

# Revista **ALCONPAT**

Latin American Journal of Quality Control, Pathology and Construction Recovery

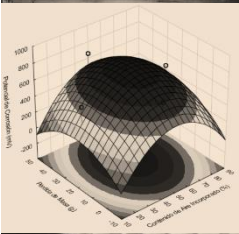
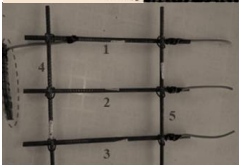
DOI: <http://dx.doi.org/10.21041/ra.v120i1>  
[editorial.revista.alconpat@gmail.com](mailto:editorial.revista.alconpat@gmail.com)

eISSN: 2007-6835

Volume 12

January - April 2022

Issue 1



Latin American Journal of Quality Control, Pathology and Construction Recovery

<http://www.revistaalconpat.org>



## **ALCONPAT Internacional**

### **Founders members:**

Liana Arrieta de Bustillos – **Venezuela**  
Antonio Carmona Filho - **Brazil**  
Dante Domene – **Argentina**  
Manuel Fernández Cánovas – **Spain**  
José Calavera Ruiz – **Spain**  
Paulo Helene, **Brazil**

### **Board of Directors International:**

#### **President of Honor**

Carmen Andrade Perdrix, **Spain**

#### **President**

Enio Pazini Figueiredo, **Brazil**

#### **General Director**

Pedro Castro Borges, **Mexico**

#### **Executive Secretary**

César Juárez Alvarado, **Mexico**

#### **Technical Vice President**

Pedro Garcés Terradillos, **Spain**

#### **Administrative Vice President**

Luis Álvarez Valencia, **Guatemala**

#### **Treasurer**

Jose Manuel Mendoza Rangel, **Mexico**

#### **Manager**

Enrique Cervera Aguilar, **Mexico**  
Paulo Helene, **Brazil**

## **Revista ALCONPAT**

### **Editor in Chief:**

Dr. Pedro Castro Borges  
Centro de Investigación y de Estudios Avanzados del  
Instituto Politécnico Nacional, Unidad Mérida  
(CINVESTAV IPN – Mérida)  
Merida, Yucatan, **Mexico**

### **Co-Editor in Chief (2022-2023):**

Dra. Edna Possan  
Universidade Tecnológica Federal do  
Paraná, Curitiba, **Brazil**

### **Executive Editor:**

Dr. José Manuel Mendoza Rangel  
Universidad Autónoma de Nuevo León,  
Facultad de Ingeniería Civil  
Monterrey, Nuevo León, **Mexico**

### **Associate Editors:**

Dr. Manuel Fernández Cánovas  
Universidad Politécnica de Madrid.  
Madrid, **Spain**

Ing. Raúl Husni

Facultad de Ingeniería - Universidad de Buenos Aires.  
Buenos Aires, **Argentina**

Dr. Paulo Roberto do Lago Helene

Universidade de São Paulo.  
São Paulo, **Brazil**

Dr. José Iván Escalante García

Centro de Investigación y de Estudios Avanzados del  
Instituto Politécnico Nacional (Unidad Saltillo)  
Saltillo, Coahuila, **Mexico**.

Dra. Oladis Troconis de Rincón  
Centro de Estudios de Corrosión  
Universidad de Zulia  
Maracaibo, **Venezuela**

Dr. Fernando Branco  
Universidade Técnica de Lisboa  
Lisboa, **Portugal**

Dr. Pedro Garcés Terradillos  
Universidad de Alicante  
San Vicente, **Spain**

Dr. Andrés Antonio Torres Acosta  
Instituto Tecnológico y de Estudios Superiores de  
Monterrey, Querétaro  
Querétaro, **Mexico**

Dr. Filippo Ubertini  
Universidad de Perugia,  
Perugia, **Italy**

Dr. Ravindra Gettu  
Instituto Indio de Tecnología de Madrás,  
Chennai, **India**

**JOURNAL OF THE LATIN-AMERICAN  
ASSOCIATION OF QUALITY CONTROL,  
PATHOLOGY AND RECOVERY OF  
CONSTRUCTION**

<http://www.revistaalconpat.org>

With great satisfaction, we present the first issue of the twelfth year of the ALCONPAT Journal.

The objective of the Journal is the publication of contributions on basic or applied research directly related to solving problems about quality control, pathology and recovery of constructions, with related case studies being welcome in these areas.

This V12N1 edition begins with a work from **Brazil**, where Emerson Félix and colleagues present an experimental investigation with the objective of evaluating the influence of the frequency of the efforts, the level of applied tension and the compressive strength of the material on the fatigue behavior of concrete. The tests were carried out considering three load frequencies (0.125, 0.25 and 0.5 Hz), two levels of maximum stress (50% and 70% of the compressive strength) and concretes with three classes of compressive strength (30, 50 and 70 MPa). The results found indicate that as the load frequency increases, the life under fatigue conditions increases exponentially. However, it was observed that the life under fatigue conditions is lower in concretes with high compressive strength, and presents an inverse relationship with the compressive strength of the material.

In the second work, Jordi Payá and colleagues from **Spain** show that alkaline activation cements (AAC) require an alkaline component for the activation of the precursor. The manufacture of the alkaline activator (AA) involves a very important energy and raw material consumption, so that the carbon footprint of AACs is fundamentally influenced by this factor. An alternative is the use of other subjects for AA preparation. In this work an exhaustive analysis of the different alternatives is carried out: silica-based materials for the preparation of alternative silicates and alkaline-based materials. Carbon footprints are compared relative to commercial Portland cements, and the effect of replacing commercial reagents with alternative activators is analyzed.

The third article comes from **Brazil**, where Fernanda Pacheco and colleagues analyze the healing potential of concrete using chemical and bacterial solutions, evaluating different materials that can be used for encapsulation. Expanded clay and perlite were used to encapsulate the agents. To analyze the effectiveness of healing, visual analysis techniques were performed using a high precision light microscope and 3D microtomography. The results pointed to a better performance of the BAC.AE mixture (bacterial solution encapsulated in expanded clay), using a bacterial solution encapsulated in expanded clay, which was able to heal cracks of up to 0.57mm. The mixtures BAC.PE (bacterial solution encapsulated in expanded perlite), bacterial solution encapsulated in expanded perlite, and SS (sodium silicate), a chemical solution added at the time of mixing to replace the water, healed cracks of 0.16 mm and 0.29 mm respectively.

In the fourth article from **Spain**, Rayara Pinto Costa and colleagues evaluate the variability in the prediction of the useful life of concrete structures through four models that estimate the natural advance of the carbonation front. The results show that there is variability in the estimated carbonation front. The models of Possan (2010) and Ekolu (2018) present estimated values close to those measured, while those of Ho and Lewis (1987) and Bob and Affana (1993) underestimate and overestimate the natural carbonation front. Only concretes without the addition of supplementary cementing materials were considered, due to model limitations. The compressive strength, CO<sub>2</sub> concentration and relative humidity have a significant influence on the results and the variability depends on the parameters considered in the models.

The fifth article, by Ronei Hoffmann Malaquias and colleagues, comes from **Brazil** and analyzes the performance of the treatment of rising humidity in walls, through the use of crystallizing and hydrophobic chemical blockers available in the Brazilian market, with their introduction by gravity. The evaluation of the rising humidity was carried out by calculating the water absorption rate in the samples, combined with the images obtained by the thermographic camera. From the results found, it was concluded that the treatment did not completely reduce the pathology in the walls, however, both products obtained a good performance, managing to considerably reduce the water absorption rates.

The sixth work of this issue is written by Carlos Fernando Gomes do Nascimento and colleagues from **Brazil**. They verify whether voids intensify the triggering of reinforcement corrosion in aerated concrete, using slabs with specific light masses. The methodology was based on four tests: visual inspection, corrosion potential, electrical resistivity and loss of mass. In relation to the L1 family, the L2 and L3 families (higher air content) were more susceptible to the corrosion of the reinforcement, as well as in the amount of lost mass of the steel bars in 90% of the cases. However, the behavior of some slabs indicates that there is a possibility that the process is asymptomatic in terms of staining, considering that the influence of the roof on the corrosion process of the steel bars was verified.

In the seventh work, from **Mexico**, Alberto Mena and Pedro Castro Borges present the practical use of the safety factor (FS) in the column repair strategy of a reinforced concrete building with historical value (almost 70 years) is presented. 80% of a building located in the historic center of the city of Campeche, Mexico, declared a World Heritage Site by UNESCO, was repaired. Strategies were used for a better use of material resources, equipment, and labor in the repair of walls, columns, slabs, and beams. One of the strategies was to use the theoretical FS to calculate the repair depth without structural consequences but fulfilling the purpose of controlling the carbonation of the concrete and maintaining the desired prediction of service life.

In the paper eight, from **Spain**, David Bru and Salvador Ivorra analyze the current state of the roof of the Basilica of Santa María, Alicante, Spain. This building dates from the 13th century and is listed. For the analysis of the efflorescences that are observed, an analysis of the construction typology is carried out, as well as a visual analysis of the state of the same, describing the existing pathological manifestations, both in the exterior area of the roofs, and in the interior area of the rooms under them. For the technical analysis of possible leaks from the roof to the interior rooms of the basilica, a

watertightness test and verification is carried out through the control of the variation of temperatures by means of thermographic analysis. The existence and position of leaks that have damaged this listed building can be concluded.

The last article that closes this issue is written by Zakaryaa Zarhri and colleagues from **Mexico**, who present a bibliometric study of the literature on the use of tire rubber in construction to promote the interest of using it as a raw material to reduce pollution at the level global. The works published in the period 1999-2020 in both Scopus and Web of Science (WoS) databases are taken into account using the Methodi Ordinatio and VOSviewer software. In this period, a total of 967 documents on the use of rubber in structural and non-structural concretes have been published and 1182 authors have contributed on the subject. Since 2010, the interest of researchers in introducing rubber in construction has increased. China, the United States and Australia are the countries with the greatest interest in researching rubber-concrete.

In this issue, for the first time, an internationally outstanding scientist who has died recently is honored with an "In Memoriam". On this occasion, the "In Memoriam" section is written by Carmen Andrade and by José Bastidas to honor José Antonio González. I met José Antonio in person in 1993 at the CNIM in Madrid. He was an extremely easy come easy go person and of whom I remember extremely enriching moments. One of them, which I will comment on here, was on my first visit, when in a spontaneous, didactic and enriching way, he gave me a personal electrochemistry class, but focused on the Resistance to Linear Polarization method. At the end of the class, he gave me his autographed book on the fight against corrosion. I was always his fan and I have had his books since then. Who better than Carmen Andrade and José Bastidas to talk about his size and hidden greatness through a humility and simplicity that is not so easy to find today. I invite you to enjoy "In Memoriam".

We are confident that the articles in this issue will constitute an important reference for those readers involved with questions of evaluations and characterizations of materials, elements and structures. We thank the authors participating in this issue for their willingness and effort to present quality articles and meet the established deadlines.

At the beginning of 2022, I must broadly acknowledge the original editorial staff and those who have joined this initiative that has led us to where we are now. But without a doubt, the greatest recognition is deserved by our authors of articles, who have trusted our journal and invested time, money and effort to publish their research work with us, despite the fact that many of them have had better options in their moment. The recognition is extended to our readers, like you, who read us and quote the RA internationally.

On behalf of the Editorial Board

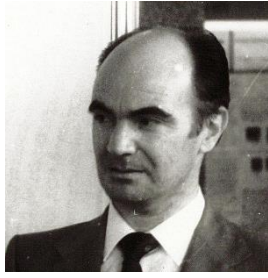


Pedro Castro Borges  
Editor in Chief

## IN MEMORIAM

José Antonio González Fernández

(1937–2021)



José Antonio González Fernández (1937–2021), left us in May 2021 after a fruitful life and excellent scientific career dedicated to research and the training of researchers. Great teacher and best person, tireless researcher who has dedicated all his knowledge and effort to the advancement of scientific knowledge. We are both one of the first and the most recent of his wardships.

In my case (Carmen) I met José Antonio at CENIM after coming into contact with Sebastián Feliu. I had just joined the Eduardo Torroja Institute where I was going to develop my Doctoral Thesis under the direction of José Calleja, the Head of the Chemistry Department. It was Calleja who suggested to me as the first topic to study the corrosion of the armor, since he had already written some work and it seemed to him of enormous importance. When I accepted it, he immediately suggested that I visit Dr. Feliu, Head of the Corrosion Department at CENIM, who directed me to the course he was giving for a doctorate in the Metallurgy chair at the Complutense University. José Antonio was then in Germany specializing in high temperature corrosion. When he returned to the laboratory a few months later, Feliu indicated that he would be the one to whom I should direct my questions. Thus, we began a fruitful collaboration in those early years until at the beginning of the 2000s my responsibilities as President of international organizations prevented me from continuing the close relationship that we had maintained for more than two decades. We had to start directing theses separately and thus continue on the same topics, but along parallel paths.

In my case (David), I had the privilege of learning with José Antonio all about Corrosion in Reinforced Concrete Structures. His scientific excellence, passion and vocation were adjectives that have accompanied and distinguished him throughout his exemplary scientific career. I also want to thank José María Bastidas for the training and scientific rigor, who is an example of research excellence at the Jose Antonio school. During my time at Cenim with José Antonio, we were pioneers in the study of the mechanisms of corrosion and passivity of steel reinforcements embedded in fly ash, a study that has had a great impact on the advancement of knowledge of the corrosion of reinforced concrete structures for his vision in the application of geopolymers as cementitious materials. In addition, you can learn with José Antonio the fundamentals of the application of galvanostatic / potentiostatic pulses for the determination of the polarization resistance through the time constant of the relaxation process for the evaluation of corrosion rate in reinforced concrete structures. I had the pleasure of accompanying him to Nashville, TN (USA), where José Antonio was awarded on the occasion of the recognition received by NACE International with the Frank Newman Speller Award in 2007, an award of merit for which he has been distinguished for his contribution to the study, diagnosis and prevention of corrosion in reinforced concrete structures. In Memory of José Antonio and to pay tribute to him, this coming year 2022, organized by the Association for Materials Protection and Performance (AMPP) and chaired jointly with Nick Birbilis, will take place a Special Symposium on Corrosion of Reinforced Concrete Structures. Among the great virtues of José Antonio, he highlighted his great capacity and generosity in training new researchers. His great talent has been an excellent example for all of us and a source of inspiration, which he always transmitted from the side of effort and tenacity, without which, the reaction would not reach its balance.

José Antonio was always available to his collaborators and was a tireless, willful worker with a lot of self-love. On a personal level, he had a very withdrawn humor, which at times was not easy to

grasp, but which was always precise, timely, and intelligent.

José Antonio's great contributions to the science of corrosion have been very notable for their international scope, where he has cultivated extensive and close relationships that have contributed to training great researchers in the international framework, being a benchmark in Ibero-American countries. Always, from the Corrosion Department of the CENIM (CSIC), where he retired a few years ago. In addition to his studies on stainless steel, which he later extended to the case of this metal reinforcement in concrete, his contributions in the use of electrochemical techniques are very important. Among them, we must mention the work with Feliu, Fullera and Andrade on the application of the Polarization Resistance ( $R_p$ ) measurement both in sulfuric acid / lead and in concrete, both of which resulted in immediate international recognition, in a few years in which the use of this way of measuring corrosion rate was highly questioned. The gravimetric verification of electrochemical losses, a verification imported from atmospheric corrosion studies where only weight losses are measured, were a crucial milestone in taking a giant step forward in demonstrating the reliability of the technique. The extension of the use of the  $R_p$  technique to large concrete structures is due to an initial impulse from Feliu, who managed to solve the mathematical equations involved and was the one who suggested the use of a guard ring, but these ideas would not have been possible without the tireless work of Jose Antonio, among others, to produce a portable corrosimeter to measure the corrosion rate with the Geocisa company and the Torroja Institute, which is still the most accurate of those marketed today.

In concrete, José Antonio diligently studied many aspects of armor corrosion such as the effect of temperature, the use of inhibitors, the application of electrochemical impedance, the use of stainless steel reinforcement, re-alkalization, and the extraction of chlorides. and a long etc. In other areas he contributed in the areas of the Corrosion Department, such as the passivation of stainless

steel in acidic media, that of aluminum and its anodization, or atmospheric corrosion.

It is very noteworthy the books he wrote on various topics of corrosion, the use of electrochemical techniques or the corrosion of armor. These books are testimony to his teaching ability and his meticulousness and rigor.

For his work he received, among others, the NACE "Frank Newman Speller Award" in 2007 for this valuable contribution to corrosion monitoring, diagnosis, and prevention of reinforced concrete Structures". He chose as his lecture the topic "Prediction of Reinforced Concrete Structure Durability by Electrochemical techniques" which was published in Corrosion 63, 9 (2007): p. 811-818.

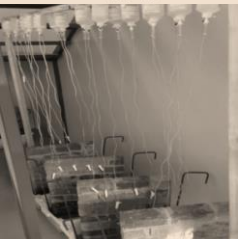
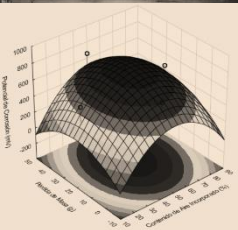
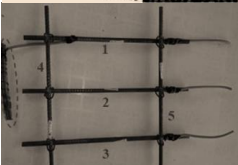
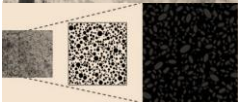
A companion of trips to congresses, of long hours measuring potentials and currents in the laboratory, and of endless scientific discussions, he rests in peace. Your teachings will serve for several generations that owe you tribute for your research vocation, scientific intuition, ability to design complex trials, rigor in the analysis of results and above all dedication, a lot of dedication to all your collaborators.

In memory of José Antonio González, great among the greats, thank you for all the knowledge and know-how that you have taught and transmitted to us. We'll miss you very much. May this memory serve to express our most sincere condolences to his entire family, his wife Mari Luz, his son José Severo, and his daughters Paloma, Mari Nieves, and Susana.

By Carmen Andrade\* and David M. Bastidas\*\*

\* International Center for Numerical Methods in Engineering (CIMNE) - Madrid- Spain

\*\* National Center for Education and Research on Corrosion and Materials Performance, NCERCAMP-UA, Dept. Chemical, Biomolecular, and Corrosion Engineering, The University of Akron, United States



## CONTENT

### BASIC RESEARCH

- |  | Page    |
|--|---------|
| <b>Felix, E. F., Carrazedo, R., Possan, E.:</b> Fatigue life of concrete: Experimental study on the influence of loading conditions and material strength.   | 1 - 15  |
| <b>Payá, J., Monzó, J., Borrachero, M. V., Soriano, L., Tashima, M. M.:</b> Alternative activators in alkali-activated cements.  | 16 – 31 |
| <b>Pacheco, F., Loeff, A., Müller, V., Ehrenbring, H. Z., Christ, R., Modolo, R. C. E., Oliveira, M. F., Tutikian, B. F.:</b> Evaluation of concrete self-healing with different insertion techniques of chemical and bacterial solutions. | 32 – 46 |
| <b>Costa, R., Franchetto, A., Gouveia, A., Ziegler, F., Pessoa, K., Garcez, M.:</b> Service life prediction for concrete structures based on carbonation front depth models.   | 47 – 60 |
| <b>Malaquias, R. H., Bruschi, G. J., Brisotto, D. S.:</b> Performance analysis of gravity chemical blockers in the treatment of rising damp in masonry walls.  | 61 – 75 |
| <b>Nascimento, C. F. G., Demétrio Filho, A. A., Silva, T. M., Teixeira, I. A. R., Neves, D. C. M., Monteiro, E. C. B.:</b> Influence of the void ratio of cellular concrete on the corrosion of steel reinforcement.                       | 76 – 97 |


### STUDY CASE

- |  |           |
|--|-----------|
| <b>Briceño-Mena, J. A., Castro-Borges, P.:</b> Practical use of the safety factor in the column repair strategy of a concrete building with historical value.        | 98 – 109  |
| <b>Bru, D., Ivorra, S.:</b> Thermographic study of the pathological manifestations due to humidity and of the conservation state of the Santa Maria Basilica's roof. | 110 – 126 |

### DOCUMENTARY RESEARCH

- |   |           |
|---|-----------|
| <b>Zarhri, Z., Rosado Martínez, W., Dominguez Lepe, J., Vega Azamar, R. E., Chan Juarez, M., Pamplona Solis, B.:</b> 30 years of rubberized concrete investigations (1990-2020). A bibliometric analysis. | 127 – 142 |
|---|-----------|

## Fatigue life of concrete: Experimental study on the influence of loading conditions and material strength

E. F. Felix<sup>1\*</sup>, R. Carrazedo<sup>1</sup>, E. Possan<sup>2</sup>

\*Contact author: [emerson.felipe.felix@gmail.com](mailto:emerson.felipe.felix@gmail.com)

DOI: <https://doi.org/10.21041/ra.v12i1.562>

Reception: 31/10/2021 | Acceptance: 07/12/2021 | Publication: 01/01/2022

### ABSTRACT

This work presents an experimental investigation aiming to evaluate the influence on the concrete fatigue behavior regarding the loading frequency, load intensity and the material's compressive strength. Tests were carried out considering three loading frequencies (0.125, 0.25 and 0.5 Hz), two levels of maximum stress (50% and 70% of the compressive strength) and concretes made with three different compressive strength (30, 50 and 70 MPa). The results point out that as the loading frequency is increased, the fatigue life increases exponentially. However, it was observed that the fatigue life is shorter in high-strength concretes, i.e., the fatigue life presented an inverse relationship with the compressive strength.

**Keywords:** concrete; cyclic compression; fatigue; low cycle fatigue; fatigue life.

**Cite as:** Felix, E. F., Carrazedo, R., Possan, E. (2022), "Fatigue life of concrete: Experimental study on the influence of loading conditions and material strength", Revista ALCONPAT, 12 (1), pp. 1 – 15, DOI: <https://doi.org/10.21041/ra.v12i1.562>.

<sup>1</sup> University of São Paulo at São Carlos School of Engineering, Brasil.

<sup>2</sup> Universidade Federal da Integração Latino-Americana (UNILA), Brasil.

#### Contribution of each author

In this work, Felix, E. F. contributed with original idea and the writing of the work (100%), experimentation (100%), data collection (100%) and discussion of results (50%). Carrazedo, R. contributed with funding acquisition (100%), supervision (100%), discussion of results (25%) and text correction (50%). Possan, E. contributed with discussion of results (25%) and text correction (50%).

#### Creative Commons License

Copyright 2022 by the authors. This work is an Open-Access article published under the terms and conditions of an International Creative Commons Attribution 4.0 International License ([CC BY 4.0](https://creativecommons.org/licenses/by/4.0/)).

#### Discussions and subsequent corrections to the publication

Any dispute, including the replies of the authors, will be published in the third issue of 2022 provided that the information is received before the closing of the second issue of 2022.



## **Vida útil à fadiga do concreto: Estudo experimental da influência das condições de carregamento e da resistência do material**

### **RESUMO**

O presente trabalho apresenta uma investigação experimental com objetivo de avaliar a influência da frequência de carregamento, intensidade da carga e resistência à compressão do material, no comportamento à fadiga do concreto. Ensaios foram realizados considerando três frequências de carregamento (0,125, 0,25 e 0,5 Hz), dois níveis de tensão máxima (50% e 70% da resistência à compressão) e concretos com três classes de resistência (30, 50 e 70 MPa). Os resultados encontrados apontam que à medida que a frequência de carregamento é aumentada, a vida útil à fadiga cresce exponencialmente. No entanto, observou-se que a vida útil à fadiga é menor em concretos de alta resistência e que a VUF apresentou uma relação inversa com a resistência à compressão.

**Palavras-chave:** concreto; compressão cíclica; fadiga; fadiga de baixo ciclo; vida útil à fadiga.

## **Vida de fatiga del hormigón: estudio experimental sobre la influencia de las condiciones de carga y la resistencia del material**

### **RESUMEN**

El presente trabajo presenta una investigación experimental con el objetivo de evaluar la influencia de la frecuencia de los esfuerzos, el nivel de tensión aplicada y la resistencia a la compresión del material sobre el comportamiento a fatiga del hormigón. Los ensayos se realizaron considerando tres frecuencias de carga (0,125, 0,25 y 0,5 Hz), dos niveles de tensión máxima (50% y 70% de la resistencia a la compresión) y hormigones con tres clases de resistencia a la compresión (30, 50 y 70 MPa). Los resultados encontrados indican que a medida que aumenta la frecuencia de carga, la vida en condiciones de fatiga aumenta exponencialmente. Sin embargo, se observó que la vida en condiciones de fatiga es menor en los hormigones de alta resistencia a la compresión, y presenta una relación inversa con la resistencia a la compresión del material.

**Palabras clave:** hormigón; compresión cíclica; fatiga; fatiga de bajo ciclo; vida de fatiga.

### **Legal Information**

Revista ALCONPAT is a quarterly publication by the Asociación Latinoamericana de Control de Calidad, Patología y Recuperación de la Construcción, Internacional, A.C., Km. 6 antigua carretera a Progreso, Mérida, Yucatán, 97310, Tel.5219997385893, [alconpat.int@gmail.com](mailto:alconpat.int@gmail.com), Website: [www.alconpat.org](http://www.alconpat.org)

Reservation of rights for exclusive use No.04-2013-011717330300-203, and ISSN 2007-6835, both granted by the Instituto Nacional de Derecho de Autor. Responsible editor: Pedro Castro Borges, Ph.D. Responsible for the last update of this issue, ALCONPAT Informatic Unit, Elizabeth Sabido Maldonado.

The views of the authors do not necessarily reflect the position of the editor.

The total or partial reproduction of the contents and images of the publication is carried out in accordance with the COPE code and the CC BY 4.0 license of the Revista ALCONPAT.

## 1. INTRODUCTION

Concrete structures are usually designed under the assumption that loads are static throughout their useful life and that the structural elements behave as linearly elastic (or with low level of damage). However, cyclic loading sources such as wind, waves, tides, temperature effects and vehicle traffic can lead to structure failure even though the stresses levels are significantly below the established in project. This occurs due to fatigue failure (Lü et al., 2004; Saini and Singh, 2020).

Fatigue is the deterioration or failure of a solid due to repeated or cyclic loading and unloading. The failure occurs due to progressive degradation of the material's microstructure developed by cyclical stresses of magnitude less than its strength (Saini and Singh, 2020). Thus, fatigue failures must be considered in the design of structural elements under cyclic loading so that damage is minimized.

In general, the magnitude of stresses is of leading importance in the analysis of endurance and service life (number of cycles  $N$  withstood before failure). The number  $N$  is described by a SN-Curve, or Wöhler curve, which is a plot that related the stress level due to cyclic loading versus the number of cycles to rupture. For most materials, the SN-Curve shows that the number of cycles reduces as the stress level is increased (Dowling, 2012).

Nowadays, only ductile materials have well-defined Wöhler curves and endurance limits. For brittle and quasi-brittle materials such as concrete, data is scatter for the several classes and types, since fatigue-related research has only increased on the last two decades, along with the substantial advances on fracture and damage mechanics and durability. Current research about the performance of concrete under cyclic loads is divided by the type of cyclic loading – tensile fatigue (Subramaniam and Shah, 2003; Chen, et al. al., 2017), tensile and compression (Lü et al., 2004), compression (Xiao et al., 2013; Lantsoght et al., 2016; Jiang et al., 2017), and flexure (Kim et al., 2013; Arora and Singh, 2016; Kasu et al., 2019; Saiani and Sinsh, 2020).

Most research aims to assess flexural fatigue strength and endurance limit, where tensile stresses are preponderant. In Brazil, for example, research is mainly devoted to flexural fatigue in beams and concrete pavements, mostly numerical and theoretical-numerical (Baroni, 2010; Junges, 2017; Mascarenhas and Carvalho, 2019). Experimental studies are incipient due to lack of equipment capable of performing cyclic loading at high speed. As an example, Medeiros (2012) carried out part of its experimental study abroad due to the unavailability of equipment for compressive fatigue tests. The author analyzed the fatigue strength gain due to the incorporation of fibers in the concrete as well as the influence of different loading frequencies.

Thus, this work evaluates the fatigue behavior of concrete, analyzing the fatigue life of concretes of low (30MPa) and high strength (50 and 70 MPa) under different loading conditions. Only cyclic compression loads with three loading frequencies (0.125, 0.25 and 0.5 Hz) and two levels of maximum stress (50% and 70% of the compressive strength) are considered in the experimental study.

## 2. FATIGUE IN CONCRETE

### 2.1 Material degradation due to cyclic loads

In a body subject to cyclic loads, microscopic cracks develop with only a small number of cycles due to the effect of material fatigue. The evolution of their size is slow, and it is related to the fatigue life expressed by the number of cycles that lead to failure ( $N_f$ ).

Fatigue life is usually classified into two stages: the nucleation of cracks, sometimes called initiation, and their propagation. In the nucleation period, the microstructural growth of cracks is observed but only with insignificant dimensions thus disregarded in the quantification of damage. On the other hand, the propagation period is characterized by the development of cracks at mesoscale. Figure 1 shows the phases that compose the fatigue life, considering aspects related to the material cracking.

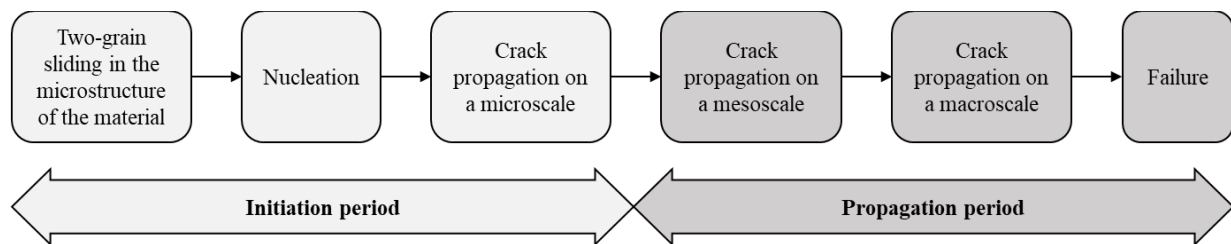


Figure 1. Fatigue life stages associated with concrete cracking.

In this sense, three stages characterize the fatigue damage of concrete, from the nucleation of the first micro-crack till rupture (as seen in Figure 2): (i) crack initiation, in which microcracks arise in discontinuities of the crystal structure due to stress concentration or in pre-existing material discontinuities; (ii) crack propagation, due to the energy accumulation at the ends of existing cracks; and (iii) failure, an abrupt rupture due to its quasi-brittle nature.

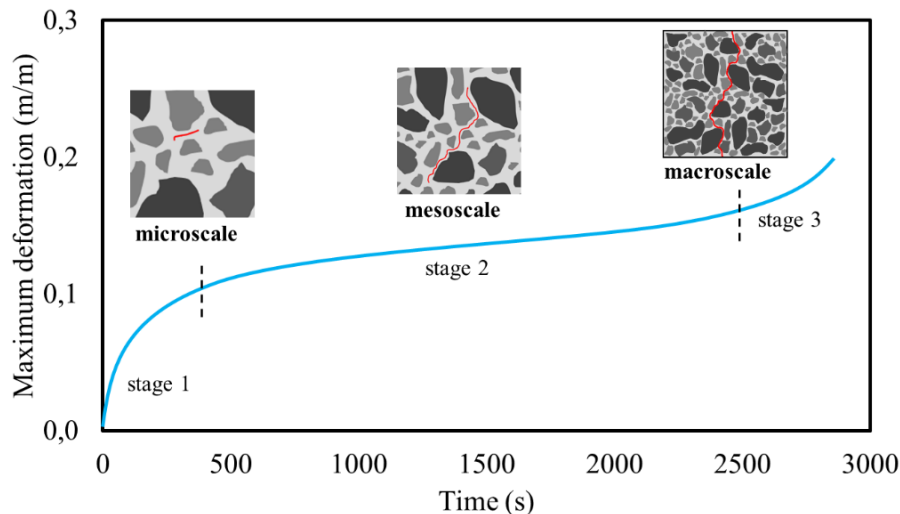


Figure 2. Development of cracks in concrete due to cyclic loading as function of time and maximum strain.

To evaluate the useful fatigue life of a concrete element, one must know the mechanical behavior of the material when subject to loading and unloading cycles. The concrete properties associated to fatigue are accessed by laboratory tests, and data are usually expressed by stresses vs number of cycles to failure or specific deformation vs number of cycles to failure, S-N curve, and  $\varepsilon$ -N curve, respectively.

Several models have been proposed to predict the fatigue life of concrete, as presented in Equations (1) to (3) (Wöhler, 1960; Raithby and Galloway, 1974; Tepfers and Kutti, 1979).

$$\frac{S_{max}}{f_{t,f}} = d + e \log(n) \quad (\text{WÖHLER, 1960}) \quad (1)$$

$$\log(N) = 13,275 - 11,39 \left( \frac{S_{max}}{f_{ck}} \right) \quad (\text{RAITHBY; GALLOWAY, 1974}) \quad (2)$$

$$\frac{S_{max}}{f_{est}} = 1 - 0,0685(1 - R) \log(N) \quad (\text{TEPFERS; KUTTI, 1979}) \quad (3)$$

where  $S_{max}$  is the maximum applied stress,  $f_{t,f}$  is the static bending tensile strength,  $N$  is the number of cycles to failure,  $d$  and  $e$  are material parameters obtained by data regression,  $R$  is the ratio between the minimum and maximum stress,  $f_{ck}$  is the concrete characteristic strength,  $f_{est}$  is the strength under analysis (tensile, compression or bending) or static tension strength of the concrete. Nevertheless, these models are usually based on S-N and  $\varepsilon$ -N curves obtained in experimental campaigns, which only attend to a small number of cases, making their general use unfeasible. According to Lee and Barr (2004), one of the reasons that make the general use of Wöhler curve unfeasible is that the parameters are obtained by data regression, and there is considerable dispersion in the fatigue tests on concrete, even under the same test conditions and sampling.

Ortega et al. (2018) report that the large dispersion in the results is associated to the sensitivity to parameters that are almost impossible to control, such as molding conditions, alignment of the specimen in the test equipment, correct imposition of maximum and minimum stresses, loading frequency and even the position of the strain gauges.

## 2.2 Factor influencing in fatigue life

The study of fatigue in concrete had its first publications in the mid-1920s with the work of Clemmer (1922), where it was observed that the degradation mechanism of concrete under cyclic loading was different from steel, and it was correlated to fracture mechanics instead. After that, until 1990s, many studies about endurance in concrete were developed, most of them focusing on the development of a general model considering the different types of fatigue tests: direct tension, tension due bending (flexural test), tension due compression (split tensile test), direct compression and cyclic tension-compression.

According to Medeiros (2012), the loading history influences the fatigue behavior of concrete, since the failure mechanism in compression, tension and bending are different. Furthermore, other parameters influence the endurance strength and service life, such as the constituent materials, moisture conditions, loading frequency, minimum and maximum applied stresses ( $R$ ), among others.

Raithby and Galloway (1974) analyzed the influence of moisture conditions in the number of cycles to failure of conventional concrete. The authors analyzed the conditions of saturated concrete, air-dried concrete for one week (Equation (2)) and oven-dried concrete for one week and found that

saturated concrete has lower service life than air-dried concrete, but practically the same as oven-dried concrete. Similar conclusions were found by Cornelissen and Lewis (1986).

Tepfers and Kutti (1979) proposed their own models to determine the useful fatigue life of concrete either by compression, tension or bending, verifying through statistical analysis that Equation (3) meets up for the different types of loading. However, Cornelissen (1984) proved that the loading mode has influence on the fatigue behavior of concrete, indicating that a single model would not adequately represent the phenomenon for different types of loading. Furthermore, Cornelissen (1984) and Zhang et al. (1996) found out that alternating stresses caused greater reduction in endurance strength.

With regard to the material constituents, there is still no consensus on the influence of the water/cement ratio ( $w/c$ ) and cement consumption, although the studies by Tepfers and Kutti (1979) and Zhang et al. (1997) shown that these parameters are indifferent to the fatigue behavior of concrete subjected to either tension or bending, affecting only the static strength of the material. As for the type of aggregate, Sparks (1982) showed that there is a strong correlation between the rate of deformation and the number of cycles until failures – concretes produced with light aggregate have shorter service life when compared to concretes produced with conventional aggregate (such as basaltic or granitic).

Finally, it is known that loading frequency ( $f$ ) exerts great influence on the fatigue behavior of concrete, and moreover, that when the frequency is increased, the fatigue life is increased. However, most works with this same statement were also developed for high frequencies ( $f > 1,0$ ) and maximum stresses varying between 75% and 95% of the compressive strength (Zhang et al., 1996). Jansen (1996) observed that frequencies between 1 and 15 Hz have little influence on endurance strength if the maximum stress is less than 75% of the concrete strength. Moreover, a reduction of 100 times in frequency reduces 10 to 30 times the number of cycles.

### 3. EXPERIMENTAL CAMPAIGN

The campaign is divided in five stages (as seen in Figure 3), whose objective is to evaluate the fatigue life of cylindrical specimens submitted to cyclic compression. The first stage is the selection and characterization of material; second stage includes dosage of concrete mixture and casting; third stage is related to static tests to define the mechanical properties; in the fourth stage, compressive fatigue tests are made; finally, in the fifth stage there is the analysis of the results. These activities are described in detail in the sequence.

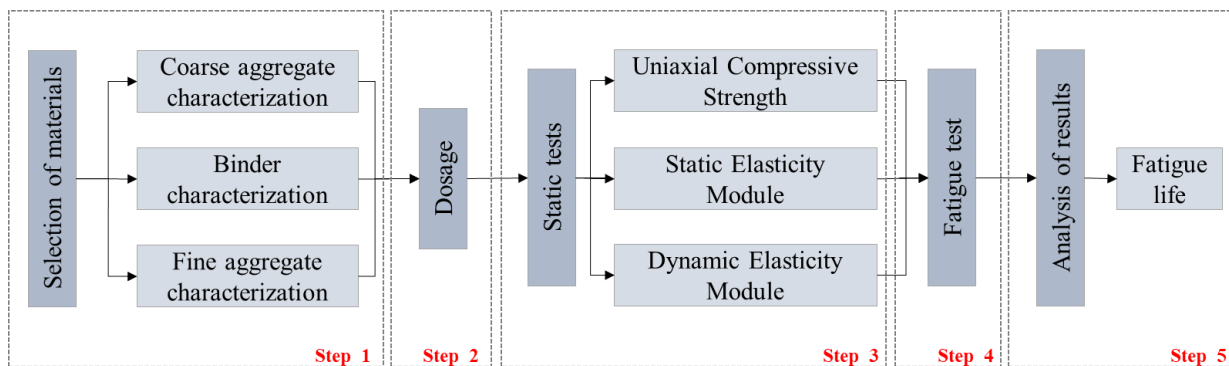


Figure 3. Experimental campaign.

### 3.1 Selection and material characterization

In this study, Portland cement CP II Z 32 was used as binder, composed with pozzolan and with 32 MPa of compressive strength. The specific mass (3.06 g/cm<sup>3</sup>) and specific surface area (3965.00 cm<sup>2</sup>/g) were determined in accordance with NBR NM 23:2001 (ABNT, 2001) and NBR 16372:2015 (ABNT, 2015), respectively.

Quartz sand and gravel of basaltic origin were used as fine and coarse aggregates, respectively. Bulk density, relative density, water absorption and fineness modulus tests were carried out, as shown in Table 1. The granulometric composition of the fine aggregate shows that it is a fine sand, according to NBR 7211 (ABNT, 2009). As for the coarse aggregate, the nominal maximum aggregate size is 9.5 mm.

Table 1. Physical properties of aggregates

Property	Fine aggregate	Coarse aggregate	Standard
Bulk density (kg/m <sup>3</sup> )	1390.00	1401.00	NBR NM 45: 2006
Relative density (kg/m <sup>3</sup> )	2520.00	2590.00	NBR NM 53: 2003
Absorption (%)	0.22	1.45	NBR NM 53, 2003
Fineness modulus	1.46	-	NBR NM 248 2003

For concretes of classes C50 and C70, it was necessary a concrete superplasticizer, composed of organic polymers, commonly used to reduce water in the concrete mixes and increasing the fluidity. Also, tap water from local supply was used.

### 3.2 Dosage and concrete pouring

For the experimental program, three different compositions were adopted, one for conventional low-strength concrete with compressive strength of 30 MPa (C30), and two for high-strength concrete, with 50 (C50) and 70 MPa (C70).

Dosage was made by ABCP method (Rodrigues, 1984) with slump fixed at 120 ± 20 mm. Initial dosage attempts were also made to obtain concretes with the desired strengths. Table 2 shows the material consumption for each dosage.

Table 2. Material consumption.

Material	Material consumption in kg/m <sup>3</sup>		
	C30	C50	C70
Cement (CP II Z 32)	353.96	395.55	553.43
Fine aggregate	800.44	1000.76	853.92
Coarse aggregate	1023.68	819.96	826.75
Water	184.19	166.37	168.92
Superplasticizer	-	2.38	4.41
Water/cement ratio	0.52	0.42	0.30

126 cylindrical specimens with 5 cm diameter and 10 cm in height were produced, 42 specimens for each composition. The specimens were casted on a vibrating plate and cured afterwards at controlled temperature and humidity at 25°C and 75%, until testing, at 28 and 90 days.

### 3.3 Static tests

Eighteen specimens were used for concrete characterization for compressive strength with static loading – six specimens at 7 days after casting, six at 28 days, and six at 90 days. In this last group, static and dynamic modulus of elasticity were also evaluated (period in which cyclic compression tests also took place). These tests were conducted in accordance with standards NBR 5739 (ABNT, 2007), NBR 8522 (ABNT, 2017) and ASTM E1876 (2015).

Notice that it was considered in this work the dynamic modulus of elasticity, since it represents the behavior of concrete under dynamic loads. The modulus was established by the impulse excitation technique (IET) is a non-destructive technique, allowing to use the specimen in subsequent tests. The variation in the dynamic modulus of elasticity as the fatigue test was also measured, as an indirect measure of damage. Besides, the static modulus of elasticity was obtained from the dynamic modulus of elasticity using Equation (4) (Popovics, 2008)

$$E_c = 0,107E_d^{1,4}\rho^{-1} \quad (4)$$

where  $E_c$  is the static modulus of elasticity (in Pa),  $\rho$  is density (in kg/m<sup>3</sup>), and  $E_d$  is the dynamic modulus of elasticity (in Pa).

### 3.4 Fatigue tests

The cylindrical specimens were subject to cyclic compression in an Instron 8805 servo-hydraulic testing system with loading capacity of  $\pm 1500$  kN. Notice that the size and compressive strength of the specimens were established by the maximum loading speed (80 kN/s) of the testing system. We also followed the experimental study carried out by Saini et al. (2015), in which it was observed that, for compressive fatigue tests, the diameter of the specimen has greater influence than the height / diameter ratio, and that the diameter of the specimen should be equal or greater than 5 cm. Saini et al. (2015) also report that the ratio between specimen diameter and maximum aggregate size should be greater than 5.0.

The servo-hydraulic system has an electronic control that receives analog signals from up to six different channels - load, displacement, or strain gauge. Figure 4a shows the adopted design for two rosette strain gauge and two LVDT, used in the specimens. Figure 4b shows the scheme used for the load controlled cyclic loading. Two configurations were defined for maximum load – 50% and 70% of the compressive strength ( $f_c$ ), and the minimum load was always 0 kN, thus the ratio between the minimum and maximum stress  $R$  is 0.00 for both cases.

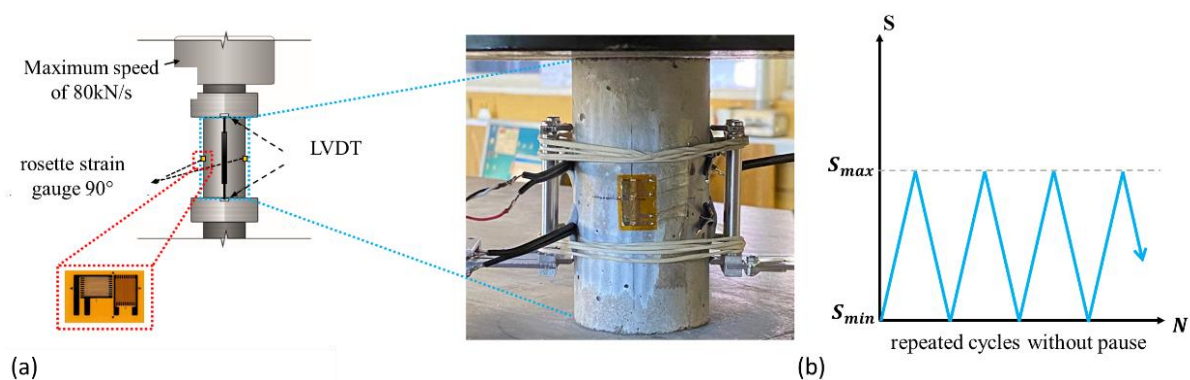


Figure 4. Arrangement (a) of instrumentation and (b) of cyclic loading.

Since three speeds of loading were adopted (0.125, 0.25 and 0.5 Hz) along with two maximum compressive strength (50% and 70% of  $f_c$ ) and three compressive strength classes (30, 50 and 70 MPa), eighteen different combinations were created. In each combination, four specimens were analyzed to establish the average number of cycles for failure. The following code was adopted: C#S#F#, where C# refers to the compressive strength class (C30 for 30 MPa, as example), S# refers to the maximum compressive strength (S7 for 70%, for instance), and F# describes the speed of loading (F125 for 0.125 Hz, F25 for 0.25 Hz and F5 for 0.5 Hz).

## 4. RESULTS

### 4.1 Material characterization

The characterization of the mechanical properties of the concretes used in the experimental study was conducted through tests of concrete compressive strength ( $f_c$ ), static modulus of elasticity ( $E_c$ ) and dynamic modulus of elasticity ( $E_d$ ).

Static compression tests were carried out on six specimens for each mix at 7, 28 and 90 days. Specimens were kept curing with controlled temperature and humidity 25°C and 75%. Figure 5a shows the obtained average for the compressive strength. Shaded areas represent mean plus standard deviation. On the other hand, Figure 5b shows averages for the evaluated mechanical properties tested at 90 days. Standard deviation is also indicated.

Results show that, at 28 days, the obtained compressive strengths are suitable for the class they were poured, with an average strength of 35.35 MPa for C30, 53.21 MPa for C50 and 73.74 MPa for C70.

An expected variation on the static modulus of elasticity was observed, as seen in Vasconcellos (2018) and Graeff and Prudencio Jr. (2016). References shows that a significant variation in the compressive strength of concrete does not necessarily mean a significant variation in the value of the modulus of elasticity, and other parameters should be evaluated, such as water/cement ratio, paste content, and aggregate/cement ratio.

As mentioned before, Equation (4) assess the static modulus of elasticity from the dynamic modulus of elasticity obtained by using the Impulse Excitation Technique. From equation (4), the static modulus for concretes C30, C50 and C70 are 35.50, 39.27 and 45.65 GPa, respectively. As comparison, the mean experimental values for the static modulus were 35.84, 38.29 and 46.05 GPa. The percentage difference was 0.94, 2.55 and 0.86% for concretes C30, C50 and C70, respectively, showing that Equation (4) is suitable to predict the static modulus of elasticity based on the dynamic modulus.

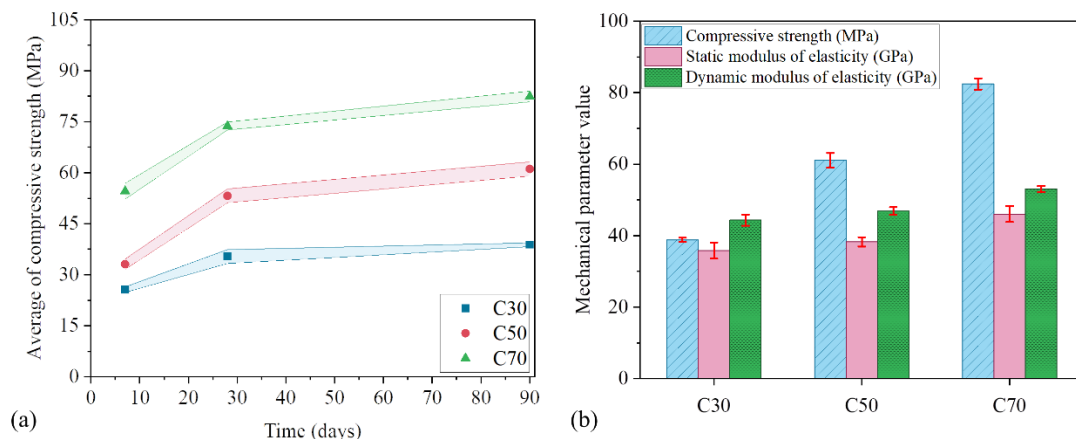


Figure 5. Mean and deviations of (a) compressive strength at 7, 28 and 90 days, and (b) compressive strength, static and dynamic modulus of elasticity at 90 days.



### 4.2 Fatigue life

Figures 6 to 8 show the number of cycles before failure that each of the four samples endure, considering the different loading scenarios and maximum compressive strength attained. They also show the average of these results (red line), and boxes representing the first and third percentiles. Besides, experimental results are also compared to the estimations obtained in Equations (2) and (3).

Equation (2) predicted a fatigue life of 38 million cycles for concrete subject to a maximum stress of 50%  $f_c$  and 200 thousand cycles for concrete subject to 70%  $f_c$ , way higher than experimental results (see Figures 6 – 8). Equation (3), on the other hand, predicted a fatigue life of 19 million cycles for concretes subject to 50%  $f_c$  and 23 thousand cycles for concrete subject to 70%  $f_c$ , also higher than the experimental results. Nevertheless, notice that these equations do not depend on neither the strength class of the concrete nor the loading conditions. Thus, models should incorporate parameters associated with the loading pattern and the material stiffness.

From Figures 6 – 8, one may notice that the number of cycles to rupture decreases as the loading frequency decreases, as also observed by Zhang et al. (1996) and Medeiros (2012). Furthermore, this behavior is present regardless the maximum applied stress (50% or 70% of  $f_c$ ), different from Jansen (1996), who states that there is almost no influence of the loading frequency in the fatigue life if maximum stresses are below 75% of the compressive strength. Nevertheless, the results found in this work follows Kim and Kim (1996), where authors point out that the fatigue life decreases as the maximum applied stress increases, especially in high-strength concrete.

Figure 9 shows the decrease in fatigue life for concretes C50 and C70 when compared to C30, when the same loading frequency and maximum stress is applied. Thus, there is positive relationship between the compressive strength of concrete and its fatigue life, especially for high-strength concretes (C50 and C70). The influence of compressive strength on fatigue life was investigated by Al-Gadhib et al. (2000) and by Kessler-Kramer et al. (2003), where authors indicate that concrete is more prone to damage as strength is increased, and this can be linked to its fatigue behavior.

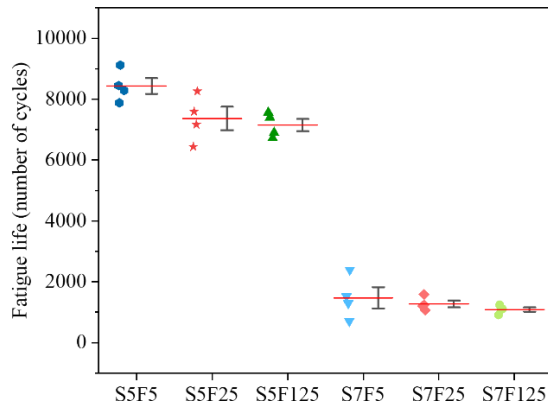


Figure 6. Fatigue life for C30.

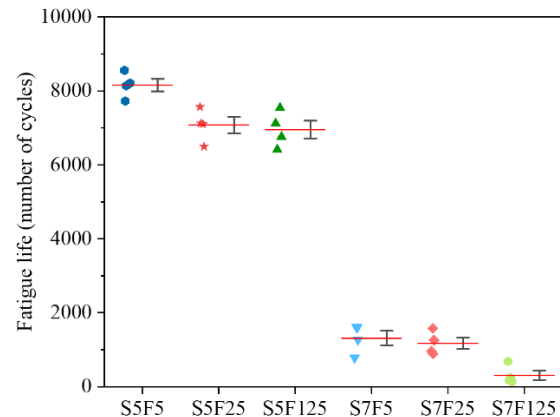


Figure 7. Fatigue life for C50.

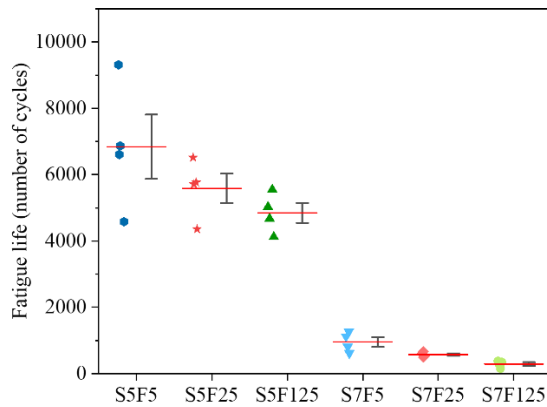


Figure 8. Fatigue life for C70.

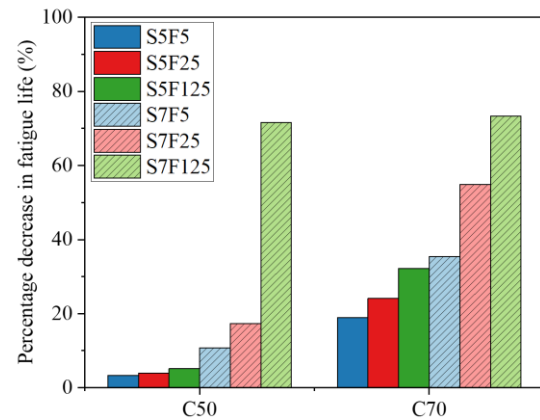


Figure 9. Variation of fatigue life of concrete C50 and C70 compared to C30.

Considering the results shown in Figure 9, it can be inferred that the reduction in fatigue life is greater for concretes submitted to higher maximum applied stresses ( $70\% f_c$ ), regardless of material strength. Furthermore, it was observed that the fatigue life is reduced as loading frequency is reduced. Thus, an increase in fatigue life is expected when loading frequency is increased, as long as the stress level is kept the same. Besides, this behavior is even noticeable in high strength concretes.

Chen et al. (2017) brings up an explanation – the cyclic loads are associated to the dynamic properties of concrete, and the dynamic properties of concrete are often superior to its static counterpart.

Finally, the usual characteristic failure mode due to compressive loads was not observed for concrete under cyclic compression. However, rupture was still more abrupt in concretes with higher compressive strength. Furthermore, the rupture abruptness was even more pronounced in cyclic tests than in static compression tests, indicating that the material brittleness should be considered as an influencing parameter in the mechanical behavior of concrete under cyclic loads.

## 5. CONCLUSIONS

The mechanical behavior of concrete subjected to cyclic compression was experimentally investigated in this work. Concretes of three compressive strength classes were submitted to different loading conditions and the fatigue life was evaluated. The following conclusions were obtained:

- The fatigue life is increased as the loading frequency is increased if the maximum stress is maintained. A plausible justification is that the dynamic property of the material is higher than the static counterpart (see Figure 6b).
- The number of cycles until rupture is reduced as the maximum stress is increased. This is associated to the inner damage, here measured by the reduction of the modulus of elasticity using a non-destructive impulse excitation technique.
- There is an inverse relationship between the compressive strength and the fatigue life, which is even more pronounced in high strength concretes.
- Dispersion of the number of cycles before failure is decreased as the loading frequency decreases, no matter the applied maximum stress. This indicates that the loading frequency should be considered in fatigue life models.

Finally, the discussion here shall be extended to other levels of maximum stress, loading frequencies and compressive strengths. It is our aim to propose SN curves for concretes subjected to cyclic compression, as well as formulations to design concrete elements under fatigue.

## 6. ACKNOWLEDGMENT

The research supported by the Brazilian National Council for Scientific and Technological Development (CNPq 141078/2018, 310564/2018-2 and 428762/2018-2) is gratefully acknowledged. This study was also financed in part by the Coordenação de Aperfeiçoamento de Pessoal de Nível Superior - Brasil (CAPES) - Finance Code 001

## 7. REFERENCES

Associação Brasileira de Normas Técnicas (2001). *NBR NM 23: Agregados – Determinação da composição granulométrica*. Rio de Janeiro.

Associação Brasileira de Normas Técnicas (2003). *NBR NM 248: Agregados – Determinação da composição granulométrica*. Rio de Janeiro.

Associação Brasileira de Normas Técnicas (2006). *NBR NM 45: Agregados – Determinação da massa unitária e do volume de vazios*. Rio de Janeiro.

Associação Brasileira de Normas Técnicas (2007). *NBR 5739: Concreto – Ensaios de compressão de corpos-de-prova cilíndricos*. Rio de Janeiro.

Associação Brasileira de Normas Técnicas (2009). *NBR 7211: Agregados para concreto – Especificações*. Rio de Janeiro.

Associação Brasileira de Normas Técnicas (2008). *NBR 8522: Concreto – Determinação do módulo estático de elasticidade à compressão*. Rio de Janeiro.

Associação Brasileira de Normas Técnicas (2009). *NBR NM 53: Agregado graúdo – Determinação da massa específica, massa específica aparente e absorção de água*. Rio de Janeiro.

Associação Brasileira de Normas Técnicas (2015). *NBR 16372: Cimento Portland e outros materiais em pó — Determinação da finura pelo método de permeabilidade ao ar (método de Blaine)*. Rio de Janeiro.

Al-Gadhib, A. H., Baluch, M., Shaalan, A., Khan, A. (2000), *Damage model for monotonic and fatigue response of high strength concrete*. International Journal of Damage Mechanics, v. 9, n. 1, p. 57-78. <https://doi.org/10.1177/105678950000900105>

Arora, S., Singh, S. P. (2016), *Analysis of flexural fatigue failure of concrete made with 100% Coarse Recycled Concrete Aggregates*. Construction and Building Materials, v. 102, n. 1, p. 782-791. <https://doi.org/10.1016/j.conbuildmat.2015.10.098>

ASTM International (2015), *ASTM E1876: Standard Test Method for Dynamic Young's Modulus, Shear Modulus, and Poisson's Ratio by Impulse Excitation of Vibration*.

Baroni, H. J. M. (2010), “*Simulação da vida útil de fadiga do concreto em vigas de tabuleiro de pontes em função do fluxo de veículos pesados*”. Tese (Doutorado). Programa de Pós-Graduação em Engenharia Civil. Universidade Federal do Rio Grande do Sul. Porto Alegre.

Chen, X., BU, J., Fan, X., Lu, J., Xu, L. (2017), *Effect of loading frequency and stress level on low cycle fatigue behavior of plain concrete in direct tension*. Construction and Building Materials, v. 133, p. 367-375. <https://doi.org/10.1016/j.conbuildmat.2016.12.085>

Clemmer, H. F. (1922), *Fatigue of concrete*. Proceedings, American Society for Testing and Materials. v. 22, n. 2, p. 408-419.

Cornellissen, H. A. W. (1984), *Fatigue failure of concrete in tension*. Heron, v. 29, n. 4, p. 2-67.

Cornelissen, H. A. W., Lewis, M. (1986) “*Fatigue experiments for the design of plain concrete pavements*” in: Workshop on Theoretical Design of Concrete Pavements, CROW-PIARC-CEMBUREAU, Report 1, Holanda.

Dowling, N. E. (2012), “*Mechanical behavior of materials: Engineering methods for deformation, fracture, and fatigue*”. Practice Hall, 4<sup>th</sup> edition, United States.

Graeff, E.; Prudêncio Jr., L. R. (2016). *Determinação do módulo de elasticidade dos concretos da central de Itajaí da Maxmohr*. [S.l.]: Relatório técnico.

Jansen A. (1996), “*Research to fatigue behaviour of topping on prefabricated concrete girders*”. Thesis (Master). Delft University of Technology. Holanda.

Jiang, C., Xianglin, G., Huang, Q., Zhang, W. (2017), *Deformation of concrete under high-cycle fatigue loads in uniaxial and eccentric compression*. Construction and Building Materials, v. 141, p. 379-392. <https://doi.org/10.1016/j.conbuildmat.2017.03.023>

Junges, P. (2017), “*Análise de fadiga em pontes curtas de concreto armado a partir de dados de sistemas B-WIM*”. Tese (Doutorado). Centro Tecnológico: Programa de Pós-Graduação em Engenharia Civil. Universidade Federal de Santa Catarina. Florianópolis.

Kasu, S. R., Deb, S., Mitra, N., Muppireddy, A. R., Kusam, S. R. (2019), *Influence of aggregate size on flexural fatigue response of concrete*. Construction and Building Materials, v. 229, p. 1-9. <https://doi.org/10.1016/j.conbuildmat.2019.116922>

Kessler-Kramer, C., Mechtcherine, V., Mueller, H. S. (2003), “*Failure of normal and high strength concrete under monotonic and cyclic tensile loading*” in: Brittle Matrix Composites 7. Woodhead Publishing. p. 277-286. <https://doi.org/10.1533/9780857093103.277>

- Kim, J. K., Kim, Y. Y. (1996), *Experimental study of the fatigue behavior of high strength concrete*. Cement and Concrete Research, v. 26, n. 10, p. 1513-1523.
- Kim, J., Yi, C., Lee, S. J., Zi, G. (2013), *Flexural fatigue behaviour of concrete under uniaxial and biaxial stress*. Magazine of Concrete Research, v. 65, n. 12, p. 757-764. [https://doi.org/10.1016/0008-8846\(96\)00151-2](https://doi.org/10.1016/0008-8846(96)00151-2)
- Lantsoght, E. O. L., Van Der Veen, C., Boer, A. (2016), *Proposal for the fatigue strength of concrete under cycles of compression*. Construction and Building Materials, v. 107, p. 138-156. <https://doi.org/10.1016/j.conbuildmat.2016.01.007>
- Lee, M. K., Barr, B. I. G. (2004), *An overview of the fatigue behavior of plain and fiber reinforced concrete*. Cement and Concrete Composites. v. 26, p. 299-305. [https://doi.org/10.1016/S0958-9465\(02\)00139-7](https://doi.org/10.1016/S0958-9465(02)00139-7)
- Lü, P., Li, Q., Song, Y. (2004), *Damage constitutive of concrete under uniaxial alternate tension–compression fatigue loading based on double bounding surfaces*. International Journal of Solids and Structures, v. 41, p. 3151-3166. <https://doi.org/10.1016/j.ijsolstr.2004.01.026>
- Mascarenhas, F. Jr. R., Carvalho, R. C. (2019), *Vida útil à fadiga da armadura longitudinal de vigas de pontes de concreto armado frente ao tráfego real de veículos pesados*. Revista ALCONPAT, v. 9, n. 3, p. 303-319. <https://doi.org/10.21041/ra.v9i3.375>
- Medeiros, A. (2012), “*Estudo do comportamento à fadiga em compressão do concreto com fibras*”. Tese (Doutorado). Departamento de Engenharia Civil: Programa de Pós-graduação em Engenharia Civil. Pontifícia Universidade Católica do Rio de Janeiro. Rio de Janeiro.
- Ortega, J. J., Ruiz, G., Yu, R. C., Afanador-García, N., Tarifa, M., Poveda, E., Zhang, X., Evangelista JR., F. (2018), *Number of tests and corresponding error in concrete fatigue*. International journal of fatigue, v. 116, p. 210-219. <https://doi.org/10.1016/j.ijfatigue.2018.06.022>
- Popovics, J. S. (2008) “*A study of static and dynamic modulus of elasticity of concrete*”. University of Illinois, Urbana, IL. ACI-CRC Final Reports.
- Raithby, K. D., Galloway, J. W. (1974), “*Effects of moisture condition, age, and rate of loading on fatigue of plain concrete*” in: ABELES Symposium: Fatigue of Concrete. ACI Publication, v. 41, p. 15-34.
- Rodrigues, P. P. F. (1984), “*Parâmetros de dosagem do concreto*.” São Paulo: ABCP, 1984.
- Saini, B. S., Singh, S. P. (2020), *Flexural fatigue life analysis of self-compacting concrete containing 100% coarse recycled concrete aggregates*. Construction and Building Materials, v. 253, p. 1-13. <https://doi.org/10.1016/j.conbuildmat.2020.119176>
- Sparks, P. R. (1982), *Influence of rate of loading and material variability on the fatigue characteristics of concrete*. ACI Journal, v. 75, n. 16, p. 331-342.

Subramaniam, K. V., Shah, S. P. (2003), *Biaxial tension fatigue response of concrete*. Cement and Concrete Composites, v. 25, n. 6, p. 617-623. [https://doi.org/10.1016/S0958-9465\(02\)00075-6](https://doi.org/10.1016/S0958-9465(02)00075-6)

Tepfers, R., Kutti, T. (1979), *Fatigue strength of plain, ordinary and lightweight concrete*. ACI Journal, v. 76, n. 29, p. 635-652.

Vasconcellos, A. T. D. (2018). “*Estudo da variabilidade do módulo de elasticidade de concretos produzidos com diferentes tipos de agregados graúdos*”. Dissertação (Mestrado). Departamento de Engenharia Civil: Programa de Pós-graduação em Engenharia Civil. Universidade Federal de Santa Catarina. Santa Catarina.

Xiao, J., Li, H., Yang, Z. (2013), *Fatigue behavior of recycled aggregate concrete under compression and bending cyclic loadings*. Construction and Building Materials, v. 38, p. 681-688. <https://doi.org/10.1016/j.conbuildmat.2012.09.024>

Zhang, B., Phillips, D. V., Wu, K. (1996), *Effect of loading frequency and stress reversal of fatigue life of plain concrete*. Magazine of Concrete Research, v. 48, n. 177, p. 361-375. <https://doi.org/10.1680/mac.1996.48.177.361>

Zhang, B., Phillips, D. V., Wu, K. (1997), *Further research on fatigue properties of plain concrete*. Magazine of Concrete Research, v. 49, n. 78, p. 241-252. <https://doi.org/10.1680/mac.1997.49.180.241>

## Alternative activators in alkali-activated cements

J. Payá<sup>1\*</sup> , J. Monzó<sup>1</sup> , M. V. Borrachero<sup>1</sup> , L. Soriano<sup>1</sup> , M. M. Tashima<sup>2</sup> 

\*Contact author: [jjpaya@cst.upv.es](mailto:jjpaya@cst.upv.es)

DOI: <https://doi.org/10.21041/ra.v12i1.568>

Reception: 08/11/2021 | Acceptance: 07/12/2021 | Publication: 01/01/2021

### ABSTRACT

Alkali-activated cements (AACs) require an alkaline component for precursor activation. As the manufacture of the alkaline activator (AA) involves significant energy and raw material uses, these factors primarily influence the carbon footprint of AACs. An alternative is to use alternative materials to prepare the AA. In this work, a comprehensive analysis of the different alternatives is carried out: silica-based materials to prepare alternative silicates and alkaline-based materials. The relative carbon footprints are compared to commercial Portland cements, and the effect of replacing commercial reagents with alternative activators is analyzed.

**Keywords:** alkali activation; alternative activators; biomass ash; industrial waste; carbon footprint.

**Cite as:** Payá, J., Monzó, J., Borrachero, M. V., Soriano, L., Tashima, M. M. (2022), “Alternative activators in alkali-activated cements”, Revista ALCONPAT, 12 (1), pp. 16 – 31, DOI: <https://doi.org/10.21041/ra.v12i1.568>

<sup>1</sup> Grupo de Investigación en Química de los Materiales (GIQUIMA), Instituto de Ciencia y Tecnología del Hormigón (ICITECH), Universitat Politècnica de València, Valencia, España.

<sup>2</sup> Grupo de Pesquisa MAC– Materiais Alternativos de Construção, Universidade Estadual Paulista (UNESP), Campus de Ilha Solteira, São Paulo, Brasil

### Contribution of each author

In this work the author, the bibliographic search activity was carried out by M. Tashima (50%) and L. Soriano (50%); the information extraction activity by J. Payá (20%), J. Monzó (20%), M.V. Borrachero (20%), L. Soriano (20%) and M. Tashima (20%); the writing of the document by J. Payá (20%), J. Monzó (20%), M.V. Borrachero (20%), L. Soriano (20%) and M. Tashima (20%); the revision of the text by J. Payá (20%), J. Monzó (20%), M.V. Borrachero (20%), L. Soriano (20%) and M. Tashima (20%); the design of figures and the adaptation to the format by J. Payá (100%); English translation (M. Tashima (100%)).

### Creative Commons License

Copyright 2022 by the authors. This work is an Open-Access article published under the terms and conditions of an International Creative Commons Attribution 4.0 International License ([CC BY 4.0](https://creativecommons.org/licenses/by/4.0/)).

### Discussions and subsequent corrections to the publication

Any dispute, including the replies of the authors, will be published in the third issue of 2022 provided that the information is received before the closing of the second issue of 2022.

## Activadores alternativos para cementos de activación alcalina

### RESUMEN

Los cementos de activación alcalina (CAA) requieren de un componente alcalino para la activación del precursor. La fabricación del activador alcalino (AA) supone un consumo energético y de materias primas muy importante, de modo que la huella de carbono de los CAA está fundamentalmente influenciada por ese factor. Una alternativa es el uso de otras materias para la preparación del AA. En este trabajo se realiza un exhaustivo análisis de las diferentes alternativas: materias de base silíceas para la preparación de silicatos alternativos y materias de base alcalina. Se comparan de forma relativa las huellas de carbono con respecto a cementos Portland comerciales, y se analiza el efecto que tiene la sustitución de reactivos comerciales por activadores alternativos.

**Palabras clave:** activación alcalina; activadores alternativos; cenizas de biomasa; residuos industriales; huella de carbono.

## Ativadores alternativos para cimentos ativados por alcalinos

### RESUMO

Os Cimentos Ativados por Alcalinos (CAA) requerem um componente alcalino para a ativação do precursor. A fabricação do ativador alcalino (AA) envolve um consumo de energia e matéria-prima muito importante, de forma que a pegada de carbono dos CAA é fundamentalmente influenciada por este fator. Uma alternativa é o uso de outros materiais para a preparação de AA. Neste trabalho é realizada uma análise exaustiva das diferentes alternativas: materiais à base de sílica para a preparação de silicatos alternativos e materiais à base de alcalinos. As pegadas de carbono são comparadas com os cimentos Portland comerciais, comparando o efeito da substituição dos reagentes comerciais por ativadores alternativos.

**Palavras-chave:** ativação alcalina; ativadores alternativos; cinza de biomassa; resíduos industriais; pegada de carbono.

### Legal Information

Revista ALCONPAT is a quarterly publication by the Asociación Latinoamericana de Control de Calidad, Patología y Recuperación de la Construcción, Internacional, A.C., Km. 6 antigua carretera a Progreso, Mérida, Yucatán, 97310, Tel.5219997385893, [alconpat.int@gmail.com](mailto:alconpat.int@gmail.com), Website: [www.alconpat.org](http://www.alconpat.org)

Reservation of rights for exclusive use No.04-2013-011717330300-203, and ISSN 2007-6835, both granted by the Instituto Nacional de Derecho de Autor. Responsible editor: Pedro Castro Borges, Ph.D. Responsible for the last update of this issue, Informatics Unit ALCONPAT, Elizabeth Sabido Maldonado.

The views of the authors do not necessarily reflect the position of the editor.

The total or partial reproduction of the contents and images of the publication is carried out in accordance with the COPE code and the CC BY 4.0 license of the Revista ALCONPAT.



*List of acronyms (in order of appearance in the text)*

Abbreviation	Meaning
AA	Alkali activator
AAC	Alkali-activated cement
MK	Metakaolin
FA	Pulverized fly ash
BFS	Blast furnace slag
CW	Ceramic waste
NS	Nanosilica
DE	Diatomaceous earth
FCC	Spent fluid catalytic cracking catalyst
WG	Sodium silicate
WD	Wasted diatomite
SF	Silica fume
GW	Glass waste
RHA	Rice husk ash
SCSA	Sugar cane straw ash
SCBA	Sugar cane bagasse ash
BLA	Bamboo leaf ash
BL	Bayer Liquor
RM	Red mud
ACS	Alkaline cleaning solution
OBA	Olive-stone biomass ash
ABA	Almond shell biomass ash
HCWA	High calcium wood ash
CCA	Corn cob ash

## 1. INTRODUCTION

The term "circular economy" has been established in most proposals on the development of humanity in global challenges (climate change, biodiversity, waste, pollution). This circular economy focuses on a production+use model that prioritizes the reduction, reuse, repair, recycling, recovery and valorization of products. Thus, products' life cycles should be extended for as long as possible by minimizing the use of natural resources and energy, and reducing waste generation and environmental pollution.

Circularity must be extended to each development, scientific, technological and human area. As many manufacturing processes are related to chemical reactions and processes are associated with pollution and waste management phenomena, the term "circular chemistry" becomes especially important (Keijer et al., 2019; Mohan and Katakajwala, 2021). Chemistry is the fundamental science for circular economy, where strategies focus on chemical innovation at atomic, molecular and structural levels.

In the construction field, and specifically in concrete technology where concrete is the most widely used material by humanity after water, technological breakthroughs must be developed according to circular chemistry. As a key binder material in concrete preparation, cement is a synthetic material made from various components. It is made up of a set of chemical compounds which, by reacting with water, develop other chemical products responsible for binders' technological properties.

In ancient times, nonhydraulic binders based on gypsum and hydrated lime were prepared by transforming natural materials. These binders were reacted with water and/or carbon dioxide (CO<sub>2</sub>) to produce stable resistant materials in certain environments. Roman engineers introduced pozzolanic materials, mainly ashes of volcanic origin, into mixtures with hydrated lime, which involved a transcendental chemical turnabout (Pavía and Caro, 2008). Many centuries later, these ancient materials were taken up again to develop new cements with pozzolanic additions.

In the late eighteenth and early nineteenth centuries, chemical processes were implemented to manufacture hydraulic binders, which culminated with Joseph Aspdin's patent in 1824: it started the Portland cement period by drastically reducing the use of hydrated lime and gypsum. Cement is the material that has been employed to make many buildings and infrastructures from that time to the present-day (Hall, 1976). The development of high-temperature chemical processes (clinkerization) allowed high-performance cements with good durability. Knowledge of the chemical reactions of Portland cement hydration and their interaction with concrete components and the environment (humidity, CO<sub>2</sub>, chlorides, etc.) allowed the evolution of the characteristics of new commercial cements based on Portland cement clinker.

In recent decades, concerns about greenhouse gases emissions from manufacturing Portland cement, perseverance to reduce the use of nonrenewable raw materials, and the requirement to improve concrete's technical performance have led the chemistry of materials toward new more sustainable, complementary and circular paths (Phair, 2006). Intensive research has been carried out on cements with a higher proportion of pozzolanic and hydraulic additions, belite cements, calcium sulfoaluminate cements, magnesia cements and alkali-activated cements (AACs).

This paper focuses on AACs, specifically on alkaline activators (AAs), their impact in carbon footprint terms, and the alternatives involved in applying circular chemistry. This paper is divided into an initial section about the basic concepts of the chemistry of AACs, followed by a comparative evaluation of the carbon footprint associated with different conventional AACs, starting with Portland clinker-based cements and finishing with a description of alternative materials of the residual origin that can be used to produce alternative AAs, along with carbon footprint-related aspects.

## 2. NATURE OF ALKALI-ACTIVATED CEMENTS AND THE ORIGIN OF COMPONENTS

Alkali-activated cements (AACs) are formed by combining two components ("two-parts" technology): the major component is the precursor, which contains  $\text{SiO}_2\text{-Al}_2\text{O}_3$  (e.g., metakaolin - MK, fly ash from coal-fired power plants - FA). Sometimes it can also contain significant amounts of CaO (blast furnace slag - BFS). The other minor component is a highly alkaline aqueous solution (sodium or potassium hydroxides, silicates and carbonates). The mixture of these two components produces cementitious substances like the alkaline aluminosilicate hydrated type (N(K)-A-S-H) or, if calcium is present, the calcium aluminosilicate hydrated type (C-A-S-H). Gels of a hybrid nature between the two previous ones, C(N,K)-A-S-H, can also be produced.

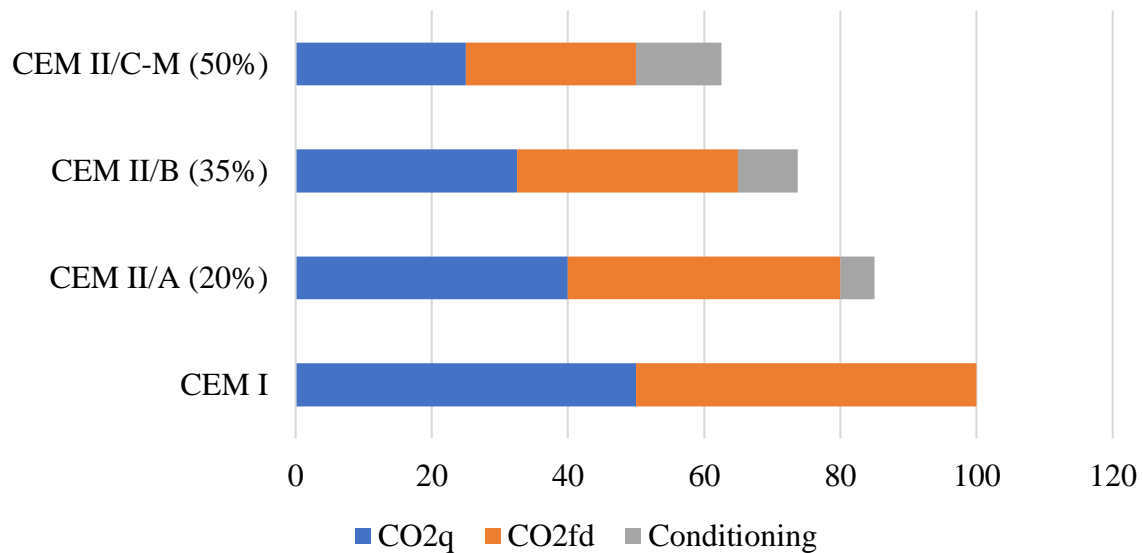
From the circular chemistry and sustainability points of view, the marked advantage of AACs lies in the fact that it is often possible to use waste from other anthropogenic industrial and agricultural activities, as well as ceramic waste (CW), BFS and FA. Circularity is not possible in other cases because the precursor is specifically manufactured, such as MK (kaolin calcination at  $800^\circ\text{C}$ ). In AACs, the application of very high temperatures is avoided, which occurs in the clinkering process of Portland cement ( $1450^\circ\text{C}$ ). The main disadvantage of AACs is that the activator is a chemically synthesized substance: e.g., hydroxides NaOH and KOH, carbonates  $\text{Na}_2\text{CO}_3$  and  $\text{K}_2\text{CO}_3$ , silicates  $\text{Na}_2\text{SiO}_3$  (waterglass) and  $\text{K}_2\text{SiO}_3$ . The manufacturing of these substances involves employing natural resources and energy, and following chemical processes that have a significant impact and move away from circularity. In recent years, the major development of AACs has taken place, when two components have been combined into one ("one-part" technology) so their application can follow the same model of traditional cements: just add water to "one-part" cement.

## 3. CARBON FOOTPRINT IN ALKALINE ACTIVATION CEMENTS

It is well-known that  $\text{CO}_2$  emissions are related to Portland cement clinker manufacturing, i.e. the carbon footprint is very large. The process involves the emissions of 850-1200 kg of  $\text{CO}_2$ /ton-clinker, which depends mainly on the applied technologies and the effectiveness of the heat recovery and insulation of industrial elements.  $\text{CO}_2$  emissions can be assigned to two main components: the chemical component on the one hand, and the energy component on the other.

The chemical component is due to limestone decarbonation. For a clinker containing 64% CaO, the amount of  $\text{CO}_2$  from the chemical component ( $\text{CO}_{2q}$ ) is approximately 500 kg of  $\text{CO}_2$ /ton-clinker. The amount of  $\text{CO}_2$  from the energy component ( $\text{CO}_{2fd}$ ) associated with fuel and electrical energy use approximately equals  $\text{CO}_{2q}$  (Luukkonen et al., 2016). Relatively speaking, we can establish a value of 100 for the  $\text{CO}_2$  emissions associated with cement with 95% clinker (cement type CEM I in the European nomenclature), with a contribution of 50 for  $\text{CO}_{2q}$  and 50 for  $\text{CO}_{2fd}$  (See Figure 1, CEM I). For cements with mineral additions, each contribution proportionally reduces: Figure 1 shows the CEM II/A (with 20% addition) and CEM II/B (with 35% addition) cases. Currently in Europe, work is being done on the standardization of CEM II/C-M cement (EN 197-5, 2021), which includes a mixture of additions (M) up to 50% (see Figure 1). For cements with additions, we must consider additional components like energy used to prepare additions (sieving, grinding, drying) in either independent or mixing processes with non-ground clinker. These additional components are named "conditioning".

Synthetic AAs have certain associated  $\text{CO}_2$ -equivalent emission values ( $\text{CO}_{2-e}$ ,  $\text{kgCO}_2/\text{kg}$ -reagent), and these values very much depend on the industrial process and the technology used in synthesis (see Table 1).



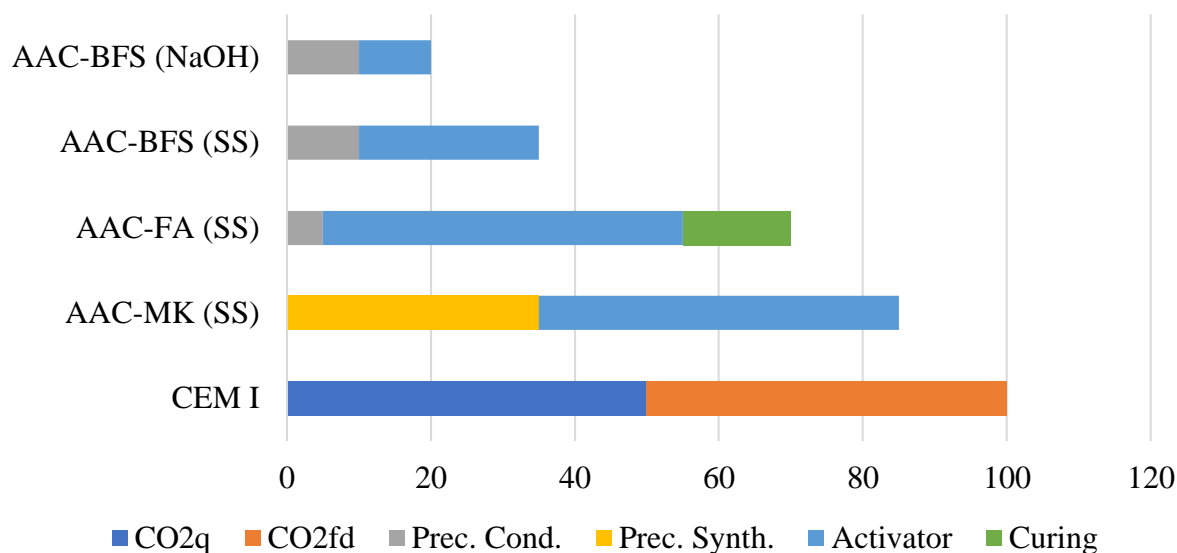
*Key: CO<sub>2</sub>q: chemical component; CO<sub>2</sub>fd: energy component; conditioning: treatment of additions, before or simultaneously with clinker.*

Figure 1. Comparison of the relative emissions of Portland cement clinker-based cements: CEM I, CEM II/A (with 20% addition), CEM II/B (with 35% addition) and CEM II/C-M (with 50% addition). Relative scale takes 100 for CEM I.

Table 1. CO<sub>2</sub> emissions for some alkaline reagents (taken from: [www.winnipeg.ca/finance/findata/matmgt/documents/2012/682-2012/682-2012\\_Appendix\\_H-](http://www.winnipeg.ca/finance/findata/matmgt/documents/2012/682-2012/682-2012_Appendix_H-))

Reagent	CO <sub>2</sub> -e kgCO <sub>2</sub> /kg-reagent
NaOH	1.12
KOH	1.94
Na <sub>2</sub> CO <sub>3</sub>	0.59
K <sub>2</sub> CO <sub>3</sub>	2.38
Na <sub>2</sub> SiO <sub>3</sub>	1.64

Metakaolin (MK)-based AACs require significant amounts of activator, especially sodium silicate SS (Weil et al., 2009). Moreover, the manufacture of MK requires the calcination of kaolin at 800°C, which involves significant energy use. An estimated calculation of the associated emissions for an MK-based AAC is shown in Figure 2: compared to CEM I, no significant advantages appear. Obviously, the lower the sodium silicate use in the dose, the more advantageous it is. Fly ash (FA)-based AACs also require vast amounts of activator. To achieve good geopolymerization development, high-temperature curing is required. Hence additional energy use is to be considered in their application (curing process). Figure 2 depicts how the corresponding relative CO<sub>2</sub> emissions are also very high. In the two previous cases based on MK and FA, the calcium content of these precursors is low, which requires a large amount of activators. With calcium-rich precursors, such as BFS, a smaller amount of activators is needed. In addition, the precursor can be activated with NaOH solution without having to resort to alkali silicate (SS or potassium silicate). Figure 2 shows the marked advantage of AAC-BFS over the relative carbon footprint compared to the previously discussed AACs. Slag requires a milling process (precursor conditioning) to improve its reactivity in the alkaline medium.



*Key: CO<sub>2</sub>q: chemical component; CO<sub>2</sub>fd: energy component; Prec. Cond. (Precursor conditioning; e.g. milling); Synth. Precursor: precursor synthesis process (e.g. calcination); Activator: associated with activator manufacturing; Curing: associated with energy use for curing.*

Figure 2. Comparison of the relative emissions of CEM I with the AACs based on metakaolin (MK), fly ash (FA), and blast furnace slag (BFS). Activators: sodium hydroxide (NaOH) and sodium silicate (SS). Relative scale takes 100 for CEM I.

## 4. ALTERNATIVE ALKALINE ACTIVATORS

As seen in the previous section, the contribution of AAs to the carbon footprint of AACs is most relevant. This means that improvements in this aspect should focus on minimizing the use of this component. One choice would be to center on improving the chemical processes of the synthesis of chemical reagents so that the associated CO<sub>2</sub>-e lowers. The other option, which is more suitable for circular economy and chemistry, is the valorization of agricultural and industrial waste for this purpose. In recent years, there have been more scientific waste valorization reports about achieving efficient activators with a smaller associated carbon footprint. These publications contain a variety of options, which can be classified as the following groups:

- Alternative activators based on silica: related to alkaline silicates, where an alkaline hydroxide is reacted with a rich-silica raw material, which is totally or partially dissolved
- Alternative activators based on alkali: in this case, the employed residual material is an alkaline, sodium or potassium-based substance
- Combined silica-AA systems

### 4.1. Alternative activators based on silica.

There are different strategies for this group: on the one hand, the use of natural silica-based resources that can be dissolved under distinct conditions; on the other hand, the availability of ashes from biomass combustion with high SiO<sub>2</sub> percentages; finally, the possibility of using some industrial waste rich in potentially reactive silica.

#### 4.1.1. Silica-based activators from natural resources.

In this section, references related to diatomaceous earth and olivine can be found.

Diatomaceous earth (DE) is a silica-rich material (generally  $\text{SiO}_2 > 80\%$ ) formed by the skeletons of diatoms, unicellular algae, which have been deposited over millions of years. This sedimentary rock presents silica in the amorphous state, which can be dissolved under alkaline conditions. Font et al. (2018) presented a study in which DE was dissolved in NaOH solution in a thermally insulated vessel. The dissolution of NaOH pellets in water increases the temperature of the aqueous medium that, in turn, enhances amorphous silica dissolution. The obtained results show the prepared activator's good performance. So these authors used this activator for the FCC precursor (fluid catalytic cracking catalyst residue). In mortars, mechanical strengths of 30 MPa after 7 curing days at room temperature were obtained without having to employ high-temperature curing.

Olivine,  $(\text{Fe}, \text{Mg})_2\text{SiO}_4$ , is a natural material that can be used to obtain nanosilica from a dissolution process with concentrated sulfuric acid and subsequent filtration (Gao et al., 2017). These authors utilized a solution prepared with nanosilica (NS) and NaOH to show that reactivity was similar to commercial sodium silicate (waterglass, SS). They applied this activator to a mixture of BFS and FA at the 70/30 ratio. The mechanical strength of concretes yielded about 57-68 MPa at 7 days and 72-82 MPa at 28 days, depending on the silica modulus ( $\text{SiO}_2/\text{Na}_2\text{O}$  molar ratio) used in the activating solution.

#### **4.1.2. Silica-based activators from industrial waste.**

This section offers examples based on residual DE, silica fume (SF) and glass waste (GW).

DE is frequently used as a component of liquid filter media, especially beer and wine. At the end of the filtration process, the residual DE (WD) contains significant amounts of potentially soluble amorphous silica. WD from beer filtrate (WD-B) was used to prepare alkaline activators with NaOH (Mejía et al., 2016). This activator was combined with a precursor consisting of a mixture of FA and MK (70/30). Paste was cured at 60°C for 24 h and subsequently cured at room temperature for up to 360 days. The compressive strength values within the range 7-360 days came close to 35 MPa. WD from wine filtrate (WD-W) was studied by Font et al. (2018). These authors evaluated the performance of the activator based on this residue. They observed a substantial improvement when WD-W was calcined at 650°C to remove the organic matter from the filtration process. The mechanical compressive strength at 28 days of the activated FCC mortars was about 20 MPa for the system with no prior WD-W calcination, and was 40 MPa for the system with calcination.

SF is a well-known and excellent pozzolan in Portland cement systems thanks to its marked fineness and high amorphous silica content. This residue, from the silicon and ferrosilicon alloys industry, can be used as raw material to produce activators. Rouseková et al. (1997) studied BFS activation with a mixture of SF and NaOH, and obtained good results. Bernal et al. (2012) studied the SF/NaOH activator in MK+BFS systems to show that silica from SF can be incorporated into the geopolymerization reaction for very short times. Mixtures of C-A-S-H, N-A-S-H, or even of N-(C)-A-S-H cementitious gels, were formed.

For GW, various chemical GW compositions can be found, although the most notable one is the amorphous state and a high percentage of silica. Since 2014, the potential of GW for manufacturing activators has been studied. The  $\text{SiO}_2$  percentages in GW fall within the 65-80% range with significant CaO and  $\text{Na}_2\text{O}$  contents (Liu et al., 2019). Several approaches have been performed to prepare the AA, as shown in Figure 3. They include melting, hydrotherma, and thermochemical methods. It has been shown that the nature and rate of formation of cementitious hydrates depend primarily on the precursor type.

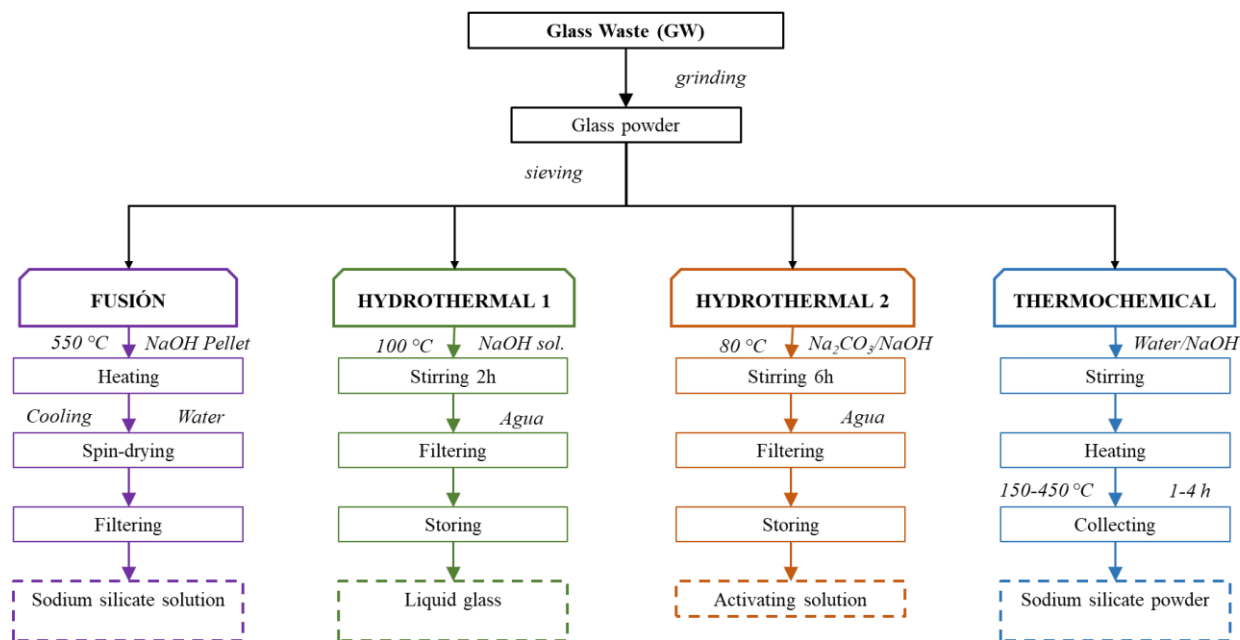


Figure 3. Methods to obtain alternative activators from glass waste (GW) (adapted from Lie et al., 2019).

#### 4.1.3. Silica-based activators from biomass ash.

This section contains the largest number of alternative activators. Biomass combustion sometimes generates the formation of a significant amount of ash (1-4%, in mass). The most significant examples are waste from rice husks, sugar cane production and bamboo leaves.

Rice husk ash (RHA) is the most widely studied. Many works have been published about using RHA to produce sodium silicate. The first bibliographic reference dates back to 2010 (Bejarano et al., 2010). The authors proposed a hydrothermal process during which they analyzed different variables: NaOH:RHA ratio, treatment time, reaction temperature and water:RHA ratio. The conclusions on the optimum parameters were NaOH:RHA=2, water:RHA=10, 100°C treatment for 120 minutes. With these proportions, the research group used this activator type in the alkaline activation of several common precursors (Mejía et al., 2016). Bouzón et al. (2014) applied an activator obtained by refluxing a mixture of NaOH solution with partially amorphous RHA, and by using FCC as a precursor to prepare mortar. Systems with excellent mechanical performance were obtained, but the authors observed that the activator was more reactive if ground RHA was used during the hydrothermal process (around 60 minutes, compared to 120 minutes for the non-ground sample). Other authors have devised methods and applications for this material (including Tong et al., 2018; Rajan and Kathirvel, 2021). Villca et al. (2021) applied an alternative RHA-based activator, produced with no energy use, but by simply heating the dissolution of NaOH pellets to dissolve the amorphous silica of RHA. This activator was applied for the first time to binary systems of lime/pozzolan and geopolymer.

Sugarcane production generates a waste product, sugarcane straw, which is usually left in fields. Using this biomass can be beneficial in energy recovery terms. The generated waste, sugarcane straw ash (SCSA), contains large amounts of silica (Moraes et al., 2018). This research demonstrated that the procedure which takes advantage of the dissolution heat of NaOH to dissolve silica is perfectly viable for SCSA and treatment should not exceed 24 h due to the gelation of the activator. Sugarcane bagasse ash (SCBA) has also been employed (Tchakouté et al., 2017) in the geopolymerization of MK. The prepared binder reached 33 MPa at 28 curing days.

Finally, bamboo leaf ash (BLA), with a SiO<sub>2</sub> percentage close to 80% (Roselló et al., 2015), is also an interesting option. BLA has been used by a thermochemical process at 300-330°C (Vinai et al.,

2021). The activator was utilized for the FA/BFS system (60/40). Compared to the SS+NaOH activator, reactivity was lower on the first 7 curing days, and the same strengths were obtained (around 43 MPa) at 28 days.

## 4.2. Alternative activators based on alkali.

Human activity also produces alkaline waste of both industrial and agricultural origins.

### 4.2.1. Alkali-based activators from industrial activities.

We can find some waste related to metallurgical activity, such as Bayer liquor, alkaline cleaning solutions and red mud.

Bayer liquor (BL) is a caustic solution prepared with NaOH, used to extract aluminum from bauxite. After filtration, the resulting solution is reusable, but has to be eventually discarded when its efficiency decreases. The waste is rich in sodium aluminate and has been employed for FA activation under different conditions (Jamieson et al., 2016).

Red mud (RM) is the solid waste generated while extracting aluminum from bauxite. It is very rich in iron oxides and silica. This sludge has a pH between 9.7 and 12.8, and has been used to activate FA (Choo et al., 2016), although the achieved strength does not exceed 2 MPa.

The last example in this category is alkaline cleaning solution (ACS), which is usually produced as waste when cleaning aluminum surfaces. It is rich in sodium hydroxide and sodium aluminate. Fernández-Jiménez et al. (2017) employed ACS at a NaOH concentration of approximately 5M to activate ground FA and GW powder. In both cases, mechanical strengths were around 10-16 MPa for FA and 2-10 MPa for GW (cured for 20 h at 85°C).

### 4.2.2. Alkali-based activators from agricultural waste.

Some agricultural waste is considered to be biomasses for energy production, and the resulting ashes are alkaline in nature. This alkaline nature is determined by the presence of calcium, especially that of potassium. This applies to olive stone ash (OBA), almond shell ash (ABA), corn cob ash (CCA), and high calcium wood ash (HCWA). The great advantage of using these ashes is that they allow "one-part" cements to be prepared as they are solid materials.

The first study on employing OBA in AAC was presented by Font et al. (2017). BFS was activated with OBA and compared to activation by means of chemical reagent KOH. The result showed that the compressive mechanical strength for the BFS/OBA system was higher (29.9 MPa vs. 16.9 MPa). Subsequent studies (De Moraes Pinheiro et al., 2018) showed the formation of cementitious gels of the C(K)-S-H, C(K)-S-A-H type, in addition to small amounts of hydrotalcite. Subsequently, Alonso et al. (2019) studied ashes from an olive biomass: both FA and bottom ashes. They observed that the alkalinity of these ashes was not sufficient to activate FA, but sufficed to activate BFS. Payá et al. (2019) employed the BFS/OBA system to produce dolomitic-based compacted earth blocks. The compressive strength of about 12 MPa for compacted blocks was obtained after 9 curing days under plastic film (to prevent water evaporation and to maintain optimal hydration conditions). The resulting blocks showed excellent resistance underwater.

Soriano et al. (2020) were the first to study the potential of almond shell ash (ABA). They found that the percentage of K<sub>2</sub>O for ABA was higher than for OBA (46.98% vs. 32.16%). They detected the presence of several calcium and potassium carbonate minerals (K<sub>2</sub>Ca(CO<sub>3</sub>)<sub>2</sub>), such as fairchildite and bütschilite, in addition to calcite (CaCO<sub>3</sub>) portlandite (Ca(OH)<sub>2</sub>) and arcanite (K<sub>2</sub>SO<sub>4</sub>). This ash performed well when combined with BFS.

Several authors have investigated the use of HCWA. Of these authors, Ban et al. (2014) characterized ash and applied it as a solid activator for FA. Ash presented a high proportion of CaO (61%) and a smaller amount of K<sub>2</sub>O (12%). The found calcium salts were calcite, portlandite and hydroxyapatite.



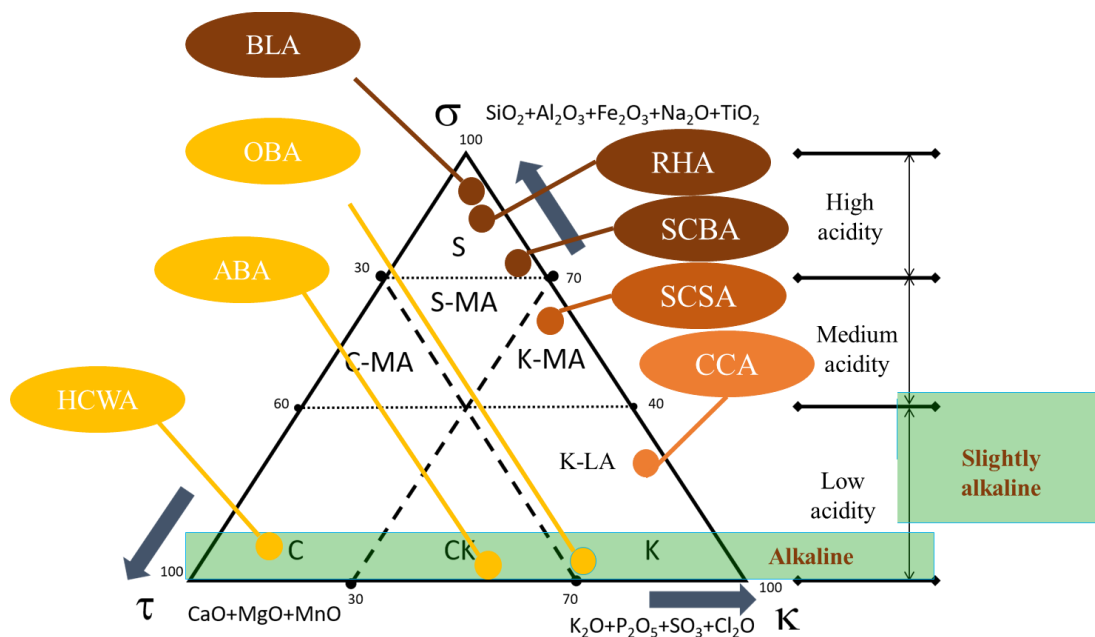
Rachis or crown CCA has also been used for MK activation (Peys et al., 2016), and 30 MPa compressive strength has been achieved for samples with a CCA:MK ratio of 1:2.

### 4.3. Combined silica-alkali systems.

AAC based on the use of alkaline ash can reduce impacts because, in some cases, both the precursor and activator come from waste. However, mechanical performance is often not very good due to the activator's silica deficiency. Thus, the development of activators containing silica and alkali could minimize this effect. Font et al. (2020) designed AAC with the BFS-OBA-RHA ternary system, in which the activator was prepared by a hydrothermal reaction between RHA and OBA at 65°C for 24 h. For a BFS-OBA-RHA dose of 9/4.5/1, 35.0, 46.2 and 67.4 MPa were obtained for mortars respectively cured for 7, 28 and 90 days at 20°C.

### 4.4. Classification of biomass ashes according to their reactivity.

Employing biomass ashes is an interesting alternative for synthesizing sustainable activators. The ternary diagram in Figure 4 illustrates an extended version of the Vassilev diagram (Vassilev et al., 2010) of the biomass ashes classification. Reactivity zones have been modified, and different ashes have been represented. In zone S (top of the diagram) we see a set of ashes that are potentially very acidic and can supply a high percentage of silicates to alternative activators: RHA, BLA and sugar cane bagasse ash (SCBA). In an intermediate situation (Zone K-MA), we find sugar cane straw ash (SCSA) whose composition contains other elements that reduce its contribution to silicate formation. Finally in low-acid materials (Zone K-LA), we find CCA, with limited silicon contribution and a high proportion of potassium. At the bottom of the diagram, where more alkaline oxides are involved, basically CaO (far left) and K<sub>2</sub>O (far right), three zones stand out: the "C" zone, which is characteristic of ashes with high calcium content, such as HCWA; the "K" zone, with a high proportion of potassium oxide, as in ABA; finally, the intermediate "CK" zone, where OBA is found.

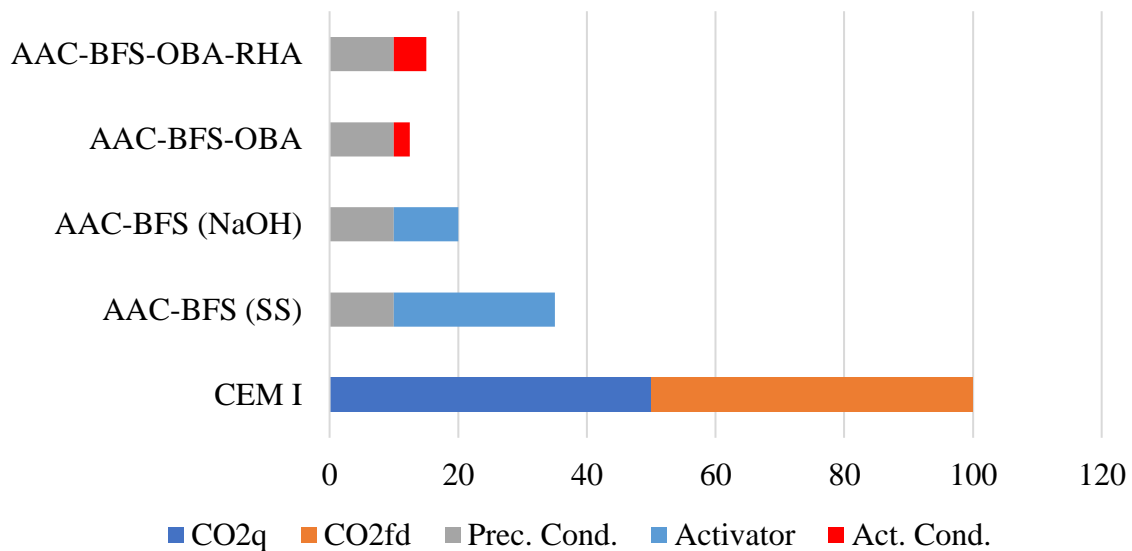


*Key: olive stone ash (OBA); almond shell ash (ABA); high calcium wood ash (HCWA); corn cob ash (CCA); sugar cane straw ash (SCSA); sugar cane bagasse ash (SCBA); rice husk ash (RHA); bamboo leaf ash (BLA).*

Figure 4. Modified Vassilev's diagram (adapted from Vassilev et al., 2010).

## 5. CARBON FOOTPRINT OF ALKALI-ACTIVATED CEMENTS USING ALTERNATIVE ALKALINE ACTIVATORS

BFS activation with synthetic activators results in relatively low CO<sub>2</sub> emissions (Figure 2). However, this can improve if alternative activators are employed. By way of example, the system with OBA is analyzed. In addition to waste recovery (and also energy recovery for biomass), the associated CO<sub>2</sub> can also slightly drop. With the BFS-OBA system (Figure 5), the conditioning of the precursor is logically the same, and only the conditioning of the activator (grinding in this case) has to be taken into account. The associated CO<sub>2</sub> emissions for the BFS-OBA-RHA system are higher because the activator must be conditioned by the hydrothermal treatment of the OBA-RHA mixture. However, this new activator enables higher mechanical strength to be achieved and, thus, extra CO<sub>2</sub> emissions can be compensated by the obtained material's mechanical performance.



*Key: CO<sub>2</sub>q: chemical component; CO<sub>2</sub>fd: energy component; Prec. Cond (milling); Activator: associated with activator manufacture; Act. Cond: activator conditioning (hydrothermal process).*

Figure 5. Comparison of relative emissions of the CEM I cements and AAC produced with alternative activators and the blast furnace slag (BFS) Precursor. Commercial activators: sodium hydroxide (NaOH) and sodium silicate (SS); alternative activators, olive stone ash (OBA) and rice husk ash (RHA). Relative scale takes 100 for CEM I.

## 6. CONCLUSIONS

The development of AACs requires the availability of both, suitable precursors and activators. The capacity to obtain precursors in sufficient quantities and locations to completely replace Portland cement is probably insufficient. Therefore, it is not easy to consider AACs to be the only solution. Their production must be taken as an alternative to Portland cements and other cement types (belite, calcium sulfoaluminate, magnesia-based). The main fact is that there are places where potentially marketable precursors are generated (ceramics, construction waste, different metallurgical slag types), and all possibilities should be exploited. The same applies to alternative activators: synthetic chemical reagents can be replaced where agricultural or industrial activities are performed, which can generate suitable components to prepare alternative activators. This circumstance may be particularly interesting in developing societies where it is not easy (basically economic) to use

Portland cement, but where there are alternative resources to manufacture AACs (construction waste, biomass, etc.).

The following conclusions about alternative activators stand out:

- a) AACs do not always result in the drastic reduction of associated CO<sub>2</sub> emissions. In some cases, the required quantities of chemical reagents represent a comparable carbon footprint to that of Portland cements
- b) Precursors like BFS require smaller quantities of activator, which results in lower CO<sub>2</sub> emissions than for other precursors like FA or MK
- c) Alternative activators can be of agricultural or industrial origin but, in any case, require complete characterization, including both necessary preconditioning studies and the potential problems of their use (presence of harmful chemical components for some applications, such as chlorides)
- d) Silica-based waste cannot be independently used because of its high acidity (mainly silica). Alkali-based waste can be independently employed. Combining both waste types can improve the mechanical behavior of AACs and enhance their uses
- e) The use of solid waste as alternative activators allows "one-part" cements to be produced. Additionally, the precursor and activator can be ground, which improves the intimate mixture of both components.

## 7. ACKNOWLEDGEMENTS

For funding, the Government of Spain, Ministry of Economy and Competitiveness (Project BIA2017-87573-C2-1-P) and FEDER funds. M.M.T. thanks the Spanish Ministry of Universities and the Universitat Politècnica de València for the "María Zambrano for the attraction of international talent" grant for the requalification of the Spanish university system funded by European Union-Next generation UE.

## 8. REFERENCES

- Alonso, M. M., Gascó, C., Morales, M. M., Suárez-Navarro, J. A., Zamorano, M., Puertas, F. (2019). *Olive biomass ash as an alternative activator in geopolymer formation: A study of strength, durability, radiology and leaching behaviour*. Cem. Concr. Compos. 104, 103384. <https://doi.org/10.1016/j.cemconcomp.2019.103384>
- Ban, C. C., Nordin, N. S. A., Ken, P. W., Ramli, M., Hoe, K. W. (2014). *The high volume reuse of hybrid biomass ash as a primary binder in cementless mortar block*. Am. J. Appl. Sci. 11, 1369–1378. <https://doi.org/10.3844/ajassp.2014.1369.1378>
- Bejarano, J., Garazón, C., Mejía de Gutiérrez, R., Delvasto, S., Gordillo, M. (2010). *In: II Simposio Aprovechamiento de residuos agro-industriales como fuente sostenible de materiales de construcción*, Valencia, Spain, November 8-9, 2010
- Bernal, S. A., Rodríguez, E. D., Mejía De Gutiérrez, R., Provis, J. L., Delvasto, S. (2012). *Activation of metakaolin/slag blends using alkaline solutions based on chemically modified silica fume and rice husk ash*. Waste Biomass Valor. 3, 99–108. <https://doi.org/10.1007/s12649-011-9093-3>
- Bouzón, N., Payá, J., Borrachero, M. V., Soriano, L., Tashima, M. M., Monzó, J. (2014). *Refluxed rice husk ash/NaOH suspension for preparing alkali activated binders*. Mater. Lett. 115, 72-74. <https://doi.org/10.1016/j.matlet.2013.10.001>

- Choo, H., Lim, S., Lee, W., Lee, C. (2016). *Compressive strength of one-part alkali activated fly ash using red mud as alkali supplier*. *Constr. Build. Mater.* 125, 21–28. <https://doi.org/10.1016/j.conbuildmat.2016.08.015>
- De Moraes Pinheiro, S. M., Font, A., Soriano, L., Tashima, M. M., Monzó, J., Borrachero, M. V., Payá, J. (2018). *Olive-stone biomass ash (OBA): An alternative alkaline source for the blast furnace slag activation*. *Constr. Build. Mater.* 178, 327–338. <https://doi.org/10.1016/j.conbuildmat.2018.05.157>
- Fernández-Jiménez, A., Cristelo, N., Miranda, T., Palomo, A. (2017). *Sustainable alkali activated materials: Precursor and activator derived from industrial wastes*. *J. Clean. Prod.* 162, 1200–1209. <https://doi.org/10.1016/j.jclepro.2017.06.151>
- Font, A., Soriano, L., Moraes, J. C. B., Tashima, M. M., Monzó, J., Borrachero, M. V., Payá, J. (2017). *A 100% waste-based alkali-activated material by using olive-stone biomass ash (OBA) and blast furnace slag (BFS)*. *Mater. Lett.* 203, 46–49. <https://doi.org/10.1016/j.matlet.2017.05.129>
- Font, A., Soriano, L., Reig, L., Tashima, M. M., Borrachero, M. V., Monzó, J., Payá, J. (2018). *Use of residual diatomaceous earth as a silica source in geopolymer production*. *Mater. Lett.* 223, 10–13. <https://doi.org/10.1016/j.matlet.2018.04.010>
- Font, A., Soriano, L., de Moraes Pinheiro, S. M., Tashima, M. M., Monzó, J., Borrachero, M. V., Payá, J. (2020). *Design and properties of 100% waste-based ternary alkali-activated mortars: Blast furnace slag, olive-stone biomass ash and rice husk ash*. *J. Clean. Prod.* 243, 118568. <https://doi.org/10.1016/j.jclepro.2019.118568>
- EN 197-5, 2021. *Cement - Part 5: Portland-composite cement CEM II/C-M and Composite cement CEM VI*.
- Gao, X., Yu, Q. L., Lazaro, A., Brouwers, H. J. H. (2017). *Investigation on a green olivine nano-silica source based activator in alkali activated slag-fly ash blends: Reaction kinetics, gel structure and carbon footprint*. *Cem. Concr. Res.* 100, 129–139. <https://doi.org/10.1016/j.cemconres.2017.06.007>
- Hall, C. (1976). *On the history of portland cement after 150 years*. *Journal of Chemical Education*, 53(4), 222.
- Jamieson, E., van Riessen, A., McLellan, B., Penna, B., Kealley, C., Nikraz, H. (2017). *Introducing Bayer liquor-derived geopolymers*. In: *Handbook of low carbon concrete*. Nazari, A. and Sanjayan, J.G. (eds), Kidlington, Oxford, United States: Elsevier.159-193. <https://doi.org/10.1016/B978-0-12-804524-4.00008-7>
- Keijer, T., Bakker, V., Slootweg, J. C. (2019). *Circular chemistry to enable a circular economy*. *Nature Chem* 11, 190–195. <https://doi.org/10.1038/s41557-019-0226-9>
- Liu, Y., Shi, C., Zhang, Z., Li, N. (2019). *An overview on the reuse of waste glasses in alkali-activated materials*. *Resour. Conserv. Recycl.* 144, 297–309. <https://doi.org/10.1016/j.resconrec.2019.02.007>
- Luukkonen, T., Abdollahnejad, Z., Yliniemi, J., Kinnunen, P., Illikainen, M. (2018). *One-part alkali-activated materials: A review*. *Cem. Concr. Res.* <https://doi.org/10.1016/j.cemconres.2017.10.001>
- Mejía, J. M., Mejía De Gutiérrez, R., Montes, C. (2016). *Rice husk ash and spent diatomaceous earth as a source of silica to fabricate a geopolymeric binary binder*. *J. Clean. Prod.* 118, 133–139. <https://doi.org/10.1016/j.jclepro.2016.01.057>

- Mohan, S. V., Katakowala, R. (2021). *The circular chemistry conceptual framework: A way forward to sustainability in industry 4.0*, Current Opinion in Green and Sustainable Chemistry, 28, 100434. <https://doi.org/10.1016/j.cogsc.2020.100434>
- Moraes, J. C. B., Font, A., Soriano, L., Akasaki, J. L., Tashima, M. M., Monzó, J., Borrachero, M. V., Payá, J. (2018). *New use of sugar cane straw ash in alkali-activated materials: A silica source for the preparation of the alkaline activator*. Constr. Build. Mater. 171, 611–621. <https://doi.org/10.1016/j.conbuildmat.2018.03.230>
- Pavía, S., Caro, S. (2008). *An investigation of Roman mortar technology through the petrographic analysis of archaeological material*. Cons. Build. Mat. 22, 1807–1811. <https://doi.org/10.1016/j.conbuildmat.2007.05.003>
- Payá, J., Monzó, J., Roselló, J., Borrachero, M. V., Font, A., Soriano, L. (2020). *Sustainable soil-compacted blocks containing blast furnace slag (BFS) activated with olive stone biomass ash (OBA)*. Sustain. 12, 1–15. <https://doi.org/10.3390/su12239824>
- Peys, A., Rahier, H., Pontikes, Y. (2016). *Potassium-rich biomass ashes as activators in metakaolin-based inorganic polymers*. Appl. Clay Sci. 119, 401–409. <https://doi.org/10.1016/j.clay.2015.11.003>
- Phair, J. W. (2006). *Green chemistry for sustainable cement production and use*. Green chemistry, 8(9), 763–780.
- Rajan, H. S., Kathirvel, P. (2021). *Sustainable development of geopolymer binder using sodium silicate synthesized from agricultural waste*. J. Clean. Prod. 286, 124959. <https://doi.org/10.1016/j.jclepro.2020.124959>
- Roselló, J., Soriano, L., Santamarina, M. P., Akasaki, J. L., José Luiz P. Melges, J. L. P., Payá, J. (2015). *Microscopy characterization of silica-rich agrowastes to be used in cement binders: bamboo and sugarcane leaves*. Microsc. Microanal. 21, 1314–1326. <https://doi.org/10.1017/S1431927615015019>
- Rouseková, I., Bajza, A., Živica, V. (1997). *Silica fume-basic blast furnace slag systems activated by an alkali silica fume activator*. Cem. Concr. Res. 27, 1825–1828. [https://doi.org/10.1016/S0008-8846\(97\)00191-9](https://doi.org/10.1016/S0008-8846(97)00191-9)
- Soriano, L., Font, A., Tashima, M. M., Monzó, J., Borrachero, M. V., Payá, J. (2020). *One-part blast furnace slag mortars activated with almond-shell biomass ash: A new 100% waste-based material*. Mater. Lett. 272, 127882. <https://doi.org/10.1016/j.matlet.2020.127882>
- Tchakouté, H. K., Rüscher, C. H., Hinsch, M., Djobo, J. N. Y., Kamseu, E., Leonelli, C. (2017). *Utilization of sodium waterglass from sugar cane bagasse ash as a new alternative hardener for producing metakaolin-based geopolymer cement*. Chemie der Erde 77, 257–266. <https://doi.org/10.1016/j.chemer.2017.04.003>
- Tong, K. T., Vinai, R., Soutsos, M. N. (2018). *Use of Vietnamese rice husk ash for the production of sodium silicate as the activator for alkali-activated binders*. J. Clean. Prod. 201, 272–286. <https://doi.org/10.1016/j.jclepro.2018.08.025>
- Vassilev, S. V., Baxter, D., Andersen, L. K., Vassileva, C. G. (2010). *An overview of the chemical composition of biomass*. Fuel, 89, 913–933. <https://doi.org/10.1016/j.fuel.2009.10.022>
- Villca, A.R., Soriano, L., Font, A., Tashima, M. M., Monzó, J., Borrachero, M. V., Payá, J. (2021). *Lime/pozzolan/geopolymer systems: Performance in pastes and mortars*. Cons. Build. Mat. 276 122208. <https://doi.org/10.1016/j.conbuildmat.2020.122208>

Vinai, R., Ntimugura, F., Cutbill, W., Evans, R. (2021). *Production of sodium silicate from bamboo leaf ash for alkali activation of binders*. Open Research Exeter. <https://ore.exeter.ac.uk/repository/bitstream/handle/10871/125925/Vinai%20et%20al.pdf?sequence=1&isAllowed=y>

Weil, M., Dombrowski, K., Buchwald, A. (2009). *Life-Cycle analysis of geopolymers*. In: Provis and van Deventer (ed), *Geopolymers Structures, Processing, Properties and Industrial Applications*. <https://doi.org/10.1533/9781845696382.2.194>

## Evaluation of concrete self-healing with different insertion techniques of chemical and bacterial solutions

F. Pacheco<sup>1\*</sup> , A. Loeff<sup>2</sup> , V. Müller<sup>3</sup> , H. Z. Ehrenbring<sup>1</sup> , R. Christ<sup>4</sup> ,  
R. C. E. Modolo<sup>3</sup> , M. F. Oliveira<sup>5</sup> , B. F. Tutikian<sup>3</sup> 

\*Contact author: [fernandapache@unisinós.br](mailto:fernandapache@unisinós.br)

DOI: <https://doi.org/10.21041/ra.v12i1.559>

Reception: 28/10/2021 | Acceptance: 07/12/2021 | Publication: 01/01/2022

### ABSTRACT

This study evaluated the self-healing potential of concrete with chemical and bacterial solutions encapsulated in different materials. The encapsulating materials were expanded clay (EC) and expanded perlite (EP). Self-healing effectiveness was evaluated visually with a high-precision optical microscope and 3D microtomography. Results pointed to improved performance of bacterial solutions encapsulated in expanded clay (BAC.EC) which were able to heal fissures of 0.57 mm. In contrast, bacterial solutions encapsulated in expanded perlite (BAC.EP) and sodium silicate replacing water during molding (SS) healed fissures of 0.16 mm and 0.29 mm, respectively.

**Keywords:** bioconcrete; self-healing; self-repairing; fissure; bacteria.

**Cite as:** Pacheco, F., Loeff, A., Müller, V., Ehrenbring, H. Z., Christ, R., Modolo, R. C. E., Oliveira, M. F., Tutikian, B. F. (2022), "Evaluation of concrete self-healing with different insertion techniques of chemical and bacterial solutions", Revista ALCONPAT, 12 (1), pp. 32 – 46, DOI: <https://doi.org/10.21041/ra.v12i1.559>

<sup>1</sup> Itt Performance, Polytechnical school, UNISINOS, São Leopoldo, Brasil

<sup>2</sup> Civil Engineering Undergraduation, Polytechnical school, UNISINOS, São Leopoldo, Brasil

<sup>3</sup> Civil Engineering Graduation, Polytechnical school, UNISINOS, São Leopoldo, Brasil

<sup>4</sup> Department of Civil and Environmental, Universidad de la Costa, Barranquilla Colombia

<sup>5</sup> Architecture Graduation, Polytechnical school, UNISINOS, São Leopoldo, Brasil

#### Contribution of each author

In this work, author Pacheco offered the original idea. Muller and Loeff were responsible for the experimentation. Ehrenbring and Christ did the tests and analysis. Modolo, Tutikian and Oliveira worked with the results interpretation and as reviewers.

#### Creative Commons License

Copyright 2022 by the authors. This work is an Open-Access article published under the terms and conditions of an International Creative Commons Attribution 4.0 International License ([CC BY 4.0](https://creativecommons.org/licenses/by/4.0/)).

#### Discussions and subsequent corrections to the publication

Any dispute, including the replies of the authors, will be published in the third issue of 2022 provided that the information is received before the closing of the second issue of 2022.

## **Análisis de la autorregeneración de matrices cementosas mediante diferentes métodos de inserción de soluciones químicas y bacterianas**

### **RESUMEN**

Este estudio analizó el potencial de curación del hormigón al utilizar soluciones químicas y bacterianas, evaluando diferentes materiales que se pueden utilizar para su encapsulación. Para encapsular los agentes se utilizaron arcilla y perlita expandidas. Para analizar la efectividad de la curación, se realizaron técnicas de análisis visual utilizando un microscopio óptico de alta precisión y microtomografía 3D. Los resultados apuntaron a un mejor desempeño de la mezcla BAC.AE (solución bacteriana encapsulada in arcilla expandida), utilizando solución bacteriana encapsulada en arcilla expandida, que fue capaz de cicatrizar grietas de hasta 0.57mm. Las mezclas BAC.PE (solución bacteriana encapsulada in perlita expandida), solución bacteriana encapsulada en perlita expandida, y SS (silicato de sodio), solución química agregada en el momento de la mezcla para reemplazar el agua, cicatrizaron grietas de 0.16 mm y 0.29 mm respectivamente.

**Palabras clave:** biohormigón; autorregeneración; autocuración; fisuras; bacterias.

## **Análise da autorregeneração de matrizes cimentícias através de diferentes métodos de inserção de soluções químicas e bacterianas**

### **RESUMO**

Este estudo analisou o potencial de cicatrização do concreto quando do uso de soluções bacterianas e soluções químicas, avaliando diferentes materiais que podem ser empregados para seu encapsulamento. Para encapsular os agentes, foram empregadas argila expandida e perlita expandida. Para analisar a eficácia da cicatrização, realizaram-se as técnicas de análise visual através de microscópio óptico de alta precisão e microtomografia 3D. Os resultados apontaram para um melhor desempenho do traço BAC.AE (soluções bacterianas encapsuladas em argila expandida), utilizando solução bacteriana encapsulada em argila expandida, que foi capaz de cicatrizar fissuras de até 0,57mm, tendo os traços BAC.PE (soluções bacterianas encapsuladas em perlita expandida) e SS (silicato de sódio) inserido na moldagem, em substituição à água, cicatrizado fissuras de 0,16 mm e 0,29 mm respectivamente.

**Palavras-chave:** bioconcreto; autorregeneração; autocicatrização; fissuras; bactérias.

### **Legal Information**

Revista ALCONPAT is a quarterly publication by the Asociación Latinoamericana de Control de Calidad, Patología y Recuperación de la Construcción, Internacional, A.C., Km. 6 antigua carretera a Progreso, Mérida, Yucatán, 97310, Tel.5219997385893, [alconpat.int@gmail.com](mailto:alconpat.int@gmail.com), Website: [www.alconpat.org](http://www.alconpat.org)

Reservation of rights for exclusive use No.04-2013-011717330300-203, and ISSN 2007-6835, both granted by the Instituto Nacional de Derecho de Autor. Responsible editor: Pedro Castro Borges, Ph.D. Responsible for the last update of this issue, Informatics Unit ALCONPAT, Elizabeth Sabido Maldonado.

The views of the authors do not necessarily reflect the position of the editor.

The total or partial reproduction of the contents and images of the publication is carried out in accordance with the COPE code and the CC BY 4.0 license of the Revista ALCONPAT.



## 1. INTRODUCTION

Concrete presents several advantages which have resulted in its widespread use (Seifan *et al.*, 2016). However, it is not immune to deterioration which prevents it from achieving desired levels of sustainability without constant repairs and adjustments. Consequently, it is essential to improve concrete durability, especially in third world countries where occurrences of structural faults in construction projects are more common (Chemrouck, 2015).

Concrete durability could be described as its ability to resist deterioration from exposure to different environmental and climatic conditions (Gjorv, 2016) or surface abrasion (Achal *et al.*, 2011). Concrete degradation is primarily caused by the appearance of fissures due to a multitude of factors and the study of self-healing concretes (SHC) represents the current trend to minimize them (Azarsa *et al.*, 2019), as is the case of this study. The core idea of SHC is that it must provide the necessary agents in the cementitious matrix so that fissures will be closed once activation conditions are met. Several innovative techniques have been tested over the past decade (Wu *et al.*, 2012) such as the use of healing agents in hollow fibers, micro-encapsulation (White *et al.*, 2001), insertion of expansive agents and mineral additives (Kishi; Ahn, 2010), shape memory materials (Abdulridha *et al.*, 2012) and bacterial solutions (Krishnapriya *et al.*, 2015).

The addition of bacterial solutions in cementitious matrices has been demonstrated to be a promising and sustainable option (Krishnapriya *et al.*, 2015; Wang *et al.*, 2017; Rais and Khan, 2021). Bacteria are required to resist the high alkalinity of cement and internal compression pressures within the matrix (Li; Herbert, 2012; Stanaszek-Tomal, 2020). The bacterial solution SHC technique relies on the insertion in the matrix of capsules of specific composition containing the bacteria alongside nutrients such as calcium lactate (Jiang *et al.*, 2020). The capsules may remain inactive for decades but, upon rupturing from concrete fissuring and exposure to humidity, become active and produce calcite (Patel, 2015).

Chemical solutions have also been determined to be an effective alternative to seal fissures in concrete (Alghamri *et al.*, 2016). Studies by Huang *et al.* (2011) and Pelletier *et al.* (2011) made use of spherical capsules with a sodium silicate solution. Upon rupture, the chemical agent reacted with calcium hydroxide in concrete to form calcium silicate hydrate (C-S-H), which sealed fissures in concrete.

The application of SHC techniques in real scale is precluded by the complexity of the encapsulating techniques under development. There are currently few studies comparing different encapsulating techniques for both bacterial and chemical solutions for insertion in cementitious matrices. Thus, the purpose of this study was to conduct a comparative analysis of bacteria encapsulated in perlite or expanded clay as well as the direct use of sodium silicate in mixing water.

## 2. FISSURING AND SELF-HEALING IN REINFORCED CONCRETE STRUCTURES

Fissures are pathological phenomena characteristic of concrete structures and denote the occurrence of an abnormal event (Bianchini, 2008). While abnormal, Ferrara *et al.* (2018) noted that preventing the occurrence of fissures in concrete still remains a challenge. Lottermann (2013) noted that some of the more common causes of fissuring are: improper curing, retraction, temperature variation, environmental aggressiveness, loading, error in project design or execution or foundation settling. It should be noted that a combination of simultaneous factors can also lead to fissuring (Gupta; Pang; Kua, 2017). Fissures are classified in accordance to their appearance in the fresh state or after hardening. Due to its effect on durability, limits on fissure opening widths are listed on national and international standards (Carmona Filho; Carmona, 2013). For example, Brazilian standards allow fissures of widths between 0.2 mm and 0.4 mm (ABNT, 2014).

The precursor study to all studies in this area was conducted by Dry (1994 apud Bianchin, 2018), which proposed the use of encapsulated polymers to obtain self-healing concrete. The study also described the phenomena involved in self-healing concrete and possible causes, as well as their intentional use to improve durability.

Since 2005, two technical committees have been created to study self-healing in cementitious materials (Cappellesso, 2018). From these, technical definitions have been agreed on that self-healing concretes were those that achieve sealing of fissures and self-regenerating concretes were those able to recover mechanical properties (Pacheco, 2020). Further classifications were defined if the mechanisms were autogenous or autonomous. Autogenous processes made use of materials already present in concrete which might not necessarily be related to self-healing. In contrast, autonomous processes made use of materials which were not found in cement but were added specifically for this purpose. This study did not include autogenous mechanisms such as the addition of pozzolans in cement.

Self-healing through autonomous mechanisms is based on micro-capsules filled with healing agents or vascular tubes (Van Tittelboom *et al.*, 2011; Wan *et al.*, 2021). Healing agents used are chemical solutions, bacterial solutions, superabsorbent polymers (SAP), permeability-reducing agents, expansive agents etc. The capsules themselves can be made from porous materials, light aggregate or others. Mila *et al.* (2019) stated that encapsulation allows for a distribution of healing agents throughout the matrix.

Chemical encapsulation consists of impregnating light and porous aggregates with a chemical solution (Alghamri; Kanellopoulos; Al-Tabbaa, 2016). Souradeep and Kua (2016) explained that the encapsulating technique could also increase the service life of chemical or biological curing agents, which resulted in higher durability and recovery of concrete. Amongst the chemical solutions, sodium silicate has been frequently used (Manoj-Prabakar *et al.*, 2017).

Bacterial healing is based in the production of calcite ( $\text{CaCO}_3$ ) (Xu *et al.*, 2020). Calcite itself is environmentally innocuous when compared to synthetic polymers currently used to repair concrete. Some of the production techniques used are calcium carbonate precipitation from bacterial hydrolysis of urea (Elzébio; Alves; Fernandes, 2017) as well as incorporation of bacterial spores or organic compounds within the concrete (Schwantes-Cezario *et al.*, 2017). However, high alkali pH in concrete could affect bacteria and cell walls might be broken down during concrete hydration. Consequently, encapsulation became a necessary protection for this technique (Jonkers; Thijssen, 2010).

### 3. MATERIALS AND METHODS

Table 1 shows the formulations and mix ratios used in this study. The reference formulation REF is based on Schwantes-Cezario *et al.* (2019).

Table 1. Formulations and mix ratios

Formulation	Cement	Sand	Perlite	w/c	Healing agent
REF	1.00	1.00	-	0.36	-
BAC.EP	1.00	0.7	0.064	0.36	<i>B.subtilis</i>
BAC.EC	1.00	0.7	0.147	0.36	<i>B.subtilis</i>
SS	1.00	1.00	-	0.18	sodium silicate

Formulations BAC.EC and BAC.EP replaced 30% of sand mass with a corresponding volume of expanded clay (EC) or expanded perlite (EP), respectively. Formulation SS included a poly-

carboxylate superplasticizer additive to increase fluidity at the proportion of 0.89% with respect to the mass of cement. Each formulation was evaluated with compression tests, flexural bending tests (to induce fissuring), visual analysis and 3-D microtomography for void space characterization.

### 3.1 Materials

Cement used in this study was Portland CP II-F-40 with filler and no pozzolanic additives. Sand was river quartz with density of 1,592.2 kg/m<sup>3</sup> and specific mass of 2,427.4 kg/m<sup>3</sup>. Sand granulometry results are shown in Figure 1 and were obtained following the procedures of standard NBR NM 248 (ABNT, 2003).

The chemical solution used was neutral sodium silicate (Na<sub>2</sub>SiO<sub>3</sub>) in liquid form, diluted in 50% of deionized water. It was selected due to its high compatibility with cementitious matrices. Due to the water present in the chemical solution, the water content (w/c) of the SS formulation was halved with respect to the others.

The bacterial solution contained an experimental *Bacillus subtilis* AP 91 strain provided by the Campinas campus of EMBRAPA (Empresa Brasileira de Pesquisa Agropecuária). Preparation and growth curve data were presented by Pacheco (2020). A sterile buffer solution of 1.06 g/L sodium phosphate (dibasic anhydrous), 0.36 g/L sodium phosphate (monobasic) and 8.17 g/L sodium chloride in deionized water was used to dilute bacteria for later encapsulation and insertion in the matrix.

Expanded perlite (EP) was provided by Pervale Minerais with granulometry between 2 mm and 4 mm, previously sifted to ensure particle size. Densities of the natural raw material and perlite impregnated with bacterial solution and covered in cement were measured as 128.43 kg/m<sup>3</sup> and 328.52 kg/m<sup>3</sup>, respectively. Perlite granulometry was conducted in accordance with the procedures of standard NBR NM 248 (ABNT, 2003) and the results shown in Figure 2.

Expanded clay (EC) was of type 0500 acquired from Global Minérios with granulometry between 2 mm and 4 mm. Clay granulometry was conducted in accordance with the procedures of standards NBR NM 45 (ABNT, 2006) and NBR NM 248 (ABNT, 2003) and the results shown in Figure 3. Densities of the natural raw material and clay impregnated with bacterial solution and covered in cement were measured as 930.39 kg/m<sup>3</sup> and 1,395.48 kg/m<sup>3</sup>, respectively.

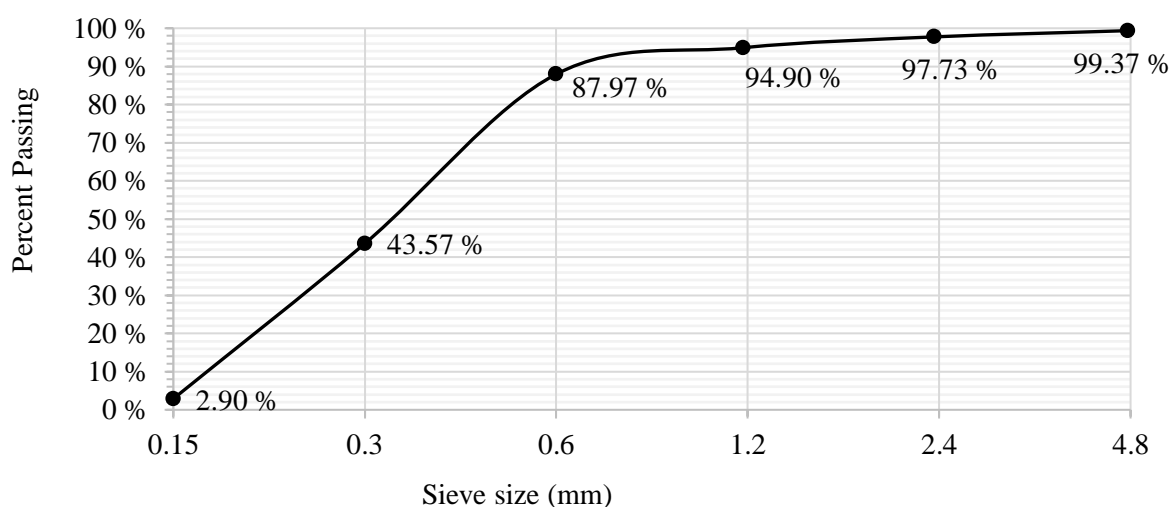


Figure 1. Granulometric distribution of river sand used in this study.

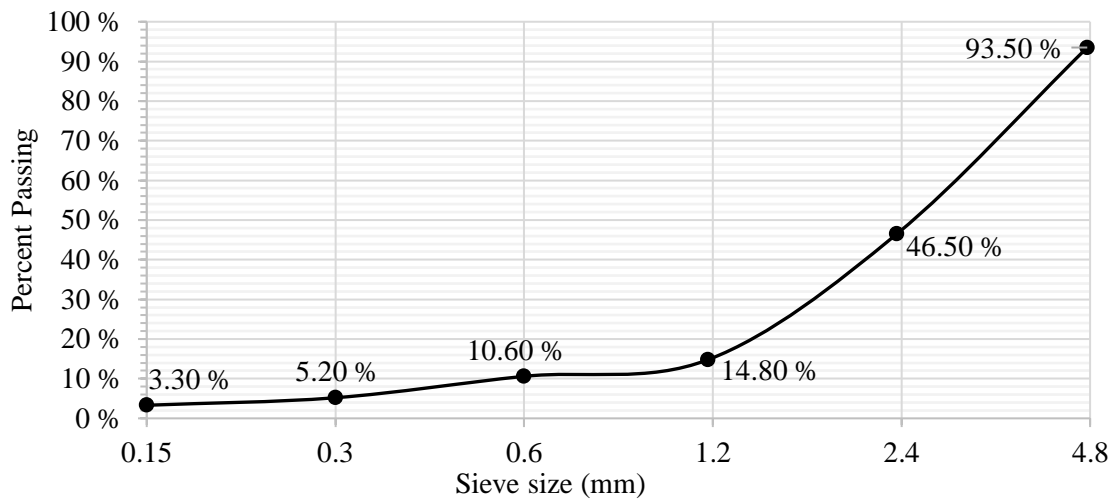


Figure 2. Granulometric distribution of expanded perlite used in this study.

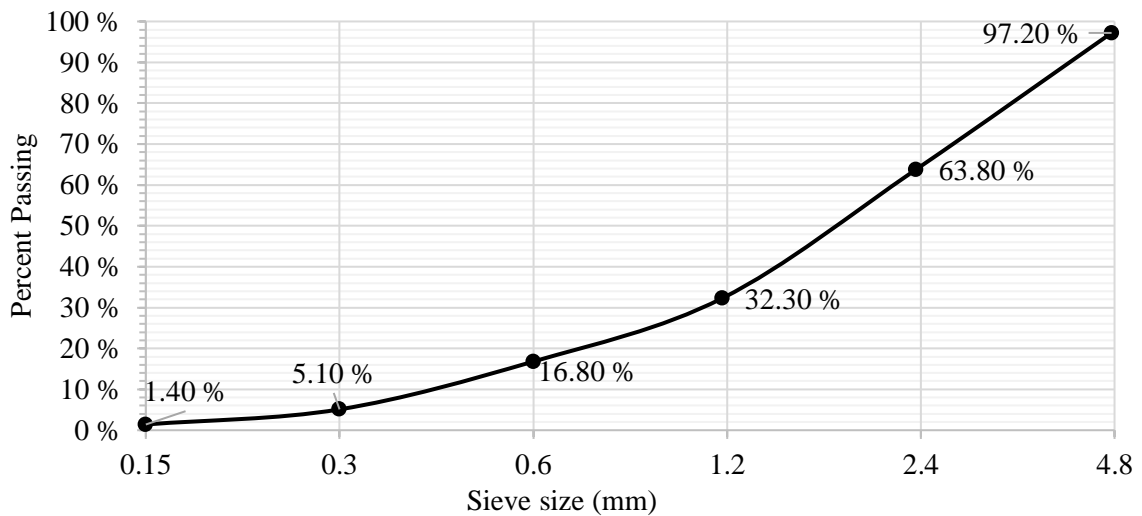


Figure 3. Granulometric distribution of expanded clay used in this study.

Chemical composition of expanded clay and expanded perlite are shown in Table 2.

Table 2. Chemical composition of light aggregates used in encapsulation

Element	EC		EP	
	Mass %	Atomic %	Mass %	Atomic %
O	42.80	58.92	43.05	57.65
Na	0.43	0.41	2.27	2.12
Mg	1.78	1.61	0.00	0.00
Al	10.23	8.35	7.18	5.70
Si	30.87	24.22	40.70	31.04
K	4.48	2.52	4.76	2.61
Ca	1.16	0.64	0.62	0.33
Ti	1.15	0.53	0.00	0.00
Fe	7.10	2.80	1.41	0.54
Total	100.00		100.00	

### 3.2 Methods

A total of 27 cylindrical test bodies (50 mm x 100 mm) and 9 prismatic test bodies (60 mm x 60 mm x 180 mm) were manufactured in accordance with standard NBR 5738 (ABNT, 2015). An additional 3 cylindrical test bodies measuring 8 mm x 30 mm were also manufactured. The prismatic test bodies were reinforced with a rebar of steel CA 60 with 5 mm of diameter placed 2 cm from the base to prevent inadvertent rupturing. After demolding, all samples were cured in a humidity and temperature-controlled chamber in accordance with the procedures of standard NBR 5738 until each testing age of 7 days, 14 days and 35 days were reached (ABNT, 2015).

#### 3.2.1 Bacterial solution encapsulation

Encapsulating material was soaked in bacterial solution and saturated in a vacuum desiccator as performed by Alghamri *et al.* (2016) and Sisomphon; Copuroglu and Fraaij (2011). Calcium lactate nutrient was also applied alongside the bacterial solution. After impregnation, both EP and EC were dried in a kiln for 48 h at 45 °C as performed by Zhang *et al.* (2017). A protection cover consisting of layers of cement was applied to the aggregates. This experimental procedure was described in more detail by Pacheco (2020).

#### 3.2.2 Testing

Compression strength tests were conducted in accordance with standard NBR 5739 (ABNT, 2018). Fissures were induced in prismatic samples with 3-point flexural bending tests in accordance with standard NBR 13279 (ABNT, 2005). Visual analyses of self-healing were conducted at initial age, 7 days, 14 days and 35 days. A 3-D microtomography test was conducted to determine void space distribution within the material. This test made use of the 3 cylindrical 8 mm x 30 mm test bodies, one for each formulation.

## 4. RESULTS AND ANALYSIS

### 4.1 Compressive strength

Compressive strength results are shown in Figure 4. Overall, compression strength levels were similar over time within each formulation, likely due to the type of cement having high strength at initial ages. The largest change in strength over time occurred for formulations SS, which varied 4.7 MPa (11.63%) between 13 days and 35 days. This was likely the result of C-S-H being produced within the matrix since its activation did not depend on fissuring (Giannaros *et al.*, 2016). However, there were significant differences in strength between formulations. Formulation BAC.EC presented the highest strength, 12.7 MPa more than the other formulations at 35 days. This was probably a result of perlite having lower density than clay but both materials being added with similar granulometries.

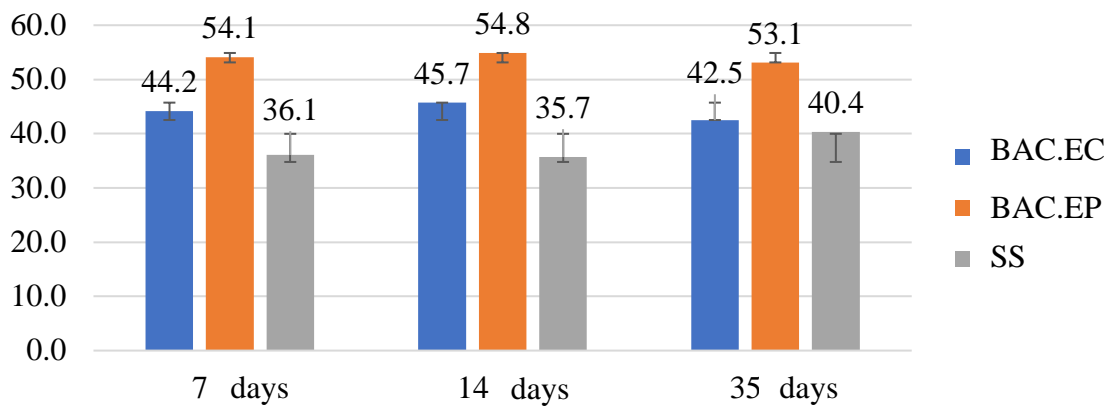


Figure 4. Average compression strength (MPa) of the formulations of this study.

The formulations of Schwantes-Cezario *et al.* (2017) used as basis for this study reached compression strengths of around 65 MPa. However, the light aggregates used in this study resulted in lower strengths as predicted by Jonkers (2011). As for SS, which lacked light aggregates, the lower strength was attributed to incomplete cement hydration due to the decrease in w/c ratio of the mixture.

#### 4.2 Surface visual analysis

Selected surface visual analyses of formulation BAC.EP are shown in Figure 5. Healing products were observed in secondary fissures and in surface deposits. Visual analysis indicated that fissure opening limited healing as no healing products were observed in the main fissures of Figure 5. This was in agreement with other studies which observed healing only in narrower fissures (Zhang *et al.*, 2016; Jiang *et al.*, 2020). Visual analysis also noted that healing occurred in plaques, attributed to the presence of calcite produced from bacterial solutions (Schwantes-Cezario *et al.*, 2018; Alghamri *et al.*, 2016).

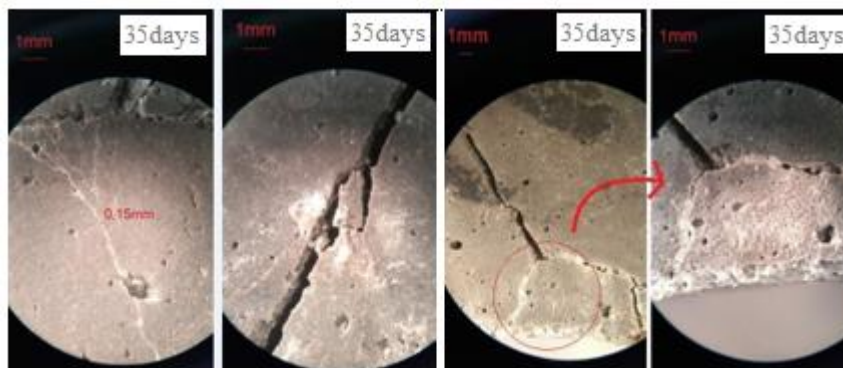


Figure 5. Sel-healing in formulation BAC.EP – Sample 1.

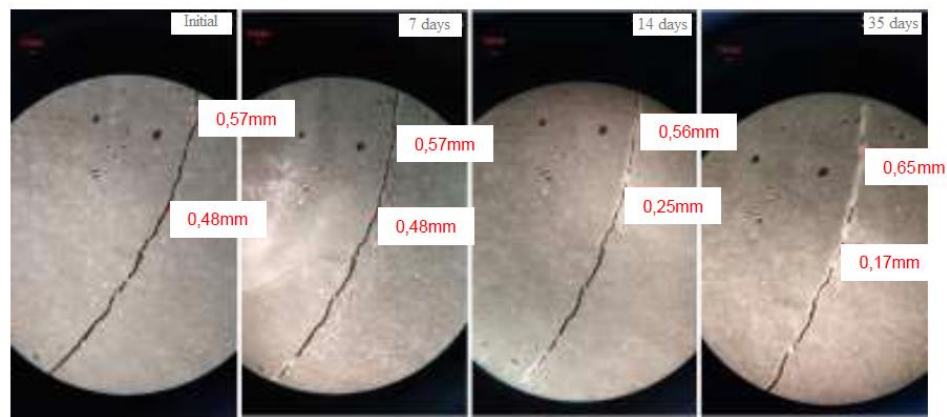


Figure 6. Self-healing in formulation BAC.EC – Sample 2.

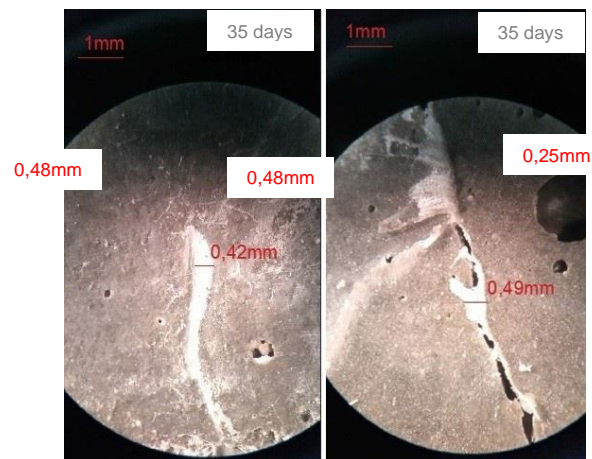


Figure 7. Self-healing in formulation BAC.EC – Samples 3 and 1.

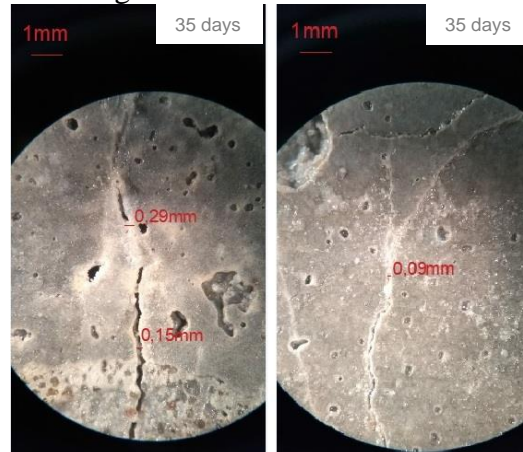


Figure 8. Self-healing in formulation SS – Samples 1 and 2.

Results for formulation BAC.EC are shown in Figure 6 with healing products forming inside the fissures. Healing was observed at several spots along the fissure and the larger fissure of 0.57 mm was completely sealed. Progressive healing was also observed with the fissure initially at 0.48 mm reducing to 0.17 mm at the final age. These results were in accordance with Zhang *et al.* (2017). The non-uniform product distribution along the fissure was likely related to the availability of perlite at the fissure location to form calcite, as noted by Alghamri *et al.* (2016). Further results for formulation BAC.EC are shown in Figure 7 with initial fissures of 0.42 mm and 0.49 mm. Healing products were formed in excess thickness than the initial opening, which were

indicative of surface deposition. This result was also attributed to the presence of calcite and similar visual results were observed by Rais and Khan (2021).

Results of formulation SS are shown in Figure 8 with fissures of 0.29 mm and 0.09 mm. Healing occurred in the form of local plaques in both samples, which were visible after 14 days. This was attributed to the presence of surface pores collecting water, which created favorable conditions to induce self-healing. The 0.29 mm fissure was also the maximum width healed for Sample 1 of formulation SS.

Overall, self-healing was observed to occur in all formulations spot-wise. This was believed to be a result of capsule dispersion inside the internal structure of the test bodies. In the case of formulation SS, a less than ideal dispersion of sodium silicate might have occurred, which was also noted by Van Tittelboom and de Belie (2013), even knowing that microtomography shows uniform dispersion. Healing was also observed to start on the fissure walls and gradually grow outwards, which was in agreement with Al-Tabbaa *et al.* (2019).

In comparison with other studies, Zhang *et al.* (2017) was able to recover fissures with openings of 0.79 mm after 28 days of curing. This difference in healing potential was likely due to the use of a *Bacillus cohnii* strain of bacteria encapsulated in perlite and coated with a geo-polymer. Jiang *et al.* (2020) also made use of *Bacillus cohnii* encapsulated in expanded perlite and observed healing of fissures of up to 0.4 mm, which were closer to the results of this study. Similarly, Liu *et al.* (2021) reported healing fissures of up to 0.25 mm.

As observed in this study, Van Tittelboom and de Belie (2013) denoted that there was no linear proportionality in fissure healing. This behavior was directly related to the availability of healing agents. Naturally, locations lacking healing agents did not generate sufficient products to close the fissure. The maximum healed fissure widths of each formulation of this study are shown in Table 3.

Table 3. Self-healing results of this study.

Formulation	Sample	Maximum healed fissure width
BAC.EP	1	0.16 mm
	2	0.14 mm
	3	0.12 mm
BAC.EC	1	0.38 mm
	2	0.57 mm
	3	0.42 mm
SS	1	0.29 mm
	2	0.22 mm
	3	No healing occurred

Table 3 shows that formulation BAC.EC was able to heal fissures much wider than the other formulations. Namely, the maximum healed fissure for BAC.EC was 0.57 mm while BAC.EP and SS were only able to heal fissures of 0.16 mm and 0.29 mm, respectively. Therefore, it was concluded that formulation BAC.EC was the most efficient of this study both from the quantity and width of fissures healed.

#### 4.3 3-D Microtomography

The 3-D Microtomography analysis was conducted at itt Fuse (Instituto Tecnológico em Ensaios e Segurança Funcional) at the Unisinos campus. Figure 9 shows results for formulation BAC.EP. In the images, EP appeared as bright yellow zones and presented a regular distribution throughout the test body with only a few concentration points. This distribution was favorable to healing since it ensured a higher probability that a fissure would rupture a capsule and release healing agent. Void



spaces were determined as 11.45% in volume of the test body, which reinforced the compression strength results as porous materials tend to have lower resistance (Yang; Jiang, 2003).

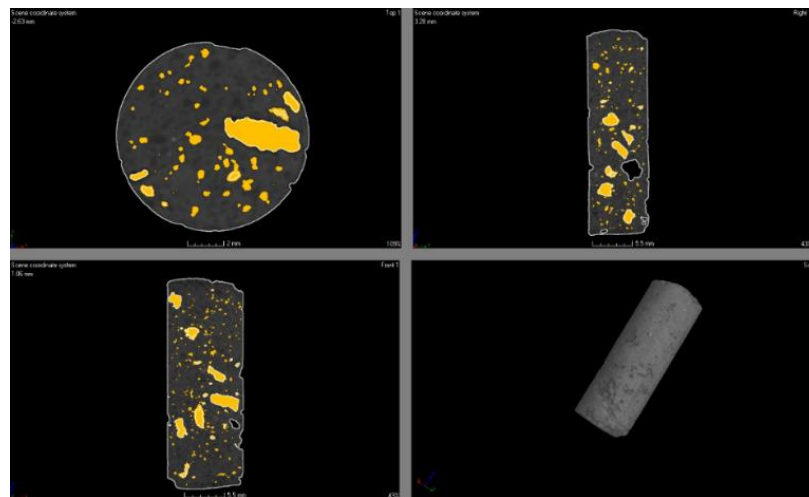


Figure 9. 3-D Microtomography results of formulation BAC.EP.

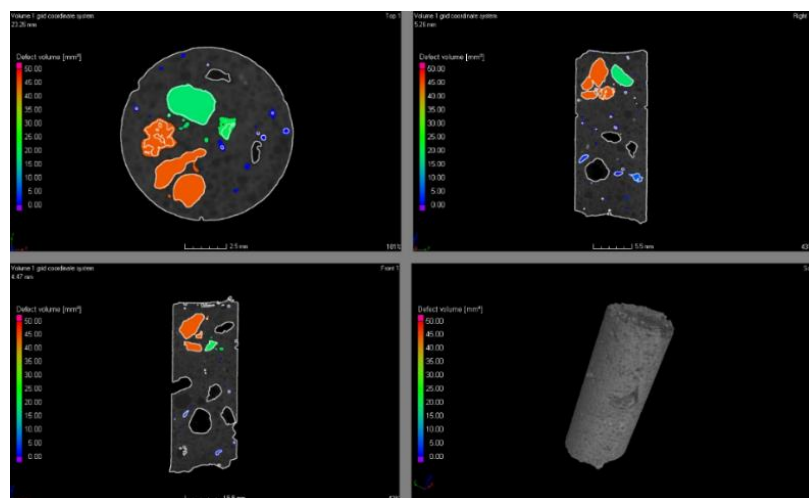


Figure 10. 3-D Microtomography results of formulation BAC.EC.

Figure 10 shows that formulation BAC.EC had an unfavorable internal distribution of expanded clay, seen as different bright colorations in the images, which could also have affected the distribution of healing agent. Void spaces in the test body were determined as 8.38% in volume, which could explain the higher compression resistance obtained for this formulation.

Figure 11 shows results for formulation SS. The images show an adequate distribution of healing agent throughout the test body, which should allow the formation of healing products throughout the sample. The void spaces were determined as 2.28% of the volume. It should be noted that since formulation SS did not contain light aggregates, the void spaces detected were attributed to compacting faults, transition zones and void spaces of the raw materials.

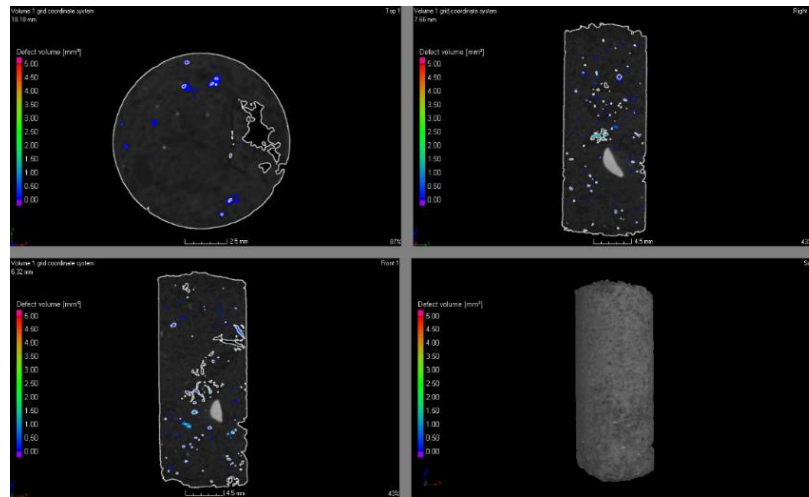


Figure 11. 3-D Microtomography results of formulation SS.

Regarding void spaces, formulations with EC and EP presented much higher values. In the case of EP, this remained even after the porous structure was impregnated with bacterial solution which was easily identifiable in the images. In the case of SS, the higher compaction resulted in lower void spaces and no deleterious effects were noted in the direct incorporation of SS in the matrix. Zhang *et al.* (2021) noted that capsule and void space distributions affect healing since they affect the distribution of healing agent. Although this effect is acknowledged, no relation was noted between the void space value and maximum healing obtained in this study. This result pointed out to a need to evaluate the distribution of capillary pores rather than their quantification in proportion to total volume. Maddalena, Taha and Garder (2021) evaluated the pores of self-healing concretes. It was noted that, just as healing occurred in the fissure, products could also form in the void spaces of the material. This raised the need of further porosity analyses to determine if concrete microstructure could improve over time but at a cost to healing product distribution.

## 5. CONCLUSIONS

Compressive strength results determined that formulation BAC.EC had the best performance with 53.1 MPa at 35 days, compared to 42.5 MPa and 40.4 MPa for formulations BAC.EP and SS, respectively. Formulation BAC.EC also presented the highest healing potential in visual analysis with a healed maximum fissure width of 0.57 mm. In comparison, formulations BAC.EP and SS healed maximum fissure widths of 0.16 mm and 0.29 mm, respectively. Healing products formed inside the fissure walls, especially for formulation SS. Fissure healing occurred spot-wise instead of uniformly along the length of the fissure.

A 3-D microtomography analysis determined that all materials in the formulations were well-dispersed in their respective cementitious matrices, but it may be different on the samples where continuous healing were not observed.

Overall, formulation BAC.EC was considered the most efficient. However, in terms of large scale production and application, formulation SS offered some benefits since it did not require capsule impregnation in order to be applied to concrete production.

## 6. ACKNOWLEDGEMENTS

The authors would like to acknowledge it Performance for their support in this study.

## 7. REFERENCES

- Associação Brasileira de Normas Técnicas (2005), *NBR 13279: Argamassa para assentamento e revestimento de paredes e tetos - Determinação da resistência à tração na flexão e à compressão*. Rio de Janeiro.
- Associação Brasileira de Normas Técnicas (2015), *NBR 5738: Concreto - Procedimento para moldagem e cura de corpos de prova*. Rio de Janeiro.
- Associação Brasileira de Normas Técnicas (2018), *NBR 5739: Concreto - Ensaio de compressão de corpos de prova cilíndricos*. Rio de Janeiro.
- Associação Brasileira de Normas Técnicas (2014), *NBR 6118: Projeto de estruturas de concreto – Procedimento*. Rio de Janeiro.
- Associação Brasileira de Normas Técnicas (2003), *NBR NM 248: Agregados - Determinação da composição granulométrica*. Rio de Janeiro.
- Associação Brasileira de Normas Técnicas (2006), *NBR NM 45: Agregados - Determinação da massa unitária e do volume de vazios*. Rio de Janeiro.
- Associação Brasileira de Normas Técnicas (2005), *NBR NM 52: Agregado miúdo - Determinação de massa específica e massa específica aparente*. Rio de Janeiro.
- Achal, V., Mukherjee, A., Reddy, M. S. (2011), *Effect of calcifying bacteria on permeation properties of concrete structures*. Journal of Industrial Microbiology and Biotechnology. 38:1229-1234, <http://dx.doi.org/10.1007/s10295-010-0901-8>
- Al-Tabbaa, A., Litina, C., Giannaros, P., Kanellopoulos, A., Souza, L. (2019), *First UK field application and performance of microcapsule-based self-healing concrete*. Construction and Building Materials. 208:669-685, <https://doi.org/10.1016/j.conbuildmat.2019.02.178>
- Alghamri, R., Kanellopoulos, A., Al-Tabbaa, A. (2016), *Impregnation and encapsulation of lightweight aggregates for self-healing concrete*. Construction and Building Materials. 124:910-921, <https://doi.org/10.1016/j.conbuildmat.2016.07.143>
- Carmona Filho, A., Carmona, T. (2013), “*Fissuração nas estruturas de concreto*”. Boletim Técnico ALCONPAT Internacional.
- Cappellesso, V. G. (2018), “*Avaliação da autocatrização de fissuras em concretos com diferentes cimentos*”, Dissertação de Mestrado em Engenharia, Universidade Federal do Rio Grande do Sul, Porto Alegre.
- Chemrouk, M. (2015), *The deteriorations of reinforced concrete and the option of high performances reinforced concrete*. Procedia Engineering. 125:713-724, <https://doi.org/10.1016/j.proeng.2015.11.112>
- Gupta, S., Pang, S. D., Kua, H. W. (2017), *Autonomous healing in concrete by bio-based healing agents – A review*. Construction and Building Materials. 146:419-428, <https://doi.org/10.1016/j.conbuildmat.2017.04.111>
- JIANG, L. et al. *Sugar-coated expanded perlite as a bacterial carrier for crack-healing concrete applications*. Construction and Building Materials, v. 232, p. 117222, 2020, <https://doi.org/10.1016/j.conbuildmat.2019.117222>
- Jonkers, H. M. (2011), *Bacteria-based self-healing concrete*. Frankfurter Afrikanistische Blätter. 8:49-79.
- Jonkers, H. M., Thijssen, A. (2010). “*Bacteria Mediated Remediation of Concrete Structures*” in: K. van Breugel, G. Ye, Y. Yuan (Eds.), 2nd International Symposium on Service Life Design for Infrastructure, [S. l.], pp. 833-840.
- Krishnapriya, S., Babu, D. L. V., Arulraj, G. P. (2015), *Isolation and identification of 60 bacteria to improve the strength of concrete*. Microbiological Research. 174:48-55, <https://doi.org/10.1016/j.micres.2015.03.009>

- Li, V. C., Herbert, E. (2012), *Robust Self-Healing Concrete for Sustainable Infrastructure*. Journal of Advanced Concrete Technology. 10:207-218, <https://doi.org/10.3151/jact.10.207>
- LIU, C et al. (2021), *Experimental and analytical study on the flexural rigidity of microbial self-healing concrete based on recycled coarse aggregate (RCA)*. Construction and Building Materials, Vol 85, <https://doi.org/10.1016/j.conbuildmat.2021.122941>
- Lottermann, A. F. (2013), “*Patologias em estruturas de concreto: estudo de caso*”, Monografia, Universidade Regional do Noroeste do Estado do Rio Grande do Sul, p. 66.
- Maddalena, R., Taha, H., Gardner, D. (2021), *Self-healing potential of supplementary cementitious materials in cement mortars: sorptivity and pore structure*. Developments in the built environment, Vol 6, <https://doi.org/10.1016/j.dibe.2021.100044>
- Mehta, P. K., Monteiro, P. J. (2014), “*Concreto: microestrutura, propriedades e materiais*”. IBRACON, São Paulo, Brasil, p. 782.
- Milla, J. et al. (2019), *Measuring the crack-repair efficiency of steel fiber reinforced concrete beams with microencapsulated calcium nitrate*. Construction and Building Materials, v. 201, p. 526–538, <https://doi.org/10.1016/j.conbuildmat.2018.12.193>
- Pacheco, F. (2020), “*Análise da confiabilidade dos mecanismos de autorregeneração do concreto em ambientes agressivos de exposição*”, Tese de Doutorado em Engenharia Civil, Universidade do Vale do Rio dos Sinos, p. 348.
- Patel, P. (2015), *Helping Concrete Heal Itself*. ACS Central Science. 1(9):470-472.
- Pelletier, M. M., Brown, R., Sshukla, A., Bose, A. (2011), *Selfhealing concrete with a microencapsulated healing agent*. University of Rhode Island, Kingston, RI, USA.
- Rais, M. S., Khan, R. A. (2021), *Experimental investigation on the strength and durability properties of bacterial self-healing recycled aggregate concrete with mineral admixtures*. Construction and Building Materials. Vol 306, Nov 2021, <https://doi.org/10.1016/j.conbuildmat.2021.124901>
- Ramachandran, S. K., Ramakrishnan, V., Bang, S. S. (2001), *Remediation of concrete using microorganisms*, ACI Mater. J. 98(1).
- Schwantes-Cezario, N., Nogueira, G. S. F., Toralles, B. M. (2017), *Biocimentação de compósitos cimentícios mediante adição de esporos de B. subtilis AP91*. Revista de Engenharia Civil IMED. 4(2):142-158, <https://doi.org/10.18256/2358-6508.2017.v4i2.2072>
- Seifan, M., Samani, A. K. and Berenjian, A. (2016), *Bioconcrete: next generation of selfhealing concrete*, Applied Microbiology and Biotechnology. 100:2591-2602, <https://doi.org/10.1007/s00253-016-7316-z>
- Sisomphon, K., Copuroglu, O., Fraaij, A. (2011), *Application of encapsulated lightweight aggregate impregnated with sodium monofluorophosphate as a selfhealing agent in blast furnace slag mortar*. Heron. 56(1-2):17-36.
- Souradeep, G., Kua, H. W. (2016), *Encapsulation Technology and Techniques in Self-Healing Concrete*. Journal of Materials in Civil Engineering. 25:864-870, [https://doi.org/10.1061/\(ASCE\)MT.1943-5533.0001687](https://doi.org/10.1061/(ASCE)MT.1943-5533.0001687)
- Stanaszek-Tomal, E. (2020), *Bacterial Concrete as a Sustainable Building Material?* 2020. Sustainability, 12, 696; <http://doi:10.3390/su12020696>
- Tittelboom, K. V., De Belie, N. (2013), *Self-Healing in Cementitious Materials - A Review*. Materials. 6:2182-2217. <https://doi.org/10.3390/ma6062182>
- Van Breugel, K. (2007). “*Is there a market for self-healing cement-based materials?*” in: First International Conference on Self Healing Materials, Noordwijk aan Zee (Netherlands), pp. 1-9.
- Xu et al. (2020), *Application of ureolysis-based microbial CaCO<sub>3</sub> precipitation in self-healing of concrete and inhibition of reinforcement corrosion*. Construction and Building Materials, Vol 265, <https://doi.org/10.1016/j.conbuildmat.2020.120364>

- Wan, P, et al. (2021), *Self-healing properties of asphalt concrete containing responsive calcium alginate/nano-Fe<sub>3</sub>O<sub>4</sub> composite capsules via microwave irradiation*. Construction and Building Materials, Vol 310, <https://doi.org/10.1016/j.conbuildmat.2021.125258>
- Wang, J., Dewanckele, J., Cnudde, V., Vlierbergue, S. V., Verstraete, W., De Belie, N. (2014), *X-ray computed tomography proof of bacterial-based self-healing in concrete*. Cement and Concrete Composites. 53:289-304, <https://doi.org/10.1016/j.cemconcomp.2014.07.014>
- Wang, J. et al. (2017), *Bacillus sphaericus LMG 22257 is physiologically suitable for self-healing concrete*. Applied Microbiology and Biotechnology, v. 101, n. 12, p. 5101–5114, <https://doi.org/10.1007/s00253-017-8260-2>
- Yang, J., Jiang, G. (2003), *Experimental study on properties of pervious concrete pavement materials*, Cement and Concrete Research. 33:381-386, [https://doi.org/10.1016/S0008-8846\(02\)00966-3](https://doi.org/10.1016/S0008-8846(02)00966-3)
- Zhang, X et al. (2021), *Effects of carrier on the performance of bacteria-based self-healing concrete*. Construction and Building Materials, Vol 305, <https://doi.org/10.1016/j.conbuildmat.2021.124771>

## Service life prediction for concrete structures based on carbonation front depth models

R. Costa<sup>1\*</sup> , A. Franchetto<sup>1</sup> , A. Gouveia<sup>1</sup> , F. Ziegler<sup>1</sup> , K. Pessoa<sup>1</sup> , M. Garcez<sup>1</sup> 

\*Contact author: [rayarapintocosta@gmail.com](mailto:rayarapintocosta@gmail.com)

DOI: <https://doi.org/10.21041/ra.v12i1.558>

Reception: 14/09/2021 | Acceptance: 02/12/2021 | Publication: 01/01/2022

### ABSTRACT

This paper seeks to evaluate the variability in predicting the service life of concrete structures through four models that estimate the natural advance of the carbonation front. The results show that there is variability in the estimated carbonation front. The models by Possan (2010) and Ekolu (2018) show estimated values close to measured ones, while Ho and Lewis (1987) and Bob and Affana (1993) tend to underestimate and overestimate the natural carbonation front, respectively. Only concretes without added supplementary cementitious materials were considered, due to model limitations. Compressive strength, CO<sub>2</sub> concentration and relative humidity have significant influence on the results and the variability depends on which parameters are considered in the models.

**Keywords:** carbonatation; service life prediction; carbonatation depth; concrete durability.

**Cite as:** Costa, R., Franchetto, A., Gouveia, A., Ziegler, F., Pessoa, K., Garcez, M. (2022), "Service life prediction for concrete structures based on carbonation front depth models", Revista ALCONPAT, 12 (1), pp. 47 – 60, DOI: <https://doi.org/10.21041/ra.v12i1.558>

<sup>1</sup> Pos Graduation Program in Civil Engineering: Construction and Infrastructure (PPGCI), Engineering School, Federal University of Rio Grande do Sul, Porto Alegre, Brazil.

#### Contribution of each author

In this work, the authors A. Franchetto; A. Gouveia; F. Ziegler; R. Costa; K. Pessoa; M. Garcez contributed to the conception of the idea and methodology of the study with 16.66% each. A. Franchetto; A. Gouveia; F. Ziegler; R. Costa; K. Pessoa participated in the research and formal analysis of the results with 20% each. A. Franchetto; A. Gouveia; F. Ziegler; R. Costa; K. Pessoa; M. Garcez provided contributions to the manuscript in the discussion of the results with 16.66% each.

#### Creative Commons License

Copyright 2022 by the authors. This work is an Open-Access article published under the terms and conditions of an International Creative Commons Attribution 4.0 International License ([CC BY 4.0](https://creativecommons.org/licenses/by/4.0/)).

#### Discussions and subsequent corrections to the publication

Any dispute, including the replies of the authors, will be published in the third issue of 2022 provided that the information is received before the closing of the second issue of 2022.

## **Predicción de la vida útil de estructuras de hormigón a partir de modelos que estiman el avance del frente de carbonatación**

### **RESUMEN**

Este artículo evalúa la variabilidad en la previsión de la vida útil de estructuras de hormigón a través de cuatro modelos que estiman el avance natural del frente de carbonatación. Los resultados muestran que hay variabilidad en el frente de carbonatación estimado. Los modelos Possan (2010) y Ekolu (2018) presentan valores estimados cercanos a los medidos, mientras que Ho y Lewis (1987) y Bob y Affana (1993) subestiman y sobreestiman el frente de carbonatación natural. Sólo se consideraron los hormigones sin adición de materiales cementantes suplementarios, debido a las limitaciones del modelo. La resistencia a compresión, concentración de CO<sub>2</sub> y humedad relativa tienen influencia significativa en los resultados y la variabilidad depende de los parámetros que se consideren en los modelos.

**Palabras clave:** carbonatación; predicción de vida útil; profundidad de carbonatación; durabilidad del hormigón.

## **Previsão da vida útil de estruturas de concreto com base em modelos para avanço da frente de carbonatação**

### **RESUMO**

Este artigo busca avaliar a variabilidade na previsão da vida útil de estruturas de concreto através de quatro modelos que estimam o avanço natural da frente de carbonatação. Os resultados mostram que há variabilidade na frente de carbonatação estimada. Os modelos de Possan (2010) e Ekolu (2018) apresentam valores estimados próximos aos medidos, enquanto Ho e Lewis (1987) e Bob e Affana (1993) tendem, respectivamente, a subestimar e superestimar a frente natural de carbonatação. Somente concretos sem adição de materiais cimentícios suplementares foram considerados, por limitações dos modelos. A resistência à compressão, concentração de CO<sub>2</sub> e umidade relativa do ar têm influência significativa nos resultados e a variabilidade depende de quais parâmetros são considerados nos modelos.

**Palavras-chave:** carbonatação; previsão de vida útil; frente de carbonatação; durabilidade do concreto.

### **Legal Information**

Revista ALCONPAT is a quarterly publication by the Asociación Latinoamericana de Control de Calidad, Patología y Recuperación de la Construcción, Internacional, A.C., Km. 6 antigua carretera a Progreso, Mérida, Yucatán, 97310, Tel.5219997385893, [alconpat.int@gmail.com](mailto:alconpat.int@gmail.com), Website: [www.alconpat.org](http://www.alconpat.org)

Reservation of rights for exclusive use No.04-2013-011717330300-203, and ISSN 2007-6835, both granted by the Instituto Nacional de Derecho de Autor. Responsible editor: Pedro Castro Borges, Ph.D. Responsible for the last update of this issue, Informatics Unit ALCONPAT, Elizabeth Sabido Maldonado.

The views of the authors do not necessarily reflect the position of the editor.

The total or partial reproduction of the contents and images of the publication is carried out in accordance with the COPE code and the CC BY 4.0 license of the Revista ALCONPAT.

## 1. INTRODUCTION

Carbonation is a phenomenon generated by the interaction between the concrete and the environment through the reaction of carbon dioxide ( $\text{CO}_2$ ) from the air with calcium hydroxide ( $\text{Ca}(\text{OH})_2$ ), a cement hydration product. The reaction provides high alkalinity in the concrete interstitial solution, forming calcium carbonate ( $\text{CaCO}_3$ ). The hydrated Portland cement of concrete has an alkaline pH (12-13), mainly due to  $\text{Ca}(\text{OH})_2$ . However, the formation of  $\text{CaCO}_3$  leads to a pH reduction that can reach 9.4 and the consequent  $\text{CaCO}_3$  precipitation to the concrete surface. The cement matrix acidification causes steel reinforcement depassivation, making it susceptible to corrosion, the primary pathological manifestation in reinforced concrete structures (PETER *et. al.*, 2008; CHEN, 2019).

The main factors that affect carbonation are temperature, relative humidity (RH),  $\text{CO}_2$  concentration, surface coating, water/cement ratio, cement type, cement and water content, curing conditions, cement matrix degree of hydration, concrete permeability, and pore network (Ribeiro *et. al.*, 2018; Li *et. al.*, 2018; Song; Kwon, 2007; Houst; Wittmann, 2002). The carbonation occurrence is low at early ages (up to 28 days, generally). However, with more prolonged  $\text{CO}_2$ -saturated environment exposure, the carbonation process becomes more evident in the concrete structure (RIBEIRO *et. al.*, 2018).

According to *NBR 15575-1: Edificações habitacionais – Desempenho Parte 1* (translation: NBR 15575-1: Residential Buildings — Performance Part 1) (ABNT, 2013), Service Life (SL) is the period in which a building and/or its systems provide the activities for which they were designed and built, meeting the performance levels established in this standard. Determining the service life of a carbonated concrete structure encompasses carbonation depth measurements and the use of mathematical models to determine the carbonation front speed affecting the structure (Possan, 2010).

The models to estimate the carbonation depth assume that the concrete is homogeneous, which does not occur in real structures since concrete consistency depends on the compaction and curing time and the relative humidity (RH) conditions of the environment. However, this assumption ensures that the properties determining the carbonation rate are similar at all concrete depths, simplifying model assumptions (Köliö *et. al.*, 2014).

Due to the various factors discussed in the previous paragraphs, no model faithfully represents concrete carbonation. Therefore, choosing which model better represents a specific concrete structure depends on its characteristics and the variables considered in the model.

Thus, this paper analyzes the variability in SL predictions through four models that estimate the concrete carbonation depth based on a database of tests performed under natural aging and exposure conditions found in the literature. A sensibility analysis was performed to identify the parameters that most influence the variations found between the values estimated by the models and those obtained experimentally.

The primary purpose of this study is to contribute to the technical-scientific community on the subject of pathological manifestations, especially in the definition of models that can better estimate the carbonation front, helping in decision-making processes related to durability and SL of reinforced concrete structures in the design stage.

## 2. METHOD

The method comprehends i) Selecting mathematical models for predicting concrete carbonation depth; ii) Creating a concrete carbonation database; iii) Comparing the concrete carbonation models; iv) Sensitivity analysis to understand carbonation depth predictions, according to the variables considered by each concrete carbonation model.



**2.1 Carbonation depth models**

**2.1.1 Possan (2010) Model**

The model proposed by Possan (2010) considers several factors that influence carbonation with manageable data input, as shown in Equation (1), where “y” (mm) is the carbonation Depth;  $k_c$  is the variable factor according to the type of cement (Table 1);  $f_c$  is the average compressive strength (MPa);  $k_{fc}$  is the variable factor for the axial compressive strength of concrete (Table 1);  $t$  is the age (years);  $ad$  is the pozzolanic addition content (% relative to the mass of cement);  $k_{ad}$  is a variable factor referring to the pozzolanic additions of the concrete (Table 1);  $CO_2$  is the  $CO_2$  content of the atmosphere (%);  $k_{CO_2}$  is a variable factor referring to the  $CO_2$  content of the environment (Table 1);  $RH$  is the average relative humidity (%\*0.01);  $k_{ur}$  is the variable factor referring to the RH (Table 1); and  $k_{ce}$  is the variable factor referring to the exposure to rain (Table 2).

$$y = k_c \left(\frac{20}{f_c}\right)^{k_{fc}} \cdot \left(\frac{t}{20}\right)^{\frac{1}{2}} \cdot \exp \left[ \left( \frac{k_{ad} \cdot ad^{\frac{3}{2}}}{40+f_c} \right) + \left( \frac{k_{CO_2} \cdot CO_2^{\frac{1}{2}}}{60+f_c} \right) + \left( \frac{k_{ur} \cdot (RH-0.58)^2}{100+f_c} \right) \right] \cdot k_{ce} \quad (1)$$

Table 1. Possan (2010) coefficients per cement type.

Cement type	Concrete characteristics			Environmental conditions	
	Cement	$f_c$	Pozzolanic addition	$CO_2$	RH
	( $k_c$ )	( $k_{fc}$ )	( $k_{ad}$ )	( $k_{CO_2}$ )	( $k_{rh}$ )
CP I	19.80	1.70	0.24	18.00	1300
CP II E	22.48	1.50	0.32	15.50	1300
CP II F	21.68	1.50	0.24	18.00	1100
CP II Z	23.66	1.50	0.32	15.50	1300
CP III	30.50	1.70	0.32	15.50	1300
CP IV	33.27	1.70	0.32	15.50	1000
CP V ARI	19.80	1.70	0.24	18.00	1300

Source: Possan, 2010.

Table 2. Possan (2010) coefficients as a function of exposure conditions.

Type of exposure	$k_{ce}$
Indoor environment protected from rain	1.3
Outdoor environment protected from rain	1
Outdoor environment unprotected from rain	0.65

Source: Possan, 2010.

**2.1.2 Ekolu (2018) Model**

The mathematical model proposed by Ekolu (2018) considers several parameters related to carbonation, such as RH and ambient temperature,  $CO_2$  concentration, structure protection, and rainfall incidence. The model estimates the carbonation depth through Equations (2) to (6), where “y” (mm) is the carbonation depth;  $e_h$  refers to the RH;  $e_s$  refers to the concrete compressive strength;  $e_{co}$  refers to the  $CO_2$  concentration in the environment;  $F_{c(t)}$  is the concrete strength growth function;  $t$  is the concrete exposure time (years);  $g$  depends on the cement type; and  $RH$  is the average RH of the environment (%).

$$y = e_h \cdot e_s \cdot e_{co} \cdot 1000 \cdot F_{c(t)}^g \cdot \sqrt{t} \quad (2)$$

$$e_h = 16. \left( \frac{RH-35}{100} \right) \cdot \left( 1 - \frac{RH}{100} \right)^{1.5} \rightarrow 50\% \leq RH \leq 80\% \quad (3)$$

$$e_s = \begin{cases} 1.0 \rightarrow \text{Protected external exposure} \\ f_{c28}^{-0.2} \rightarrow \text{Unprotected external exposure} \end{cases} \quad (4)$$

$$e_{co} = \begin{cases} \alpha f_{c28}^r \rightarrow 20 < f_c < 60 \text{MPa} \\ 1.0 \rightarrow f_c > 60 \text{MPa} \end{cases} \quad (5)$$

$$F_{c(t)} = \frac{t}{a+bt} \cdot f_c \rightarrow f_c = f_{c28} \text{ ou } f_{cbn} \quad (6)$$

The “ $e_{co}$ ” can be determined through (5) by inserting, if necessary, the concrete compressive strength at 28 days of curing ( $f_{c28}$ ) and the respective correction coefficients “ $\alpha$ ” and “ $r$ ” from Table 3.  $F_{c(t)}$  is obtained through (6), and the coefficients “ $a$ ” and “ $b$ ” (Table 4) depend on the values of concrete strength ( $f_{c28}$ , when considering concrete strength at 28 days and  $f_{cbn}$ , when considering long-term concrete strength), as well as concrete ages. The “ $g$ ” coefficient applied in (2) should be consulted in Table 5.

Table 3. Ekolu (2018) coefficients for  $e_{co}$  equation.

Coefficient	CO <sub>2</sub> concentration in atmosphere (ppm)				
	200	300	500	1000	2000
$\alpha$	1.40	1.00	2.50	4.50	14.00
$r$	-0.25	0.00	-0.25	-0.40	-0.67

Source: Ekolu, 2018.

Table 4. Ekolu (2018) coefficients for  $F_{c(t)}$  equation.

Compressive strength	Concrete age	a	b
$f_{c28}$	$t < 6$ anos	0.35	$0.6 - t^{0.5}/50$
	$t > 6$ anos	$0.15t$	$0.5 - t^{0.5}/50$
$f_{cbn}$	$t < 15$ anos	0.35	$1.15 - t^{0.6}/50$
	$t > 15$ anos	$0.15t$	$0.95 - t^{0.6}/50$

Source: Ekolu, 2018.

Table 5. Ekolu (2018) coefficients for  $g$  equation.

Supplementary cementitious materials (SCM)	Cement type*	Conductance factor “g”
20% SCM	CEM I, CEM II/A	-1.5
30% fly ash	CEM II/B, CEM IV/A	-1.4
50% slag	CEM III/A	

\*According to British standard BS EN 197-1

Source: Ekolu, 2018.

### 2.1.3 Ho e Lewis (1987) Model

Ho and Lewis (1987) proposed an improvement for the model proposed by Tuutti (1982) by adding a parameter for initial carbonation, as shown in Equation 8. The carbonation depth is represented by the factor  $e_c$  (mm);  $e_0$  is the initial carbonation depth (mm);  $k$  is the carbonation coefficient

(mm/year)<sup>0.5</sup>, and  $t$  is the time (years).

$$e_c = e_0 + k\sqrt{t} \tag{7}$$

The model proposed by Ho and Lewis (1987) does not indicate how to determine the carbonation coefficient ( $k$ ). Thus, different proposals have been developed for determining the coefficient, such that proposed by Helene (1997), which takes into account the cement type, the CO<sub>2</sub> concentration, and the concrete compressive strength, as shown in Equations (8) to (10). The carbonation coefficient is represented by the factor  $k$  (mm/year)<sup>0.5</sup>;  $fck$  is the compressive strength (MPa) and;  $CCO_2$  is the CO<sub>2</sub> concentration (%).

Concrete (Equation 9):

$$k = (21.46617 - 0.35765 \cdot fck) \cdot \sqrt{CCO_2} \tag{8}$$

Concretes with pozzolanic cement (Equation 10):

$$k = 1.1 \cdot (21.46617 - 0.35765 \cdot fck) \cdot \sqrt{CCO_2} \tag{9}$$

Concrete with blast furnace cement (Equation 11):

$$k = 1.2 \cdot (21.46617 - 0.35765 \cdot fck) \cdot \sqrt{CCO_2} \tag{10}$$

**2.1.4 Bob e Affana (1993) Model**

Bob and Affana (1993) model is also based on the model developed by Tuutti (1982), but the authors considered that concrete carbonation depth was related to more factors, such as air RH, cement type, and concrete compressive strength. In the model, presented in Equation (11), the carbonation depth is represented by the factor “ $y$ ” (mm);  $c$  is the coefficient related to cement type (Table 6);  $k$  is the coefficient dependent on the air humidity (Table 6);  $f_c$  is the compressive strength of concrete (MPa);  $t$  is the time (years) and;  $d$  is the coefficient referring to the amount of CO<sub>2</sub> (Table 6).

$$y = 150 \cdot \left(\frac{c \cdot k \cdot d}{f_c}\right) \cdot \sqrt{t} \tag{11}$$

Table 6 – Coefficients  $k$ ,  $d$  and  $c$  of the Bob e Affana (1993) model.

Relative humidity	$k$
RH ≤ 60	1.0
70 ≤ RH ≤ 75	0.7
80 ≤ RH ≤ 85	0.5
RH ≥ 90	0.3
CO <sub>2</sub> concentration	$d$
CO <sub>2</sub> ≤ 0.03%	1.0
0.03 < CO <sub>2</sub> ≤ 0.1%	2.0
Cement type	$c$
Portland cement PC40 and PC45	0.8
Portland cement PC50 and PC55	1.0

Portland cement + 15% mineral addition	1.2
Portland cement + 30% mineral addition	1.4
Portland cement + 50% mineral addition	2.0

Source: Bob e Affana, 1993.

## 2.2 Database

A literature review was conducted to create the database presented in Table 7. A total of 300 data were selected from papers that evaluated different concrete mixes under the effects of natural carbonation. Subsequently, with this group of data, a new screening was performed to select the data that could effectively be used in the carbonation models used in this paper (referred in section 3.1). A total of 24 data were used for the development of this paper, as shown in Table 7, where ET corresponds to the exposure time and ec to the carbonation depth.

Table 7. Database.

Data	ET (year)	w/c	Cement	fck 28 (MPa)	CO <sub>2</sub> (%)	RH (%)	Exposure	cd (mm)
Possan (2010)	7.00	0.80	PC V	19.80	0.035	0.70	oepr	12.01
	12.00	0.80	PC V	19.80	0.035	0.70	oepr	15.1
Pauletti (2009)	2.50	0.40	PC I	38.96	0.071	0.70	oeur	1.31
	4.83	0.40	PC I	38.96	0.071	0.70	oeur	2.00
Tasca (2012)	2.00	0.55	PC V	45.90	0.035	0.65	iepr	0.92
	4.00	0.55	PC V	45.90	0.035	0.65	iepr	1.41
	14.00	0.55	PC V	45.90	0.035	0.65	iepr	6.35
Nardino et al. (2018)	3.33	0.61	PC V	30.00	0.053	0.70*	iepr	6.00
	6.41	0.61	PC V	30.00	0.053	0.70*	iepr	8.10
	7.80	0.61	PC V	30.00	0.053	0.70*	iepr	7.44
Rozière et al. (2009)	1.00	0.63	PC V*	47.80	0.053	0.50	oeur*	1.20
	1.00	0.63	PC V*	36.20	0.053	0.50	oeur*	10.90
Ribeiro et al. (2018)	10.00	0.65	PC V	32.30	0.015	0.55	oeur	11.90
	10.00	0.44	PC II F	54.20	0.015	0.55	oeur	3.00
Sanjuan et al. (2003)	2.00	0.69	PC V	17.00	0.030	0.50	iepr	7.00
	2.00	0.49	PC V	28.00	0.030	0.50	iepr	5.00
Ferreira (2013)	3.00	0.55	PC II F	24.8	0.034	0.65	oeur	7.56
	7.00	0.55	PC II F	24.8	0.034	0.65	oepr	12.86
	9.00	0.55	PC II F	24.8	0.034	0.65	oepr	13.89
	10.00	0.55	PC II F	24.8	0.034	0.65	oepr	13.57
	3.00	0.55	PC II F	24.8	0.034	0.65	oepr	10.00
	7.00	0.55	PC II F	24.8	0.034	0.65	oepr	15.36
	9.00	0.55	PC II F	24.8	0.034	0.65	oepr	16.80
10.00	0.55	PC II F	24.8	0.034	0.65	oepr	15.96	

RH - relative humidity; oepr - outdoor environment protected from rain; oeur - outdoor environment unprotected from rain; iepr - indoor environment protected from rain; ET - exposure time, cd - carbonate depth; \* - estimated data.

### 2.3 Model comparison and sensitivity analysis

A comparison of the real carbonation depth (mm), in relation to the estimated carbonation depth, was performed and the error (mm and %) was quantified. In addition, the sensitivity level of the models was determined, taking into account three factors: compressive strength (MPa); CO<sub>2</sub> concentration (%); ambient RH (%). A simulation of natural carbonation scenarios was made, where some factors varied while others remained fixed. The factors stipulated for the scenarios were defined based on the information obtained from the database. The carbonation depths were delimited for a period of 50 years. With these factors in mind, three scenarios were determined, as described in Table 8.

Table 8. Description of scenarios A, B, and C.

<b>Scenario A – varies compressive strength at 28 days</b>				
Compressive strength (MPa)	40		20	
Relative humidity (%)	65		65	
Carbon dioxide (%)	0.035		0.035	
Environment type	Indoor		Indoor	
Cement type	PC V		PC V	
<b>Scenario B – varies carbon dioxide from the environment</b>				
Compressive strength (MPa)	40		40	
Relative humidity (%)	65		65	
Carbon dioxide (%)	0.03		0.07	
Environment type	Indoor		Indoor	
Cement type	PC V		PC V	
<b>Scenario C – varies relative humidity of the environment</b>				
Compressive strength (MPa)	40	40	40	40
Relative humidity (%)	30	50	70	90
Carbon dioxide (%)	0.035	0.035	0.035	0.035
Environment type	Indoor	Indoor	Indoor	Indoor
Cement type	PC V	PC V	PC V	PC V

### 3. RESULTS AND DISCUSSION

Figure 1 (a) shows a tendency for the models to generate different results from those observed in the experiments. These observations are more explicit for Bob and Affana (1993) model, which overestimated, and Ho and Lewis (1987) model, which underestimated the carbonation depths.

Data presented in Figure 1 (b) allows a comparison of the carbonation depths estimated by each model, relative to the real carbonation depths. The dashed red line represents equivalent results for the estimated and real values, obtained experimentally: points above the dashed line represent values that were overestimated by the model, while values under the dashed line represent underestimated estimates for carbonation depth. It can be observed that the Ho and Lewis (1987) model underestimates carbonation depths, while the Bob and Affana (1993) model overestimates them. The carbonation data estimated by Possan (2010) and Ekolu (2018) models, on the other hand, are closer to the dashed line, but still underestimate the carbonation depth.

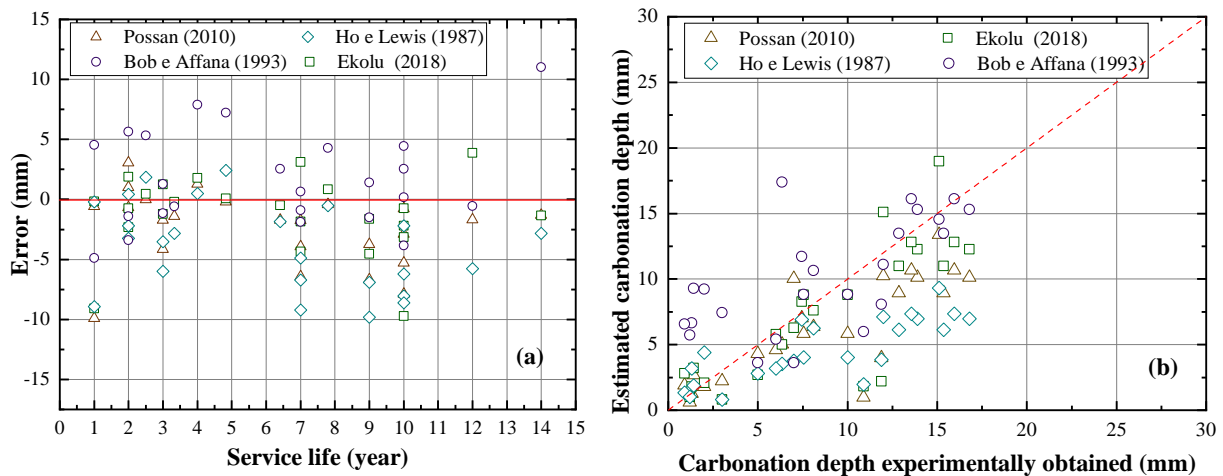


Figure 1. Errors for carbonation depths as a function of time (a) and comparison between estimated and experimentally obtained carbonation depths (b).

Figure 2 (a) shows the sensitivity analysis results for the models regarding the compressive strength, considering values between 20 and 40 MPa, in the natural carbonation process during 50 years. The figure shows carbonation depths and SL with the minimum concrete cover of 25 mm stipulated by NBR 6118 (2014) for reinforced concrete structures in urban environments (moderate aggressiveness, class II).

In all models of scenario A, the increase in concrete compressive strength results in lower carbonation depths. This behavior is consistent with that predicted in the literature since lower w/c ratios reduce the matrix porosity and carbonation depths, determining concrete strength (TUUTTI, 1982; HO and LEWIS, 1987; KULAKOWSKI, 2002).

The reduction in carbonation depth caused by increasing the compressive strength of concrete from 20 to 40 MPa, considering results for the same period, is approximately 68.55%, 70.3%, 49.97%, and 50% for the models of Possan (2010), Ekolu (2018), Ho and Lewis (1987), Bob and Affana (1993), respectively. These values are obtained by fixing the formula variables of each method and varying the compressive strength. The compressive strength factor exerts more influence on the carbonation depths estimated by the models of Ho and Lewis (1987) and Bob and Affana (1993). In addition, the Possan (2010) and Bob and Affana (1993) models predict that 20 MPa concrete would not be able to meet an SL of 50 years with a concrete cover of 25 mm under the conditions stipulated for Scenario A. For the other models, 20 MPa concrete would already meet this requirement.

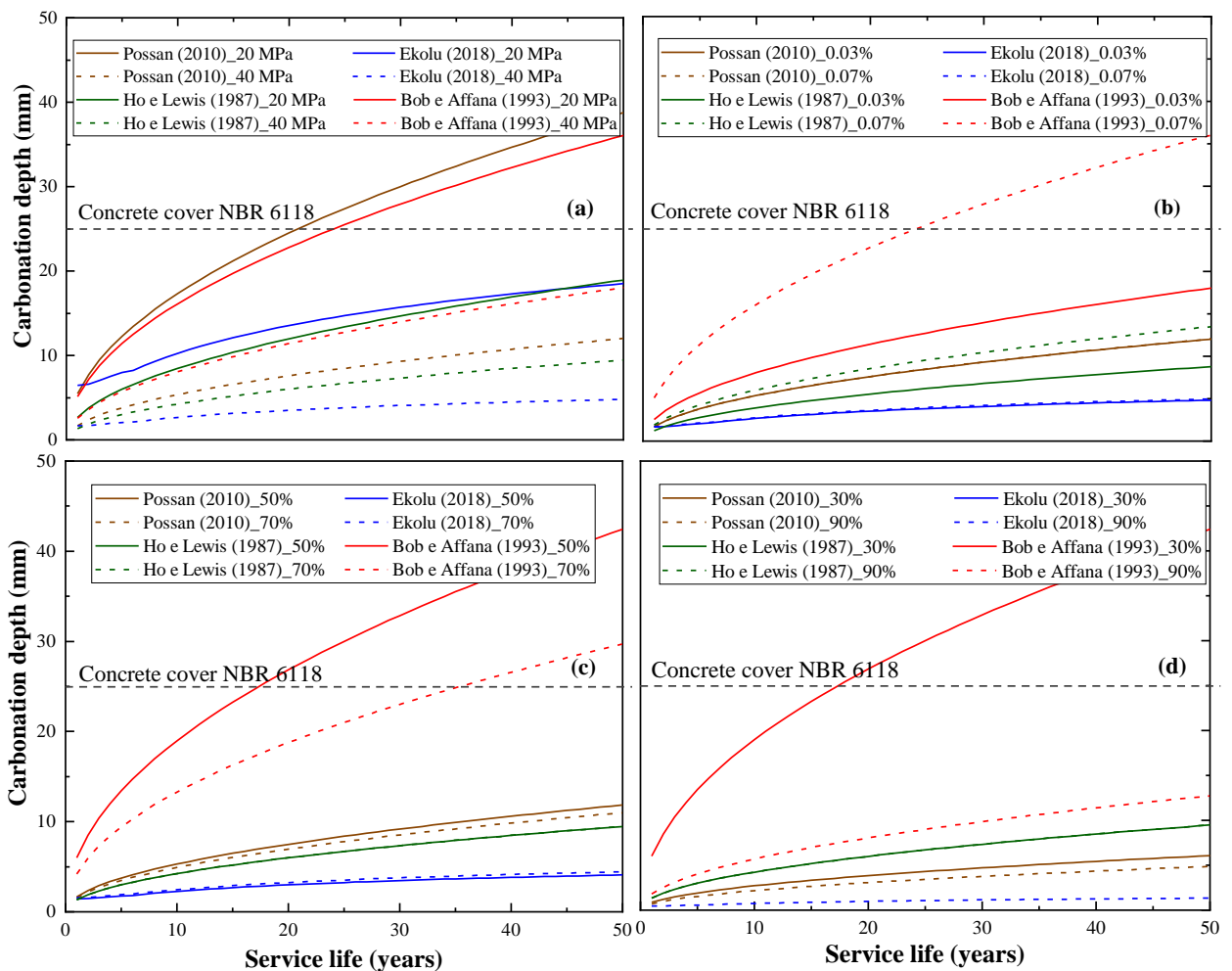


Figure 2. Service life and carbonation depth in relation to compressive strength - Scenario A - (a), carbon dioxide in the environment - Scenario B - (b), relative humidity of 50 and 70% - Scenario C - (c) and relative humidity of 30 and 90% - Scenario C - (d).

Figure 2 (b) shows the sensitivity regarding the  $\text{CO}_2$  concentration. The  $\text{CO}_2$  concentrations were delimited based on the values obtained from the database and definitions presented in the publication of Possan (2010). Concentrations of 0.03% and 0.07% were then stipulated in the natural carbonation process during the 50 years. Pires (2016) presents  $\text{CO}_2$  concentration as one of the intervening factors in the carbonation process of concrete, and Cadore (2008) suggests that the carbonation front speed is directly related to  $\text{CO}_2$  concentration, i.e., the carbonation speed increases by increasing  $\text{CO}_2$  concentration.

Note in Figure 2 (b) that although carbonation increases by increasing  $\text{CO}_2$  levels, this growth is lower in the Possan (2010) and Ho and Lewis (1987) models. The carbonation depth increase caused by the  $\text{CO}_2$  concentration growth is approximately 0.17%, 2.89%, 53.84%, and 100%, on average, for Possan (2010), Ekolu (2018), Ho and Lewis (1987), Bob and Affana (1993) models, respectively. This result indicates that the  $\text{CO}_2$  factor of the Possan (2010) and Ekolu (2018) models exert less influence on the estimated carbonation depths for Scenario B compared to the other mentioned models. The Bob and Affana (1993) model suggests that in environments with 0.07%  $\text{CO}_2$ , concrete would not meet a 50-year SL with a 25 mm concrete cover under the conditions stipulated for Scenario B.

Figure 2 (c) illustrates the sensitivity to the ambient RH in the natural carbonation process for 50 years. The selected RH are extreme values found in the literature for the natural carbonation

processes (Pauletti, 2009; Tasca, 2012; Rozière, 2009; Nardino, 2019).

For scenario C, the increase of ambient RH reduces the carbonation depth for Possan (2010) and Bob and Affana (1993) models. However, while Possan (2010) model presents a 7.16% decrease on average, the Bob and Affana (1993) model results in a 30% decrease, which suggests that Bob and Affana (1993) model is more sensitive to this variable. For Ekolu (2018) model the carbonation depth increases by 8.44% on average. On the other hand, for Ho and Lewis (1987) model, the carbonation depths remain unchanged with the 20% increment in RH, which can be explained by the fact that the RH is not an input data, and therefore, the model is not sensitive to this factor.

Since RH is a relevant factor for the carbonation process, it should be accounted for, directly or indirectly, in SL prediction models by natural carbonation processes. The water present in the pores is responsible for dissolving the CO<sub>2</sub>, forming carbonic acid (H<sub>2</sub>CO<sub>3</sub>) and Ca(OH)<sub>2</sub>, resulting in CaCO<sub>3</sub> (Pauletti, 2009). The volume and composition of pore water are influenced by factors such as the w/c ratio, curing time, temperature, and even the RH of the environment (Vieira et al., 2016). The literature also indicates that excessive or low RH environments are not conducive to the natural carbonation process. In the first situation, the concrete pores would be filled with water, hindering the penetration of CO<sub>2</sub> for H<sub>2</sub>CO<sub>3</sub> formation. On the other hand, in low RH conditions, the water in the concrete pores would be insufficient to generate more accelerated natural carbonation rates since water is required to generate H<sub>2</sub>CO<sub>3</sub> (Félix et al., 2017; POSSAN et al., 2017; Elsalamawy et al., 2019; Dierfeld et al., 2020).

Considering Scenario C, results of Possan (2010) and Bob and Affana (1993) show a reduction in carbonation depths due to the RH increase from 50 to 70%, which suggests that the pore saturation is predicted in these ranges of ambient RH. In contrast, the Ekolu (2018) model results suggest that these RH contents are conducive to the carbonation process. In this regard, Chen et al. (2018) observed an increase in carbonation depth with an increase in ambient RH, with a peak of about 70%. Data obtained through the Ekolu (2018) model in Scenario C follows the one suggested by these authors.

For a better understanding, Possan (2010), Ekolu (2018), and Bob and Affana (1993) models were then tested in Scenario C, considering 30% and 90% RH. The results are shown in Figure 2 (d). For the Possan (2010) method, lower carbonation depths are obtained in 30% - 90% RH range compared to 50% - 70%. While the 50-year average carbonation depths for 50% and 70% RH are 8.01 mm and 7.43 mm, respectively, for 30% and 90% RH these values change for 4.10 and 3.28 mm, respectively. This indicates that the model is sensitive to both excess and low RH conditions. Also, in Ekolu (2018) model, the 30% RH generates negative values, while 90% predicts significantly lower results than 50% and 70%. Thus, the model recognizes the 50% -70% RH range as the more favorable for the carbonation process. For Bob and Affana (1993) model, on the other hand, 30% RH results in carbonation depths equivalent to those estimated for 50% RH, since the model considers RH ranges instead of individual values. As the same coefficient (1.0) is used for RH equal to or below 60%, the model is not sensitive to RH below 60%. The same happens for RH values equal to or greater than 90%, where the coefficient 0.3 is adopted. However, the model considers that for RH equal to or below 60% the carbonation depth is higher than for RH equal to or greater than 90%. For 30% an average carbonation of 28.68 mm depth was obtained for 50 years, while for 90% the value was 8.6 mm. Figure 2 (c) also indicates that according to Bob and Affana model (1993), concrete in environments with 50 and 70% RH would not meet a 50-year SL with a 25 mm concrete cover in the conditions stipulated for Scenario C. Furthermore, according to Bob and Affana (1993) model, concrete in environment with 30% RH, and conditions as in Scenario C, Figure 2 (d), would not meet the 50-year SL for a 25 mm concrete cover.



## 4. CONCLUSION

The main considerations that can be made based on the results discussed in this paper are:

- The Possan (2010) and Ekolu (2018) models result in carbonation depths closer to those found experimentally;
- The Ho and Lewis (1987) model tends to underestimate the carbonation depth;
- The Bob and Affana (1993) model tends to overestimate the carbonation depth;
- The Ho and Lewis (1987) and Bob and Affana (1993) models showed a more significant influence of the compressive strength on the carbonation depths;
- The CO<sub>2</sub> concentration factor of the Possan (2010) and Ekolu (2018) models exert the slightest influence on the estimated carbonation depths for Scenario B compared to the other models;
- The Bob and Affana (1993) model has the highest sensitivity to the RH variable, while the Ho and Lewis (1987) model has no data input for this variable.

The Possan (2010) and Bob and Affana (1993) models with 20 MPa concrete in Scenario A, Bob and Affana (1993) model with concrete exposed to 0.07% CO<sub>2</sub> in the environment in Scenario B, and Bob and Affana (1993) model with concrete exposed in 30%, 50% and 70% RH environment in Scenario C, would not be able to meet a SL of 50 years with a concrete cover of 25 mm under the stipulated conditions.

Thus, it can be seen that there is variability in the results of carbonation front estimated by the selected models compared to the real results of natural carbonation. This variability occurs to a greater or lesser extent depending on the parameters considered in the model equations. The sensitivity analysis performed with compressive strength, CO<sub>2</sub> concentration, and relative humidity shows that these variables significantly influence the results issued by the models and, therefore, should be considered in the equations.

## 5. ACKNOWLEDGMENTS

We thank the Universidade Federal do Rio Grande do Sul (UFRGS) and the Graduate Program in Civil Engineering: Construction and Infrastructure (PPGCI), for providing the necessary subsidies for the development of this study.

## 6. REFERENCE

- Associação Brasileira de Normas Técnicas. (2013). *NBR 15575-1: Edificações habitacionais — Desempenho Parte 1: Requisitos gerais*. Rio de Janeiro.
- Associação Brasileira de Normas Técnicas. (2014). *NBR 6118: Projeto de estruturas de concreto — Procedimento*. Rio de Janeiro.
- Bob, C., Afana, E. (1993). “*On-site assessment of concrete carbonation*”. Proceedings of the International Conference Failure of Concrete Structures, RILEM, Bratislava: (Rep. Eslovaca), pp. 84–87.
- Cadore, W.C. (2008), “*Estudo da camada de cobrimento de protótipos de concreto com altos teores de adições minerais e cal hidratada*”, Dissertação de Mestrado, Universidade Federal de Santa Maria, p.149.
- Chen, T., Gao, X. (2019), *Effect of carbonation curing regime on strength and microstructure of Portland cement paste*. Journal of CO<sub>2</sub> Utilization, 34:74-86. <https://doi.org/10.1016/j.jcou.2019.05.034>
- Chen, Y., Liu, L., Yu, Z. (2018), *Effects of Environmental Factors on Concrete Carbonation Depth and Compressive Strength*. Materials, 11, 2167. <https://doi.org/10.3390/ma11112167>

- Dierfeld, S. G. et al. (2020), *Understanding the carbonation of concrete with supplementary cementitious materials: a critical review by RILEM TC 281-CCC*. Materials and Structures, 53:136. <https://doi.org/10.1617/s11527-020-01558-w>
- Elsalamawy, M., Mohamed, A. R., Kamal, E. M. (2019), *The role of relative humidity and cement type on carbonation resistance of concrete*. Alexandria Engineering Journal 58(4):1257–1264. <https://doi.org/10.1016/j.aej.2019.10.008>
- Ekolu, S. O. (2018), *Model for practical prediction of natural carbonation in reinforced concrete: Part 1-formulation*. Cement and Concrete Composites. 86:40-56. <https://doi.org/10.1016/j.cemconcomp.2017.10.006>
- Ferreira, M. B. (2013), “*Estudo da carbonatação natural de concretos com diferentes adições minerais após 10 anos de exposição*”, Dissertação de Mestrado, Universidade Federal de Goiás, p. 197.
- Félix, E. E., Carrazedo, R., Possan, E. (2017), *Análise paramétrica da carbonatação em estruturas de concreto armado via Redes Neurais Artificiais*. Revista ALCONPAT, 7(3), pp. 302-316. <https://doi.org/10.21041/ra.v7i3.245>
- Helene, P. (1997). “*Vida útil das Estruturas de Concreto*”. in: IV Congresso Iberoamericano de Patologia das Construções. Anais. Porto Alegre: RS (Brasil).
- Ho, D. W. S., Lewis, R. K. (1987), *Carbonation of concrete and its prediction*. Cement and Concrete Research, 17(3):489-504. [https://doi.org/10.1016/0008-8846\(87\)90012-3](https://doi.org/10.1016/0008-8846(87)90012-3)
- Housty, Y. F., Wittmann, F. H. (2012), *Depth profiles of carbonates formed during natural carbonation*. Cement and Concrete Research, 32(12):1923-1930. [https://doi.org/10.1016/S0008-8846\(02\)00908-0](https://doi.org/10.1016/S0008-8846(02)00908-0)
- Köliö, A. et al. (2014), *Durability demands related to carbonation induced corrosion for Finnish concrete buildings in changing climate*. Engineering structures, 62-63:42-52. <https://doi.org/10.1016/j.engstruct.2014.01.032>
- Kulakowski, M. P. (2002), “*Contribuição ao estudo de carbonatação de concretos e argamassas compostos com adição de sílica ativa*”, Tese de Doutorado, Universidade Federal do Rio Grande do Sul, Porto Alegre: RS (Brasil), p. 180.
- Li, D. et al. (2018), *Evaluating the effect of external and internal factors on carbonation of existing concrete building structures*. Construction and Building Materials, 167:73-81 <https://doi.org/10.1016/j.conbuildmat.2018.01.127>
- Nardino, C. et al. (2019) “*Previsão de vida útil de estruturas por modelos matemáticos e carbonatação natural*” in: 4º Simpósio Paranaense de Patologia das Construções, Curitiba:PR (Brasil), pp. 300-311. <https://doi.org/10.4322/2526-7248.052>
- Pauletti, C. (2009). “*Estimativa da carbonatação natural de materiais cimentícios a partir de ensaios acelerados e de modelos de predição*”, Tese de Doutorado, Universidade Federal do Rio Grande do Sul, Porto Alegre:RS (Brasil), p. 285.
- Peter, M. A. et al. (2008), *Competition of several carbonation reactions in concrete: A parametric study*. Cement and concrete research, 38(12):1385-1393. <https://doi.org/10.1016/j.cemconres.2008.09.003>
- Pires, P. F. (2016). “*Estudo da carbonatação avançada em concretos contendo adições minerais*”, Dissertação de Mestrado, Universidade Federal de Goiás. p. 141.
- Possan, E. (2010), “*Modelagem da carbonatação e previsão de vida útil de estruturas de concreto em ambiente urbano*”, Tese de Doutorado, Universidade Federal do Rio Grande do Sul. p. 263.
- Possan, E. et al. (2017), *CO2 uptake potential due to concrete carbonation: A case study*. Case Studies in Construction Materials, 6:147-161. <https://doi.org/10.1016/j.cscm.2017.01.007>
- Ribeiro, D. V. et. al. (2018), “*Corrosão e Degradação em Estruturas de Concreto: Teoria, Controle e Técnicas de Análise e Intervenção*”. Elsevier, Rio de Janeiro, Brasil, p. 426.
- Ribeiro, A. B., Santos, T., Gonçalves, A. (2018), *Performance of concrete exposed to natural*

- carbonation: Use of the *k*-value concept. *Construction and Building Materials*. 175:360–370. <https://doi.org/10.1016/j.conbuildmat.2018.04.206>
- Rozière, E., Loukili, A., Cussigh, F. (2009), *A performance based approach for durability of concrete exposed to carbonation*. *Construction and Building Materials* 23(1):190–199. <https://doi.org/10.1016/j.conbuildmat.2008.01.006>
- Sanjuán, M., Andrade, C., Cheyrezy, M. (2003), *Concrete carbonation tests in natural and accelerated conditions*. *Advances in Cement Research*, 15(4):171–180. <https://doi.org/10.1680/adcr.2003.15.4.171>
- Song, H., Kwon, S. (2007), *Permeability characteristics of carbonated concrete considering capillary pore structure*. *Cement and Concrete Research*, 37(6):909-915. <https://doi.org/10.1016/j.cemconres.2007.03.011>
- Tasca, M. (2012), “*Estudo da carbonatação natural de concretos com pozolanas: monitoramento em longo prazo e análise da microestrutura*”. Dissertação de Mestrado, Universidade Federal de Santa Maria, p. 178.
- Tuutti, K. (1982), “*Corrosion of Steel in Concrete*”. Swedish Cement and Concrete Research Institute, Stockholm, Sweden, p.468.
- Vieira, R. E. et al. (2016). “*Aspectos sobre a extração e composição da água de poro de pasta de cimento hidratado com vista à durabilidade do concreto armado*”. in: 7 Congresso Brasileiro de Cimento - CBCI, São Paulo: SP (Brasil), pp. 15.

## Performance analysis of gravity chemical blockers in the treatment of rising damp in masonry walls

R. H. Malaquias<sup>1</sup>, G. J. Bruschi<sup>2</sup>, D. S. Brisotto<sup>3\*</sup>

\*Contact author: [daiane.brisotto@ufsc.br](mailto:daiane.brisotto@ufsc.br)

DOI: <https://doi.org/10.21041/ra.v12i1.561>

Reception: 31/10/2021 | Acceptance: 07/12/2021 | Publication: 01/01/2022

### ABSTRACT

The objective of this work is the performance analysis of the rising damp treatment in walls, through the use of chemical blockers (i.e., crystallizing and water repellent) available in the Brazilian market, with their introduction by gravity. As there are no standardized tests for such a study, experiments conducted by other researchers were used as a reference. The evaluation of the rising damp was achieved by the calculation of the water absorption rate in the specimens, allied with the images obtained by the thermographic camera. From the results, it was concluded that the treatment did not completely reduce the pathological manifestation in the walls, but both products performed well and managed to reduce the water absorption rate considerably.

**Keywords:** rising damp; pathological manifestation; chemical barrier.

**Cite as:** Malaquias, R. H., Bruschi, G. J., Brisotto, D. S. (2022), “*Performance analysis of gravity chemical blockers in the treatment of rising damp in masonry walls*”, Revista ALCONPAT, 12 (1), pp. 61 – 75, DOI: <https://doi.org/10.21041/ra.v12i1.561>

<sup>1</sup> Universidade Regional do Alto Uruguai e das Missões - URI Campus Erechim, Brasil.

<sup>2</sup> Universidade Federal do Rio Grande do Sul. Universidade de Trás-os-Montes e Alto Douro, Brasil.

<sup>3</sup> Universidade Federal de Santa Catarina, Brasil.

#### Contribution of each author

All authors equally contributed to the study conception and design. Material preparation and data collection were performed by Ronei. Data analysis was performed by Ronei (75%) and Giovanni Jordi Bruschi (25%). The first draft of the manuscript was written by Giovanni Jordi Bruschi and all authors commented on previous versions of the manuscript. All authors read and approved the final manuscript. In addition, Dr. Daiane de Senna Brisotto were responsible for the supervision of the research.

#### Creative Commons License

Copyright 2022 by the authors. This work is an Open-Access article published under the terms and conditions of an International Creative Commons Attribution 4.0 International License ([CC BY 4.0](https://creativecommons.org/licenses/by/4.0/)).

#### Discussions and subsequent corrections to the publication

Any dispute, including the replies of the authors, will be published in the third issue of 2022 provided that the information is received before the closing of the second issue of 2022.

## **Análisis del rendimiento de bloqueadores químicos por gravedad en el tratamiento de la humedad ascendente en muros de mampostería**

### **RESUMEN**

El objetivo de este trabajo es analizar el desempeño del tratamiento de la humedad ascendente en paredes, mediante el uso de bloqueadores químicos cristalizantes e hidrófugos disponibles en el mercado brasileño, con su introducción por gravedad. La evaluación de la humedad ascendente se realizó calculando la tasa de absorción de agua en las muestras, combinada con las imágenes obtenidas por la cámara termográfica. De los resultados encontrados se concluyó que el tratamiento no redujo por completo la patología en las paredes, sin embargo, ambos productos obtuvieron un buen desempeño, logrando reducir considerablemente las tasas de absorción de agua.

**Palabras clave:** humedad ascendente; patología; barreras químicas.

## **Análise de desempenho de bloqueadores químicos por gravidade no tratamento de umidade ascendente em paredes de alvenaria**

### **RESUMO**

O objetivo deste trabalho é a análise de desempenho do tratamento da umidade ascensional em paredes, através do uso de bloqueadores químicos cristalizantes e hidrofugantes disponíveis no mercado brasileiro, com a introdução dos mesmos por gravidade. A avaliação da umidade ascendente deu-se pelo cálculo da taxa de absorção de água nos corpos de prova, aliado com as imagens obtidas pela câmera termográfica. A partir dos resultados encontrados concluiu-se que o tratamento não reduziu por completo a patologia nas paredes, porém ambos os produtos obtiveram um bom desempenho, conseguindo reduzir consideravelmente as taxas de absorção de água.

**Palavras-chave:** umidade ascensional; patología; barreira química.

### **Legal Information**

Revista ALCONPAT is a quarterly publication by the Asociación Latinoamericana de Control de Calidad, Patología y Recuperación de la Construcción, Internacional, A.C., Km. 6 antigua carretera a Progreso, Mérida, Yucatán, 97310, Tel.5219997385893, [alconpat.int@gmail.com](mailto:alconpat.int@gmail.com), Website: [www.alconpat.org](http://www.alconpat.org)

Reservation of rights for exclusive use No.04-2013-011717330300-203, and ISSN 2007-6835, both granted by the Instituto Nacional de Derecho de Autor. Responsible editor: Pedro Castro Borges, Ph.D. Responsible for the last update of this issue, Informatics Unit ALCONPAT, Elizabeth Sabido Maldonado.

The views of the authors do not necessarily reflect the position of the editor.

The total or partial reproduction of the contents and images of the publication is carried out in accordance with the COPE code and the CC BY 4.0 license of the Revista ALCONPAT.

## 1. INTRODUCTION

The presence of moisture in buildings is recurrent and can generate serious pathological manifestations for the constructive system. Porous building materials (e.g. bricks and concrete) facilitate the transport of gases and liquids present in the environment and, in combination with other environmental factors, may lead to biological attacks, salt crystallization, chemical attacks, frost damage, etc (Sandrolini and Franzoni 2006; Bertolini, 2010). The development of these pathologies can occur due to poor execution or lack of waterproofing system, causing aesthetic impact and degradation of the structures and coatings. Furthermore, in the most serious cases, problems associated with human health (Franzoni, 2018).

As a consequence of the complexity of its treatment, one of the most challenging types of moisture manifestation is the rising damp. Worldly recognized, this phenomenon manifests itself when groundwater flows into the base of a construction and ascends through the pore structure by capillarity (Massari and Massari, 1993; Alfano, 2005; Henriques, 2007). Although it occurs with a certain frequency, it corresponds to a complex phenomenon with great behavioral unpredictability (Torres, 2014; Guimarães et al., 2016).

Many repair systems have been proposed to solve this problem. The main masonry repair techniques can be subdivided into four large groups conforming to their function (Henriques, 1994): (i) solutions to prevent the access of water from the ground; (ii) solutions to remove the excess water; (iii) solutions to stop water rising; and (iv) solutions to hide anomalies. When well adapted and executed, solutions to prevent the access of water from the ground are the most efficient repair technique in the treatment of rising damp. This solution can be performed either by reducing the absorbent section, increasing the base ventilation or through physical and chemical barriers. Although the system does not act as the origin of the phenomenon of capillary ascension, it prevents the water from reaching excessive capillary heights (Torres, 2013; Freitas et al., 2008). Currently, the implementation of chemical barriers is one of the most widely utilized methods to manage and solve the rising damp phenomena. This technique consists of creating holes in the wall along a horizontal profile, usually spaced 10 to 15 cm, as close to the ground as possible on one or both sides of the masonry, depending mainly on the wall thickness (Dreyer and Hecht, 2001; Alfano et al., 2006; Lubelli et al., 2013). The chemical additives introduced into the holes can function by filling the pores (creating a waterproof layer in the masonry) and/or making the pores water repellent (inhibiting capillary transport). Among the pore-filler substances, also known as crystallizers or cover-pores, acrylamides, epoxy resins, alkali silicates, and inorganic silicates stand out. As for water repellent products, the most preeminent types are the organometallics, siliconates, silicones, and siloxanes. These products can have an organic solvent or be aqueous solutions or emulsions in water, being found with different viscosities (liquid, cream and gel) (Lubelli et al., 2013; Socoloski and Masuero, 2019).

One of the main problems associated with the application of chemical barriers is the difficulty of introducing the product into the pores, since they are on a large scale, filled with water. In order to present effectiveness, the chemical product must interact with all pores and voids, creating a hydrophobic or impermeable horizontal layer that prevents the access of water. If the horizontal barrier is not continuous, the water can still flow and the ascending moisture will not be interrupted. Therefore, the introduction of the product, applied with pressure/injection or gravity feed/impregnation, should be implemented aiming the layering of the treated zones (Hees et al., 2018).

The application of chemical barriers by gravity feed or impregnation (Figure 1(a)) is based on the gravity force and the materials capillarity and can be performed by inserting the chemical products without complex apparatus (Torres, 2014). In accordance with most Brazilian manufacturers, the drilling must be performed at a 45° inclination and the holes should be saturated before the insertion

of the products, promoting an improvement on the dispersal and consequently in the entire process (Socoloski, 2015). The application of the chemicals must be integral and continuous encompassing the entire treated area. The non-intrusive behavior in conjunction with the versatility of this technique results in a worldwide acknowledgment of its usage in historical buildings. However, in order to demonstrate its efficiency, some years can be required (Carrio, 1997). In the application by injection, as shown in Figure 1 (b), the fluid is pumped onto the wall by pressure, using an injection pump with special nozzles that prevent the products retraction. Several sets of mouthpieces can be attached simultaneously to the injection pump or the injection can be executed independently (Luso, 2002). The injection pressure is not necessarily constant and can vary from applicator to applicator, but it must not exceed 0.4 MPa. This range prevents the possible degradation on the constituent materials of the treated walls (Henriques, 1994).

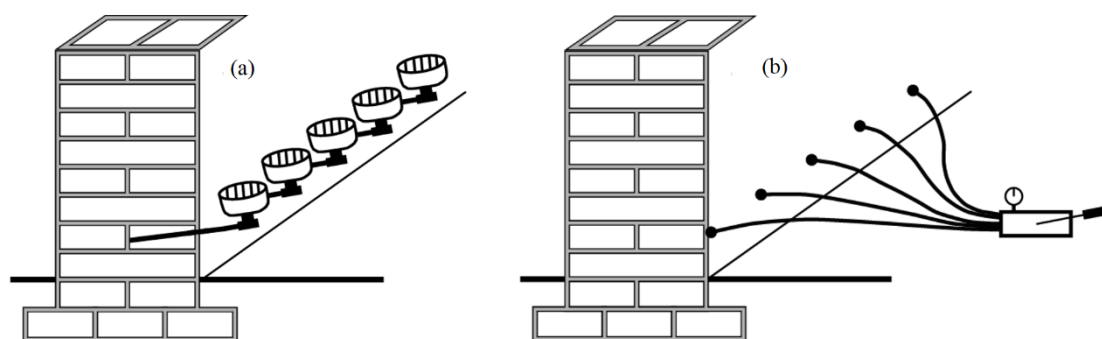


Figure 1. Introduction of chemical barriers: (a) by gravity and (b) by injection. Adapted from Henriques (1994).

The utilization of chemical barriers, either by injection or by gravity, has been widely investigated (Alfano et al., 2006; Freitas, 2014; Franzoni, 2014; Franzoni, 2018; Socoloski et al., 2019). The research have been performed in the laboratory, on single building materials (Vanhellemon et al., 2008), assemblies of materials (Hacquebord et al., 2013) and on-site (Larsen, 2012). Although it is difficult to compare the results of different researches, considering that the experimental methods usually are not convergent, the available studies provide a valuable indication of the dispersal capacity and drying efficiency of the chemical products (Franzoni et al., 2016). The dispersal capacity should be seen as a key-factor for the creation of functional and steady chemical barriers, considering that a non-steady behavior may enable the capillary flow (Hacquebord et al., 2013). This capacity depends on the nature of the solvent and its water miscibility, as well as the chemical products viscosity. These factors are essential for the pore water displacement (I'Anson and Hoff, 1988).

Despite the existence of several methods and products to solve the rising damp problem, as discussed above, scientific research on their effectiveness, both in the laboratory and in the field, is still scarce. In addition to not being as effective as expected, the treatment solutions may aggravate the pathological manifestations if the decision-making process is inappropriate. Hence, there is substantial demand for experimental results that provide evidence on the functioning, effectiveness and limitations of these repair systems, allowing an improved comprehension of their behavior and consequently a higher success rate when applied in real masonry.

Within this context, this research aims to experimentally study the rising damp treatment on walls with the use of chemical barriers by gravity, through blocking products of distinct chemical bases. For this purpose, a crystallizing product (active silicate base) and a water repellent product (oligomeric silane-siloxanes based) were comparatively analyzed.

## 2. MATERIALS

In this study, six small walls were constructed with the use of ceramic solid bricks and multiuse industrialized mortar. The samples were submitted to the treatment procedure of rising damp with two different chemical-based blocking products.

### 2.1 Ceramic bricks

Solid ceramic bricks of 190 x 90 x 50 mm (with tolerances up to 3 mm in dimensions) were adopted. Since there was no technical standard for the water absorption test in solid bricks, NBR 15270 (ABNT, 2005) was applied as a substitution. Six samples were prepared following five steps: (i) removal of loose particles and dust; (ii) drying process at 105 °C for 24 hours; (iii) weighing for the determination of the dry mass parameter ( $d_m$ ); (iv) immersion of each sample in water during 24 hours (in room temperature).; and (v) new weighing for the determination of the wet mass parameter ( $w_m$ ). The water absorption rate of the bricks ( $WA$ ) is determined according to (1) and the results obtained can be visualized in Table 1.

$$WA(\%) = \frac{w_m - d_m}{d_m} \times 100 \quad (1)$$

Table 1. Water absorption rate of the ceramic bricks.

Property	Sample						Average (%)
	1	2	3	4	5	6	
Dry mass (g)	1605.48	1597.80	1587.41	1622.99	1586.27	1682.45	25,48
Wet mass (g)	1994.56	2021.41	2017.26	2043.88	2012.05	2057.58	
WA (%)	24.23	26.51	27.08	25.93	26.84	23.30	

### 2.2 Industrialized mortar

For the laying of the bricks a multiuse industrialized mortar was applied. The industrialized multiuse mortar was chosen due to the improved quality control of the product, avoiding possible variations in the results. This product is composed by Portland cement, mineral aggregates and chemical additives, with resistance to compression of 1.2 MPa and ratio of water/dry materials of 0.2. The mortar was prepared by mixing water until the suitable consistency and homogeneity parameters were achieved. The minimal consistency (i.e., 20 ± 5 cm) was determined following the NBR 13276 (ABNT, 2005). For the execution of the base of the walls, a mortar with 8 MPa resistance was utilized.

### 2.3 Chemical blockers

Initially, a research was carried out on the available waterproofing products for the treatment of rising damp in the Brazilian industry. Only one product of each chemical base (one crystallizing and one water repellent) was chosen for the research, due to the low availability of water repellent products for this type of treatment. The crystallizing product, named product A (65% active content), was commercially available in 1-liter and 25-liter containers. The water-repellent product, named product B (9% active content), was offered only in 18-liter containers. The characterization of the chemical blockers, provided by the manufacturers, is presented in Table 2. The crystallizing chemical blocker was characterized according to its pH and the rate of solids whereas the water repellent chemical blocker according to its pH and specific mass.



Table 2. Chemical blockers characterization.

Product	pH	Active content	Specific mass	Manufacturer info
Crystallizing (A)	11	65%	-	Active silicate base
Water repellent (B)	6.5 to 8	9%	1 kg/m <sup>3</sup>	Oligomeric silane siloxane base

### 3. RESEARCH METHOD

#### 3.1 Sample execution

In order to simulate a real wall, mini walls (50 x 50 x 9 cm) were molded according to the methodology presented by Socoloski (2015), which was based on the models of Rirsch and Zhang (2010) and Freitas et al. (2008). The dimensions adopted were the largest possible considering that they had to be carried by two people, not exceeding the limit of up to 50 kg. A total of six specimens were prepared, two for the application of the crystallizing product (PA1 and PA2), two for the water repellent product (PB1 and PB2) and two as reference (T1 and T2) without any chemical treatment.

The base of the constructed walls had approximately 50 millimeters of height, executed in a reinforced mortar, with 250 millimeters galvanized square mesh for the prevention of shear rupture. Steel bars were inserted into the mortar base, serving as hooks for the handling of the specimens, as shown in Figure 2(a). After 21 days curing process, the walls were constructed onto the bases. The specimens were composed by 2.5 bricks per row, totaling 8 rows, with vertical joints interspersed as in a real masonry, as shown in Figure 2(b). The contact of the wall with soil moisture is given through the foundation, made of cementitious materials.



Figure 2. (a) Base of the wall and (b) Finished wall.

#### 3.2 Efficiency of the chemical products

##### 3.2.1 Mass and water absorption rate

This test provided the main parameter on the performance analysis of the treatment against rising damp. The procedures were based on the research developed by Socoloski (2015), according to the following phases:

- Mass measurement of all specimens (dry mass before treatment), 21 days after their execution.
- Saturation of the mortar bases (Figure 3).

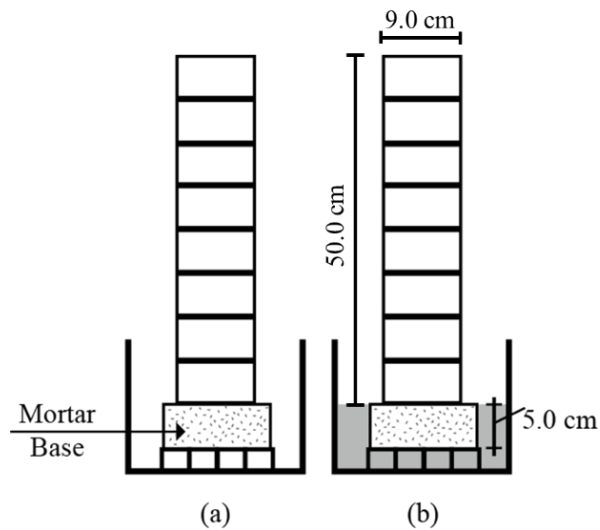


Figure 3. Specimen base saturation: (a) dry wall; (b) base in contact with water. Adapted from Socoloski (2015).

- c) Verification of the stabilization of the mass of the walls, which occurred between day 7 and 8, indicating the stabilization of the water absorption. Measurement of the walls mass on day 8 (wet mass before treatment).
- d) Computation of the water absorption rate before treatment, with the mass values obtained before and after the saturation of the bases.
- e) Treatment of the walls with chemical blockers, inserted at 45°, with holes at a height of 100 mm and spaced by 100 mm each, with a total of 5 holes per wall. In order to ensure the watertightness of the scheme, the product was inserted with a system of bottles, allowing the control of the speed and volume injection (Figure 4).



Figure 4. Application of waterproofing products.

- f) New saturation of the bases (water layer of 50 mm) for 28 days. During this period the mass was measured at 7, 14 and 28 days respectively.
- g) After 28 days, the specimens were removed from the water and placed at room temperature until the stabilization of the mass, which occurred in 20 days. Mass measurement on the 20th day (dry mass after treatment);
- h) The saturation process of the bases was repeated, with the treated walls, to quantify the preventive action. After 8 days a new mass measurement (wet mass after treatment) was performed to calculate the water absorption rate after treatment.
- The water absorption rate was calculated with the difference between the dry and wet mass, divided by the contact area of the walls and the mortar base, in accordance with Equation 2.

$$\text{Absorption rate (kg/m}^2\text{)} = \frac{w_m - d_m}{A} \quad (2)$$

Where “ $w_m$ ” represents the wet mass of the wall, “ $d_m$ ” the dry mass of the wall and “ $A$ ” the contact area of the first row of bricks with the humidity.

### 3.2.2 Thermography

The thermography test, considered as qualitative or complementary, allows the mapping of a region, distinguishing areas of different temperatures. Thus, this test was utilized to monitor the moisture distribution on the specimens.

The FLIR T440 thermographic camera was utilized and, during the image capturing, some parameters of the equipment were fixed, such as the emissivity (0.81) and the distance between the specimen and the camera (2 m), aiming an improved resolution. The atmospheric temperature measured by the camera, at the time of the experiment, was 23 °C. In addition, to improve the performance of the equipment, a dark background was assembled and installed behind the specimens, enhancing the sharpness of the images.

Using the software PSPP2018 the maximum and minimum wall temperatures were determined over the entire test period. The color scales adopted were the same for all images to allow the visual comparison. It is important to note that in this test, the camera provides only the recording of the temperature parameter, not including moisture rate or any other information. Thus, although the images contribute for a diagnosis, they are not necessarily decisive on the analysis

### 3.2.3 Cost analysis

In order to evaluate the cost of executing this type of treatment, the value of each product was investigated, and its consumption was measured considering the thickness (90 mm) and length (1 m) of the tested walls. Therefore, it was possible to estimate which of the chemical blockers presented the best cost-benefit (i.e., the lowest cost per linear meter of treated wall).

## 4. RESULTS AND DISCUSSION

### 4.1 Mass measurement and water absorption rate estimation

The mass of each tested specimen was recorded in order to calculate the absorption rate before and after the chemical treatment. The results are presented in Table 3 and Figure 5.

Table 3. Mass measurement and water absorption rate before and after treatment.

Sample	Contact area (m <sup>2</sup> )	Before treatment				After treatment				Average reduction (%)
		Dry mass - 21 days of cure after confection (kg)	Wet mass - 8 days of water contact with the base (kg)	Absorption rate (kg/m <sup>2</sup> )		Dry mass - 21 days drying (kg)	Wet mass - 8 days of water contact with the base (kg)	Absorption rate (kg/m <sup>2</sup> )		
				Per sample	Average			Per sample	Average	
T1	0.045	52.68	54.60	42.24	45.87	52.50	54.40	41.80	44.55	2.88
T2	0.045	51.65	53.90	49.50		51.60	53.75	47.30		
PA1	0.045	49.50	50.95	56.11	49.51	49.00	49.90	19.80	20.35	58.90
PA2	0.045	50.60	52.50	42.90		50.55	51.50	20.90		
PB1	0.045	47.90	50.45	31.90	36.85	47.60	48.25	14.30	11.00	70.15
PB2	0.045	48.50	50.45	41.80		48.20	48.55	7.0		

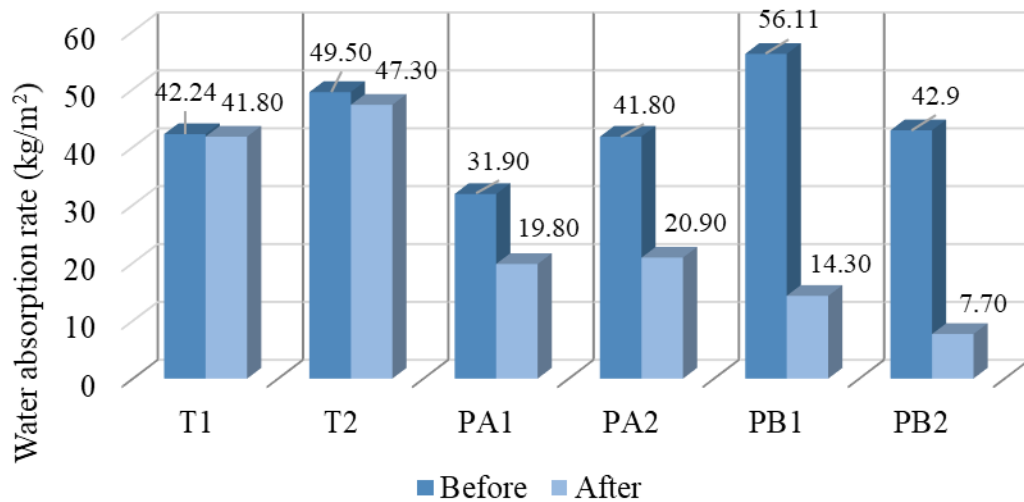


Figure 5. Mass measurement and water absorption rate before and after treatment.

The values in Table 3 demonstrate that before the beginning of treatment an increase in the specimens' mass occurred when exposed to humidity. However, according to Figure 5, the results show that both products were capable of considerably reducing the absorption rates of the treated specimens. The application of the crystallizing product resulted in an average reduction of 58.9% in the water absorption rate, while for the water repellent product this reduction was 70.15%. The

fact that the control walls showed a small decrease in mass and, consequently, a decrease in the absorption rate (2.88%), was already expected due to the equivalence process evidenced between the evaporation and absorption rate and, since this research analyzed a miniature wall, the process occurred faster than it normally would when compared to a natural size construction.

Table 4. Specimens mass during treatment.

Specimen	Mass during treatment (kg)		
	7 days	14 days	28 days
<b>T1</b>	-	-	54.25
<b>T2</b>	-	-	53.55
<b>PA1</b>	50.85	50.20	49.80
<b>PA2</b>	52.30	51.65	51.35
<b>PB1</b>	49.75	48.95	48.45
<b>PB2</b>	50.30	49.65	49.20

The mass measurements during the treatment (7, 14 and 28 days after the blockers application) are shown in Table 4. The results are equivalent to the obtained by Socoloski (2015) for both types of chemical blockers, with the lowest mass values obtained at 28 days of saturation. This can be explained by the fact that, over time, the rate of evaporation exceeds the rate of absorption (this index decreases as the pores are crystallized or with water-repellent behavior due to the chemical action). In addition, the mass reduction was certainly superior with the water repellent product. These results can be visualized in Figure 6.

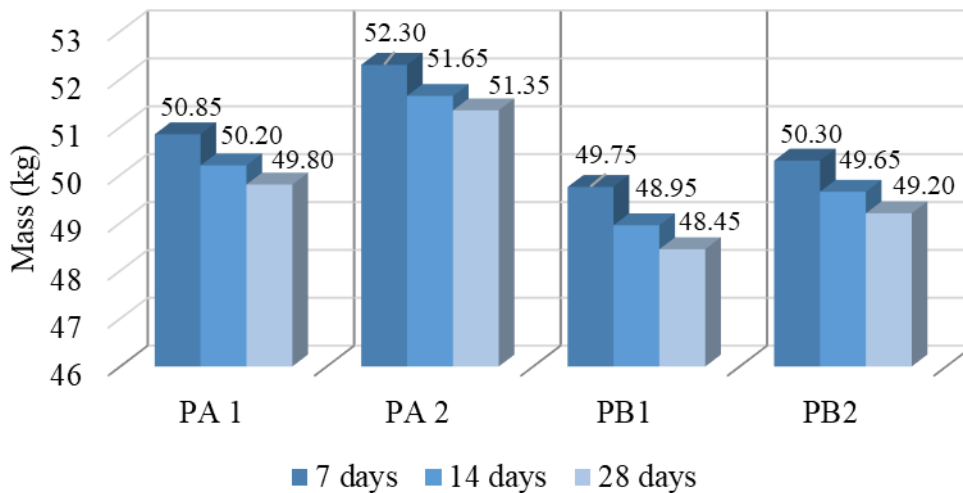


Figure 6. Comparison between masses during treatment.

In pursuance of the performance evaluation of the products, for the prevention of the rising damp phenomenon, Figure 7 shows a comparison between wet mass before and after the treatment. Although prevention is not the main focus of the evaluated method, the results demonstrate the potential of using the products as a preventive resource in construction.

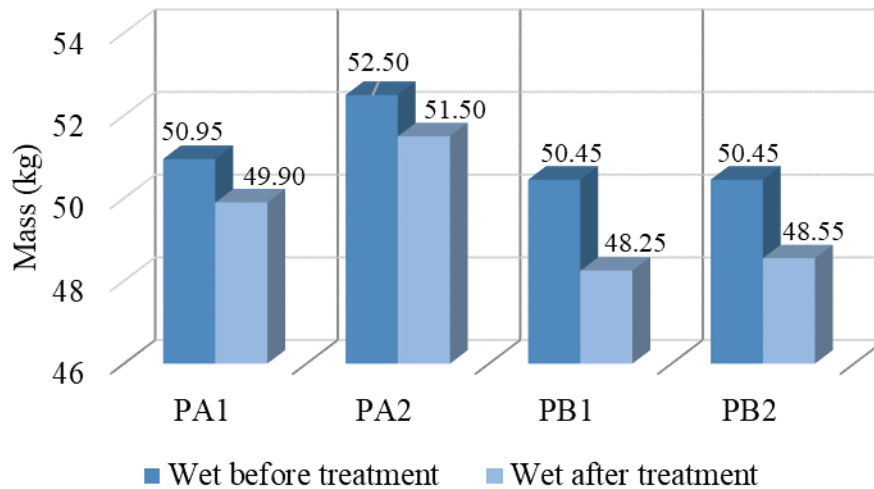


Figure 7. Comparison between wet masses before and after treatment.

In order to confirm if the reductions in the absorption rate were significant, the results were statistically treated and analyzed using the variance method (ANOVA). The outcome is presented in Table 5 and classify the difference as significant.

Table 5. Variance analysis

Property		Square sum	Levels of freedom	Square mean	Fisher test	Significant
Absorption	Between groups	1199,11	2	599.55	47.95	Yes
	Within groups	37,51	3	12.50	-	-
	Total	1236,62	5	-	-	-

In order to verify the dissimilarities of the groups, the post-hoc Fischer test was performed. It was observed that, statistically, there was no significant difference between the results comparing the crystallizing and water repellent products. However, when compared to untreated samples (control group), a significant reduction in the average absorption rate was obtained, indicating the efficacy of the treatment (Figure 8).

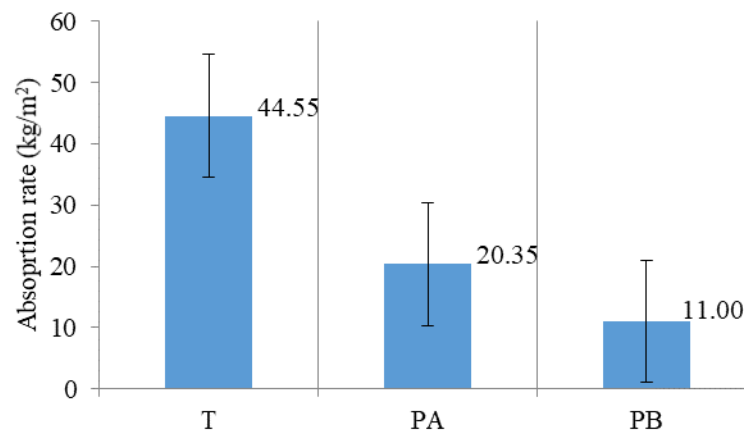


Figure 8. Comparison between the average absorption rates after treatment.

### 4.2 Thermography

The images obtained by the thermography test, Figures 9 to 12, qualitatively demonstrate the specimens' temperature before the treatment (dry wall and wet wall) and at 28 days of treatment. Areas with lighter colors, orange tones, represent higher temperatures (i.e. drier regions).

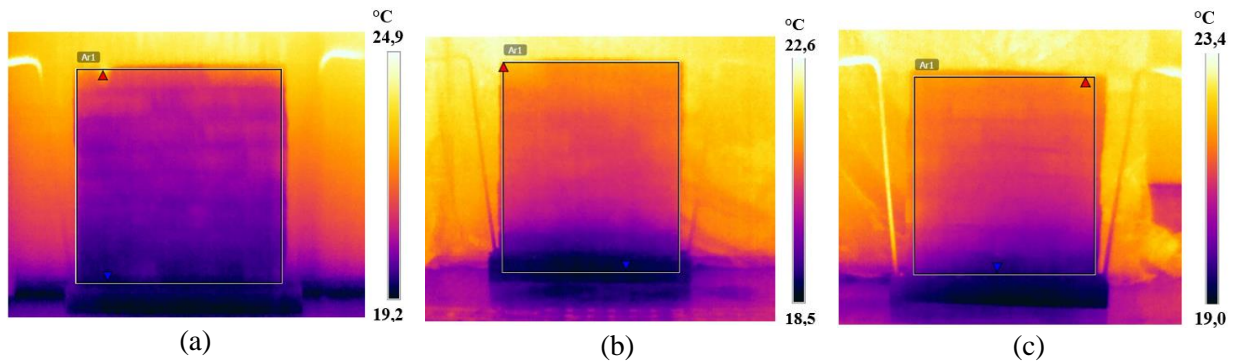


Figure 9. Sample PA1: a) dry wall; b) humid wall; and c) wall at 28 days

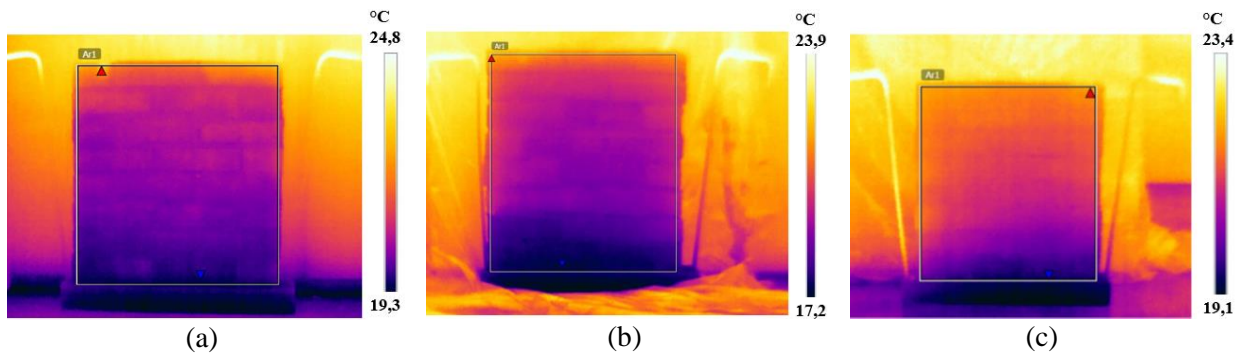


Figure 10. Sample PA2: a) dry wall; b) humid wall; and c) wall at 28 days

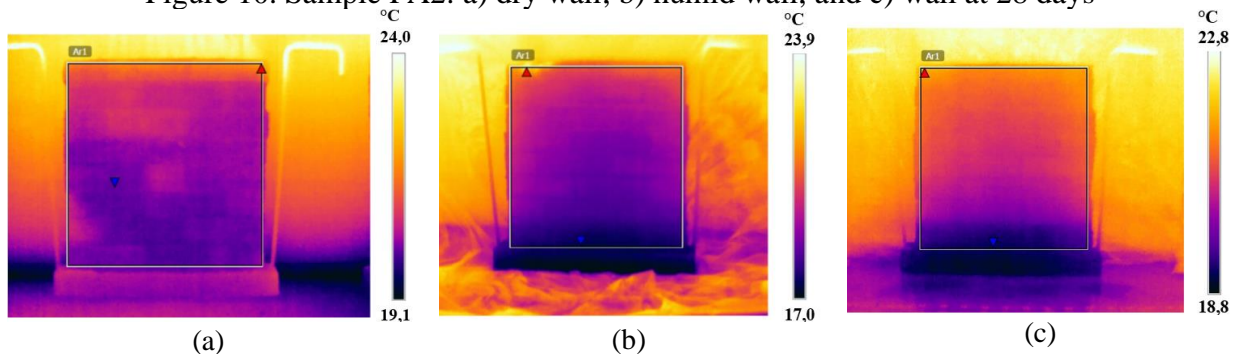


Figure 11. Sample PB1: a) dry wall; b) humid wall; and c) wall at 28 days

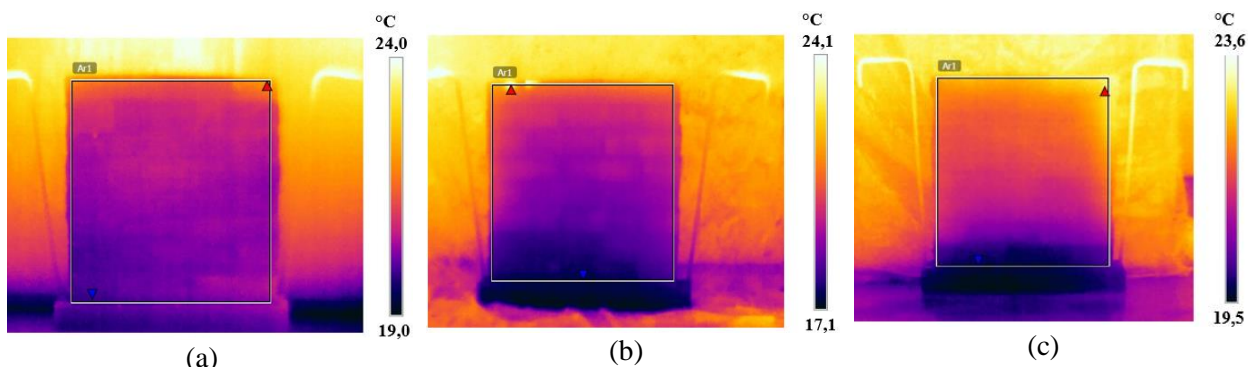


Figure 12. Sample PB2: a) dry wall; b) humid wall; and c) wall at 28 days

In general, the images initially show that, before the treatment and with the dry wall, there was moisture distributed throughout the entire wall, except in the top part and on the edges, due to the greater air contact of these locations. After the saturation of the bases, the walls show an accentuated dark blue band, near the base, which characterizes the presence of ascensional humidity. At 28 days of treatment, a reduction of the moisture range was observed, indicating a favorable outcome of the applied products.

#### 4.3 Cost analysis

When analyzing the performance of the products, both were absorbed by the walls in a period of approximately 1 day, with a consumption per hole of 125 ml for product A (crystallizing) and 60 ml for product B (water repellent). Although the reduction in the water absorption rate, caused by the two products, did not show a statistical difference, the water repellent product presented the best cost-benefit, reaching almost 1/5 of the value of the crystallizing product, as shown in Table 6.

Table 6. Cost analysis

Analysis Parameter	Product		
	A (Crystallizing)		B (Water repellent)
Packing volume (L)	1.00	25.00	18.00
Price (R\$)	36.50	595.00	189.00
Consumption (l/m)	1.25	1.25	0.60
Cost (R\$/m)	45.63	29.75	6.30

The cost per linear meter of the water repellent product was R\$ 6.30, while for the crystallizing product it reached R\$ 29.75, representing an increase of more than 4 times.

## 5. CONCLUSIONS

- It was verified that both products presented a significant reduction in the average water absorption rates of the specimens.
- The crystallizing product generated an average reduction, when compared to the untreated walls, of 32% in the water absorption rate, while the water repellent product 28.18%. However, statistically, this difference was not significant, indicating that both present the same performance.
- Regarding the cost-benefit (a decisive factor in the selection of the blocker), it was concluded that the water repellent product had an advantage over the crystallizing, with a cost about 5 times lower.
- Although the injection system, utilized in this research, was designed to prevent leakage and to control the application velocity, the injection was occasionally obstructed during the application of the crystallizing product, showing the necessity of studying the ideal injection speed. The execution of this technique outside the laboratory environment would probably generate ergonomics problems, due to its complexity on the equipment scope. The necessity of studies on new methods of product application is presented as indispensable on the creation of a more practical in situ system.
- Finally, it should be noted that the occurrence of rising damp is not a simple pathology and the search for knowledge and new techniques, that can improve the performance of buildings and reduce treatment costs, is of great importance.



## 6. REFERENCES

- Alfano, G., Chiancarella, C., Cirillo, E., Fato, I. F. (2006), *Long-term performance of chemical damp-proof courses: twelve years of laboratory testing*. Building and Environment. 41:1060-1069. <https://doi.org/10.1016/j.buildenv.2005.04.017>
- Associação Brasileira de Normas Técnicas. (2005). *NBR 13276: Argamassa para assentamento e revestimento de paredes e tetos – Preparo da mistura e determinação do índice de consistência*. Rio de Janeiro.
- Associação Brasileira de Normas Técnicas. (2005). *NBR 15270: Componentes cerâmicos parte 3: Blocos cerâmicos para alvenaria estrutural e de vedação – Métodos de ensaio*. Rio de Janeiro.
- Bertolini, L. (2010), “*Materiali da costruzione: degrado, prevenzione, diagnose, restauro*”, Editore CittàStudi; 2ª ed., Sondrio/Italy.
- Carrió, J. M. (1997), “*Patología de Cerramientos y Acabados Arquitectónicos*”, Munilla-Leria; 2ª ed., Madrid/Spain.
- Dreyer, J., Hecht, C. (2001), *Injection methods for retrofitting of moisture damaged constructions*. Transactions on the Built Environment. 55: 517-526.
- Franzoni, E. (2018), *State-of-the-art on methods for reducing rising damp in masonry*. Journal of Cultural Heritage. 31: S3-S9. <https://doi.org/10.1016/j.culher.2018.04.001>
- Franzoni, E. (2014), *Rising damp removal from historical masonries: a still open challenge*. Construction and Building Materials. 54: 123-136.
- Franzoni, E., Rirsch, E., Paselli, Y. (2016). “*Laboratory models for the assessment of the effectiveness of chemical damp-proofing in masonry: existing methods and some proposals for new fixtures*”, in: International RILEM Conference Materials, Paris.
- Freitas, R. J. G. (2014), “*Técnicas de tratamento/controle da humidade ascensional – Catálogo*”, Masters Thesis, Faculdade de Engenharia da Universidade do Porto, Porto.
- Freitas, V.P.; Torres, M.I.M.; Guimarães, A. S. (2008), “*Humidade Ascensional*”, FEUP edições; 1.ª ed., Porto/Portugal.
- Guimarães, A. S., Delgado, M. P. Q., De Freitas, V. P. (2016), *Treatment of rising damp in historic buildings: experimental campaign of wall base ventilation and interface effect analysis*. Cultural Heritage. 20: 733-738. <https://doi.org/10.1016/j.culher.2016.02.012>
- Hacquebord, A., Lubelli, B., Lubelli, R., Nijland, T. (2013), *Evaluation of spreading and effectiveness of injection products against rising damp in mortar/brick combinations*. Procedia Chemistry. 8: 139–149. <https://doi.org/10.1016/j.proche.2013.03.019>
- Hess, R. P. J., Lubelli, B. H. A. (2018), *New test methods to verify the performance of chemical injections to deal with rising damp*. Journal of Cultural Heritage. 31: S52-S59.
- Henriques, F. M. A. (1994), “*Humidade em Paredes*”. Lisboa: Laboratório Nacional de Engenharia Civil.
- Henriques, F. M. A. (2007), “*Humidade em Paredes*”. Lisboa: Laboratório Nacional de Engenharia Civil.
- I'anson, S. J., Hoff, W. D. (1988), *Chemical injection remedial treatments for rising damp–I. The interaction of damp-proofing fluids with porous building materials*. Building and Environment. 23: 171-178. [https://doi.org/10.1016/0360-1323\(88\)90001-7](https://doi.org/10.1016/0360-1323(88)90001-7)
- Larsen, P. L. (2012), *Determination of water content in brick masonry walls using a dielectric probe*. Journal of Architectural Conservation. 18, 47-62. <https://doi.org/10.1080/13556207.2012.10785103>
- Lubelli, B., Van Hees, R. P. J., Hacquebord, A. (2013), *Experimental study of the distribution of chemical products against rising damp in substrates with different water saturation degrees*. Construction and Building Materials. 40: 891-898. <https://doi.org/10.1016/j.conbuildmat.2012.11.062>

- Luso, E. (2002), “*Contribuição para intervenções no Centro Histórico de Bragança*”. Masters Thesis, Universidade de Minho, Minho.
- Massari G., Massari I. (1993), *Damp Buildings, Old and New*. ICCROM, 17: 2-30.
- Rirsch, E., Zhang, Z. (2010), *Rising damp in masonry walls and the importance of mortar properties*. Construction and Building Materials. 24: 1815-1820. <https://doi.org/10.1016/j.conbuildmat.2010.04.024>
- Sandrolini, F., Franzoni, E. (2016), *An operative protocol for reliable measurements of moisture in porous materials of ancient buildings*. Building and Environment. 41: 1372-1380. <https://doi.org/10.1016/j.buildenv.2005.05.023>
- Socoloski, R. F. (2015), “*Tratamento de umidade ascensional em paredes através de barreiras químicas por gravidade*”, Masters Thesis, Universidade Federal do Rio Grande do Sul, Porto Alegre.
- Socoloski, R. F., Masuero, A. B. (2019), *Evaluation of the efficiency of the treatment for rising damp on walls through the insertion of chemical barriers by gravity*. Construction and Building Materials. 210: 660-672. <https://doi.org/10.1016/j.conbuildmat.2019.03.018>
- Torres, I. M. (2013), *Wall base ventilation system to treat rising damp: the influence of the size of the channels*. Journal of Cultural Heritage. 15: 121-127. <https://doi.org/10.1016/j.culher.2013.03.005>
- Torres, R. J. de M. M. (2014), “*Humidades ascensionais em paredes de alvenaria de edifícios antigos*”, Masters Thesis, Instituto Superior Técnico (IST), Lisboa, 2014.

## Influence of the void ratio of cellular concrete on the corrosion of steel reinforcement

C. F. G. Nascimento<sup>1\*</sup> , A. A. Demétrio Filho<sup>2</sup> , T. M. Silva<sup>3</sup> , I. A. R. Teixeira<sup>2</sup> ,  
D. C. M. Neves<sup>2</sup> , E. C. B. Monteiro<sup>1,2</sup> 

\*Contact author: [carlosfernando.gn@gmail.com](mailto:carlosfernando.gn@gmail.com)

DOI: <https://doi.org/10.21041/ra.v12i1.507>

Reception: 06/09/2020 | Acceptance: 09/12/2021 | Publication: 01/01/2022

### ABSTRACT

The objective of this study was to understand whether voids intensify the triggering of reinforcement corrosion in cellular concrete, for slabs with light specific masses. The methodology was based on four tests: visual inspection, corrosion potential, electrical resistivity, and mass loss. In relation to the L1 family, the L2 and L3 families (higher air content) were shown to be more susceptible to reinforcement corrosion and mass loss from the steel bars in 90% of cases. However, the behavior of some slabs indicates the possibility of the process being asymptomatic with regard to staining, considering that the influence of the cover on the corrosion of the steel bars was verified.

**Keywords:** void ratio; lightweight concrete; reinforcement corrosion.

**Cite as:** Nascimento, C. F. G., Demétrio Filho, A. A., Silva, T. M., Teixeira, I. A. R., Neves, D. C. M., Monteiro, E. C. B. (2022), "Influence of the void ratio of cellular concrete on the corrosion of steel reinforcement", Revista ALCONPAT, 12 (1), pp. 76 – 97, DOI: <https://doi.org/10.21041/ra.v12i1.507>

<sup>1</sup>Laboratório de Estruturas e Materiais de Construção Civil, Universidade Católica de Pernambuco, Recife/PE, Brasil.

<sup>2</sup>Laboratório Avançado de Materiais de Construção Civil, Universidade de Pernambuco, Recife/PE, Brasil.

<sup>3</sup>Departamento de Materiais de Construção Civil, Universidade Federal de Santa Catarina, Florianópolis/SC, Brasil.

#### Contribution of each author

In this work, the author A. A. Demétrio Filho, contributed with the original idea and with the conception of the study. The author E. C. B. Monteiro was responsible for the supervision and guidelines for writing the paper. The author I. A. R. Teixeira contributed 60% and the author D. C. M. Neves 40% of the data collection. Author C. F. G. Nascimento was responsible for summarizing the results, discussions and laboratory analysis. Finally, the author T. M. Silva contributed with the closing and conclusions of the paper.

#### Creative Commons License

Copyright 2022 by the authors. This work is an Open-Access article published under the terms and conditions of an International Creative Commons Attribution 4.0 International License ([CC BY 4.0](https://creativecommons.org/licenses/by/4.0/)).

#### Discussions and subsequent corrections to the publication

Any dispute, including the replies of the authors, will be published in the third issue of 2022 provided that the information is received before the closing of the second issue of 2022.

## **Influência do índice de vazios do concreto celular na corrosão das barras de aço**

### **RESUMEN**

O objetivo deste estudo foi compreender se os vazios intensificam o desencadeamento da corrosão de armaduras no concreto celular, utilizando placas com massas específicas leves. A metodologia foi baseada em quatro testes: inspeção visual, potencial de corrosão, resistividade elétrica e perda de massa. Em relação à família L1, as famílias L2 e L3 (maior teor de ar) mostraram ser mais suscetíveis à corrosão de armaduras, bem como na quantidade de massa perdida das barras de aço, em 90% dos casos. Entretanto, o comportamento de algumas placas indica que existe a possibilidade de o processo ser assintomático em relação ao manchamento, considerando que a influência do cobrimento foi verificada no processo de corrosão das barras de aço.

**Palavras-chave:** índice de vazios; concreto leve; corrosão das armaduras.

## **Influencia del porcentaje de vacíos del concreto celular en la corrosión del acero de refuerzo**

### **RESUMEN**

El objetivo de este estudio fue comprender si los vacíos intensifican el desencadenamiento de la corrosión de la armadura en el hormigón celular, utilizando losas con masas específicas ligeras. La metodología se basó en cuatro pruebas: inspección visual, potencial de corrosión, resistividad eléctrica y pérdida de masa. En relación con la familia L1, las familias L2 y L3 (mayor contenido de aire) se mostraron más susceptibles a la corrosión de las armaduras, así como en la cantidad de masa perdida de las barras de acero en el 90% de los casos. Sin embargo, el comportamiento de algunas losas indica que existe la posibilidad de que el proceso sea asintomático en cuanto a la mancha, considerando que se verificó la influencia de la cubierta en el proceso de corrosión de las barras de acero.

**Palabras clave:** porcentaje de vacíos; hormigón ligero; corrosión del refuerzo.

### **Legal Information**

Revista ALCONPAT is a quarterly publication by the Asociación Latinoamericana de Control de Calidad, Patología y Recuperación de la Construcción, Internacional, A.C., Km. 6 antigua carretera a Progreso, Mérida, Yucatán, 97310, Tel.5219997385893, [alconpat.int@gmail.com](mailto:alconpat.int@gmail.com), Website: [www.alconpat.org](http://www.alconpat.org)

Reservation of rights for exclusive use No.04-2013-011717330300-203, and ISSN 2007-6835, both granted by the Instituto Nacional de Derecho de Autor. Responsible editor: Pedro Castro Borges, Ph.D. Responsible for the last update of this issue, Informatics Unit ALCONPAT, Elizabeth Sabido Maldonado.

The views of the authors do not necessarily reflect the position of the editor.

The total or partial reproduction of the contents and images of the publication is carried out in accordance with the COPE code and the CC BY 4.0 license of the Revista ALCONPAT.

## 1. INTRODUCTION

Reinforced concrete is one of the most commonly-used construction materials in the world due to its physical and mechanical properties, which includes issues regarding its durability. These factors stimulate interest in the search for new technologies and new compounds as proposed improvements of certain characteristics or to its applicability (Mechtcherine et al., 2020; Nguyen; Castel, 2020; Kanellopoulos et al., 2020).

Improvements to materials technology has made it possible to produce concrete with special characteristics, such as lightweight concrete used for thermal insulation. The widespread use of this material is particularly attributed to its benefits of reducing specific mass and density, savings related to formwork, reinforcement, and in transportation costs, in the case of precast structures (Khodabakhshian et al., 2018; Zhang et al., 2020).

Cellular concrete is another type of low-density material, which is the main object of study in this paper, where it has been produced with additives that produce air bubbles within the concrete, decreasing its specific mass (Stumm; Schweike; Stemmermann, 2018; Trong; Asamoto; Matsui, 2018; He et al., 2018; He et al., 2019). Considering the many uses of cellular concrete because of to its lightness and lower specific weight, there is concern regarding the use of this material for reinforced concrete structural members, due to its potential behavior with regard to the propagation of steel reinforcement corrosion from the number of voids within the material and its lower mechanical strength (Du et al., 2020).

Concrete durability is an essential issue, as it makes it possible to understanding a material's performance throughout a structure's lifetime (Kashani et al., 2017). Moreover, it can be affected by the action of external aggressive agents, such as chloride ions or carbon dioxide - CO<sub>2</sub> (Shon et al., 2018; Nascimento et al., 2021).

One of the principal problems related to the durability of reinforced concrete is the corrosion of steel bars leading to the degradation or loss of the structural properties of the material. According to Badar et al., (2014), good quality concrete provides the necessary conditions to promote the pH of the passivation layer of the steel.

The central question of this study is to determine if the voids present from the incorporation of air within the cellular concrete mitigate the corrosion of the steel bars and make the process asymptomatic, i.e., without cracks or stains on the external face of the element? This hypothesis becomes viable by observing that concrete that undergoes a freeze-thaw cycle can be protected by the intentional incorporation of air.

In summary, then, the main objective of the study is to evaluate the behavior of reinforced concrete elements under the corrosion process when using cellular concrete (with incorporated air). This research not only provides a reference to determine the behavior of cellular concrete, but also as a proposal that covers some useful information for its application in the construction industry.

In summary, the main objective of this study is to evaluate the behavior of reinforced concrete elements under corrosion when using cellular concrete (with incorporated air). This study not only provides a reference to determine the behavior of cellular concrete, but also gives information useful for its application in the construction industry.

## 2. EXPERIMENTAL PROCEDURE

### 2.1 Materials

To manufacture the cellular concrete, the parameters studied by Mariz (2013), who performed durability evaluations on cellular concrete, were used. The test parameters were selected as the initial basis for the dosing procedures and their results, in terms of specific mass, were similar to those analyzed in this study.

The type of cement used was the national brand CPV – ARI MAX. This type of agglomerate was chosen due to its quick strength gain and absence of additives.

The added mineral content contained in other types of cement could contribute to the thinning and filling of pores within the concrete, which hinders the entry of aggressive agents and, consequently, prevents the corrosion of the steel bars from starting.

Natural fine aggregate of quartz origin (sand), from the Recife Metropolitan Area, was used. The natural sand was purchased for its specific physical characteristics and was acquired in a humid state, making it necessary to correct its water content through natural drying. To ensure the proper moisture content, 600 g of material were placed in an oven for 24 hours at a temperature of  $100^{\circ}\text{C} \pm 2^{\circ}\text{C}$  and, following this, 300 g were used for the granulometric characterization test, taking into account the fine aggregate granulometry according to the NBR NM 248 standard (ABNT, 2003). It was necessary to analyze the optimum usage zone of the fine aggregate (sand), because it can influence the ideal density of the cementitious composite (concrete). Through the aggregate particle size distribution, it was possible to obtain parameters such as the fineness modulus (FM) of 2.93 and the maximum diameter ( $D_{\text{max}}$ ) of 4.5 mm, classifying the material as fine aggregate with well-distributed medium grains. The results can be seen in (Figure 1).

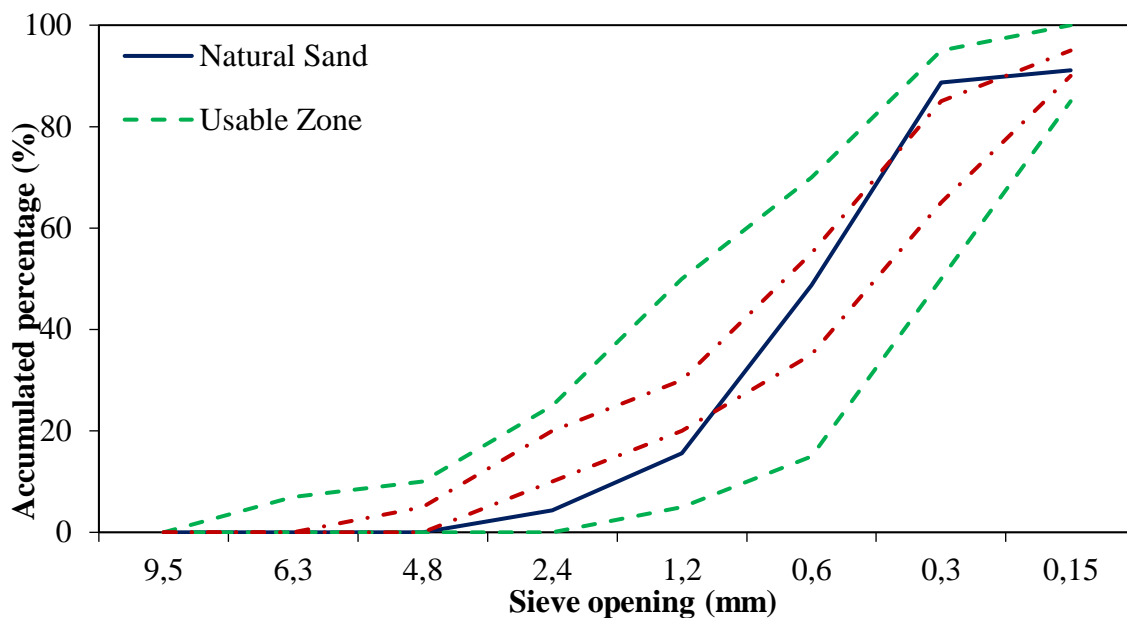


Figure 1. Granulometric curve (fine aggregate).

The coarse aggregates (gravel) were also analyzed and, the granulometric classification showed them to have a  $D_{\text{max}}$  of 12.5 mm and an FM of 6.48. This value was chosen by taking into account the thickness of the concrete plate ( $e = 50$  mm), respecting the recommendation that  $D_{\text{max}}$  be less than or equal to  $1/4$  of the smallest dimension of the mold. The granulometric curve of the material was not determined in this study, but the type of aggregate used was classified as gravel 1.

The additives used were: additive 1 - Techniflow 520, from MC Bauchemie. This plasticizer was used in the concrete matrix dosage with normal specific mass (family R); additive 2 - Gethal 2011, from Gethal. This is an atmospheric-based concentrated organic/chemical additive. It is used in the production of concrete with specific mass lower than  $2000 \text{ kg/m}^3$  (L1, L2, and L3 families).

After preliminary tests, the uniform mix used to produce the specimens was:  $1_{\text{Cement}} : 2.2_{\text{Sand}} : 2.6_{\text{Gravel}} : 0.60_{(w/c)}$  by weight, which is, in mass,  $353 \text{ kg/m}^3$  of cement,  $776.6 \text{ kg/m}^3$  of sand,  $917 \text{ kg/m}^3$  of gravel, and 211.8 liters of water;  $M\% = 55\%$  (mortar content);  $A\% = 10.5\%$  (water-dry matter ratio); and Plasticizer additive =  $0.6\%$ . For the light concrete, the plasticizer additive was replaced by an air filter ( $0.1\%$  of the cement mass), varying the mixing time.

## 2.2 Methods

### 2.2.1 Preparation of the steel bars

Before testing, the bars were sanitized according to the G1-03 international standard (ASTM, 2017). A total of 72 steel bars of each gauge (6.3 mm, 8.0 mm, and 10.0 mm) were cut to a length of 30 cm, and 48 bars of each gauge were cut to a length of 20 cm. Following this, the steel bars were placed in a solution of 500 ml of hydrochloric acid, 3.5 g of hexamethylenetetramine, and 1 L of water, for 15 minutes. Then, they were washed under running water with the help of steel brushes, to remove the surface oxide layer and impurities. After drying, the bars were weighed before inducing the corrosive process.

### 2.2.2 Specimens used for analysis

The methodology used to develop this study was organized to be able to understand the behavior of lightweight reinforced concrete elements (cellular concrete) undergoing corrosion of its steel reinforcement. Throughout the process, the material elements were evaluated through electrochemical tests (corrosion potentials and resistivity) and physical tests on the steel bars (mass loss and tensile strength). The specimens were configured in the form of a plate, (35 cm wide x 35 cm high x 5 cm thick) as shown in (Figure 2).

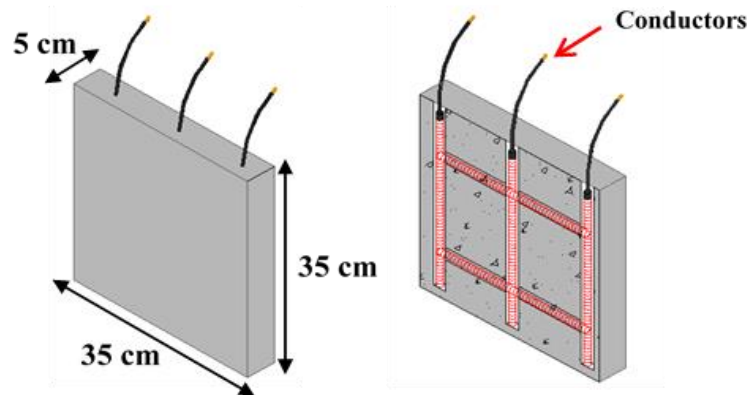


Figure 2. Schematic representation of the test specimen configuration.

The copper conductors made it possible to electrically connect the steel bars from the exterior, thereby controlling the corrosion potential. The choice of 5-cm-thick plates was made in order to facilitate the activation of the corrosive process through the entrance of chloride ions, by reducing the distance between the bar and the external surface. The samples were distributed between concrete having a common specific mass (reference) and three types of cellular concrete families (L1, L2 and L3) with light specific masses. This distribution can be seen in (Table 1).

Table 1. Number of plates developed and their mechanical behavior.

Concrete family	Specific mass in the fresh state (kg/m <sup>3</sup> )	Steel gauges – CA 50 (mm)			Total number of specimens	Compressive strength (MPa)
		6.3	8.0	10.0		
<b>R</b>	2.3	6	6	6	18	33.5
<b>L1</b>	1.9	6	6	6	18	8.94
<b>L2</b>	1.7	6	6	6	18	2.15
<b>L3</b>	1.5	6	6	6	18	0.61

For purposes of analysis, a steel mesh made of three vertical bars and two horizontal bars was developed, making a total of five steel bars in each concrete mold. The vertical bars serve as connecting elements for the three horizontal bars (Figure 3), creating a greater density of steel within the plate and, consequently, increasing the possibility of observing the characteristic symptoms of steel corrosion.

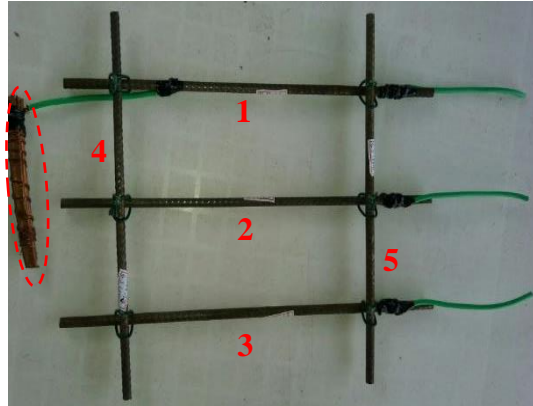


Figure 3. Organization and connection of the steel bars.

To produce the specimens, eight 18-mm thick slabs (2.10 m x 1.20 m) of coated wood were used. The coated formwork was chosen to provide a better surface finish for the concrete slabs and, in addition, to optimize their production, transportation, and concreting. A rectangular mold of dimensions (1.50 m x 0.65 m x 0.35 m), with internal partitions, was chosen. Each rectangular mold contained 36 forms. This mold is shown in (Figure 4).



Figure 4. Rectangular mold capable of producing 36 specimens.

### 2.2.3 Concrete specimen production and formwork removal

A total of 72 slabs (35 cm x 35 cm x 5 cm) were produced, and cylindrical specimens were also made for the mechanical characterization tests, but those results were not presented in this study. Due to the thinness of the plates, in order to facilitate the concreting operation and to guarantee a good finishing and filling of the molds, no spacers were used to align the steel mesh. The bars were centered inside the molds by hand. After removing the plates, they were kept protected from direct rain and sunlight for 28 days, and the wetting and drying process using a salt water solution was started. Before the start of the corrosion process, a visual inspection and photographic registration was performed to maintain the external physical characteristics of the plates.



### 2.2.4 Inducing corrosion of the steel bars

Two procedures were used to induce corrosion in the steel bars within the concrete plates. The first procedure, called (type 1), used the principle of galvanic corrosion. The copper functions as a cathode and the steel becomes the anode, losing electrons (corrosion). The material was also connected to the steel mesh (Figure 5 (a) and (b)) of each plate, located at the bottom of the formwork.

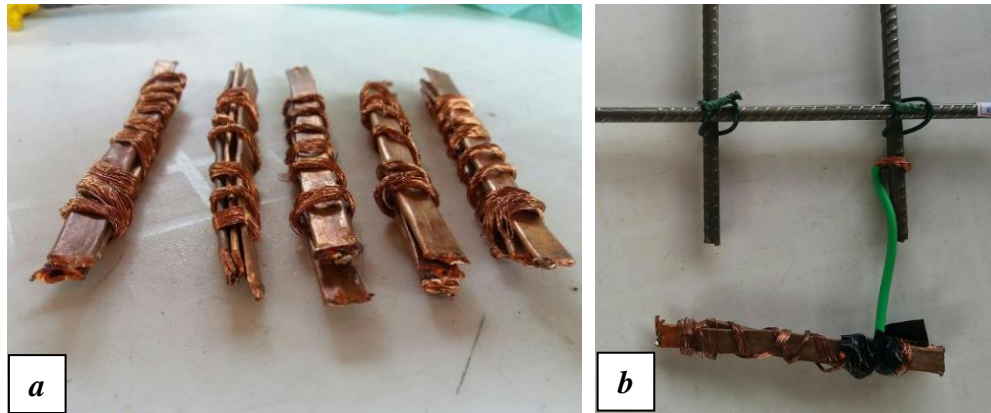


Figure 5. (a) Copper used to induce galvanic corrosion; (b) Material connected to the steel mesh.

The second procedure (type 2) to induce corrosion was performed by passing the already molded concrete slabs (Figure 6 (a) and (b)), through repeated wet and dry cycles with 5% NaCl (sodium chloride) solution, following procedures found in the literature and in the study conducted by Ye et al., (2017). After 28 days, visual inspection and electrochemical tests (potential and resistivity) were performed, before beginning the plate immersion process. A complete cycle consisted of three days of immersion (with about 25 cm of water covering the plates) and four days of air drying (protected from direct sunlight).

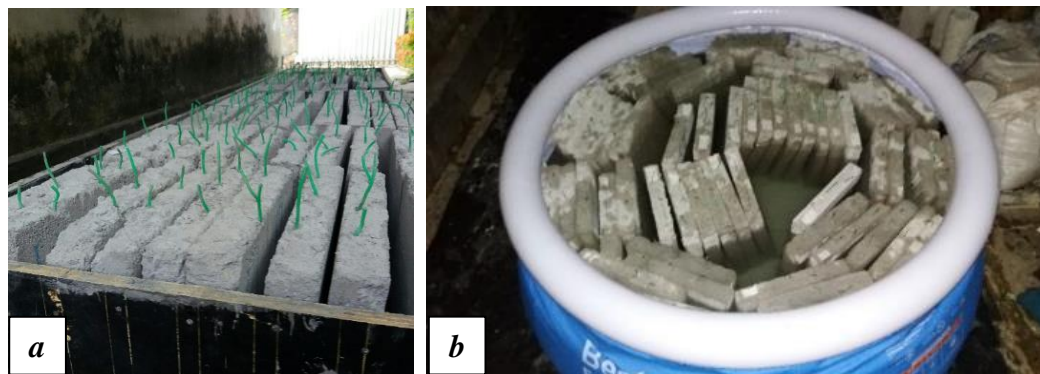


Figure 6. (a) Cast concrete specimens; (b) Concrete slabs in NaCl solution for induction of chloride ions.

### 2.2.5 Tests for control of concrete production

During the production of the concrete, two tests were performed to control its characteristics. These were: specific mass of concrete in the fresh and hardened state, performed according to NBR 9833 (ABNT, 2008) with the result obtained for lightweight concrete according to the procedures instituted by NBR 12644 (ABNT, 2014).

Concrete characterization tests were performed for each family according to their specific mass, in order to have comparative parameters and their respective behaviors for the steel bar corrosion process.

**2.2.6 Covering of the steel bars and thickness of the concrete plates**

In order to verify the covering of the steel bars on both faces of the slabs after concreting, electromagnetic sensors were used. This equipment, Hilti's Ferroskan PS200, was used to estimate the average covering of the bars on each of the slabs. In addition, images were taken to verify the positioning of the bars. A and B were nomenclatures given to the faces of the plates to represent the positioning of the steel mesh, as indicated in (Figure 7).

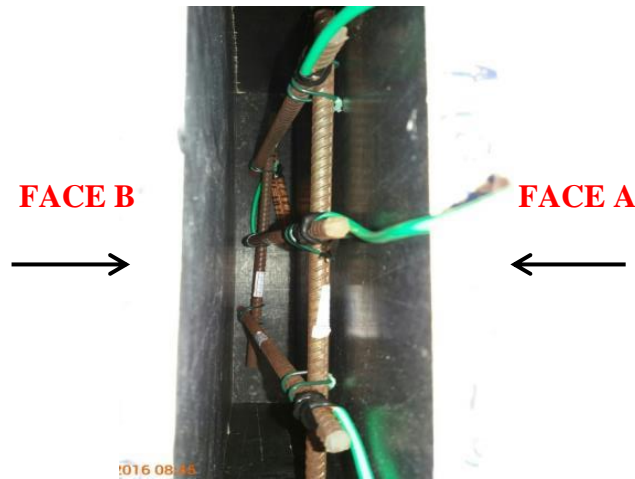


Figure 7. Schematic representation of faces A and B of the plates.

The thickness of the plates was measured with a tape to calculate the coverage of the steel bars in relation to face A.

**2.2.7 Physical monitoring tests**

The physical monitoring test was divided into two phases: visual inspection of the slabs and mass loss. With regard to visual inspection, a first analysis was performed a few days after concreting and before beginning the wetting and drying cycles. During the study period, other visual inspections were performed at the end of each immersion cycle to monitor the evolution of degradation. To analyze the visual appearance of the slabs, a criterion was developed for this study based on the existence of corrosion stains and characteristic cracks that can appear on the surface, as shown in (Table 2).

Table 2. Criterion for visual evaluation of the degradation of the slab.

Without stains or cracks	Not relevant	●
Up to three small stains	Slight deterioration	●
Between four and five small stains and/or one large one	Moderate	●
More than five small stains and/or more than one large one	High	●
Cracks and spots of corrosion	Very high	●

The second type of physical monitoring test was the evaluation of the mass of the bars lost at the end of the corrosion process. With this information, it was possible to verify which plates and which families were most affected by exposure to the aggressive agent. After removing all of the steel bars, they were cleaned with a solution of hydrochloric acid and water to remove all concrete residues that may have adhered to the bars, as well as any excess corrosion products. After a thorough cleaning, each bar was weighed to verify its mass loss, comparing the values before and after the study period. NBR 7480 (ABNT, 2007) indicates the requirements and criteria for the use of steel bars for reinforced concrete. In this case, the standard establishes a value for the mass of the bars per unit length, according to each gauge, as well as tolerance values.

### **2.2.8 Electrochemical monitoring tests**

Two types of tests were used to monitor the evolution and likelihood of corrosion of the steel bars present in the slabs over time: corrosion potential and resistivity of the concrete surface. The corrosion potential test was performed according to C 876 (ASTM, 2015), which provides guidelines to evaluate the test criteria. The equipment used was Canin+ from Proceq+. Twelve points on each plate were tested: three horizontal lines, one at the top, one in the middle, and one at the bottom, with four points on each line. These points were located 10 cm apart. In this way, it was possible to map the full corrosion potential of the plates.

To measure the surface resistivity of the concrete, the four-electrode method (Wenner method) was used, with the Resipod equipment from Proceq. As with the corrosion potential test, water was sprayed onto the concrete surface before taking readings. As recommended by TC154-EMC (RILEM, 2003), each resistivity measurement taken was an average of five readings taken a few millimeters apart. Before the start of each wetting and drying cycle, in other words, after the four-day drying period and immediately prior to re-immersion of the slabs in water, the electrochemical monitoring tests mentioned above were performed.

## **3. RESULTS AND DISCUSSIONS**

The central question of this study is whether or not the corrosion of steel bars in cellular concrete can be asymptomatic (without cracks or stains), different from traditional concrete and, for this, some considerations must be made. No cracks were observed in any of the cellular concrete slabs nor in the reference mixture (R). As for staining, only 7 slabs (10%) were asymptomatic, three from the R family and four from the L1 family.

It was not possible to state, based only on the conditions of this study, that the corrosion of steel bars in lightweight concrete will not generate cracking. Namkung et al., (2019) and Pachla et al., (2021) state that, for higher mass loss values, greater than those found here, a greater volume of corrosion products is generated, leading to greater expansion stresses and, consequently, the emergence of micro cracks.

According to Zhang et al., (2020), porosity and pore size have a significant effect on the mechanical behaviors of cellular concrete. The initial compaction phase of the material depends on porosity to a certain degree, which is explained by the collapse and compaction of surface pores or defects. Although 90% of the slabs had staining at different intensities, the variable covering of these slabs must be taken into account.

Stains occurred most frequently on face "A". When analyzing the estimated amount of covering, in general, for all families, face "A" was thinner than face "B". It is possible that different behaviors might be found with greater and more uniform coverage.

An interesting piece of information about the slabs from the L1 family, which were asymptomatic, is related to their coverage of the steel bars. Three of the four had thinner covers than the family average, and still showed no crack formation. These results do not agree with the analyses performed by Green (2020), who reported that the corrosion process, and consequently the staining, was independent of the covering of the steel bars and occurred expressively in aggressive environments.

The plates from families L2 and L3, the most porous ones, were visually classified as being more degraded, which was also verified by the loss of mass seen in the electrochemical monitoring tests. There was also a marked decrease in compressive strength when larger amounts of air were integrated into the concrete. Some of the slabs had a greater steel bar mass loss, and the L3 family had the second highest loss percentage.

For higher levels of mass loss, it is expected that a greater amount of corrosion products will be formed and this will appear more intensely on the surface of the slabs, as seen in the study by Du et al., (2020). However, the result of some of the plates, with regard to the corrosion process and staining was contrary to expectations. These slabs were visually classified as having mild degradation. This is an example where there is a possibility of the pores "absorbing" the stains (Figure 8 (a) and (b)) and in (Figure 9 (a) and (b)). This behavior was also seen by Liu et al., (2020) and Liu et al., (2021).

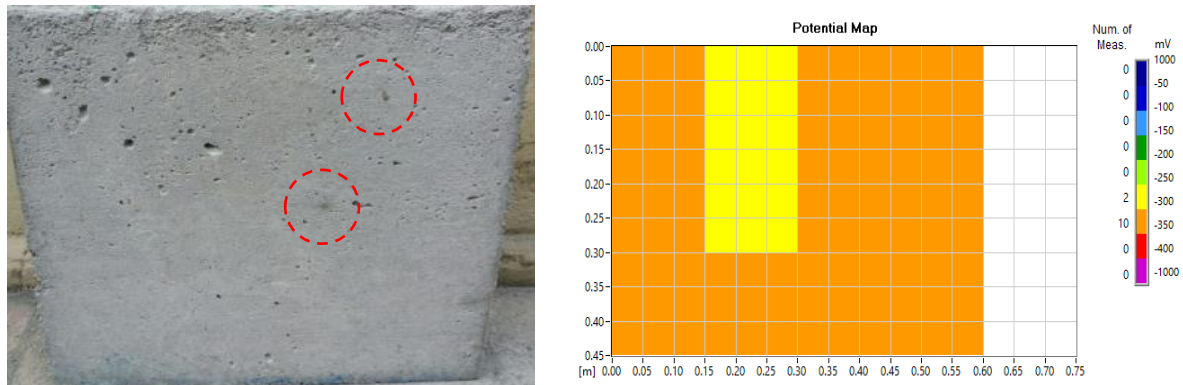


Figure 8. (a) "Absorption" of corrosion products through the pores; (b) Map of corrosion potential (no severe effects apparent).

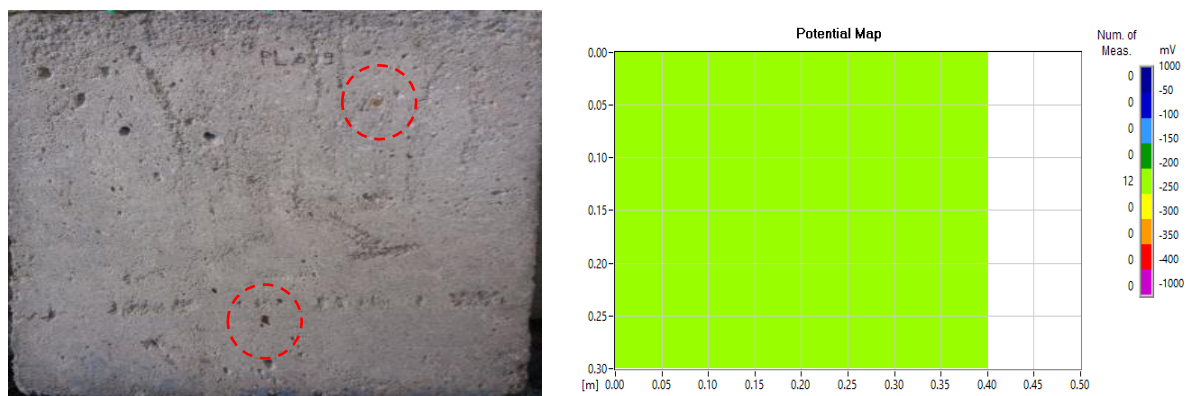


Figure 9. (a) "Absorption" of corrosion products through the pores; (b) Map of corrosion potential (no severe effects apparent).

Even if this is only an isolated occurrence, it should not be ignored. With respect to durability and other concrete properties, it was observed that the lightweight concrete studied was more susceptible to steel bar degradation than the reference concrete.

Chung et al., (2019), Dong et al., (2020), and Al-Shwaiter, Awang, and Khalaf (2021) reported that the incorporation of low-density materials into concrete reduces energy consumption, with characteristics that meet the minimum mechanical properties to be effectively used as building materials.

### 3.1 Visual inspection

Of the 18 slabs in each family, 67% of the R group were classified as having a light degree of degradation and two were not relevant. The second "best" family in terms of least visual degradation, L1, had only two slabs classified as having a high degree of degradation. The two most visually degraded families, according to the proposed classification, were L2 and L3, having 44% and 61% of the slabs classified with a high degree of degradation, respectively. These analyses can be better seen in (Figure 10).

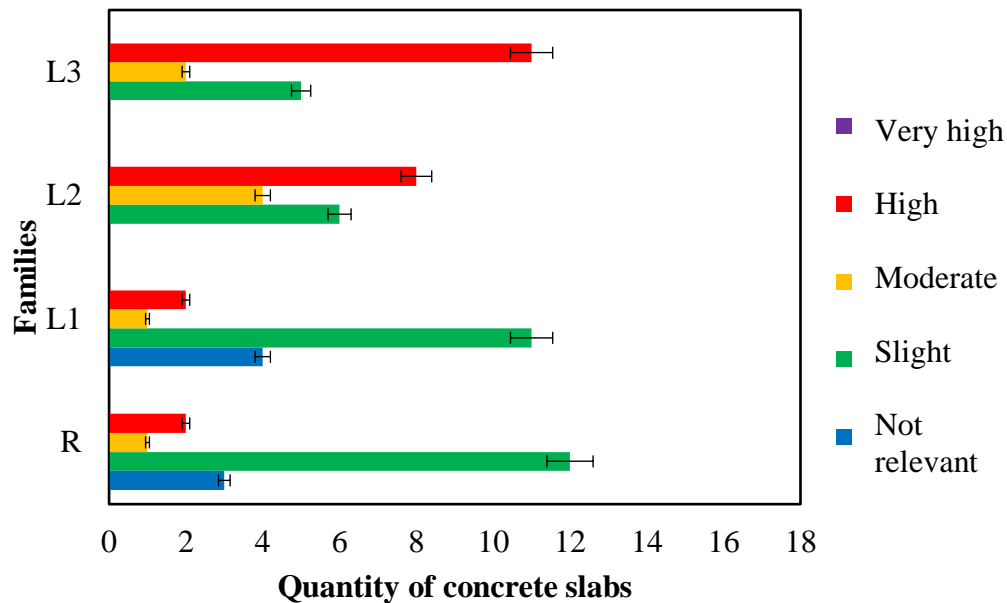


Figure 10. Qualitative classification of the level of visual degradation of the slabs.

Regarding the physical behavior of the concrete slabs, it was noticed that the  $\text{Na}^+\text{Cl}^-$  (sodium chloride) solution triggered the corrosion of the steel bars, where some stains could be seen on the surface of the slabs. In (Figure 11 (a) and (b)), corresponding to plate family R, a high level of degradation was not evidenced and the values on corrosion potential map ranged from -350 mV to -400 mV.

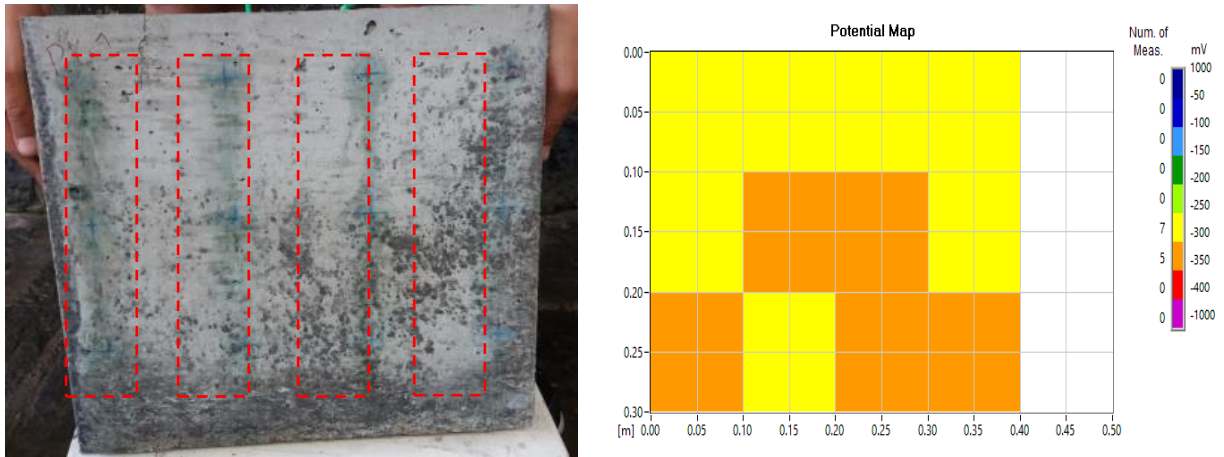


Figure 11. (a) Effects of surface degradation on the concrete slabs; (b) Map showing the corrosion potential (mild effects).

As for the slabs of family L1, it was noticed that the degradation caused by the presence of sodium chloride affected the durability of the steel bars, as seen in (Figure 12 (a) and (b)). The corrosion occurred at specific points on the plate and the surface stains occurred in the regions where the concrete layer was thinner. The mapping of the corroded steel bars, showed that the corrosion potential values ranged from -250 mV to -350 mV.

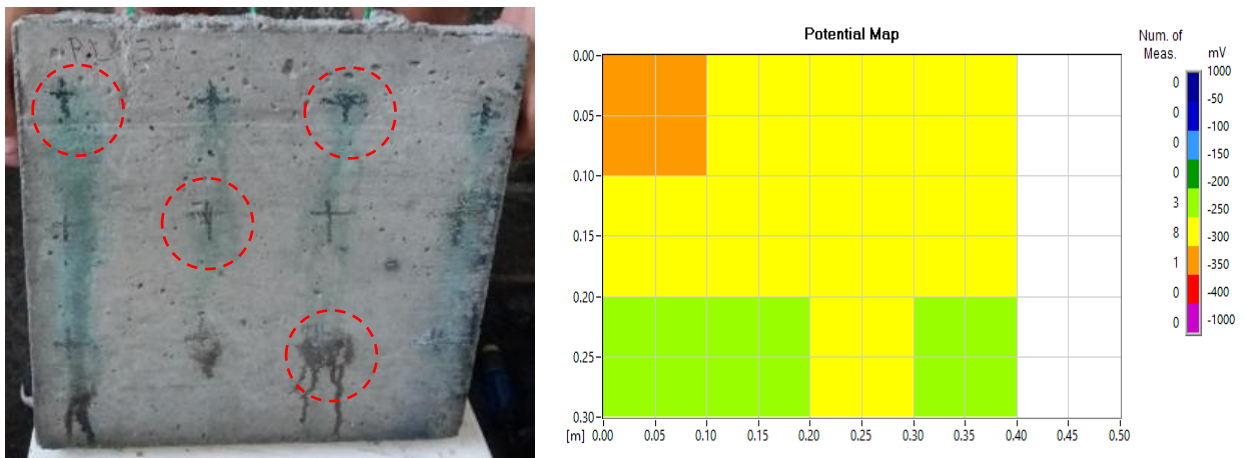


Figure 12. (a) Effects of surface degradation on the concrete slabs; (b) Map of corrosion potential (mild effects).

The degradation of the steel reinforcement within the concrete slabs of families L2 and L3 was the most severe, and the surface stains caused by the transport of oxides to the surface occurred because the physical behavior inside the material. The incorporated air content resulted in a higher void index that facilitated the ingress of chloride ions, leading to corrosion and pitting. The mapping of the corroded steel bars showed corrosion potential values ranging from -400 mV to -1000 mV for both families, as shown in (Figure 13 (a) and (b)) and (Figure 14 (a) and (b)).

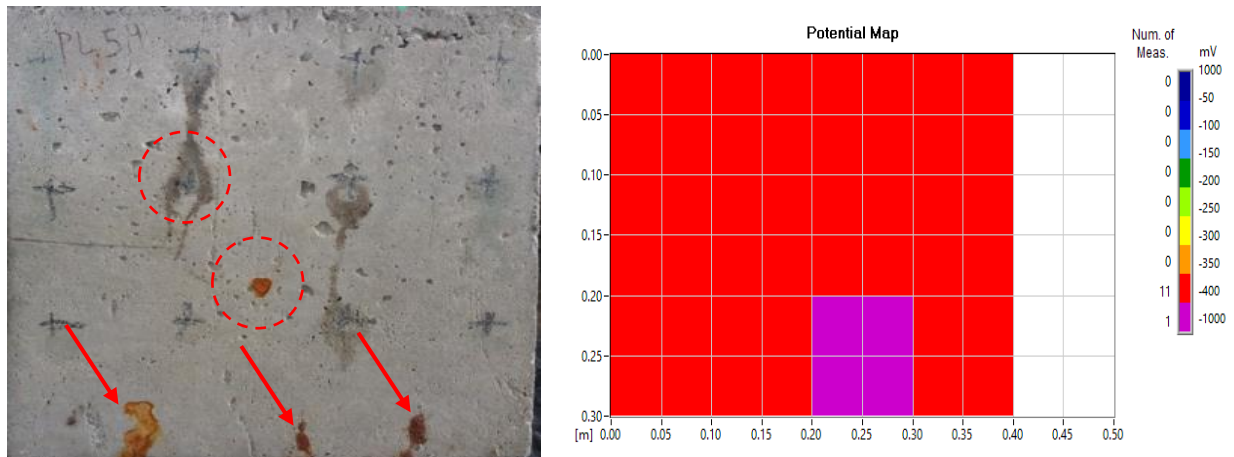


Figure 13. (a) Effects of surface degradation on the concrete slabs; (b) Map of corrosion potential (severe effects).

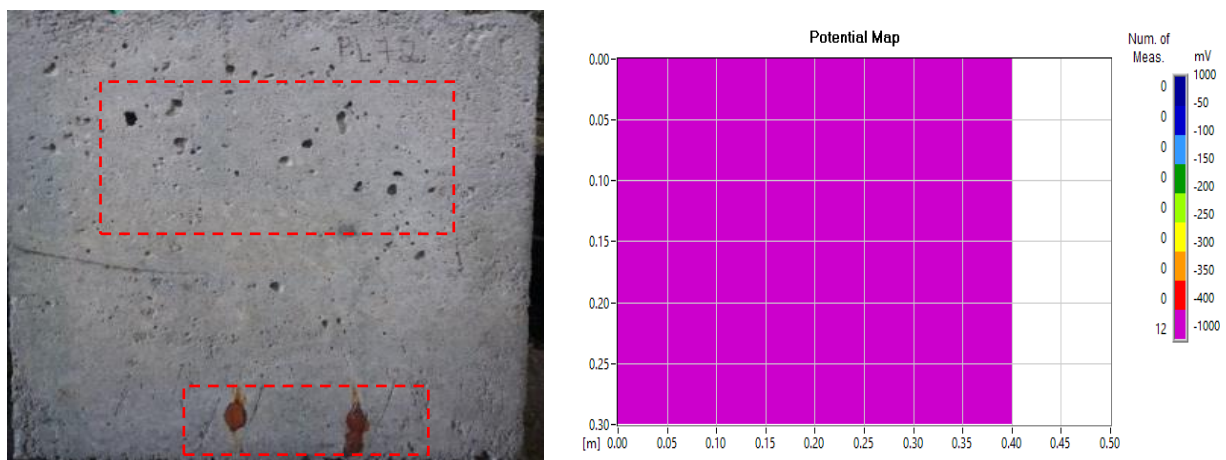


Figure 14. (a) Effects of surface degradation on the concrete slabs; (b) Map of corrosion potential (severe effects).

### 3.2 Corrosion potential

The evaluation criteria followed the procedures proposed by C 876 (ASTM, 2015). Values that are more electronegative than  $-350$  mV have a 90% probability of corrosion, while values more electropositive than  $-200$  mV have only a 10% probability of corrosion.

Values between these limits lie in the uncertainty range. During the experimental period, six tests were performed to measure the corrosion potential of the plates. The first was performed only a few days after concreting and the second immediately before the start of the NaCl immersion cycles. The other tests were performed during the study to follow the evolution of the corrosion of the steel bars contained in the concrete slabs.

The results of the corrosion potential tests for each family can be seen in (Figure 15). It is understood that the value representing the corrosion potential of the plate should be the most electromechanical (i.e., the one in the worst condition) among the 12 measured points.

The darkest points seen after the test, show the regions where readings were taken in an area of (10 cm x 10 cm). Among the 12 measurements of the corrosion potential, 10 fall within the region of uncertainty, but with values close to the safe range. The other two points were within an area having less than 10% probability of corrosion.

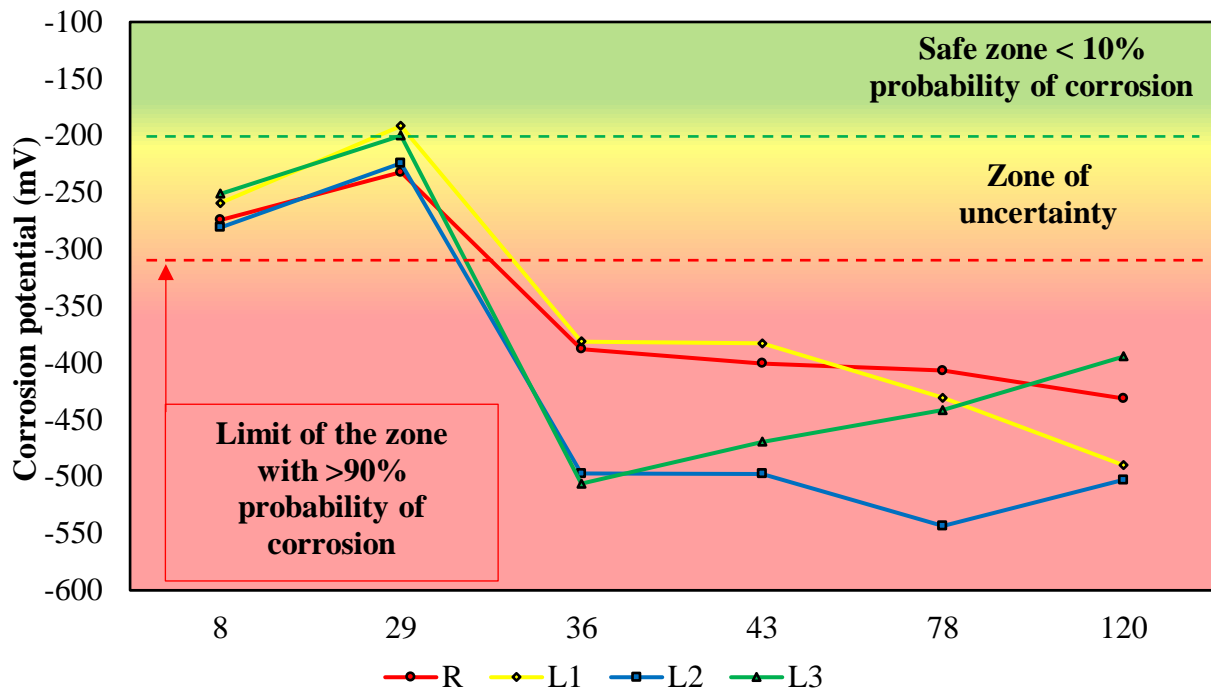


Figure 15. Behavior of the average corrosion potential of the families over time.

Some commentary can be made regarding the variation in corrosion potential for the slabs from all families. The first readings, taken only a few days after concreting, are located in the uncertainty zone. According to Hou et al., (2021) this occurs due to the presence of lime on the concrete surface or because of the formation of a water film on the steel bar.

With the second measurement, there was a tendency for the potential to shift towards the "safe" zone, with a corrosion probability of less than 10%. This behavior is attributed to the longer curing period, with the plates being drier and more protected. Immediately after the second reading, the immersion cycles were begun.

For the third reading (after 36 days), a sudden drop in the corrosion potential can be verified, especially for the most porous families (L2 and L3). When comparing the L3 family with the R family, it can be seen that the measurement of the corrosion potential at 120 days is less electronegative, -394 mV compared to the result for the R family of -431 mV, i.e., a difference of 9%, due to the high electrolytic activity of the chloride ions.

### 3.3 Electrical resistivity

To understand the effects of electrical resistivity on cellular concrete, it is necessary to analyze the microstructural parameters of the material, however, this was not a variable studied in this article. According to She et al., (2018) and Han, Lee, and Byun (2021) the formation of voids or micropores in the matrix of the cement composite enhances the diffusion of aggressive agents such as NaCl. The size of these pores can vary from 100  $\mu\text{m}$  to 350  $\mu\text{m}$ , and they can occur in different shapes, as shown in (Figure 16). The authors also state that, the larger the pore radius, the higher the electrical resistivity, ranging from 2  $\mu\text{m}$  to 5  $\mu\text{m}$ .



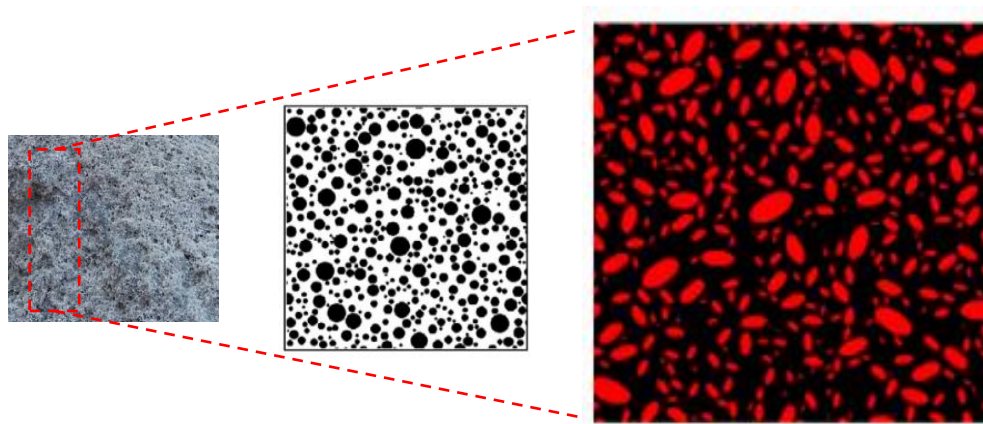


Figure 16. Examples of randomly-distributed pores having different shapes and a randomly-generated microstructure with radii between 2  $\mu\text{m}$  to 5  $\mu\text{m}$ . Source: Adapted from She et al., (2018).

The monitoring of reinforced concrete structures is necessary, because there are environments where they are required to have a longer service life. One of the issues to be evaluated is the degree of structural degradation due to permeability by sodium chloride (Yi et al., 2020). According to Lynch, Farrar, and Michaels (2016), electrical resistivity is a parameter used in damage detection, but this technique may not be feasible for some cement composites, due to the uncertain influence of many factors on the measurements obtained. Consequently, there are several studies on the influence of individual factors that improve the reliability of the results, such as: specimen geometry, water/cement ratio, types of percussive materials, aggregate size, curing conditions, and the presence of steel bars (Sanchez et al., 2016). For this study, concrete slabs containing steel bars were developed and the electrical resistivity was measured during the NaCl permeability period, with higher values initially observed for families L2 and L3 of 22.9 K $\Omega$ .cm and 36.2 K $\Omega$ .cm, respectively, which can be seen in (Figure 17).

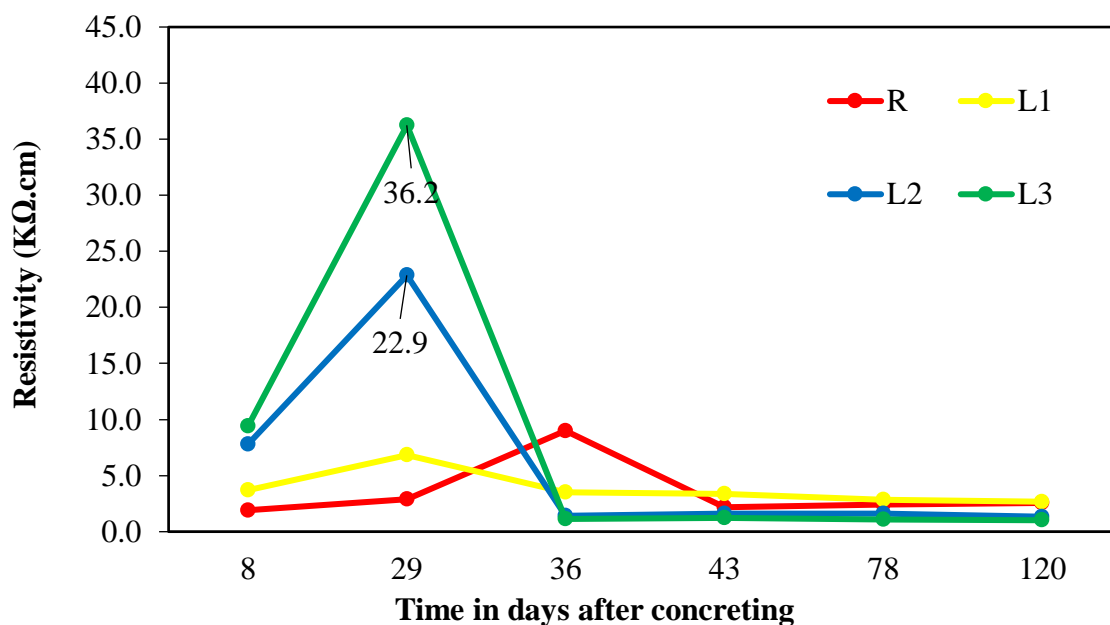


Figure 17. Behavior of concrete surface resistivity over time.

A study conducted by Dong et al., (2020), corroborated the results obtained in this study, as the electrical resistivity of their samples increased sharply from 4.5 KΩ.cm to 16 kΩ.cm in 29 days. To better contextualize this point, a longer "resting" period in a dry place protected from rain and sun enhances resistivity up to 29 days, specifically for cement matrices with higher levels of incorporated air (which can more easily lose retained moisture), due to the number of pores formed. After the start of the immersion process, a sharp drop in resistivity was observed, remaining between values of 1 to 10 KΩ.cm until the end of the study period, indicating a high activity/corrosion rate, according to the adopted criteria. The data agree with the studies conducted by Michel, Sørensen, and Geiker (2021), whose results indicated no significant difference in electrical resistivity, ranging from 0.5 to 2.5 KΩ.cm.

The studies conducted by Alnahhal et al., (2021) and Lokeshwari et al., (2021) indicate that the use of lower density materials in cellular concrete can improve electrical resistivity, where it ranges from 2.5 kΩ.cm to 5.0 kΩ.cm. Their results do not agree with those obtained in this study, because the higher the percentage of incorporated air, the higher the corrosion rate of the steel bars. This behavior can possibly be explained by the constant presence of chloride ions (strong electrolytes, facilitating ionic movement) and the possible retention of moisture within the concrete plates, because they were laid out to air dry for periods of 4 days.

All of the concrete families showed similar electrical resistivity behavior on the slab surfaces. According to Dong et al., (2020), more intense hydration can lead to higher cement consumption and, above all, high temperatures between the inside and outside of the concrete due to the heat released. This process can form microstructures that facilitate the passage of chloride ions into the cement composite and, in turn, lower the electrical resistivity. On the other hand, the first one hundred days of curing are significant in ensuring a sufficient electrical resistivity to contain the diffusivity of chloride ions, because the denser the material is, the lower its porosity.

### 3.4 Mass loss

The total mass loss of the steel bars per family followed a sequence, as shown in (Figure 18). Families L2 and L3, besides demonstrating higher electronegative corrosion potential values and a more degraded visual appearance (quantitatively and qualitatively), also obtained higher steel mass loss values (absolute and percentage).

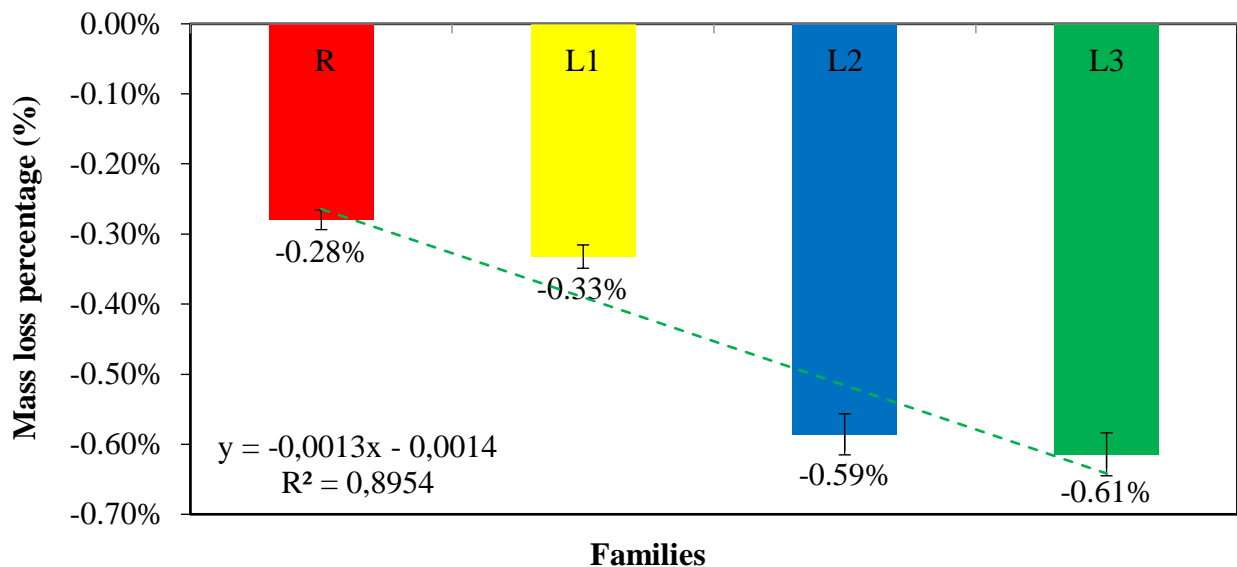


Figure 18. Percentage of total mass loss from steel bars by family.

In the analyses performed, it was observed that the concrete plates had a percentage mass loss from the steel bars of close to 2%, but when they were analyzed together (as families), this value ranged between 0.6% to 1%. A longer period of immersion in the NaCl solution would probably produce higher values of mass loss, but this was not necessary for this study, because the results obtained are considerable with regard to the formation of corrosion products. Family L3 had the highest percentage mass loss (Figure 19), when compared with families L1 (Figure 20) and L2 (Figure 21). This behavior may have occurred due to the fixed air content formed when mixing the material in the cement matrix. Another variable that can be taken into account is the mixing time for the concrete mixes, which was between 5 min and 20 min, where the air content formed varied between 5% and 40%.



Figure 19. Mass loss from steel bars (L3).



Figure 20. Mass loss from steel bars (L2).



Figure 21. Mass loss from steel bars (L1).

In (Figure 22), it can be seen that, the higher the percentage of air incorporated within the cement composite (cellular concrete), the greater the total loss of mass from the steel bars, because the voids index facilitates the entry of aggressive agents. The advance of the corrosion products against the content of incorporated air grows exponentially as can be seen by the  $R^2 = 0.9482$ .

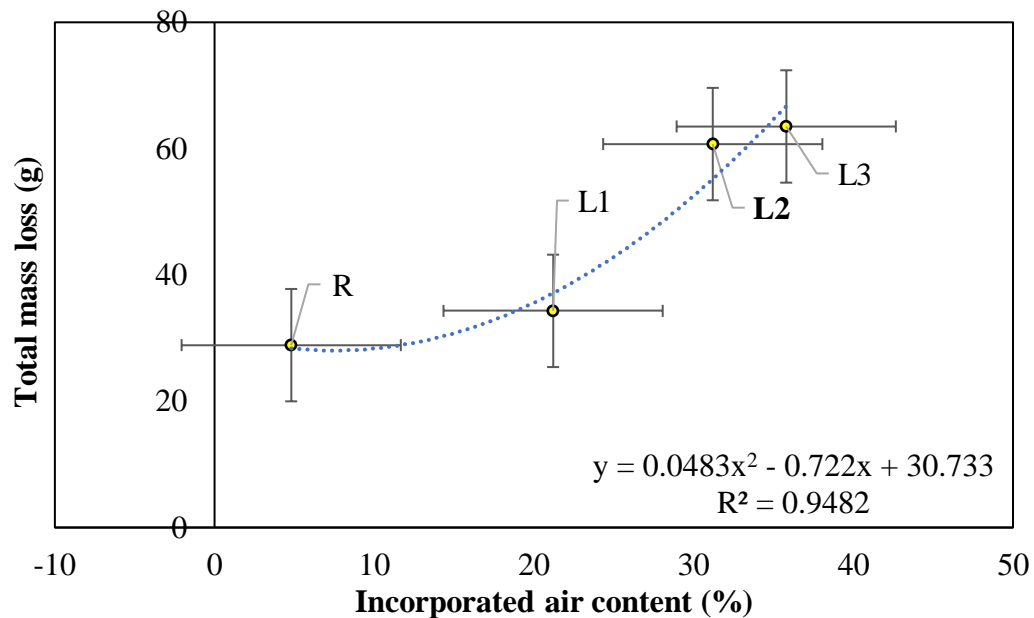


Figure 22. Linear regression of the data obtained.

The mass loss from the L3 family (cellular concrete) was 55% higher than that of the R family (reference concrete). These results show that the incorporated air content of the concrete should be less than 10%, because it interferes in the improvement of mechanical properties and, moreover, enhances the corrosion of the steel bars within the material.

Concrete masses with low resistance tend to have less electropositive ( $E_{corr}$ ) values, highlighting that the readings for corrosion potential are not always due to the exposure time of the material in aggressive environments, but also to the type of additive used and the mass loss from the steel bars within the cement composite. To better contextualize this point, in (Figure 23 (a)), it was noticed that all families (R, L1, L2, and L3) had corrosion potential readings between -250 mV and -600 mV, but the data were not statistically different at 5% variance, as shown in the Pareto diagram (Figure 23 (b)).

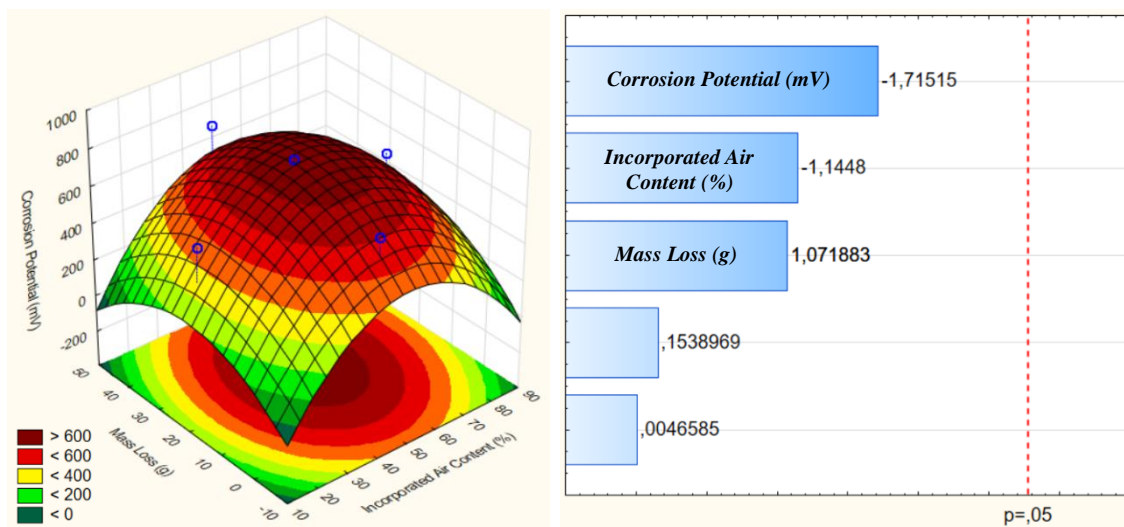


Figure 23. (a) Response surface for the variables that influence the corrosion potential (b) Pareto diagram.

## 4. CONCLUSIONS

When investigating whether reinforcement corrosion in cellular concrete may be asymptomatic, the presence of cracks was not observed for any family of concrete tested. However, it is necessary to point out that the non-occurrence of cracks was specific to the parameters used in this study. For example, the cover used (5 mm) and the severe conditions of exposure to wetting and drying in a NaCl solution. Other considerations were relevant to the tests performed, such as:

- With regard to staining, despite the high incidence of this symptom, its occurrence may be related to the variable covering thickness between the slab faces (A and B). However, the concrete families with higher levels of incorporated air, had greater water absorption, and lower density and compressive strength.
- With regard to the tests, families L2 and L3 (higher air content) presented more visual degradation, and also had the greatest steel mass loss. Therefore, given the results and analysis, the initial hypothesis can be discarded, because according to the results obtained, a greater incorporation of air did not mitigate corrosion, but instead led to an increase in the probability of the concrete presenting reinforcement corrosion.
- The visual inspection analyses found the R group to have 67% of its slabs classified as lightly degraded and two being not relevant. With a percentage of 0.1%, the L1 family had lower degradation than the L2 and L3 families, which had 44% and 61% of their slabs,

respectively, classified as highly degraded.

- With regard to the corrosion potential, the R, L1, L2, and L3 families all had the same behavior after 29 days, with measurements more electropositive than -200 mV. During the 120 days, the corrosion potential of the L3 family was less electronegative, possibly due to the high electrolytic activity of chloride ions in the innermost layers of the cellular concrete.
- With regard to electrical resistivity, after 29 days, the L2 and L3 families showed a large increase due to the internal stability of the voids and the presence of easily-lost water. This behavior provides the cellular concrete of both families with an insignificant corrosion risk, because it is greater than 20 K $\Omega$ .cm. After 36 days, all families presented a very high risk of corrosion, with values between 0 and 5 K $\Omega$ .cm.

## 5. ACKNOWLEDGMENTS

This study is of great relevance to the scientific/academic community and would not have been possible without the collaboration of all participants. We would also like to thank the University of Pernambuco, the Catholic University of Pernambuco and, above all, the research funding agencies, CNPq “*Conselho Nacional de Desenvolvimento Científico e Tecnológico*” and CAPES “*Coordenação de Aperfeiçoamento de Pessoal de Nível Superior*”.

## 6. BIBLIOGRAPHIC REFERENCES

- ABNT – Associação Brasileira de Normas Técnicas. (2003), *NBR NM 248: Agregados – Determinação da composição granulométrica*. Rio de Janeiro.
- ABNT – Associação Brasileira de Normas Técnicas. (2007), *NBR 7480: Aço destinado a armaduras para estruturas de concreto armado – Especificação*. Rio de Janeiro.
- ABNT – Associação Brasileira de Normas Técnicas. (2008), *NBR 9833: Concreto fresco - Determinação da massa específica, do rendimento e do teor de ar pelo método gravimétrico*. Rio de Janeiro.
- ABNT – Associação Brasileira de Normas Técnicas. (2014), *NBR 12644: Concreto celular estrutural – Determinação da densidade do concreto no estado fresco*. Rio de Janeiro.
- Al-Shwaiter, A., Awang, H., Khalaf, M. A. (2021), *The influence of superplasticiser on mechanical, transport and microstructure properties of foam concrete*. Journal of King Saud University – Engineering Sciences. 1(1):1-9. <http://dx.doi.org/10.1016/j.jksues.2021.02.010>
- Alnahhal, A. M., Alengaram, U. J., Yusoff, S., Singh, R., Radwan, M. K. H., Deboucha, W. (2021), *Synthesis of sustainable lightweight foamed concrete using palm oil fuel ash as a cement replacement material*. Journal of Building Engineering. 35(1):1-12. <http://dx.doi.org/10.1016/j.jobbe.2020.102047>
- ASTM G1-03, Standard Test Method for Corrosion Potentials of Uncoated Reinforcing Steel in Concrete*, ASTM International, West Conshohocken, PA, 2017.
- ASTM C876-15, Standard Test Method for Corrosion Potentials of Uncoated Reinforcing Steel in Concrete*, ASTM International, West Conshohocken, PA, 2015.
- Badar, S., Patil, K. K., Bernal, S. A., Provis, J.L., Allouche, E. N. (2014), *Corrosion of steel bars induced by accelerated carbonation in low and high calcium fly ash geopolymer concretes*. Construction and Building Materials, 62(1):79-89. <http://dx.doi.org/10.1016/j.conbuildmat.2014.03.015>
- Chung, S-Y., Elrahman, M. A., Kim, J-S., Han, T-S., Stephan, D., Sikora, P. (2019), *Comparison of lightweight aggregate and foamed concrete with the same density level using image-based characterizations*. Construction and Building Materials. 211(1):988-999. <http://dx.doi.org/10.1016/j.conbuildmat.2019.03.270>

- Dong, Y., Su, C., Qiao, P., Sun, L. (2020), *Microstructural crack segmentation of three-dimensional concrete images based on deep convolutional neural networks*. Construction and Building Materials. 253(1):1-12. <http://dx.doi.org/10.1016/j.conbuildmat.2020.119185>
- Dong, W., Huang, Y., Lehane, B., Ma, G. (2020), *XGBoost algorithm-based prediction of concrete electrical resistivity for structural health monitoring*. Automation in Construction. 114(1):1-11. <http://dx.doi.org/10.1016/j.autcon.2020.103155>
- Du, F., Jin, Z., She, W., Xiong, C., Feng, G., Fan, J. (2020), *Chloride ions migration and induced reinforcement corrosion in concrete with cracks: a comparative study of current acceleration and natural marine exposure*. Construction and Building Materials. 263(1):1-11. <http://dx.doi.org/10.1016/j.conbuildmat.2020.120099>
- Green, W. K. (2020), *Steel reinforcement corrosion in concrete – an overview of some fundamentals*. Corrosion Engineering, Science and Technology. 55(4):289-302. <http://dx.doi.org/10.1080/1478422x.2020.1746039>
- Han, W., Lee, J. S., Byun, Y. H (2021), *Volume, strength, and stiffness characteristics of expandable foam grout*. Construction and Building Materials. 274(1):1-16. <http://dx.doi.org/10.1016/j.conbuildmat.2020.122013>
- He, T., XU, R., Chen, C., Yang, L., Yang, R., Yongqi, D. (2018), *Carbonation modeling analysis on carbonation behavior of sand autoclaved aerated concrete*. Construction and Building Materials. 189(1):102-108. <http://dx.doi.org/10.1016/j.conbuildmat.2018.08.199>
- He, X., Zheng, z., Yang, J., Su, Y., Wang, T., Strnadell, B. (2019), *Feasibility of incorporating autoclaved aerated concrete waste for cement replacement in sustainable building materials*. Journal of Cleaner Production. 19(2):2-49. <https://doi.org/10.1016/j.jclepro.2019.119455>
- Hou, L., Li, J., Lu, Z., Niu, Y. (2021), *Influence of foaming agent on cement and foam concrete*. Construction and Building Materials. 280(1):1-13. <http://dx.doi.org/10.1016/j.conbuildmat.2021.122399>
- Kanellopoulos, A., Savva, P., Petrou, M. F., Ioannou, I., Pantazopoulou, S. (2020), *Assessing the quality of concrete – reinforcement interface in Self Compacting Concrete*. Construction and Building Materials. 240(1):1-12. <http://dx.doi.org/10.1016/j.conbuildmat.2019.117933>
- Khodabakhshian, A., Brito, J., Ghalehnovi, M., Shamsabadi, E. A. (2018), *Mechanical, environmental and economic performance of structural concrete containing silica fume and marble industry waste powder*. Construction and Building Materials. 169(1):237-251. <http://dx.doi.org/10.1016/j.conbuildmat.2018.02.192>
- Kashani, A., Ngo, T. D., Mendis, P., Black, K. R., Hajimohammadi, A. (2017), *A sustainable application of recycled tyre crumbs as insulator in lightweight cellular concrete*. Journal of Cleaner Production. 17(3):1-32. <https://doi.org/10.1016/j.jclepro.2017.02.154>
- Liu, X., Ni, C., Meng, K., Zhang, L., Liu, D., Sun, L. (2020), *Strengthening mechanism of lightweight cellular concrete filled with fly ash*. Construction and Building Materials. 251(1):1-14. <http://dx.doi.org/10.1016/j.conbuildmat.2020.118954>
- Liu, X., Sun, D., Liu, D., Meng, K., Ni, C., Shao, Z., Sun, L. (2021), *Simulation of ultrasonic propagation in porous cellular concrete materials*. Construction and Building Materials. 285(1):1-13. <http://dx.doi.org/10.1016/j.conbuildmat.2021.122852>
- Lynch, J. P., Farrar, C. R., Michaels, J. E. (2016), *Structural health monitoring: technological advances to practical implementations*. Proceedings of the Ieee. 104(8):1508-1512. <http://dx.doi.org/10.1109/jproc.2016.2588818>
- Lokeshwari, M., Bandakli, B. R. P., Tarun, S. R., Sachin, P., Kumar, V. (2021), *A review on self-curing concrete*. Materials Today: Proceedings. 1(1):1-6. <http://dx.doi.org/10.1016/j.matpr.2020.12.859>

- Mariz, J. C. (2013), “*Avaliação comparativa do comportamento mecânico de concretos leves com ar incorporado*”. Monograph presented as a partial requirement for Bachelor's degree in Civil Engineering from the Polytechnic School of Pernambuco – University of Pernambuco.
- Mechtcherine, V., Michel, A., Liebscher, M., Schneider, K., Großmann, C. (2020), *Mineral-impregnated carbon fiber composites as novel reinforcement for concrete construction: material and automation perspectives*. Automation in Construction. 110(1):1-8. <http://dx.doi.org/10.1016/j.autcon.2019.103002>
- Michel, A., Sørensen, H. E., Geiker, M. R. (2021), *5 years of in situ reinforcement corrosion monitoring in the splash and submerged zone of a cracked concrete element*. Construction and Building Materials. 285(1):1-12. <http://dx.doi.org/10.1016/j.conbuildmat.2021.122923>
- Namkung, H., Lee, Y.-J., Park, J.-H., Song, G.-D., Choi, J. W., Kim, J.-G., Park, S.-J., Park, J. C., Kim, H.-T., Choi, Y.-C. (2019), *Influence of herbaceous biomass ash pre-treated by alkali metal leaching on the agglomeration/sintering and corrosion behaviors*. Energy. 187(1):1-13. <http://dx.doi.org/10.1016/j.energy.2019.115950>
- Nascimento, C. F. G., Silva, T. M., Teixeira, I. A. R., Silva, F. G. A., Neves, D. C. M., Pedrosa, P. G. V., Valões, D. C. P., Monteiro, E. C. B. (2021), *Influência do agregado reciclado na durabilidade do concreto armado frente a corrosão de armadura desencadeada por carbonatação acelerada*. Conjecturas, 21(4):569-599. <http://dx.doi.org/10.53660/conj-237-801>
- Nguyen, Q. D., Castel, A. (2020), *Reinforcement corrosion in limestone flash calcined clay cement-based concrete*. Cement And Concrete Research. 132(1):1-15. <http://dx.doi.org/10.1016/j.cemconres.2020.106051>
- Pachla, E. C., Silva, D. B., Stein, K. J., Marangon, E., Chong, W. (2021), *Sustainable application of rice husk and rice straw in cellular concrete composites*. Construction and Building Materials. 283(1):1-11. <http://dx.doi.org/10.1016/j.conbuildmat.2021.122770>
- RILEM TC 154-EMC. Recommendations of RILEM TC 154-EMC: *Electrochemical techniques for measuring metallic corrosion Half-cell potential measurements – Potential mapping on reinforced concrete structures*. ISSN: 1359-5997. RILEM Publications SARL. Vol 36, 2003.
- Sanchez, J., Andrade, C., Torres, J., Rebolledo, N., Fulla, J. (2016), *Determination of reinforced concrete durability with on-site resistivity measurements*. Materials and Structures. 50(1):1-10. <http://dx.doi.org/10.1617/s11527-016-0884-7>
- She, W., Zhao, G., Cai, D., Jiang, J., Cao, X. (2018), *Numerical study on the effect of pore shapes on the thermal behaviors of cellular concrete*. Construction and Building Materials. 163(1):113-121. <http://dx.doi.org/10.1016/j.conbuildmat.2017.12.108>
- Shon, C. S., Lee, D., Kim, J. H., Chung, C. W. (2018), *Freezing and thawing resistance of cellular concrete containing binary and ternary cementitious mixtures*. Construction and Building Materials. 168(1):73-81. <https://doi.org/10.1016/j.conbuildmat.2018.02.117>
- Stumm, A., schweike U., Stemmermann, P. (2018), *Nanostructured high insulating autoclaved aerated concrete*. Mauerwerk. 22(5):329-334. <http://dx.doi.org/10.1002/dama.201800024>
- Trong, L. N., Asamoto, S., Matsui, k. (2018), *Sorption isotherm and length change behavior of autoclaved aerated concrete*. Cement and Concrete Composites. 94(1):136-144. <http://dx.doi.org/10.1016/j.cemconcomp.2018.09.003>
- Ye, H., Jin, X., Fu, C., Jin, N., Xu, Y., Huang, T. (2017), *Influence of combined carbonation and chloride ingress regimes on rate of ingress and redistribution of chlorides in concretes*. Construction and Building Materials, 140(1):173-183. <https://doi.org/10.1016/j.conbuildmat.2017.02.121>
- Yi, Y., Zhu, D., Guo, S., Zhang, Z., Shi, C. (2020), *A review on the deterioration and approaches to enhance the durability of concrete in the marine environment*. Cement and Concrete Composites, 113(1):1-14. <https://doi.org/10.1016/j.cemconcomp.2020.103695>

- Zhang, S., Cao, K., Wang, C., Wang, X., Wang, J., Sun, B. (2020), *Effect of silica fume and waste marble powder on the mechanical and durability properties of cellular concrete*. Construction and Building Materials, 241(1):1-17. <http://dx.doi.org/10.1016/j.conbuildmat.2019.117980>
- Zhang, S., Cao, K., Wang, C., Wang, X., Deng, G., Wei, P. (2020), *Influence of the porosity and pore size on the compressive and splitting strengths of cellular concrete with millimeter-size pores*. Construction and Building Materials. 235(1):1-19. <http://dx.doi.org/10.1016/j.conbuildmat.2019.117508>



## Practical use of the safety factor in the column repair strategy of a concrete building with historical value

J. A. Briceño-Mena<sup>1</sup> , P. Castro-Borges<sup>1\*</sup> 

\*Contact author: [pcastro@cinvestav.mx](mailto:pcastro@cinvestav.mx)

DOI: <https://doi.org/10.21041/ra.v12i1.569>

Reception: 09/11/2021 | Acceptance: 21/12/2021 | Publication: 01/01/2022

### ABSTRACT

In this paper the practical use of the safety factor (FS) in the column repair strategy of a reinforced concrete building with historical value (almost 70 years) is presented. 80% of a building located in the historic center of the city of Campeche, Mexico, declared a World Heritage Site by UNESCO, was repaired. Strategies were used for a better use of material resources, equipment, and labor in the repair of walls, columns, slabs, and beams. One of the strategies was to use the theoretical FS to calculate the repair depth without structural consequences but fulfilling the purpose of controlling the carbonation of the concrete and maintaining the desired prediction of service life.

**Keywords:** repair; reinforced concrete; durability; security factor.

**Cite as:** Briceño-Mena, J. A., Castro-Borges, P. (2022), “Practical use of the safety factor in the column repair strategy of a concrete building with historical value”, Revista ALCONPAT, 12 (1), pp. 98 – 109, DOI: <https://doi.org/10.21041/ra.v12i1.569>

<sup>1</sup>Departamento de Física Aplicada, Centro de Investigación y de Estudios Avanzados del Instituto Politécnico Nacional, Unidad Mérida, Mérida, Yucatán, México.

#### Contribution of each author

In this work the author J.A. Briceño-Mena contributed with the field experimentation activity (60%), data collection (50%), writing of the work (50%), discussion of results (50%); the author P. Castro-Borges contributed with the original idea, field experimentation (40%), data collection (50%), writing of the work (50%), discussion of results (50%).

#### Creative Commons License

Copyright 2022 by the authors. This work is an Open-Access article published under the terms and conditions of an International Creative Commons Attribution 4.0 International License ([CC BY 4.0](https://creativecommons.org/licenses/by/4.0/)).

#### Discussions and subsequent corrections to the publication

Any dispute, including the replies of the authors, will be published in the third issue of 2022 provided that the information is received before the closing of the second issue of 2022.

## Uso práctico del factor de seguridad en la estrategia de reparación de columnas de un edificio de concreto con valor histórico

### RESUMEN

En este trabajo se presenta el uso práctico del factor de seguridad (FS) en la estrategia de reparación de columnas en un edificio de concreto reforzado con valor histórico (casi 70 años). Se llevó a cabo la reparación del 80% de un edificio ubicado en el centro histórico de la ciudad de Campeche, México, declarado patrimonio de la humanidad por la UNESCO. Se utilizaron estrategias para una mejor utilización de los recursos materiales, equipamiento y mano de obra en la reparación de muros, columnas, losas y trabes. Una de las estrategias fue usar el FS teórico para calcular la profundidad de reparación sin consecuencias estructurales, pero cumpliendo la finalidad de controlar la carbonatación del concreto, y manteniendo la predicción deseada de vida de servicio. **Palabras clave:** reparación; concreto reforzado; durabilidad; factor de seguridad.

## Uso práctico do fator de segurança na estratégia de reparo de pilar em um edifício de concreto com valor histórico

### RESUMO

Neste artigo discute-se o uso prático do fator de segurança (FS) na estratégia de reparo de pilares em um edifício de concreto armado com valor histórico (quase 70 anos). 80% de um prédio localizado no centro histórico da cidade de Campeche, no México, declarado Patrimônio da Humanidade pela UNESCO, foi reformado. Estratégias foram utilizadas para um melhor aproveitamento dos recursos materiais, equipamentos e mão de obra na reparação de paredes, pilares, lajes e vigas. Uma das estratégias foi utilizar o FS teórico para calcular a profundidade de reparo sem consequências estruturais, mas cumprindo o objetivo de controlar a carbonatação do concreto, e manter a previsão de vida útil desejada.

**Palavras-chave:** reparar; concreto reforçado; durabilidade; fator de segurança.

### Legal Information

Revista ALCONPAT is a quarterly publication by the Asociación Latinoamericana de Control de Calidad, Patología y Recuperación de la Construcción, Internacional, A.C., Km. 6 antigua carretera a Progreso, Mérida, Yucatán, 97310, Tel.5219997385893, [alconpat.int@gmail.com](mailto:alconpat.int@gmail.com), Website: [www.alconpat.org](http://www.alconpat.org)

Reservation of rights for exclusive use No.04-2013-011717330300-203, and ISSN 2007-6835, both granted by the Instituto Nacional de Derecho de Autor. Responsible editor: Pedro Castro Borges, Ph.D. Responsible for the last update of this issue, Informatics Unit ALCONPAT, Elizabeth Sabido Maldonado.

The views of the authors do not necessarily reflect the position of the editor.

The total or partial reproduction of the contents and images of the publication is carried out in accordance with the COPE code and the CC BY 4.0 license of the Revista ALCONPAT.

## 1. INTRODUCTION

One of the common problems in concrete repairs is the misuse of structural specifications to know the depth to which they must be made, when faced with problems due to chlorides or carbonation. This results in a poorly optimized use of labor, equipment and materials that leads, not only to wrong repairs and the return of the problem, but also to a lack of sustainability in the entire process. This building with an internal space of more than 600 m<sup>2</sup> and an approximate height of 20 m, and a frame-based structure, involved a demolition and subsequent construction of a new 4-level building. However, this plan was reconsidered because the building was approximately 70 years old and was located in the historic center of the city of San Francisco de Campeche, Campeche, Mexico (Figure 1), declared a World Heritage Site in 1999 by the United Nations Educational, Scientific and Cultural Organization (UNESCO). This place is protected by federal authorities such as the National Institute of Fine Arts and Literature (INBAL, in Spanish) and the National Institute of Anthropology and History (INAH, in Spanish). Therefore, rather than a demolition process, a repair strategy had to be considered that met the conditions established by the federal authorities, whereas much of the structure was preserved as possible (80%). For this reason, an extensive study was carried out on the durability of the property. Therefore, the parts that would remain standing prior to an intervention that would involve the repair and/or reinforcement of the different structural elements were defined, avoiding the initial demolition processes, and adapting it to the required conditions. It was proposed to attach a new internal structure to the building that has already been repaired, thus maintaining its exterior architecture, and rescuing interior areas.

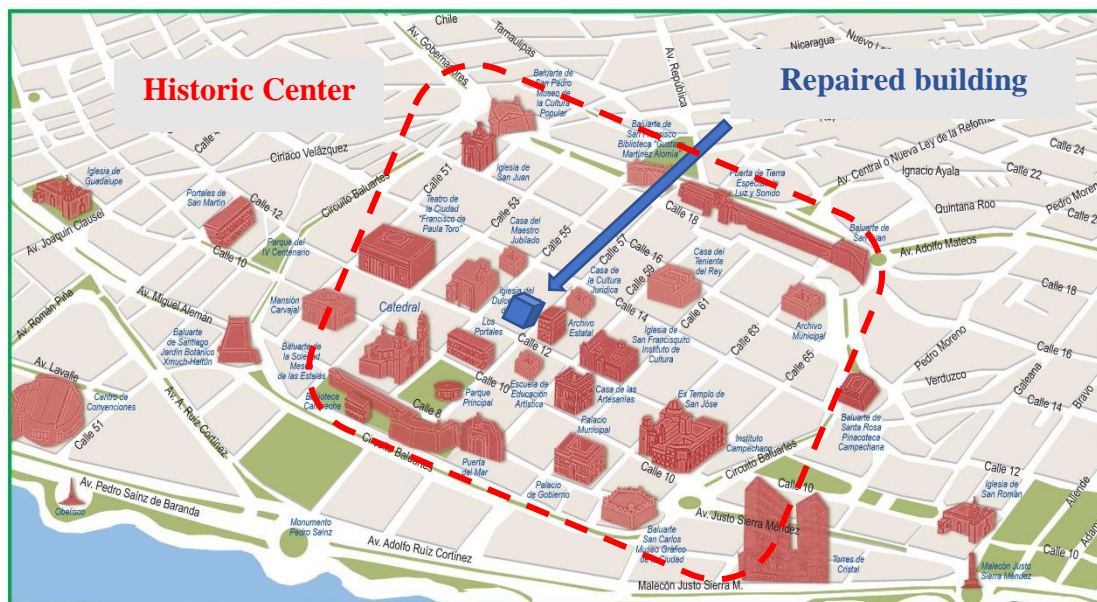


Figure 1. Location of the structure within the protected area of Campeche <sup>1</sup>

The structure had as its primary function that of being a cinema, later it functioned as a parking lot and was finally abandoned. These changes in use and abandonment were factors that potentiated the damage, as partially observed in the photos of Figure 2.

<sup>1</sup> <https://programadestinosmexico.com/descubre-mexico/mapas/mapas-de-ciudad-de-campeche.html>



Figure 2. State of the structure before being repaired.

To develop an optimal repair, a structural analysis should be considered where the construction processes to be carried out during said intervention are considered since, during this process, loads can be added or removed due to the demolition of elements, vibrations, changes in the same properties of the repair materials, changes in resistance, shoring, among others (Ministerio de Vivienda y Urbanismo – Minvu, 2018; Allen, 1991). Therefore, it is important to establish the values with which it will work, such as the old and new resistance of the elements, safety factors, to name a few. In the present work it is illustrated, for the case of the columns, how the safety factor (SF) was used for the repair of the former Selem cinema.

### 1.1 The safety factor as a criterion for the durability of the repair

It was found in the literature the information about the Security Theory (González Cueto Vila and Quevedo Sotolongo, 2007) which, in general, consists of relating the security level (H) (equation 1), defined as  $H = 1 - pf$ , where  $pf$  is the probability of failure. This level of security depends on all the variables that intervene in the design of the structure and how they can vary. The general equation that governs the theory of security is:

$$H \geq H^n \quad (1)$$

Where:  $H^n$  is the safety level of the design.  
 $H$  is the level of safety of the work.

In Civil Engineering, it can be understood as safety to prevent the structure from exceeding the permissible limit state, which is where it is considered that the structural behavior is acceptable (Ridell and Hidalgo, 2010). The SF is the one that relates the load or stress (C) to be applied to the structure with the maximum capacity (R) that it can withstand, that is, its maximum resistance.

$$SF = \frac{C}{R} \quad (2)$$

The SF is considered at the moment in which a structural element is being designed but it must also be considered when repairs are made since it has a direct relationship with the resistance of the material itself, as well as in the dimensions of the section of the elements. The SF is based on two coefficients (ACI 318-19, 2019), a coefficient of increased loads that consists of fictitiously increasing the load that will be applied to the structure when it is subjected to real loads during use. That is, multiplying the expected real load by a safety factor of increased load. The other coefficient is the reduction in the resistance of the material that makes up the element. The strength of the materials is reduced compared to the maximum allowable stresses. That is, dividing the resistance of the materials by a safety coefficient of reduction of resistance. Therefore, considering an element that in theory will have loads higher than the real ones and with a lower resistance than its own, there will be confidence in the security provided by the element even under very unfavorable conditions during its useful life.

Putting a practical fictitious example, the SF can be understood as follows: supposing that a column, which was designed to support 6 tons of load and 2 beams will rest on it, and each of these will transfer a load of 2 tons to the column. Therefore, it can be seen that the SF is 1.5 ( $SF = 6/4 = 1.5$ ). Although in this example it was treated as a simple subject, in reality it is something much more complex. Various criteria must be considered, such as live loads (the people who will use the building), dead loads (furniture, for example), accidental loads, as well as environmental factors.

## 2. METHODOLOGY OF THE REPAIR PROCESS

### 2.1 Damage inspection

Before carrying out any intervention in the structure, it was necessary to carry out an inspection of the damage, based on Mexican regulations (NMX-C-505-ONNCCE, 2016; NMX-C-520-ONNCCE, 2018), to establish the repair strategies. These inspections have already been published (Briceño-Mena et al, 2021) and can be consulted in the literature for more details. These inspections had 4 main axes:

- Visual, to identify the damaged areas that require a greater intervention and possible causes of pathological problems such as areas of humidity, as well as detachments, cracks, etc.
- Mechanics, to know the state of the concrete such as its mechanical resistance and to be able to establish the resistance of the new concrete to be used.
- Electrochemistry, to know the state of the steel, how damaged it could be due to pathological problems.
- Chemistry, to determine the aggressive agents that are causing damage to structural elements.

## 2.2 Repair strategies

After the inspection carried out, it was found that the structural and architectural elements could be intervened for their consolidation with the new structure to be built inside the building as part of its change of use. All repair strategies were established to be able to provide the structure with a new service life and durability against current and future pathological problems to which it could be subjected, considering the mechanical characteristics of the elements themselves, as well as the use of the safety factors (NMX-C-530-ONNCCE, 2018; Val and Stewart, 2002; Melchers, 2001). These strategies were based on previous experiences and on the literature such as the Rehabilitar Manual (Helene and Pereira, 2003). The purpose of these repairs was to remove damaged concrete or that presented a pathological problem such as carbonation, as well as to ensure structural stability with the recalculation and restructuring of the amount of steel necessary in the elements, in addition to ensuring the adequate coating according to the structural requirements. Figure 3 shows processes of deterioration of the structure. To define the repair strategies, it was necessary to establish the types of repairs to be used:



Figure. 3. Carbonation and detachment of concrete.

### 2.2.1 Localized superficial repair (LSR)

This repair refers to those elements that present damage to the concrete with little depth and extension in relation to the dimensions of the structural element. Therefore, a repair was established in specific areas where cracks are observed at a depth no greater than 3 cm or before reaching the reinforcing steel.

### 2.2.2 Uniform superficial repair (USR)

This repair strategy is similar to the localized superficial repair since it will be carried out at a depth no greater than 3 cm, or before reaching the reinforcing steel, but contemplating the repair in a relatively large extension according to the dimensions of the structural element, delimiting for the works a maximum extension on the element of 1.5 m.

### 2.2.3 Localized deep repair (LDR)

This repair will be carried out in the structural elements where damage with a relatively small extension has been identified, with a depth greater than 3 cm, affecting the concrete behind the reinforcements.

### 2.2.4 Uniform deep repair (UDR)

As in the localized deep repair section, the repair is performed at a depth beyond the steel. However, as it was uniform, the repair was established in maximum sections of 1.5 m, due to structural issues.

### 3. APPROACH AND USE OF THE SAFETY FACTOR IN REPAIRS

The proposed repair techniques were carried out to apply strategies in the construction processes that allow avoiding unnecessary processes such as demolition, which would lead to the generation of rubble and garbage and even more so in important areas such as a world heritage site.

As an initial starting point to carry out the repair, it was important to analyze each element individually, its behavior, its maximum bearing load, its state, and later project it at a general level relating it to all the structural elements, thus obtaining a global behavior. In this way, it was possible to carry out the intervention considering all the possible factors of affectation and minimizing collateral damage of the repair process. This in turn leads to personnel training to prepare repairs since, at present, both workers and engineers are unaware of these issues, which causes an incorrect use of tools, materials, and equipment.

Although a repair strategy can be carried out by trained people, it is always important to consider safety and risk factors when working.

The SF theory was put into practice in the repair process of the structure described in this work. For this, the support of manuals, regulations, literature, and own experience was required to establish with the best criteria the ideal strategy per element. As previously mentioned, thanks to the previous inspection, the degree of damage was established and with it the repair strategy. Although 4 possible ones were established, in this work only what is related to uniform deep repair will be discussed (see Figure 4).

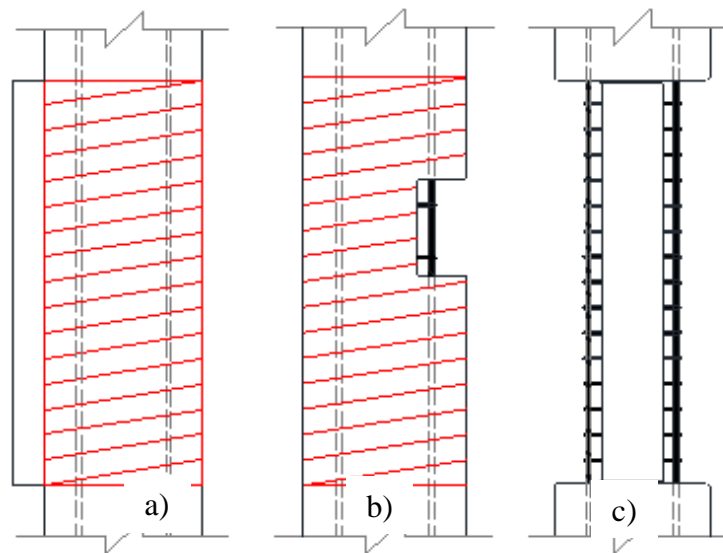


Figure 4. Uniform deep repair: a) Delimitation of the area to be demolished, b) scarification started, c) final section after scarification

To carry out the repairs, it was necessary to establish the criteria with which they would be carried out. In the case of this structure, there were elements of different dimensions, for which universal repair criteria were established but they had to be verified before their execution. An UDR may or may not be large in relation to the size of the element. However, in this case and in order not to resort to materials, labor and time as is the case with the installation of stabilization struts, it was determined for practicality that the best thing was to carry out the repairs in sections of 1.5 linear meters. The following is an example of a rectangular type of column. The typical column (see Figure 5) had a cross section of 30x35 cm and with the help of the mechanical tests carried out it was possible to obtain the average compressive strength of the concrete, which is greater than 200 kg/cm<sup>2</sup>. Considering the cross section of the element and the minimum resistance obtained, it can

be deduced that the column can support an axial load of 210,000 kg. Now, if the concrete in poor condition is scarified, and it is repaired beyond the reinforcement, remembering that the uniform deep repair is the one that occurs beyond 3 cm or behind the reinforcement, the new cross section of the element is 25x30 cm. If this new cross section is used and the compressive strength obtained previously with the extracted cylinders, it can be determined that the structure, even with the reduction in the concrete section, can support 150,000 kg. If it is considered that, at least, the element was designed with an SF of 1.5, then the structure was initially designed to carry a load of 140,000 kg safely. Therefore, even after scarifying, the item to be repaired can still withstand the loads exerted as it can resist up to 150,000 kg. This could not be entirely true since it is not an analysis that considers all the possible effects that may exist at the time of making the repairs. However, it is a good strategy to be carried out in the field since it allows a quick appreciation of how far one can intervene without structurally affecting the element and to be able to continue with the repair work once the diagnosis has been made.

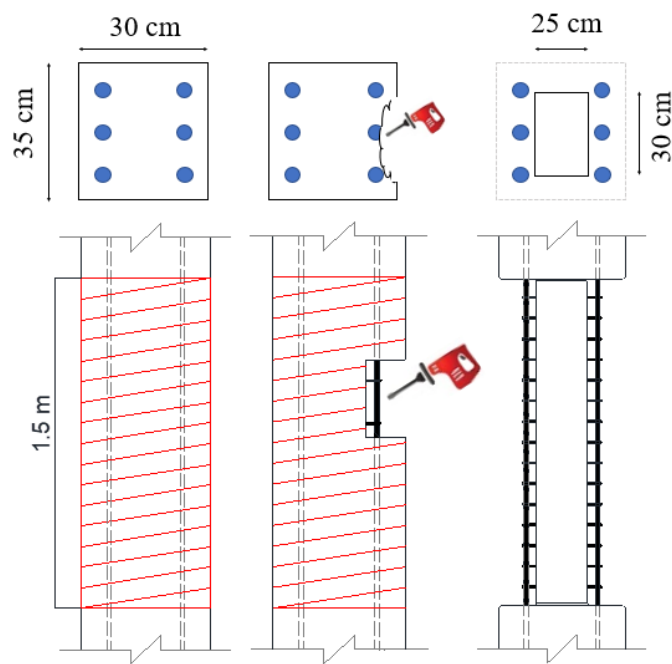


Figure 5. Criterion for delimitation and scarification of repairs

For the repair process, a guide was made which could be easily followed by the workers and which in turn was repeatable in various elements. This process can be seen in Figure 6. To carry out the repairs and in order to control various problems such as temperature contractions, modulus of elasticity, etc., it was decided to use some concrete with similar characteristics to carry out the repair of the elements.





Mechanical scarification to remove bad concrete and uncover reinforcing steel.



Measurement of the diameter of the reinforcing steel, if the loss of diameter was greater than the allowable, the steel was completed or replaced. In some cases, full transverse reinforcing steel was placed due to excessive wear.



Holes were drilled for the placement of new steel to replace the corroded one. For its correct anchoring, a high-performance epoxy resin was injected for high loads.



Before carrying out the installation, the base of all the elements was covered with an asphalt waterproofing around the floor to avoid any penetration of moisture or corrosive agents.



Due to previous inspection experience, it is recommended to apply an oxide converter to the steel.



Prior to casting, a bonding primer was applied to ensure the homogenization of the new concrete with the old one, this also has the function of a sealer.



Post-casting and post-stripping, a curing membrane was applied to the concrete to ensure durability.

Figure 6. Uniform deep repair process

Naturally, the work of the workers involved on some occasion the breaking of the concrete cross section or going beyond the minimum section required according to the SF. In these cases, the precautions included not only punctual shoring, but also considering the monolithism of the structure when transferring the excess loads from the section contemplated to the neighboring elements.

With this work, it has been possible to demonstrate in a simple way the ease and confidence with which an UDR in columns can be approached, considering a simple calculation of the SF. Figure 7 shows a night view of the building already recovered.



Figure 7. View of the intervention building

## 4. CONCLUSIONS

The purpose of this work was to present the practical case of repairing the columns of a 70-year-old reinforced concrete structure, which was in a state of abandonment and its total demolition had been planned. By mandate of the authorities, a durability study was carried out, which resulted in changing the demolition project to a repair one. To carry out this repair, it was necessary to consult different educational sources such as previous experiences that led to the creation of a practical manual for workers. This manual was based on durability criteria as well as design specifications that allow for safe operation. The SF played an important role in determining the redress mechanism, which resulted in significant savings in resources and time. With these repair procedures it is projected to have a durable structure that can fulfill the established service life with preventive maintenance.

## 5. ACKNOWLEDGMENTS

The authors are grateful for the support of Coppel SA de CV, UACAM, Cinvestav, INAH and INBA. J.A. Briceño-Mena is grateful for the Conacyt doctoral scholarship.

## 6. REFERENCES

- American Concrete Institute (2019), *ACI 318-19 Requisitos de Reglamento para Concreto Estructural*. Primera impresión: junio 2019. ISBN 978-1-64195-060-2
- Allen, D. E. (1991), “Limit states criteria for structural evaluation of existing buildings” *Canadian Journal of Civil Engineering*, vol. 18, no. 6, pp. 995–1004, doi: <https://doi.org/10.1139/I91-122>
- Briceño-Mena, J. A., Balancán-Zapata, M. G., Castro-Borges, P., Pérez-López, T. (2021), “Extending the Service Life of a Historical Concrete Building”, *Materials Performance*, pp. 1–8, 2021. URL: <https://materialsperformance.com/articles/coating-linings/2021/04/extending-the-service-life-of-a-historical-concrete-building>
- González Cueto Vila, A. V., Quevedo Sotolongo G. (2007), “Aplicación de la teoría de seguridad al diseño de cimentaciones en arenas. Chequeo de linealidad” *Revista Ingeniería de Construcción* Vol. 22 No. 2, pp. 81–88, [www.ing.puc.cl/ricvol](http://www.ing.puc.cl/ricvol). <https://scielo.conicyt.cl/pdf/ric/v22n2/art02.pdf>
- Ridell C. R., Hidalgo O. P. (2010), *Diseño Estructural*, Quinta. Pontificia Universidad Católica de Chile. I.S.B.N. 956-14-0463-X
- Helene, P., Pereira, F. (2003), *Manual de rehabilitación de estructuras de hormigón - reparación, refuerzo y protección*. Red Rehabilitar, Ciencia y Tecnología para el Desarrollo (CYTED), 2003.
- Ministerio de Vivienda y Urbanismo - Minvu (2018), *Vol. 4. Manual De Reparaciones Y Refuerzos*

*Estructurales*. Editor: División Técnica de Estudio y Fomento Habitacional – Ditec, Minvu, ISBN: 978-956-9432-85-9. Gobierno de Chile, febrero de 2018.

Melchers, R. E. (2001), “*Assessment of existing structures—approaches and research needs*” J. Struct. Eng., vol. 127, no. 4, pp. 406–411, doi: [https://doi.org/10.1061/\(ASCE\)0733-9445\(2001\)127:4\(406\)](https://doi.org/10.1061/(ASCE)0733-9445(2001)127:4(406))

Organismo Nacional de Normalización y Certificación de la Construcción y Edificación S. C. (2016) *NMX-C-505-ONNCCE, Industria de la Construcción – Inspección Preliminar de Daños en Estructuras de Concreto Hidráulico con Criterios de Durabilidad - Procedimientos*.

Organismo Nacional de Normalización y Certificación de la Construcción y Edificación S. C. (2018), *NMX-C-520-ONNCCE, Industria de la Construcción-Inspección Detallada de Daños en Estructuras de Concreto Hidráulico con Criterios de Durabilidad-Procedimientos*.

Organismo Nacional de Normalización y Certificación de la Construcción y Edificación S. C. (2018) *NMX-C-530-ONNCCE, Industria de la construcción – Durabilidad – Norma general de durabilidad de estructuras de concreto reforzado – Criterios y Especificaciones*.

Val, D. V., Stewart, M. G. (2002), “*Safety Factors for Assessment of Existing Structures*,” J. Struct. Eng., vol. 128, no. 2, pp. 258–265, doi: [https://doi.org/10.1061/\(ASCE\)0733-9445\(2002\)128:2\(258\)](https://doi.org/10.1061/(ASCE)0733-9445(2002)128:2(258))

## Thermographic study of the pathological manifestations due to humidity and of the conservation state of the Santa Maria Basilica's roof

D. Bru<sup>1</sup>\*, S. Ivorra<sup>1</sup>

\*Contact author: [david.bru@ua.es](mailto:david.bru@ua.es)

DOI: <https://doi.org/10.21041/ra.v12i1.567>

Reception: 01/11/2021 | Acceptance: 13/12/2021 | Publication: 01/01/2022

### ABSTRACT

This paper analyzes the current state of the roof of the Basilica of Santa Maria, Alicante, Spain. This building dates back to the 13th century and is catalogued. For the analysis of the efflorescence observed, an analysis of the constructive typology is carried out, as well as a visual analysis of the state of the same, describing the existing pathological manifestations, both in the exterior area of the roofs, as well as in the interior area of the rooms under them. For the technical analysis of the possible leaks from the roof to the interior rooms of the basilica, a watertightness test and the verification through the control of the variation of temperatures by means of thermographic analysis are carried out. It can be concluded the existence and position of leaks that have damaged this listed building.

**Keywords:** thermography, humidities, filtrations, efflorescence, historical building.

**Cite as:** Bru, D., Ivorra, S. (2022), “*Thermographic study of the pathological manifestations due to humidity and of the conservation state of the Santa Maria Basilica's roof*”, Revista ALCONPAT, 12 (1), pp. 110 – 126, DOI: <https://doi.org/10.21041/ra.v12i1.567>

<sup>1</sup>Departamento de Ingeniería Civil, Escuela Politécnica Superior, Universidad de Alicante, Alicante, España.

#### Contribution of each author

In this work the author David Bru contributed 100% with the data collection and experimentation activity, with the original idea activity, writing of the work and discussion of the results in 50%. The author Salvador Ivorra contributed with the activity of original idea, writing of the work and discussion of the results by 50%.

#### Creative Commons License

Copyright 2022 by the authors. This work is an Open-Access article published under the terms and conditions of an International Creative Commons Attribution 4.0 International License ([CC BY 4.0](https://creativecommons.org/licenses/by/4.0/)).

#### Discussions and subsequent corrections to the publication

Any dispute, including the replies of the authors, will be published in the third issue of 2022 provided that the information is received before the closing of the second issue of 2022.

## **Estudo termográfico das manifestações patológicas devidas à umidade e do estado de conservação da cobertura da Basílica de Santa Maria**

### **RESUMO**

Este trabalho analisa o estado atual da cobertura da Basílica de Santa María, Alicante, Espanha. Este edifício data do século XIII e está catalogado. Para a análise das eflorescências observadas foi efetuada uma análise da tipologia da construção, bem como uma análise visual do estado dela, descrevendo as manifestações patológicas existentes, tanto na zona exterior das coberturas, como na área interna dos ambientes abaixo dela. Para a análise técnica de possíveis vazamentos através da cobertura para os ambientes interiores da basílica, foi efetuado um ensaio de estanqueidade e verificação através do controle da variação de temperatura por meio de análise termográfica. O procedimento foi adequado para entender e comprovar a existência e localização de vazamentos que danificaram este edifício.

**Palavras-chave:** termografia, umidade, infiltração, eflorescência, edifício histórico.

## **Estudio termográfico de las manifestaciones patológicas por humedades y del estado de conservación de la cubierta de la Basílica de Santa María**

### **RESUMEN**

El presente trabajo analiza el estado actual de la cubierta de la Basílica de Santa María, Alicante, España. Este edificio data del siglo XIII y está catalogado. Para el análisis de las eflorescencias que se observan se realiza un análisis de la tipología constructiva, así como un análisis visual del estado de las mismas, describiendo las manifestaciones patológicas existentes, tanto en la zona exterior de las cubiertas, como en la zona interior de las salas bajo las mismas. Para el análisis técnico de las posibles filtraciones de la cubierta a las salas interiores de la basílica se realiza una prueba de estanquidad y la verificación a través del control de la variación de temperaturas mediante análisis termográfico. Se puede concluir la existencia y posición de filtraciones que han dañado este edificio catalogado.

**Palabras clave:** termografía, humedades, filtraciones, eflorescencias, edificio histórico.

### **Legal Information**

Revista ALCONPAT is a quarterly publication by the Asociación Latinoamericana de Control de Calidad, Patología y Recuperación de la Construcción, Internacional, A.C., Km. 6 antigua carretera a Progreso, Mérida, Yucatán, 97310, Tel.5219997385893, [alconpat.int@gmail.com](mailto:alconpat.int@gmail.com), Website: [www.alconpat.org](http://www.alconpat.org)

Reservation of rights for exclusive use No.04-2013-011717330300-203, and ISSN 2007-6835, both granted by the Instituto Nacional de Derecho de Autor. Responsible editor: Pedro Castro Borges, Ph.D. Responsible for the last update of this issue, Informatics Unit ALCONPAT, Elizabeth Sabido Maldonado.

The views of the authors do not necessarily reflect the position of the editor.

The total or partial reproduction of the contents and images of the publication is carried out in accordance with the COPE code and the CC BY 4.0 license of the Revista ALCONPAT.

## 1. INTRODUCTION

The purpose of this work is the technical assessment of the current pathological manifestations of the waterproofing system in the roof of the Basilica of Santa Maria, Alicante, Spain, Figure 1. The Basilica of Santa Maria, located at coordinates 38°20'46"N 0°28'45"W and less than 300 m from the coastline, has been catalogued as an Asset of Cultural Interest within the monuments listed in the Valencian Cultural Heritage. The oldest parts of the building have been dated between the 13th and 14th centuries. From the architectural point of view, the structure has a single nave without transept, with side chapels located between the buttresses and a polygonal apse, Figure 2. The main nave is covered by six ribbed vaults with pointed arches, separated from each other by toral arches, which together with the ribs start from the capital in a solution typical of the late fifteenth century and the first decades of the sixteenth century (Beviá et al, 1997).

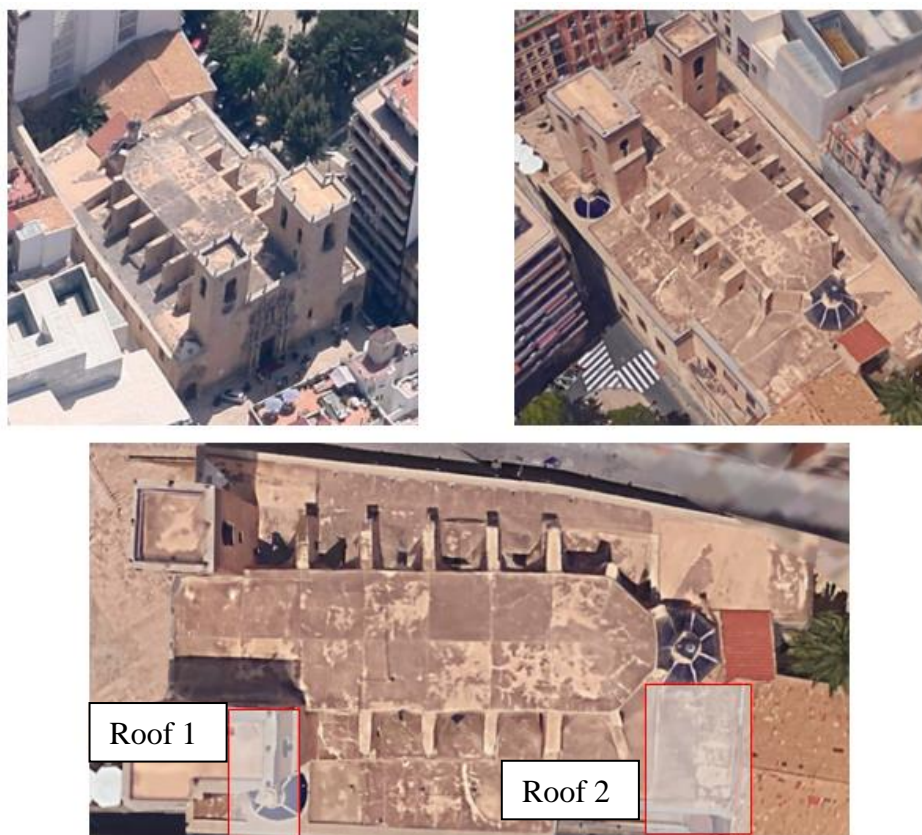


Figure 1. Aerial view of the Basilica of Santa María, Alicante. Sup. left: northwest facade. Sup. right: Southeast facade. Below: Plan view of the Basilica of Santa Maria, Alicante. Identification of study roofs. Source: Images ©2016 Google, Map data ©2016 Google, Inst. Geogr. Nacional.

Regarding the main materials that constitute the masonry elements of the Basilica of Santa Maria, no laboratory studies have been carried out to identify their origin. However, and according to the historical data, we provide in the present investigation the data associated with the rocks of the same origin arranged in the Civil Palaces of Gravina Street (Louis et al. 2001), close to the location of the Basilica. The data obtained from this research allow us to classify the typology of the rock used, its compressive strength and absorption coefficient. In this sense, the rock consists of a biocalcarene with variable grain size, from medium to coarse sand and even microconglomerate (>2mm), with a high porosity and a compressive strength of 6.1 MPa. On the other hand, in relation to the absorption coefficient, values between 6% and 15% are shown. In this sense, it is important

to highlight the high value of the same in comparison with other limestone or marl type stones, with values between 0.56% and 2.05% (Thomas et al. 2008). Other data associated with the calcite content and density of this material are shown in Table 1.

Finally, Louis et al (2001), also highlight an important aspect for the analysis of pathologies due to the presence of moisture in this type of materials. Specifically, they evaluate the presence of efflorescence and highlight the highly detrimental effect of salt crystallization in the process of alveolar erosion and especially in areas with facades exposed to the sea wind, since this effect favors the crystallization of salts and contributes with a large amount of sea salt due to the sea spray effect. These statements are confirmed by the presence of halite in the efflorescence on the inside of the structure. In addition, they show that part of the sodium chloride from the marine environment or from the infiltration water has reached part of the analyzed building due to capillarity phenomena. Therefore, based on the previous results of Louis et al (2001), the hypothesis of the presence of salts in the constituent materials of the Basilica analyzed can be affirmed.

Table 1. Compositional data and some physical properties of the San Julián Stone (Brotóns et al. 2013).

<b>San Julián Stone</b>	<b>Quarry</b>	<b>Buildings</b>
Calcite (%)	80-85	65-85
Water absorption (%)	7.6-15.1	6.2-13.0
Real density (g/cm <sup>3</sup> )	2.64-2.67	2.59
Apparent density (g/cm <sup>3</sup> )	1.85-2.29	1.8-2.4

The building analyzed in this study is framed within the typologies of historical constructions, being its constructive approach very different from the buildings of today. From the hygrothermal point of view, its main difference is its conception as a building permeable to water (in vapor or liquid form), both from the exterior and from the interior (Paricio, 1985), unlike current buildings that are designed as isolated elements, to avoid the loss of energy to the exterior. Schematically, the building studied, as mentioned in section 1, has a perimeter enclosure that is estimated (with the available means) to have a very thick sheet. This fact causes that, facing the action of external water, the external part of the leaf in contact with the water gets wet and diffuses the water in liquid form through the thickness of the wall. The advance of the water through the wall forms a "wet front" until the precipitation ceases. This amount of water remains absorbed in the masonry due to the high absorption capacity of the constituent materials of the masonry and then evaporates on both sides of the wall. Therefore, it is possible to intuit the importance of the thickness and permeability of the material, in order to prevent the wet front from appearing inside the room and, above all, so that once the source of humidity is finished, the water evaporates in the shortest possible time, especially to avoid overlapping of wet fronts between different precipitation cycles. Therefore, it is also clear that the evacuation of water in this type of building occurs in a deferred manner by diffusion and evaporation. Therefore, it is common to observe in this type of building processes of saturation of the facing by rainwater, once the pores are saturated, and surface runoff processes along the facing, producing the wetting of other areas of the element arranged for the enclosure of the construction.

On the other hand, in relation to the dynamic phenomena of water inside the building in the form of vapor, it is important to note that, due to the absence of plastic sheets or vapor barriers such as those currently used in modern roofs and enclosures, the building was characterized as eminently permeable. It is common for the minimum specific humidity of a room to be the same as that of the outside, since the air is able to penetrate from the outside without being subjected to any barrier process. Therefore, the usual problems of this type of construction when faced with humidity in its



original conception was to try to eliminate the excess vapor generated inside the rooms due to human respiration and perspiration, in order to equalize the specific humidity inside the room to that of the outside. Thus, as mentioned above, if the room did not have windows or openings to eliminate the excess water vapor accumulated in the room, it was eliminated either by diffusion through the walls, convection through openings and slits, or by absorption of the vapor in the materials, which was then transferred to the environment when it was dried.

Once the technical conception of the approach to the enclosure systems of the historic buildings has been considered, it is necessary to analyze the possible causes that generate the formation of damp, since this is the main reason for the writing of this study. The presence of humidity can be due to filtration processes by direct contact with water or by capillarity. In both cases, the transfer of water through the masonry may entail the entrainment of soluble salts, either from the rock itself or from the seepage water itself. Such soluble salts can be retained in the enclosures when the water evaporates, crystallizing in the pores and causing the appearance of efflorescence (Giovannacci et al, 2017). The saturation of the pores due to the presence of salt crystallization decreases the evaporation processes and causes a displacement of the moisture stains due to the search for new exit zones of the water vapor present in the porous materials.

On the other hand, if the accumulation of salts mentioned above corresponded to hygroscopic salts, these would tend to retain water from the air when the relative humidity exceeds a certain limit value, which could generate a false mechanism of the presence of moisture due to hygroscopic condensation, with the possible appearance of stains, but caused simply by the absorption of water vapor from the air due to the effect of the hygroscopicity of the salts and not by the real presence of a source of water by filtration or capillarity. For this reason, a general cause of moisture pathology in historic buildings is the appearance of efflorescence due to local seepage phenomena caused years ago that have subsequently been reactivated. That is to say, the appearance of new moistures on the masonry would not be due to the real presence of a new water seepage, but due to the hygroscopicity of the salts on the surface of the rocks. Grossi and Esbert (Grossi and Esbert, 1994) show a deep bibliographical review on the effects of soluble salts in the deterioration of monumental rocks. In this sense, in the interior of the analyzed church, different efflorescences and stains are observed, which suggest the existence of filtrations, Figure 2.

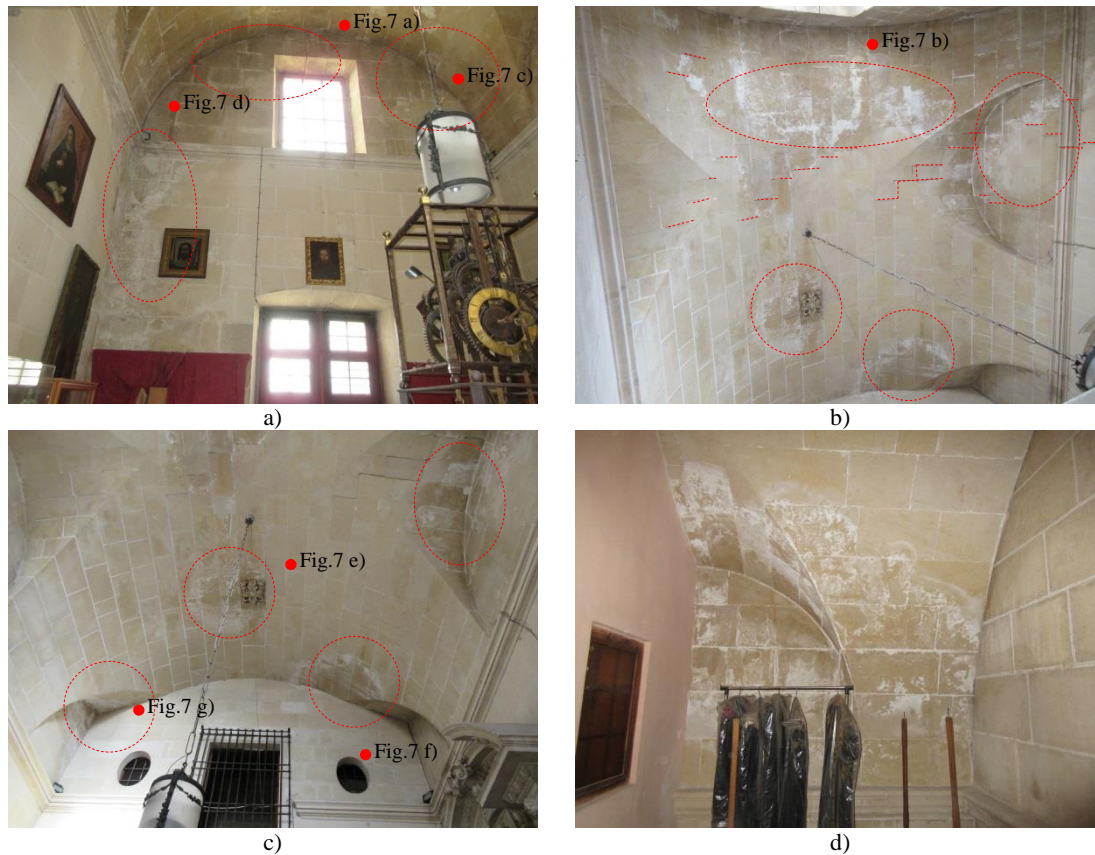


Figure 2. Photos of rooms under roof 2: a) East facade, b) Lower view of the roof, c) Lower view of the roof with vault partition wall, d) Upper adjoining room after division with partition wall. Photos of rooms under roof 1: e) Lower view of the roof area next to the exterior facade, f) Lower view of the roof in contact with the body of the church. Figures a), b), c) include the tomography points of Figure 7 with a red dot.

## 2. EXPERIMENTAL PROGRAM

A comparative visual analysis has been carried out, based on the performance of a watertightness test, analyzing the state of the rooms before and after the flooding process of the roofs, with the aim of detecting leaks with quick access from the roof. Finally, an analysis was performed from infrared thermography of both the roof and the aforementioned rooms, in order to detect the existence of localized thermal bridges and areas of significant moisture presence (Takeda, 2018), (Silva et al, 2019).

In order to determine the general operating conditions of the roof in relation to the slopes, the state of the waterproofing support, as well as the state of execution of the singular elements, such as edges, junctions, drains and joints, it was proposed to perform a watertightness test in order to observe the appearance or not of humidities under the roof or in the walls, paying attention to the critical points associated with construction details according to the regulations in use at the date of waterproofing of the roof (NBE QB-90). The watertightness test consisted of flooding to a level approximately 3-7 cm above the drainage level, ensuring a sufficiently low overload level so as not to affect the structural safety conditions of the roof. The flooding was maintained for 72h, the drains being sealed with a plastic waterproofing system in order to prevent the water level on the roof from decreasing. Finally, once the time required for the watertightness test had elapsed, the sealing systems of the drains were removed in order to maintain their current operation.

On the other hand, in order to determine the presence of humidities and possible thermal bridges, which show an incorrect functioning of the roof, a test was carried out using a FLIR E30 model thermographic camera, based on the provisions of the EN 13187:1998 standard. Some recently published examples of the application of this technique can be found in the following references (Vijay et al, 2019), (Valluzzi et al, 2019), (Lucchi, 2018), (Ruiz Valero, et al, 2019), (Garrido et al, 2020), (Martínez-Garrido et al, 2018), (Zhang et al, 2018), (Barreira et al, 2020) and (Barbosa et al, 2021)).

The test was performed during two consecutive days. During the first day, the thermal recording of decks 1 and 2, as well as the room under room 2, was performed. This recording was carried out between 19:45 and 20:45. The maximum and minimum values ranged throughout the day between 10.7 °C and 17.4 °C, recording a value at the time of data collection of 15 °C outside, and 16.7°C, with a relative humidity value between 38-40%. On the other hand, for the data recorded on the second day, January 15, the maximum and minimum temperature values reached values between 16.6 °C and 8.7 °C, registering a value of 13°C outside and 15.9 °C at the time of data collection, with a relative humidity value between 52%. During this second day, the rooms under deck 1 were analyzed, as well as the building annexed to the room under deck 2. The test consisted of analyzing the critical points detected during the visual inspection phases, in order to corroborate the results experimentally. In relation to the surface, a granular material with emissivity value 0.95 was considered based on the library of materials provided by the manufacturer, homogeneous for all the surfaces analyzed. Other published examples related to the emissivity of this type of materials can be found in (Barreira et al, 2021).

### 3. RESULTS AND DISCUSSIONS

In relation to the analysis of the water flow during the watertightness test, the results show that in the case of roof 1, the upper zone channels the water perimetrically towards the gutter through the established slopes. In the case of roof 1, in the lower zone, it was possible to verify that the slopes converge in the drainage area. The absence of overflows prevents the evacuation of water in the event of saturation of the drain due to the accumulation of solid elements at its entrance. This fact makes it easier for the level of stagnant water to reach the side wall of the Communion chapel, favoring the entry of water at the intersection of the vertical wall-skirt.

Regarding the results of the thermographic analysis of roof 1, Figure 3 shows the images for both the upper and lower areas of the roof. Figure 3 (a) shows an overview of the upper part of the roof. In this image, all the possible pathological manifestations previously mentioned can be identified. In the first place, it can be seen how after the watertightness test and the pouring of the water on part of the vertical façade enclosures and 10 h after the test, part of the humidity is preserved due to the high absorption capacity of the stone in the facing. In this image, it can also be seen how the area of the parapet, the water has accumulated more than in the area located just in the area of the gutter. A detail of this area can be seen in Figure 3c, where it can be observed not only the entry and accumulation of water in the lower area, but also the water filtered through the joints between the masonry pieces. On the other hand, it should also be noted the abrupt change in thermal characteristics at the joint between the parapet and the wall corresponding to the rigid protection of the upper skirt, Figure 3a-3c. The joint between the two materials is clearly observed and it can be seen how part of the water poured from the end of the skirt has dripped down the facing, being stored in the area of the joint, due to the absence of the correct realization of the detail of the end of the skirt. In relation to the gutter, however, no leakage problems have been detected. On the other hand, Figure 3b shows a detail of the gutter for the passage of the installations. In this image, it can be seen in green, the rear area of the gutter, where water has been stored, due to the lack of watertightness of the joint and the absence of a protection device to prevent water from dripping

down the face and leaking behind the gutter. On the other hand, Figure 3d shows a detail of the lack of watertightness of the right end of the parapet, in the area of connection of the end of the skirt, the parapet and the buttress, marking the area that is currently very deteriorated, being an obvious sign of lack of waterproofing. Also in relation to waterproofing problems, it can be seen in Figure 3e, the absence of the waterproofing in the contact area of the lower skirt with the parapet, as well as the presence of vegetation in the rightmost area of the photo, where the temperature is higher. In addition, the current state of waterproofing of the damaged area of the sill can be evaluated by means of this image. The results shown by thermography did not show the presence of watertightness problems. Finally, Figures 3g-3h show the dammed area during the test, where the process of capillary rise through the facing can be clearly observed, clearly exceeding the 5 cm of waterproofing strip currently in place at the junction of the skirt with the vertical facing, in the areas where it has been placed, since there is an absence of this construction detail in various parts of the lower skirt.

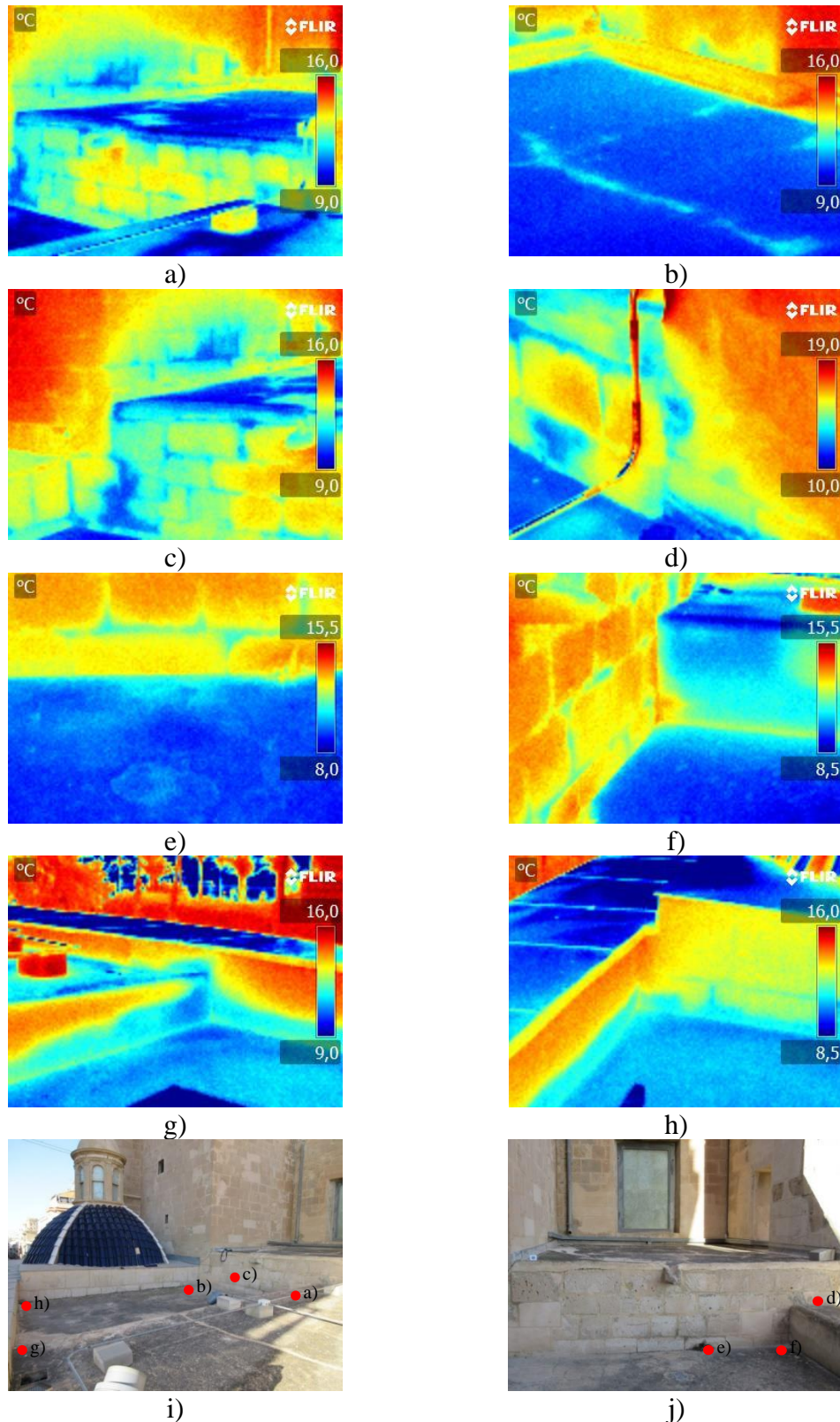


Figure 3. Thermography of roof 1: a) General view of the upper area, b) Detail of the installations gutter, c) Moisture in vertical facing and corner of parapet, filtration through masonry joints, d) Lack of watertightness in parapet and buttress, e) Lower skirt and vertical facing, f) Lateral connection of parapet skirt, g) and h) Capillarity, i) and j) location of the thermographs. The red dots indicate the location of the thermography in the associated image.

In relation to the results of the analysis of roof 2, Figure 4a and 4b show the detail of the absence of the perimeter joint, showing the difference in temperatures in the areas where the mortar is totally deteriorated, and the joint is without mortar between the end of the skirt and the facing. It is important not to confuse this with the red line associated with the passage of an installation pipe, since the area analyzed is the one associated with the end of the connection with the vertical face of the facade. These images show the lack of thermal insulation in the sections of the vertical facing, as well as areas with a colder tone, due to the water spilled during the load test. Figures 4c and 4d show a detail of this area without thermal camera application. On the other hand, Figure 4e shows the side skirt end zone. In this image it can be seen how the lack of thermal insulation in the vertical facing sections, as well as areas of colder tone, due to the water poured during the load test. This area is shown in a more greenish tone in the middle area of the photo. Also noteworthy is the contrast at the skirt end joint, clearly showing the position of the horizontal joint between the upper material and the support material. This joint, represented as a yellow line with cyan tones, presents an important state of deterioration, as could be observed during the visual analysis of the roof, Figure 4g. Finally, Figure 4f shows a detail of the perimeter end of the skirt, in the area near the access door to the roof. Figure 4 also includes digital camera images of the areas analyzed by thermal imaging. The comparison of these images allows observing the benefits of the use of thermography in the detection of pathologies, being this a support technique to the visual inspection.

On the other hand, Figures 5, 6 and 7 show the details of the temperature distribution inside the three interior rooms analyzed. It should be noted that due to the low levels of thermal differences between the different structural elements that make up the enclosure, the sharpness of the images does not show such a differentiated behavior as in the case of the analysis of the roofs. In order to increase the thermal contrast, in some rooms the spotlights were kept on before the test was carried out, in order to ensure the position of the edges of the room, once the thermal photos were taken, since these were taken with the light off.

Analyzing the thermal behavior of the room under the lower area of roof 1, Figure 5, referred to throughout the study as the room adjacent to the Communion Chapel, it can be seen in Figure 5a, corresponding to the corner of connection between the exterior facade and the main arch that gives access to the Communion Chapel and, arranged in the area near the presence of the drain in the roof at the top, that the thermal difference between the part corresponding to the facade and the roof of the vault is clearly defined. However, with the climatic conditions recorded during the test, the presence of specific thermal irregularities in the potentially damaged areas associated with the connection between the facade and the toral arch of the groin vault analyzed were not detected. Also, part of the exterior window is observed, which serves as a reference in order to be able to frame the photo. Figure 5b shows a detail of the window area. In this image, the cold spot effect is clearly visible due to the higher thermal transparency of the glass compared to the high thicknesses of the facade. In addition, the lack of thermal insulation in the connection areas between the facade and the roof can be observed, clearly marking the junction edge between the two, and showing a temperature gradient from the beginning to the central area of the vault. In Figure 5c, the thermography of the other corner of the exterior facade is shown, similar to that described in Figure 5a. As can be seen, in this image there are no relevant signs of pathology, being detected only the thermal gap between the vertical faces and the roof of the vault. Finally, Figure 5d shows a general image of the roof. This image shows the presence of a part of the roof slightly colder than the other, mainly due to the effect of the accumulation of water during the test.

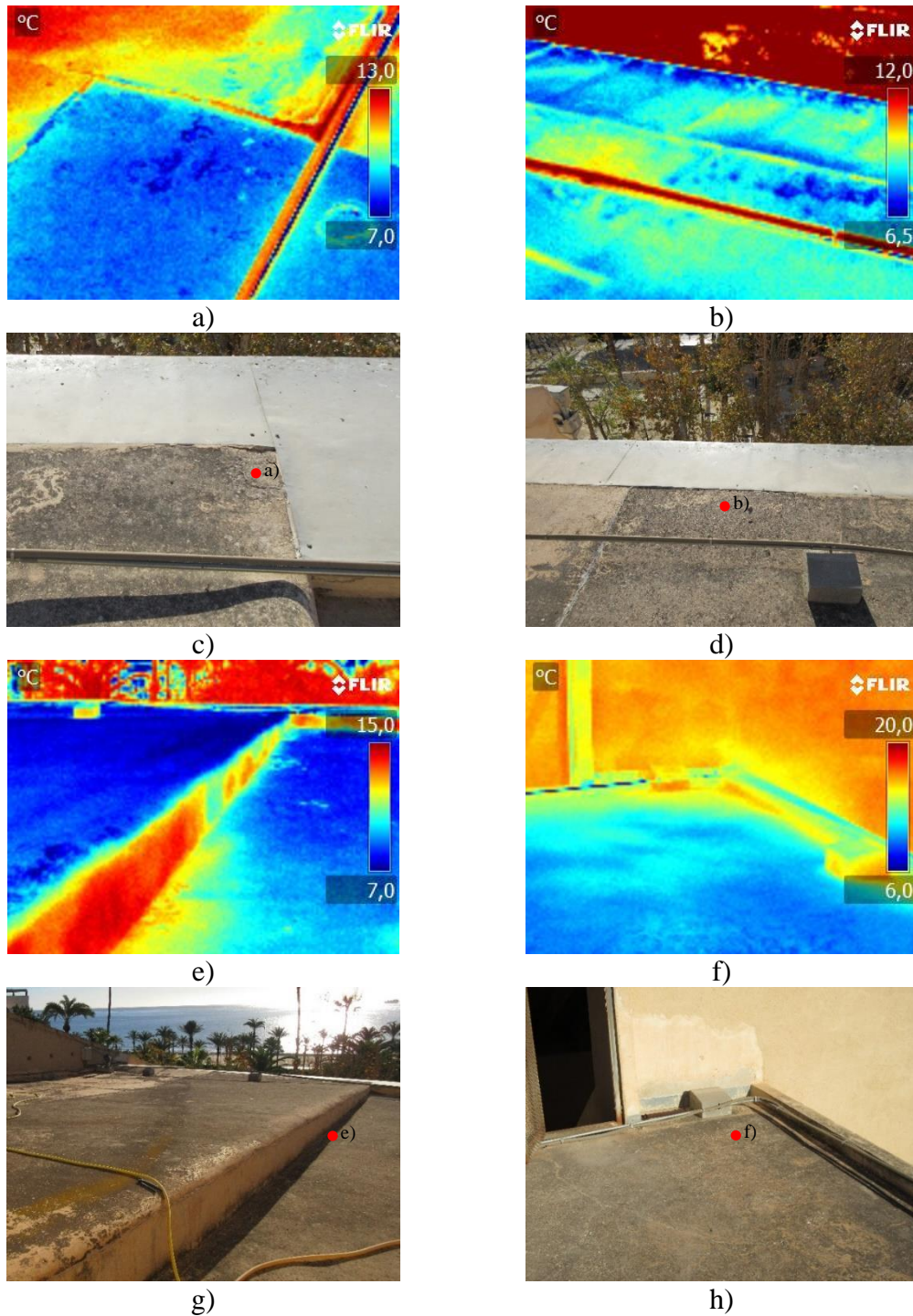


Figure 4. Thermography roof 2: a) Deterioration of perimeter joint, b) Detail of failure in perimeter joint in contact of the skirt with the facade, c) and d) Image a) and b) with digital camera, e) Detail of the lateral end of the skirt and connection with the roof, f) Perimeter zone of the skirt in the access area to the roof; g) and h) Image e) and f) with digital camera. The red dots indicate the location of the thermography in the associated image.

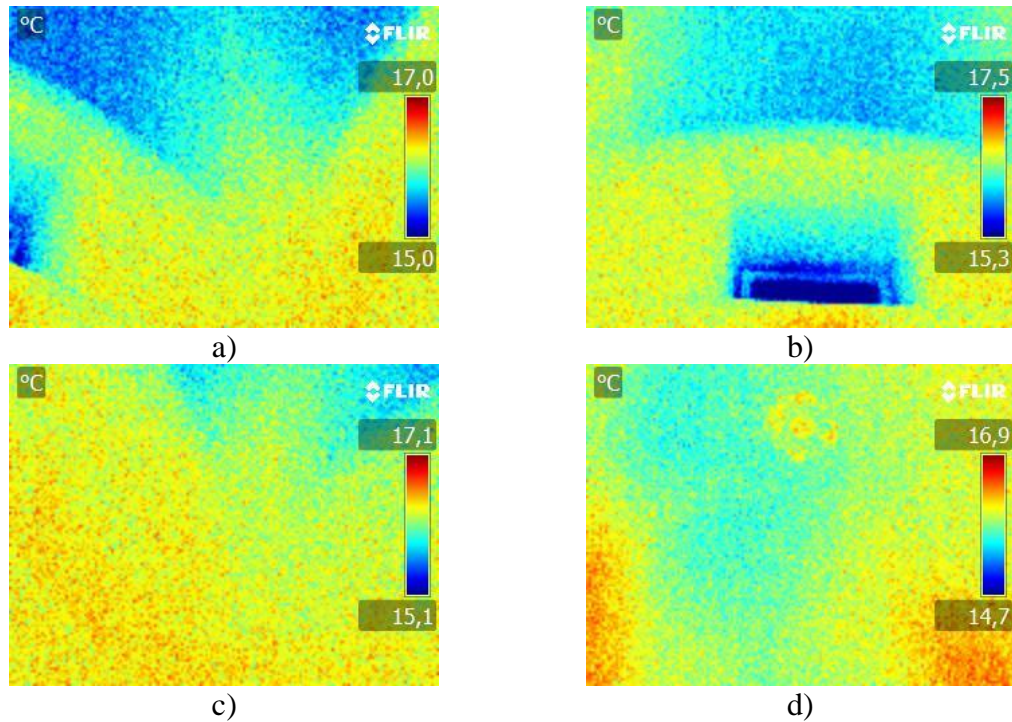


Figure 5. Thermography of rooms under roof 1, adjacent to the Communion Chapel: a) Connection of the main arch with the exterior facade, in the area of access to the Communion Chapel, b) Connection of the facade with the roof in the window area, c) Second corner of the facade wall, equivalent to image (a), d) General view of the roof from below.

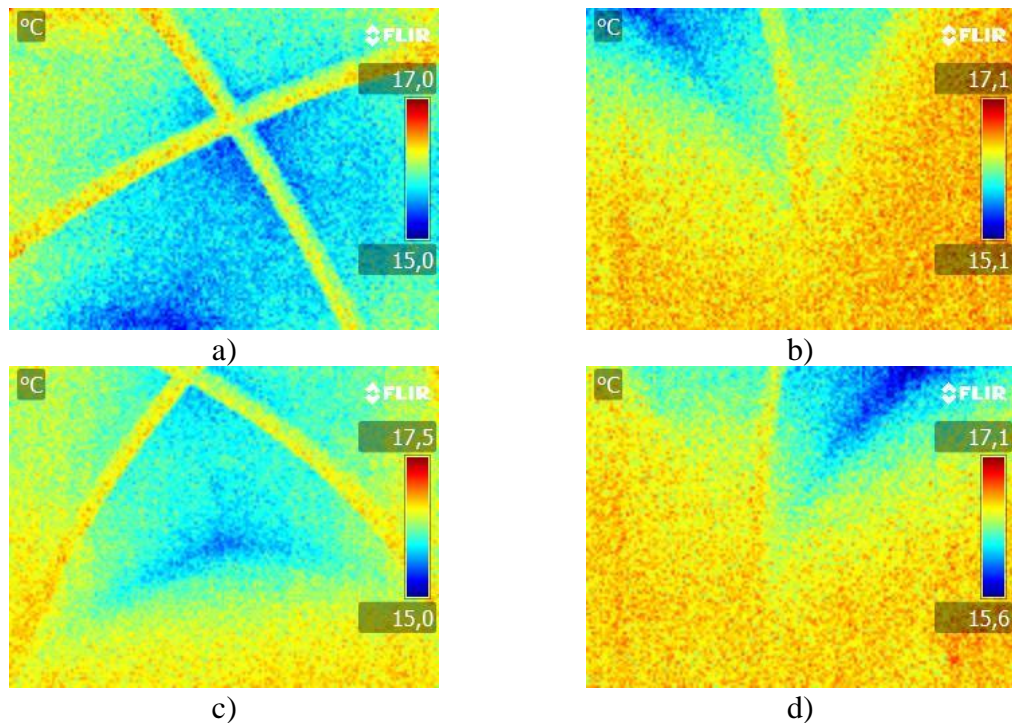


Figure 5. Thermography of rooms under roof 1, adjacent to the side building: a) General view of roof, b) Connection between facade and side corner, c) Connection between facade and roof, d) Connection between facade and opposite side corner.



In relation to the analysis by thermography carried out for the room located in the side nave, adjacent to the central nave of the basilica, Figure 6 shows the distribution of temperatures in the different critical points analyzed in the previous sections. First, Figure 6a shows a lower view of the groin vault roof. It can be observed the difference in temperatures between the perpendicular arches and the rest of the plementery that makes up the vault roof. On the other hand, Figure 6b and 6d show the detailed thermography of the connection corners between the perpendicular arches and the facade walls. A pattern of behavior similar to those described for the previous room is observed, with the difference of the higher temperature of the start of the arches. It should be noted that the analysis of these points was carried out without the presence of nearby light sources before or during the test, so the thermal distribution is due to the hygrothermal equilibrium between the exterior and the interior of the building. Finally, Figure 5c shows the same problem of lack of insulation as in the previous room, due to the connection joint between the vertical facing and the roof.

Finally, in relation to the thermography analysis carried out for the room under deck 2, Figure 7 shows the distribution of temperatures in the different critical points analyzed in the previous sections. In general, the thermal behavior is very similar to those detected in the previous rooms, except that in this case a high thermal difference between the points of the interior facade and the roof has not been observed. That is, Figures 7a, 7b, 7c and 7d show the detail of the contact between the facade and the roof, showing the thermal leaks in the upper part of the window area, as well as in the window itself. Figure 7e shows a thermography of the part of the roof corresponding to the anchorage of the chandelier, where a uniform distribution of temperatures is observed without the presence of detected damage. In Figures 7f and 7g, the thermographies associated to Figures 7c and 7d are observed, but in this case, in the facade opposite to the exterior one. In this case, the thermal variations can be observed in the areas affected by the heating of the light sources. This is due to the presence of cold spots in the contact zones between the side wall and the facade. These cold spots, especially those detected in Figure 7g, are related to the detected moisture stains. In these images, the coldest circular hole is shown as a reference to locate the position of the photos. It is important to point out that such humidity stains, besides being related to the presence of a cold zone, are also related to the presence of a water accumulation zone in the upper part of deck 2, close to the dome. In this area the water collected in the dome is discharged, and the lack of lateral sealing at the end of the skirt, together with the low level of ventilation in the room shown, cause the increase in humidity, and thus the appearance of such efflorescence.

Finally, it should be noted the presence of a leak detected in the annex building with access to room 2. This leak is on the roof of the upper floor. It has not been possible to detect whether the presence of moisture is due to an error in the tile roof, or in the roof 2 itself. However, due to its geometric position, it is very close to the position of the roof drain, which could be a sign of a lack of watertightness of the roof.

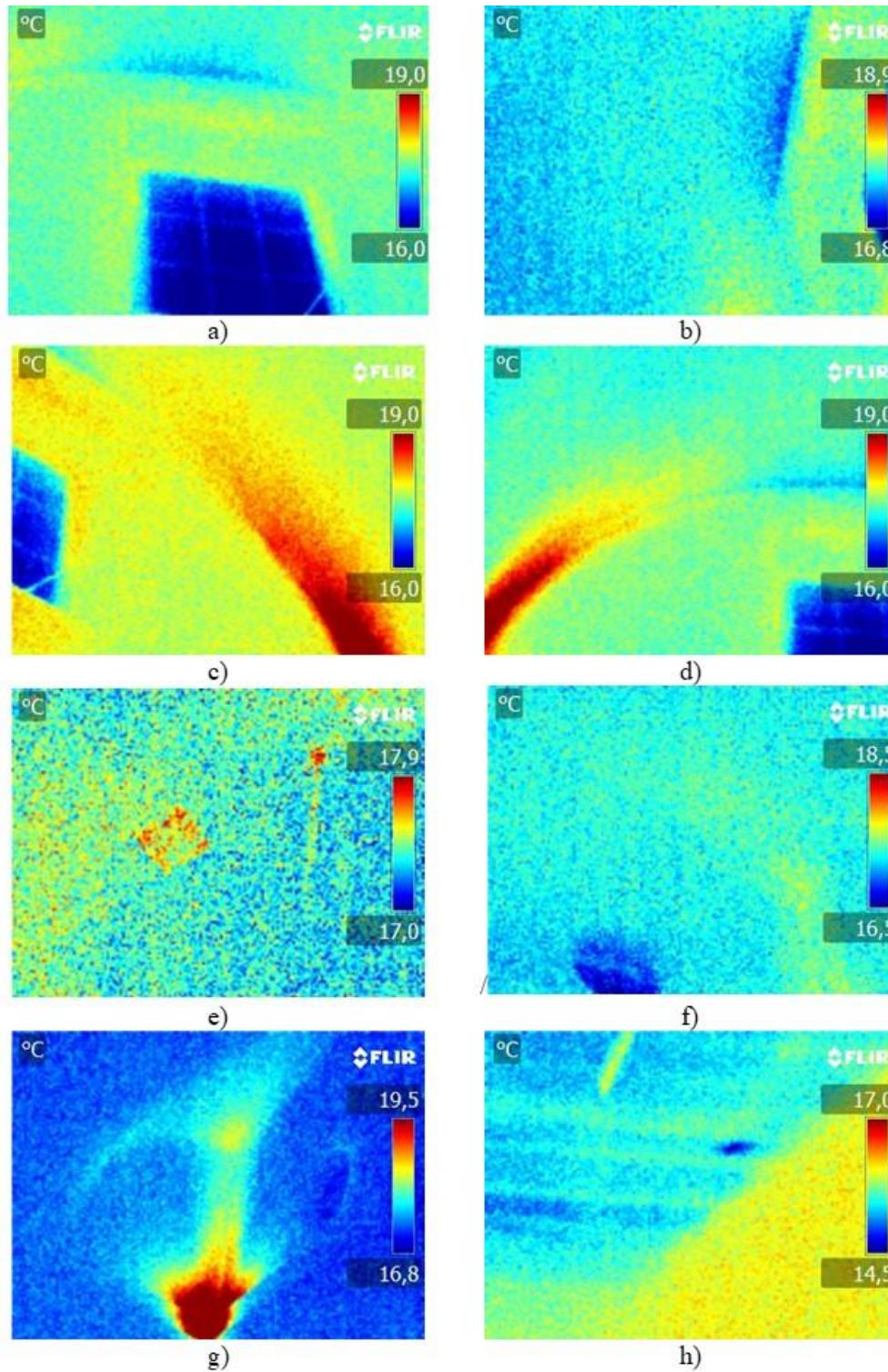


Figure 7. Thermography of room under roof 2: a) window and slab area, b) lower view of roof, c) connection view of slab side wall, d) connection view of slab side wall, e) central area of roof, f) view of rear dividing wall, g) connection view of side wall and rear wall, h) leak in outbuilding area.

## 4. CONCLUSIONS

After carrying out the technical assessment study of the state of watertightness and the analysis of humidities of the roofs analyzed in the basilica of Santa Maria, it can be concluded that the current state of the roof does not meet the minimum technical conditions based on the current state of the construction details according to the provisions of the regulations (NBE QB-90). Likewise, the state of humidity and efflorescence present in the interior areas is due to a problem of hygroscopic condensation, because the humidity increases due to the proximity to the maritime area, as well as the lack of ventilation of the interior rooms studied. In addition, this pathology is intensified by the possible filtration problems caused during the months of October and November, due to the higher level of rainfall. This water accumulates in the interior of the construction elements and eliminates excess humidity by vapor transmission as the thermal conditions of the building change. In addition, the presence of sea salts in nearby buildings and the high absorption capacity of the materials studied, show a behavior prone to the dragging of salts in solution during the rainy season, which favors the appearance of efflorescence, which increases the risk of condensation moistures. On the other hand, in relation to the use of thermographic analysis techniques, the images have made it possible to detail existing pathologies with greater precision, especially those due to thermal leaks and areas of moisture accumulation, which are imperceptible during visual exploration. This fact highlights the feasibility of using thermography to identify pathologies in masonry buildings that could be hidden by coatings or geometric conditions that prevent their detection with the naked eye. In addition, by using this technique it is possible to more accurately delimit the repair surfaces from the point of view of a future intervention compared to a direct visual analysis without thermography as commented by Barbosa (Barbosa et al, 2021).

## 5. ACKNOWLEDGEMENTS

The authors wish to thank the Bishopric of Orihuela-Alicante for their willingness to carry out this study on a catalogued property.

## 6. REFERENCES







- Barbosa, M.T.G., Rosse, V. J., Laurindo, N. G. (2021), “*Thermography evaluation strategy proposal due moisture damage on building facades*”, Journal of Building Engineering, 43, art. no. 102555, DOI: <https://doi.org/10.1016/j.jobbe.2021.102555>
- Barreira, E., Almeida, R.M.S.F., Simões, M.L., Rebelo, D. (2020), “*Quantitative infrared thermography to evaluate the humidification of lightweight concrete*”, Sensors (Switzerland), 20 (6), art. no. 1664, DOI: <https://doi.org/10.3390/s20061664>
- Barreira, E., Almeida, R.M.S.F., Simões, M.L. (2021), “*Emissivity of building materials for infrared measurements*”, Sensors, 21 (6), art. no. 1961, pp. 1-13. DOI: <https://doi.org/10.3390/s21061961>
- Bevià García, M., Azuar Ruiz, R. (2005), “*Santa María descubierta: Arqueología, arquitectura-cerámica: Excavaciones en la Iglesia de Santa María de Alicante (1997-1998)*”. Alicante. Fundación MARQ. ISBN: 84-609-7478-2
- Brotóns, V., Tomás, R., Ivorra, S., Alarcón, J.C. (2013), “*Temperature influence on the physical and mechanical properties of a porous rock: San Julian's calcarenite*. Engineering Geology”, 167, pp. 117-127. DOI: <https://doi.org/10.1016/j.enggeo.2013.10.012>

- Giovannacci, D., Brissaud, D., Mertz, J.-D., Mouhoubi, K., Bodnar, J.-L. (2017), “*Nonintrusive tools to detect salts contamination in masonry: Case study of Fontaine-Chaalis church*”, Proceedings of SPIE - The International Society for Optical Engineering, 10331, art. no. 1033103. DOI: <https://doi.org/10.1117/12.2269727>
- Grossi, C. M. Esbert, R. M. (1994), “*Las sales solubles en el deterioro de rocas monumentales. Revisión bibliográfica*”. Materiales de Construcción, Vol. 44, nº 235. DOI: <https://doi.org/10.3989/mc.1994.v44.i235.579>
- Louis, M., García del Cura, M. A., Spairani, Y., de Blas. D. (2001), “*The Civil Palaces in Gravina Street, Alicante: building stones and salt weathering*. Materiales de Construcción”, Vol. 51, nº262. DOI: <https://doi.org/10.3989/mc.2001.v51.i262.369>
- Lucchi, E. (2018), “*Applications of the infrared thermography in the energy audit of buildings: A review*”, Renewable and Sustainable Energy Reviews, 82, pp. 3077-3090. DOI: <https://doi.org/10.1016/j.rser.2017.10.031>
- Paricio Ansuateguie, I. “*La construcción de la Arquitectura. Institut de Tecnologia de la Construcció de Catalunya*”, 1985, T.2, p. 26. ISBN: 978-84-7853-375-6
- Norma Básica de la Edificación. Cubiertas con materiales bituminosos: “*NBE QB-90*”. Gobierno de España.
- Ruiz Valero, L., Flores Sasso, V., Prieto Vicioso, E. (2019), “*In situ assessment of superficial moisture condition in façades of historic building using non-destructive techniques*”, Case Studies in Construction Materials, 10, art. no. e00228, DOI: <https://doi.org/10.1016/j.cscm.2019.e00228>
- Silva, G. P., Batista, P. I. B., Povóas, Y. V. (2019), “*Uso de termografía infrarroja para estudiar el desempeño térmico de paredes: una revisión bibliográfica*”, Revista ALCONPAT, 9(2), pp. 117 – 129, DOI: <http://dx.doi.org/10.21041/ra.v9i2.341>
- Takeda, T. Mazer, W. (2018), “*Potencial da análise termográfica para avaliar manifestações patológicas em sistemas de revestimentos de fachadas*”, Revista ALCONPAT, 8 (1), pp. 38 – 50, DOI: <http://dx.doi.org/10.21041/ra.v8i1.181>
- Valluzzi, M.R., Lorenzoni, F., Deiana, R., Taffarel, S., Modena, C. (2019), “*Non-destructive investigations for structural qualification of the Sarno Baths, Pompeii*”, Journal of Cultural Heritage, 40, pp. 280-287. DOI: <https://doi.org/10.1016/j.culher.2019.04.015>
- Vijay, P.V., Tulasi Gadde, K., Gangarao, H.V.S. (2019), “*Structural Evaluation and Rehabilitation of Century-Old Masonry and Timber Buildings*”, Journal of Architectural Engineering, 25 (2), art. no. 05019001, DOI: [https://doi.org/10.1061/\(ASCE\)AE.1943-5568.0000350](https://doi.org/10.1061/(ASCE)AE.1943-5568.0000350)
- Garrido, I., Solla, M., Lagüela, S., Fernández, N. (2020), “*Irt and gpr techniques for moisture detection and characterisation in buildings*”, Sensors (Switzerland), 20 (22), art. no. 6421, pp. 1-38. DOI: <https://doi.org/10.3390/s20226421>
- Martínez-Garrido, M.I., Fort, R., Gómez-Heras, M., Valles-Iriso, J., Varas-Muriel, M.J. (2018), “*A comprehensive study for moisture control in cultural heritage using non-destructive techniques*”, Journal of Applied Geophysics, 155, pp. 36-52. DOI: <https://doi.org/10.1016/j.jappgeo.2018.03.008>
- Zhang, F., Zhang, X., Li, Y., Tao, Z., Liu, W., He, M. (2018), “*Quantitative description theory of water migration in rock sites based on infrared radiation temperature*”, Engineering Geology, 241, pp. 64-75. DOI: <https://doi.org/10.1016/j.enggeo.2018.05.006>

Thomas, c., Lombillo, I., Setién, J., Polanco, J. A., Villegas, L. (2008), “*Absorción por capilaridad y consolidación de materiales pétreos del patrimonio histórico construido impermeabilizados y reforzados con productos hidrofugantes y consolidantes comerciales*”. Tecnología de la rehabilitación y la gestión del patrimonio construido (REHABEND). ISBN: 978-84-692-5650-3.

UNE EN 13187 (1998). “*Prestaciones térmicas de edificios. Detección cualitativa de irregularidades en cerramientos de edificios. Método de infrarrojos*”. Asociación Española de Normalización.

## 30 years of rubberized concrete investigations (1990-2020). A bibliometric analysis

Z. Zarhri<sup>1\*</sup> , W. Rosado Martinez<sup>2</sup> , J. Dominguez Lepe<sup>2</sup> , R. E. Vega-Azamar<sup>2</sup> , M. Chan Juarez<sup>2</sup> , B. Pamplona Solis<sup>2</sup> 

\*Contact author: [z.zarhri@gmail.com](mailto:z.zarhri@gmail.com)

DOI: <https://doi.org/10.21041/ra.v12i1.554>

Reception: 31/08/2021 | Acceptance: 09/12/2021 | Publication: 01/01/2022

### ABSTRACT

This work presents a bibliometric study of the literature on the use of recycled rubber from tires in the construction industry to promote its use as a ‘raw’ material to reduce pollution at a global level. Published papers between 1990 and 2020 in both databases Scopus and Web of Science (WoS) were taken into account using the *Methodi Ordinatio* and the VOSviewer software. A total of 967 documents on the use of recycled rubber in structural and non-structural concrete have been published during this time frame and 1182 authors have contributed on the subject. Since 2010, the interest of researchers to introduce recycled rubber in construction applications has increased markedly. China, the United States of America and Australia are the leading countries in rubberized concrete research.

**Keywords:** rubberized concrete; construction; crumb rubber; bibliometric analysis; *Methodi Ordinatio*.

**Cite as:** Zarhri, Z., Rosado Martinez, W., Dominguez Lepe, J., Vega Azamar, R. E., Chan Juarez, M., Pamplona Solis, B. (2022), “30 years of rubberized concrete investigations (1990-2020). A bibliometric analysis”, Revista ALCONPAT, 12 (1), pp. 127 – 142, DOI: <https://doi.org/10.21041/ra.v12i1.554>

<sup>1</sup> CONACYT-Tecnológico Nacional de México/I.T. Chetumal; Insurgentes 330, C.P. 77013, Chetumal, Quintana Roo, Mexico

<sup>2</sup> Tecnológico Nacional de México/I.T. Chetumal; Insurgentes 330, C.P. 77013, Chetumal, Quintana Roo, Mexico.

#### Contribution of each author

In this work, William Rosado Martinez made the bibliometric studies and contribute to the discussion and the redaction of the manuscript (30%). Zakaryaa Zarhri supervised the whole work and wrote the document in English(30%). Jose Antonio Dominguez Lepe (10%), Ricardo Enrique Vega Azamar (10%) and Maritza Chan Juarez (10%) they three contributed to the discussion of the results and the correction of the manuscript. Blandy Berenice Pamplona Solis contribute to the methodology and results of the document (10%).

#### Creative Commons License

Copyright 2022 by the authors. This work is an Open-Access article published under the terms and conditions of an International Creative Commons Attribution 4.0 International License ([CC BY 4.0](https://creativecommons.org/licenses/by/4.0/)).

#### Discussions and subsequent corrections to the publication

Any dispute, including the replies of the authors, will be published in the second issue of 2022 provided that the information is received before the closing of the third issue of 2022.

## 30 años de investigaciones sobre concreto con caucho (1990-2020). Un análisis bibliométrico

### RESUMEN

Este trabajo presenta un estudio bibliométrico de la literatura sobre el uso del caucho reciclado de las llantas en la industria de la construcción para promover el interés de utilizarlo como materia prima para reducir la contaminación a nivel global. Se consideraron los trabajos publicados en el período 1990-2020, tanto en las bases de datos de Scopus como de Web of Science (WoS), y se utilizó el *Methodi Ordinatio* y el software VOSviewer para llevar a cabo el análisis. En este período de tiempo, se ha publicado un total de 967 documentos sobre el uso del caucho en concretos estructurales y no estructurales y han contribuido 1182 autores en el tema. Desde 2010, ha aumentado notablemente el interés de los investigadores por introducir el caucho reciclado en aplicaciones constructivas. China, Estados Unidos y Australia son los países líderes en la investigación del concreto con caucho reciclado proveniente de los neumáticos.

**Palabras clave:** concreto con caucho reciclado; construcción; polvo de neumático; análisis bibliométrico; *Methodi Ordinatio*.

## 30 anos de investigações sobre concreto com adição de borracha (1990-2020). Uma análise bibliométrica

### RESUMO

Este trabalho apresenta um estudo bibliométrico da literatura sobre o uso de borracha reciclada de pneus na indústria da construção para promover seu uso como matéria-prima para reduzir a poluição em nível global. Artigos publicados entre 1990 e 2020 em ambas as bases de dados Scopus e Web of Science (WoS) foram levados em consideração usando o *Methodi Ordinatio* e o software VOSviewer. Nesse período, foram publicados 967 documentos sobre o uso de borracha reciclada em concreto estrutural e não estrutural e 1182 autores contribuíram com o assunto. Desde 2010, o interesse dos pesquisadores em introduzir borracha reciclada em aplicações de construção aumentou significativamente. China, Estados Unidos da América e Austrália são os países líderes na pesquisa de concreto com adição de borracha.

**Palavras-chave:** concreto com adição de borracha; construção; borracha fragmentada; análise bibliométrica; *Methodi Ordinatio*.

### Legal Information

Revista ALCONPAT is a quarterly publication by the Asociación Latinoamericana de Control de Calidad, Patología y Recuperación de la Construcción, Internacional, A.C., Km. 6 antigua carretera a Progreso, Mérida, Yucatán, 97310, Tel.5219997385893, [alconpat.int@gmail.com](mailto:alconpat.int@gmail.com), Website: [www.alconpat.org](http://www.alconpat.org)

Reservation of rights for exclusive use No.04-2013-011717330300-203, and ISSN 2007-6835, both granted by the Instituto Nacional de Derecho de Autor. Responsible editor: Pedro Castro Borges, Ph.D. Responsible for the last update of this issue, Informatics Unit ALCONPAT, Elizabeth Sabido Maldonado.

The views of the authors do not necessarily reflect the position of the editor.

The total or partial reproduction of the contents and images of the publication is carried out in accordance with the COPE code and the CC BY 4.0 license of the Revista ALCONPAT.

## 1. INTRODUCTION

Inadequate management and disposal of solid waste is one of the activities most affecting the environment. An increase in waste generation of up to 70% is expected by 2050, from 2.01 billion tons in 2016, a total of 3.4 billion tons of annual waste is projected for the year 2050, according to the World Bank in the 2018 report “What a Waste 2.0: A Global Snapshot of Solid Waste Management to 2050” (World Bank, 2019).

Especially, when it comes to rubber and waste tires, due to their nature and polluting potential, this kind of wastes have to be processed and buried in sanitary landfills as final disposal method, however, this may lead to soil and subsoil contamination. Therefore, it is important to find a way to partially or totally reuse this waste so that it can be transformed from a potentially polluting material into a raw material for the industry at the end of its lifespan. Waste tires are one of the most polluting materials because vulcanization is an irreversible process, making it difficult to create a waste plan. For the appropriate treatment of this type of waste, the industry has special recycling facilities from which byproducts can be obtained such as fibers from tire recycling, granulated rubber, rubber in the form of chips, rubber powder as well as steel fibers (Thomas et al., 2016).

One of the offered solutions is to use it as a ‘raw’ material (Perez, 2015). At present, the scientific community has recognized the problem this represents which is why different alternatives for the use of rubber from both waste and the recycling industry have been proposed and analyzed for its application in some engineering areas. This entails economic development, job creation, as well as the fulfillment of a main objective: the reduction of pollutants in the environment (Al-Salem et al., 2009; Ghosh, 2019; Ruwona et al., 2019; Yang et al., 2018).

This bibliometric analysis is based on the search for the most relevant articles on the subject, as well as an in-depth analysis of the selected literature, with the aim of collecting data on the importance of the study of rubber for the scientific community.

This article has the purpose of carrying out a quantitative analysis on how the study of concrete with rubber addition has evolved between 1990 and 2020, with the aim to compile and analyze the most important research articles using the bibliometric method *Methodi Ordinatio* (Pagani et al., 2015b) in order to obtain the most relevant articles based on the journals’ impact factor, the number of citations as well as the year of publication (De Campos et al., 2018). This article is aimed at researchers and practitioners of the subject requiring an extensive analysis of the existing literature for future works.

## 2. EXPERIMENTAL PROCEDURE

To carry out the work, the Scopus and Web of Science (WoS) databases were considered to be of greater importance (but mostly that of Scopus) in the development of the bibliometric analysis for the literature research, contemplating a search period between January 1990 and November 2020. Once these variables had been selected, the databases were explored using the keyword ‘rubberized concrete’ as a starting point. A total of 610 articles were found in the Scopus database and a total of 357 articles in that of WoS. Based on these results, the main keywords were selected.

A database in Comma Separated Values (CSV) and Text File (TXT) formats was subsequently generated for further analysis in a software tool for the construction and visualization of bibliometric networks called VOSviewer. Figure 1 shows the diagram of keywords from Scopus and WoS databases based on the frequency of repetition of the words.



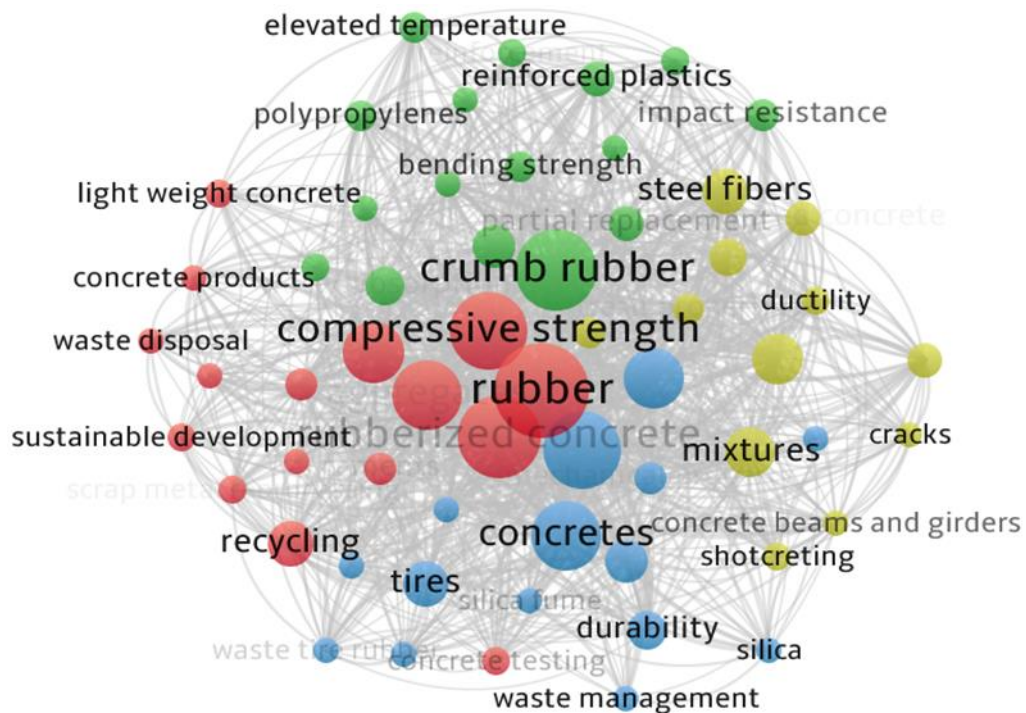


Figure 1. Bibliometric map created with VOSviewer showing the frequency (keyword co-occurrence) of keywords presented in ‘rubberized concrete’

For the bibliometric analysis, the *Methodi Ordinatio* method (Pagani et al., 2015a) was used, which consists of 9 stages:

- Phase 1: Establishment of the search intention: The purpose of the search was to analyze the information in the databases on the subject ‘rubberized concrete’.
- Phase 2: Preliminary search in the database with the keyword ‘rubberized concrete’.
- Phase 3: Final decision on the keywords combination for the search in databases: ‘crumb rubber’, ‘behavior’, ‘mechanical properties’, ‘performance’, ‘strength’, ‘rubberized concrete’, ‘concrete’, ‘aggregate’, ‘durability’ and ‘tire rubber’.
- Phase 4: Final search in the databases; the Boolean operators used were: ‘crumb rubber’ AND ‘behavior’ AND ‘mechanical properties’ AND ‘performance’ AND ‘strength’ AND ‘rubberized concrete’ AND ‘concrete’ AND ‘aggregate’ AND ‘durability’ AND ‘tire rubber’. Results were exported in csv and txt format for later analysis in VOSviewer.
- Phase 5: Information filtering: From the previous phase, the articles to be filtered were obtained, then further filtering was carried out until obtaining the most relevant papers for the application of the *InOrdinatio* equation.
- Phase 6: Identification of impact factor, year of publication and number of citations: With the results obtained from the search in both databases (Scopus and WoS), the analysis by number of citations and year of publication was carried out. The journal impact factor was obtained through the Clarivate Analytics Incites Journal Citation Reports database or the Scopus Source List.
- Phase 7: Obtention of the articles ranking: Once phases 1 to 6 were completed, the *InOrdinatio* index equation was used to calculate the articles ranking. This equation considers total citations, impact factor and a weight factor provided by the researcher, which ranges from 1 to 10.

$$InOrdinatio = \left(\frac{IF}{1000}\right)^{\alpha} + \alpha (\text{research year} - \text{publication year}) + \sum Ci$$

where,

IF = impact factor (JCR, CiteScore, SJR or SNIP)

$\alpha$  = coefficient (1 to 10) that evaluates the importance of the year in which the article was published

Research year = year in which the research was carried out

$\sum Ci$  = total number of citations of the article

In order to consider not only long-established publications, an alpha value of seven was chosen (Pamplona Solis et al., 2019). An alpha value near to one ( $\alpha = 1$ ) generates portfolios with classic articles, but if recent papers are more important for the research, then the alpha value should be closer to 10.

- Phase 8: Articles search: Once the articles ranking had been obtained using the *InOrdinatio* method, their full version was obtained through a reference management software tool such as Mendeley, Citavi or Zotero.
- Phase 9. Final reading and systematic analysis of the articles: A systematic review can be an extensive and laborious work; *Methodi Ordinatio* helps to create an ordered list of all relevant articles to facilitate the researcher's analysis.

VOSviewer is a software designed to complement this type of methodologies. Information that can be extracted is the keyword frequency, which is displayed based on the circles area. The smaller ones represent keywords that are not so relevant, while those in the middle (and larger) represent relevant keywords in the different published articles. For example, the word ‘rubber’ is more relevant for obvious reasons. However, in some articles with the same keyword, topics of interest such as pretreatment of the material or the rubber-cement interface can be found. Compared with ‘steel fibers’, which are the steel fibers extracted from the used tires, there is little interest of researchers, since there is less presence of this keyword. This made it clear that this diagram provides an overview of the studied topics and does not reflect any final results, it is a procedure prior to filtering.

### 3. RESULTS AND DISCUSSION

The objective of the search was to find articles containing the word ‘rubberized concrete’ either in the title, abstract or keywords in the period between 1990 and 2020.

The use of rubber in concrete was chosen as the main topic for the analysis, so the first search for articles was carried out considering the inclusion of the initial keyword ‘rubberized concrete’. Priority was given to articles in English language, as well as those in the Scopus database. For the analysis period, 610 articles have been registered in Scopus as well as 357 in WoS. The first publication registered in the Scopus database was one by the American Society for Testing and Materials (ASTM) in 1990. The highest scientific production occurred in 2020 with 125 published articles according to the Scopus database and a total amount of 97 articles in WoS. In Figure 2, it can be observed in greater detail how the study of this material for construction applications has been increasing.

Results obtained show the increased trend of the study of rubber use in concrete mixes in the last ten years and highlight the most relevant articles using the *InOrdinatio* index.

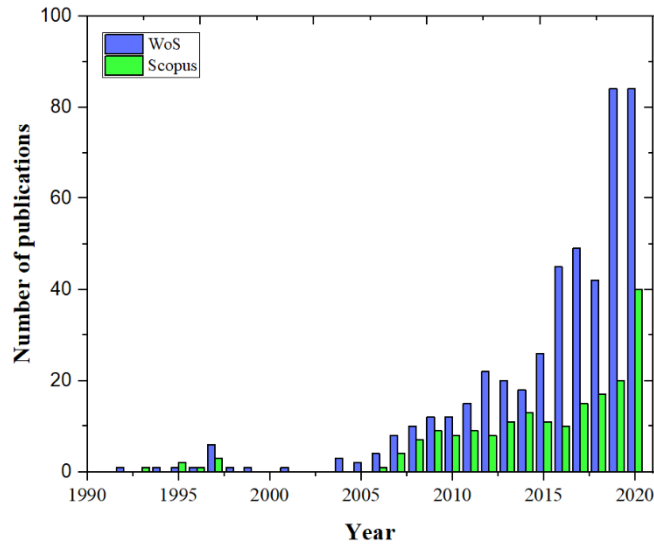


Figure 2. Number of articles published per year

Figure 2 shows that, although the frequency in the study of rubber in concrete is somewhat inconsistent in terms of the number of articles published per year, in the last ten years, scientists have taken this issue in their research works with more frequency. This resulted in a higher productivity of articles (apparently, the trend will continue to rise in the upcoming years) and is currently being sought as an alternative to mitigate global pollution caused by waste tires.

According to the Scopus database, there are a total of 610 articles published on the topic ‘rubberized concrete’ and a total of 1182 authors, between January 1990 and November 2020.

Figure 3 demonstrates that the year with the highest scientific activity was 2020 with a total of 409 authors. The research trend on the subject has increased substantially over the years.

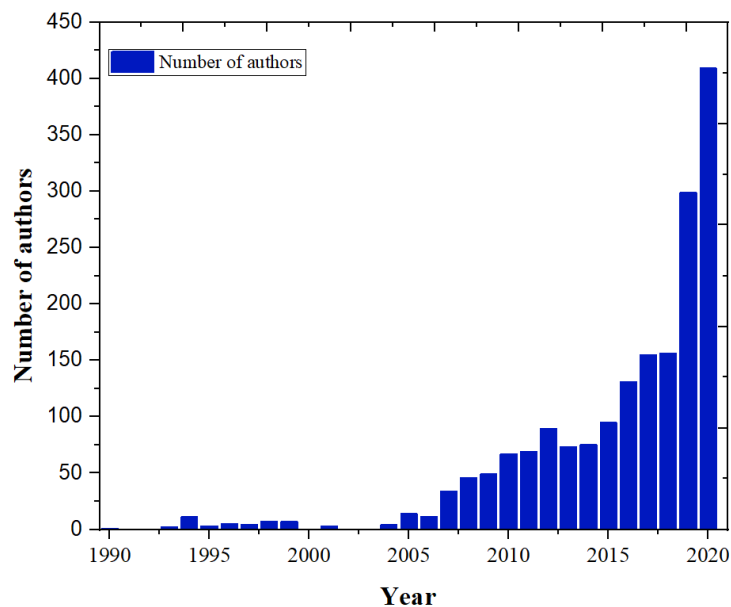


Figure 3. Number of authors per year, 1990-2020.

Figure 4 shows the top ten countries with the greatest number of contributions on the topic ‘rubberized concrete’, the first ten places have been considered based on the quantity of articles published per year.

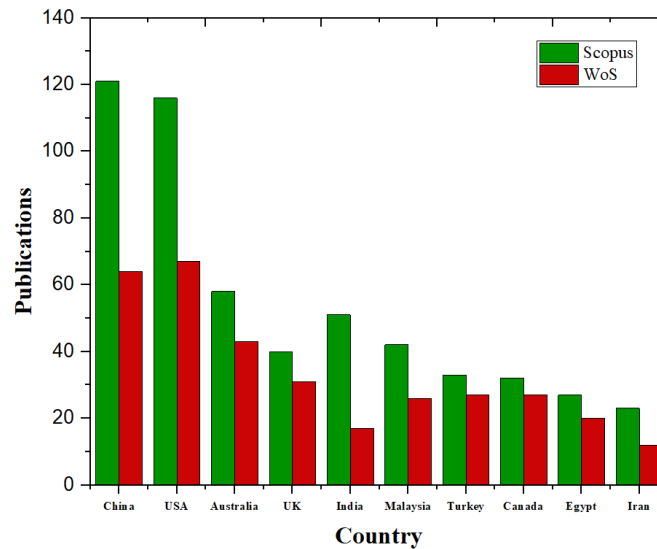


Figure 4. Top 10 of countries with the largest number of publications (Scopus and WoS).

The country with the highest scientific productivity is China with 121 articles published according to Scopus, and 64 according to WoS, followed by the United States in second place and Australia in the third place.

Once the set of articles was defined for the analysis of the literature, the search was carried out in both Scopus and Web of Science. For this, the following Boolean commands were used: ‘TITLE-ABS-KEY (rubberized AND concrete) AND PUBYEAR > 2009 AND PUBYEAR < 2021’ for Scopus, and ‘TITLE-ABS-KEY (rubberized AND concrete) AND PUBYEAR > 1989 AND PUBYEAR < 2021’ for WoS. For the case of WoS, the entire collection was taken into consideration, whereas for Scopus, the entirety of the database was considered.

The total portfolio of articles is made up of a total of 967. Figure 4 depicts how, during the application of *InOrdinatio* method, the articles were being discarded due to relevance issues or because *InOrdinatio* value was not high enough to be taken into account in the final portfolio of documents to be analyzed. Table 1 shows the articles that met the criteria established for an alpha value of 7. The quantity of articles to be analyzed for the *InOrdinatio* rank was significant, given the recent increase in productivity on the subject, compared to the past decade, however, the articles met the minimum or a greater value. This, due to various factors such as insufficient number of citations or low impact factor of the journal to reach the proposed value.

Table 1. Number of articles before and after the applied filters

Filter	Portfolio articles	Crossing articles	Remaining articles	%
WoS	610			
Scopus	357			
Gross portfolio	967			100
Duplicated	140	140	827	85.52
Reviews, book chapters, conference papers	98	98	729	75.38
Articles published before 2010	105	105	624	64.52
<i>In Ordinato</i> < 75	617	617	7	0.72
Total discarded papers	911			
Total considered papers	7			

Table 2. List of articles classified by *InOrdinatio* order in the final portfolio.

Author	Title	Year	InOrdinatio Alfa= 7	InOrdinatio
Pelisser et al.	Concrete made with recycled tire rubber: Effect of alkaline activation and silica fume addition (Pelisser et al., 2011)	2011	1	280.007246
Najim et al.	Mechanical and dynamic properties of self-compacting crumb rubber modified concrete (Najim & Hall, 2012)	2012	2	181.004419
Su et al.	Properties of concrete prepared with waste tire rubber particles of uniform and varying sizes (Su et al., 2015a)	2014	3	135.007246
Thomas et al.	Recycling of waste tire rubber as aggregate in concrete: durability-related performance (Thomas et al., 2016)	2016	4	132.007246
Onuaguluchi et al.	Hardened properties of concrete mixtures containing pre-coated crumb rubber and silica fume (Onuaguluchi & Panesar, 2014)	2014	5	121.007246
Xue et al.	Rubberized concrete: A green structural material with enhanced energy-dissipation capability (Xue & Shinozuka, 2013)	2013	6	104.004419
Youssf et al.	An experimental investigation of crumb rubber concrete confined by fibre reinforced polymer tubes (Youssf et al., 2014)	2014	7	87.004419

Despite that most of the analyzed articles have been published recently, this affects the final portfolio of articles since many of them did not have enough citations to meet an *InOrdinatio* value of 7 or greater (Table 2). However, this does not mean that there will not be articles in the future becoming a reference for the study of rubber in construction applications, specifically in structural and non-structural concrete. An example is the rubber-cement interface which, in the future, will be very useful for the development of concrete mixes with rubber addition based on this topic of research. Other researchers have provided data that will be useful for long-term investigations into the use of rubber as a mix in composite materials and structural efficiency (Ataria & Wang, 2019). The most important articles, according to this analysis, are listed in Table 2.

Other authors have also provided a summary of 30 years of research of rubber as a building material providing an extensive analysis on pretreatment, mechanical properties, physical properties and other useful data (Roychand et al., 2020).

During the *InOrdinatio* analysis, a total of 967 articles were initially considered in the analysis. After the application of filter number two, a total of 382 articles were considered for the final analysis. Table 3 shows the ten most frequent keywords used in studies of rubber in concrete as well as their frequency. These articles were subsequently analyzed in the VOSviewer software where it can be seen that the keyword with the highest presence in most of the articles is ‘rubber’ with a total of 355 and the one with the least frequency is “mechanical properties” with a total of 82.

Table 3. Top 10 keyword concurrences in the bibliometric analysis

Keyword	Concurrence
rubber	355
rubberized concrete	305
concretes	234
compressive strength	218
aggregates	162
concrete aggregates	127
crumb rubber	128
tires	95
tensile strength	94
mechanical properties	82

Figure 5 depicts that the priority of the researchers is to incorporate rubber in the construction industry, according to the literature. Given that it is a global pollution concern, this trend is reflected in the use of the different keywords are presented in the above-mentioned table. Also, in rubberized concrete, one of the problems that researchers have tried to improve over the years is compressive strength, issue of utmost importance in concrete performance since it is one its main functions, so the study of this specific property is a priority. For that reason, its frequency is greater when compared to other mechanical properties. Note that differences can be found when changing the Boolean commands, so the results may be different and more specific.

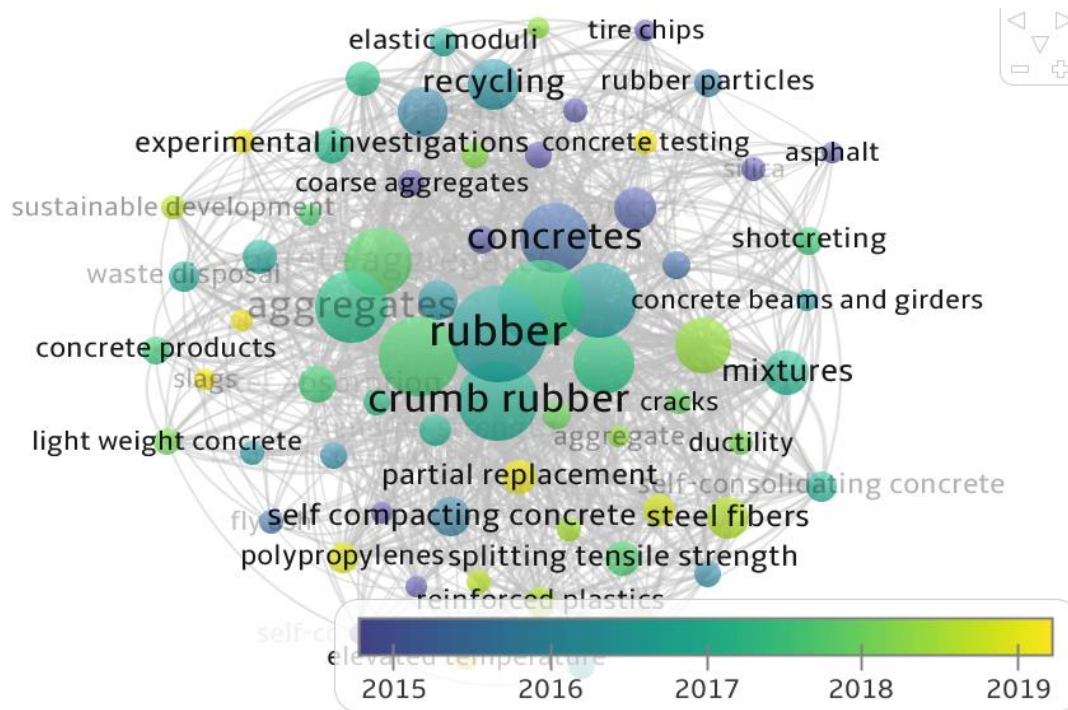


Figure 5. Keyword’s diagram based on their concurrency

During the 30 years timespan of this study of rubber in concrete, 1,182 authors have participated in the investigation of the subject. Authors with the highest number of citations and published articles are listed in Table 4. However, it was until 2010 that the subject presented a considerable increase in the production of articles and related documents in which different studies intended to improve the properties of concrete with the addition of rubber in industrial applications.

Table 4. Top 10 authors based on published documents and citations

Author	Documents	Citations
Mills J. E.	20	414
Youssf O.	18	399
Hassanli R.	17	234
Silvestre N.	11	187
Guadagini M.	14	166
Pilakoutas K.	14	166
Ma X.	11	164
De Brito J	9	147
Duarte A. P. C.	8	141
Julio E.	8	141

Regarding productivity, Mills J.E. has 414 citations and 20 documents until 2020, being the author with the highest productivity. On the other hand, Duarte A. P. C. and Julio E. with 8 documents and 141 citations occupy the last two places of the top ten. Figure 6 represents, graphically, the behavior of the data presented in Table 4. This diagram aims to show co-authorship, which is reflected in productivity. This helps to provide a starting point to know what authors to consult to carry out a research in the field of concrete with addition of rubber.

During the period between years 1990-2020, considered in this work, since the publication of the first article according to the Scopus database in 1990, the number of articles published per year was less than 10 until 2007.

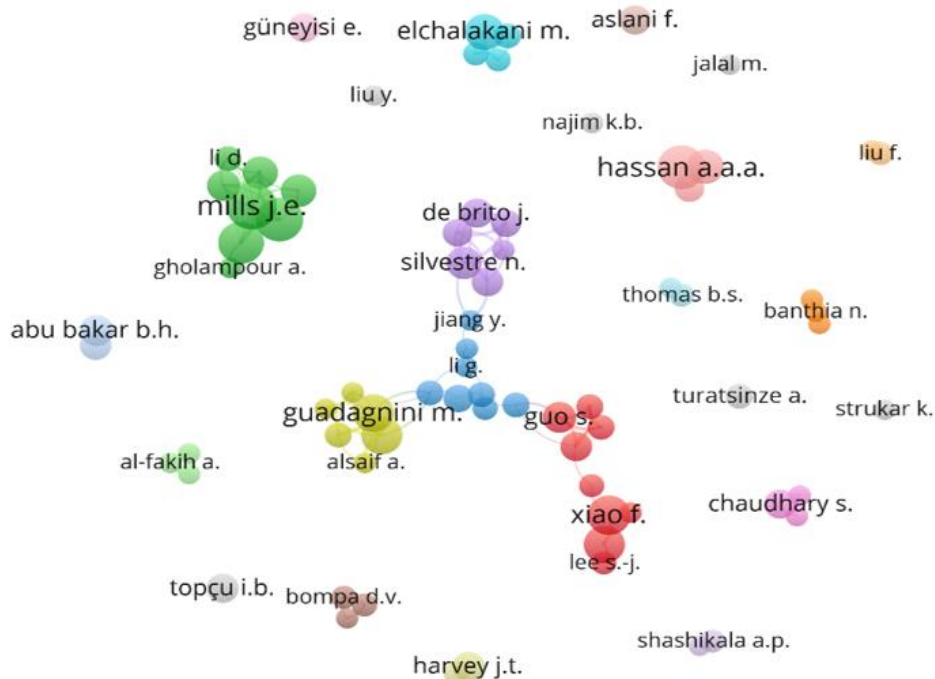


Figure 6. Co-authorship diagram based on ‘rubberized concrete’ publications

During the period from 1990 to 2020, a total of 610 documents have been published according to the Scopus database. An inconsistent trend can be noticed in the publications until 2007, and from that year on, productivity began to increase significantly to this day. For a better analysis, Table 5

contains data of the articles published per year.

Table 5. Productivity of articles by year of the topic ‘rubberized concrete’

Year	Articles	Year	Articles	Year	Articles
1990	1	2001	2	2012	38
1991	0	2002	0	2013	27
1992	0	2003	0	2014	26
1993	1	2004	6	2015	30
1994	5	2005	5	2016	51
1995	2	2006	6	2017	58
1996	3	2007	9	2018	53
1997	6	2008	16	2019	87
1998	4	2009	21	2020	111
1999	2	2010	17		
2000	0	2011	23		
<b>Total</b>	<b>610</b>				

China, despite being the first country with the highest research productivity, is the ninth most cited, being Iran the one occupying the first position with 482 citations, so despite its low productivity. it is placed in the first position (Table 6). This trend may be due to the fact that the articles published by Iranian researchers have a higher journal impact factor when compared to Chinese researchers which impact factor is not that high. An example of this is Su et al. (2015b) and Chen et al. (2019) which, despite not being old articles can be considered classics on the subject.

Table 6. Top 10 of the most cited countries.

Country	Citations
Iran	482
Turkey	435
Canada	362
United States of America	282
Australia	271
India	231
Iraq	148
Egypt	113
China	84
Malaysia	65

Australia and the United States have a similar productivity-citation ratio. These being the most important countries when both variables are considered. However, Iran presents the highest number of citations and the 10th place in document productivity. Figure 7 shows a graphical representation of the collaboration between countries and how they are linked to each other. It is a complement to diagram in Figure 6, but it focuses on collaboration between countries in an attempt to specify which places in the world have an interest in the subject in terms of scientific productivity.



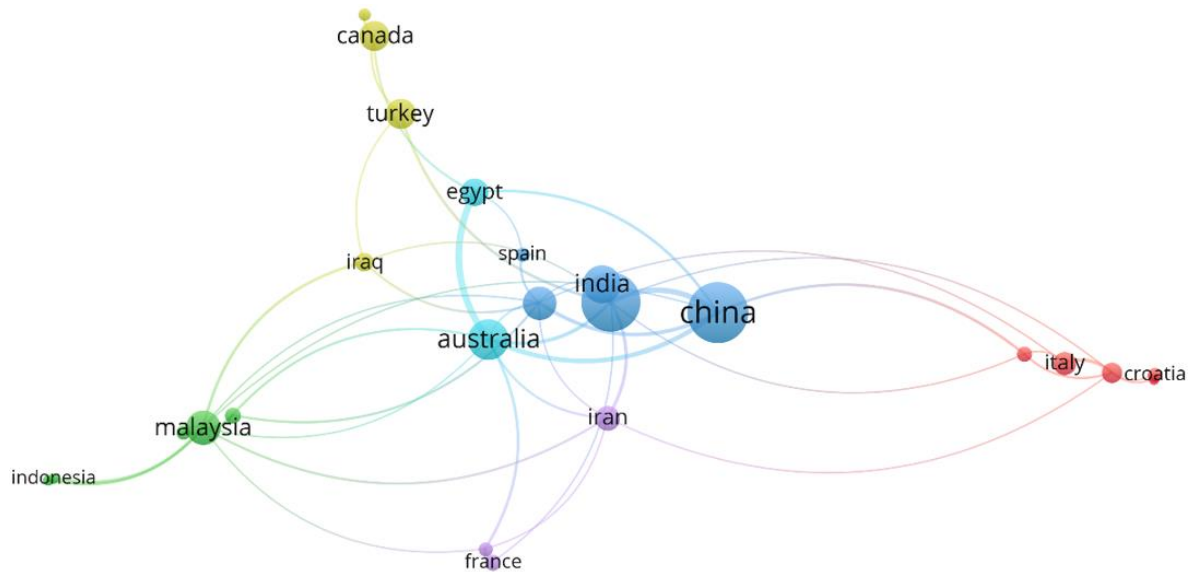


Figure 7. Country collaboration diagram based on co-authorship of publications on the topic 'rubberized concrete'

The journal with the highest productivity is *Construction and Building Materials* with an impact factor of 4.69. However, the journal with the highest impact factor is *Journal of Cleaner Production* with an IF of 7.10, these impact values are according to Clarivate Analytics.

The aims and scope of the journals are mainly construction, materials science and environmental issues. In general, most of the research focuses on sustainable construction (Su et al., 2015b), alternative materials (Yang et al., 2018) and, in some cases, mechanical analysis of structures (Ataria & Wang, 2019) (Table 7).

Table 7. Productivity of publications and citations by journal

Source	Documents	Citations
Construction and Building Materials	115	3739
Journal of Cleaner Production	32	1354
Journal of Materials in Civil Engineering	23	1291
Engineering Structures	8	153
ACI Materials Journal	13	187
Materials and Structures/Materiaux et Constructions	11	403
Materials	14	86
Composite Structures	8	82
Journal of Building Engineering	7	142
Structures	6	95

The three journals with the highest number of citations are *Construction and Building Materials* with 3739 citations, *Journal of Cleaner Production* with 1354 and *Journal of Materials in Civil Engineering* with 1291. These three journals are the ones with the highest productivity and quantity of citations in the world (Table 7). Figure 8 shows graphically how the data behaves and gives an idea of which are the most important journals that the authors consider for their publications. It is a complement to Table 7 and gives us a visual representation of the data presented in this table.

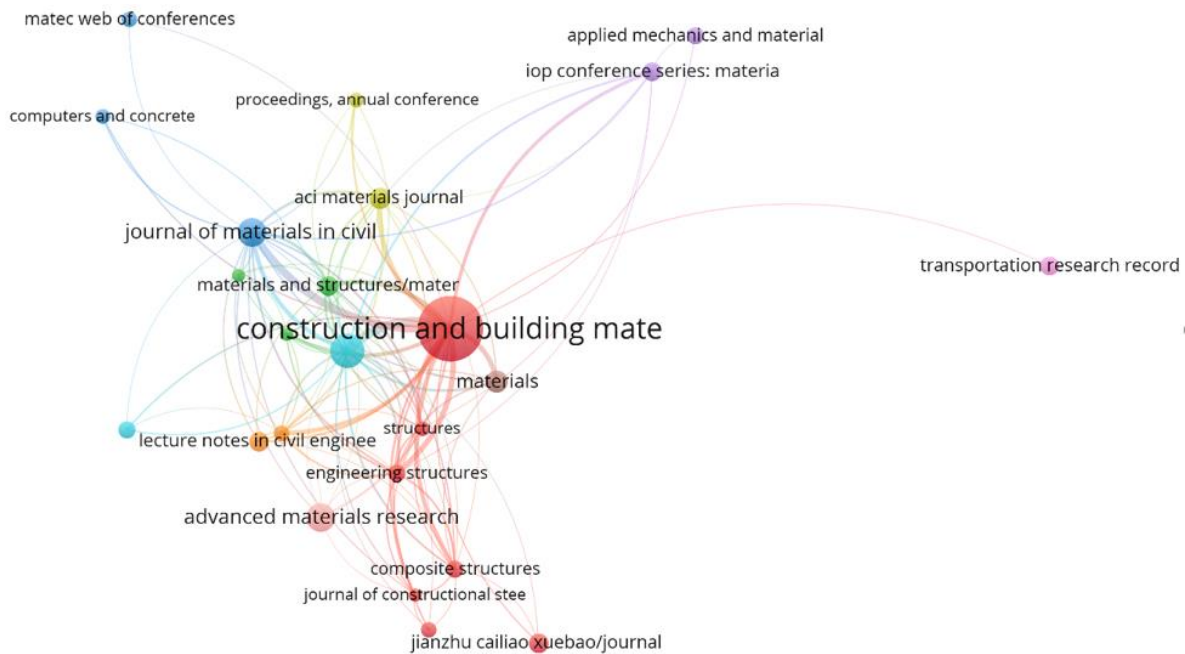


Figure 8. Bibliometric map based on the citations of the most relevant journals on the topic ‘rubberized concrete’

#### 4. CRITICAL REVIEW OF THE MAIN CONTRIBUTIONS AND CURRENT NEEDS OF CONCRETE WITH TIRE WASTE

It was possible to verify that the use of silica fume improves the mechanical resistance of concrete with the addition of rubber (rubber concrete). Only a 14% reduction in compressive strength can be obtained. However, it would be interesting to investigate how compressive strength can be affected or improved with the complement of silica fume. Silica fume is also considered an interface improver between rubber and cement, so it can be proposed for the design of concrete mixes with rubber addition as a cementitious material to improve the interface between rubber and cement (Pelisser et al., 2011).

The mechanical and dynamic properties of self-compacting concrete were investigated, granulated rubber was used as a substitute for fine aggregate, coarse aggregate and both (fine and coarse aggregate). The mechanical properties of concrete with rubber addition in this case are enough to be used in a real environment. However, the results of the dynamic properties tests surpassed the data obtained in the tests carried out on conventional concrete. Continuity of this work may be conducted by performing a seismic analysis which may shed some light on the application of this material in structural elements such as foundations (Najim & Hall, 2012).

Research related to durability issues in concrete with rubber addition concluded that less penetration of chlorides is obtained for a 7.5% of addition. In terms of acid attack, a decrease in weight and compressive strength was observed. In turn, energy dissipation capacity of concrete may increase with the addition of rubber. This property has a potential application in structures exposed to earthquakes. It was concluded that the addition of rubber reduces the response to vibrations (Tomas et al., 2016).

The influence of particle size on the addition of rubber was also investigated. It was concluded that the addition of rubber in concrete affects the workability and permeability when compared to a conventional concrete. Specifically, the larger the size improved the above-mentioned properties. More rigorous investigation may be done to analyze granulometry and determine an optimal particle size of rubber for better physical properties with respect to the ASTM C 33 standard which

may give a parameter for an application from a more technical point of view, as well as guidelines to create a design system for concrete mixes with rubber addition (Youssf et al., 2014).

## 5. CONCLUSION

This article had the purpose of analyzing the last 30 years of research on rubber and its application in structural and non-structural concrete through the *Methodi Ordinatio* analysis. A bibliometric analysis of the literature showed that, since 2010, scientists have considered the impact of pollution worldwide caused by waste tires, which leads the scientific community to find a way to reduce it through reuse.

During these 30 years, 967 documents on the use of rubber in structural and non-structural concrete have been published in the 1990-2020 timespan and 1182 authors have contributed on the subject up to the time of writing this article.

Different properties have been studied such as compressive strength, volume of rubber in concrete mixes as well as the granulometry of rubber particles and their possible influence on concrete strength.

Currently, new studies reveal data that will serve in future research such as the behavior of the rubber-cement interface and the potential that rubber has when used in composite materials. All this opens a new stage in the research of this material for its direct application in different types of situations in the construction industry.

According to the literature analysis, concrete with rubber addition has a lower mechanical resistance than conventional concrete and, also, mechanical resistance decreases as the volume of rubber increases in the concrete mix although the potential as an addition in composite materials shows that the incorporation of rubber can be beneficial in structural applications. The use of different particle sizes in the addition of rubber is a subject that still requires a more in-depth study since conclusive data on the granulometry of the addition and its effect on concrete are lacking. Currently, it is theoretically known that size can influence compressive strength and porosity, however, there are no specific sizes that allow a design standard for concrete mixes with rubber addition.

In a global context, it can be observed that, according to the analyzed data, since 2010, the interest of researchers in introducing rubber in construction applications has increased markedly in order to reduce pollution at a global level. However, there is still a lack of regulations for its use under real conditions, such as granulometry values and a mix design methods for this specific addition, so more research has to be undertaken on the characteristics of this material so that it can be regulated for its appropriate use.

## 6. ACKNOWLEDGEMENTS

The authors acknowledge of the support of the Catedra CONACYT Project number 746, LNS Project number 202101008N and the CONACYT Fronteras project (2096029).

## 7. REFERENCES

- Al-Salem, S. M., Lettieri, P., Baeyens, J. (2009). *Recycling and recovery routes of plastic solid waste (PSW): A review*. Waste Management, 29(10), 2625–2643. <https://doi.org/10.1016/j.wasman.2009.06.004>
- Ataria, R. B., Wang, Y. C. (2019). *Bending and shear behaviour of two layer beams with one layer of rubber recycled aggregate concrete in tension*. Structures, 20, 214–225. <https://doi.org/10.1016/j.istruc.2019.03.014>

- Chen, Z., Li, L., Xiong, Z. (2019). *Investigation on the interfacial behaviour between the rubber-cement matrix of the rubberized concrete*. Journal of Cleaner Production, 209, 1354–1364. <https://doi.org/10.1016/j.jclepro.2018.10.305>
- de Campos, E. A. R., Pagani, R. N., Resende, L. M., Pontes, J. (2018). *Construction and qualitative assessment of a bibliographic portfolio using the methodology*, Methodi Ordinatio. Scientometrics, 116(2), 815–842. <https://doi.org/10.1007/s11192-018-2798-3>
- Ghosh, S. K. (Ed.). (2019). *Waste Management and Resource Efficiency: Proceedings of 6th IconSWM 2016*. Springer Singapore. <https://doi.org/10.1007/978-981-10-7290-1>
- Najim, K. B., Hall, M. R. (2012). *Mechanical and dynamic properties of self-compacting crumb rubber modified concrete*. Construction and Building Materials, 27(1), 521–530. <https://doi.org/10.1016/j.conbuildmat.2011.07.013>
- Onuaguluchi, O., Panesar, D. K. (2014). *Hardened properties of concrete mixtures containing pre-coated crumb rubber and silica fume*. Journal of Cleaner Production, 82, 125–131. <https://doi.org/10.1016/j.jclepro.2014.06.068>
- Pagani, R. N., Kovalski, J. L., Resende, L. M. (2015a). *Methodi Ordinatio: A proposed methodology to select and rank relevant scientific papers encompassing the impact factor, number of citation, and year of publication*. Scientometrics, 105(3), 2109–2135. <https://doi.org/10.1007/s11192-015-1744-x>
- Pagani, R. N., Kovalski, J. L., Resende, L. M. (2015b). *Methodi Ordinatio: A proposed methodology to select and rank relevant scientific papers encompassing the impact factor, number of citation, and year of publication*. Scientometrics, 105(3), 2109–2135. <https://doi.org/10.1007/s11192-015-1744-x>
- Pamplona Solis, B., Cruz Argüello, J. C., Gómez Barba, L., Gurrola, M. P., Zarhri, Z., Trejo Arroyo, D. L. (2019). *Bibliometric Analysis of the Mass Transport in a Gas Diffusion Layer in PEM Fuel Cells*. Sustainability, 11(23), 6682. <https://doi.org/10.3390/su11236682>
- Pelisser, F., Zavarise, N., Longo, T. A., Bernardin, A. M. (2011). *Concrete made with recycled tire rubber: Effect of alkaline activation and silica fume addition*. Journal of Cleaner Production, 19(6–7), 757–763. <https://doi.org/10.1016/j.jclepro.2010.11.014>
- Perez, J. G. (2015). *Plan de Manejo de Neumáticos Usados de Desecho*. 79.
- Roychand, R., Gravina, R. J., Zhuge, Y., Ma, X., Youssf, O., Mills, J. E. (2020). *A comprehensive review on the mechanical properties of waste tire rubber concrete*. Construction and Building Materials, 237, 117651. <https://doi.org/10.1016/j.conbuildmat.2019.117651>
- Ruwona, W., Danha, G., Muzenda, E. (2019). *A Review on Material and Energy Recovery from Waste Tyres*. Procedia Manufacturing, 35, 216–222. <https://doi.org/10.1016/j.promfg.2019.05.029>
- Su, H., Yang, J., Ling, T.-C., Ghataora, G. S., Dirar, S. (2015a). *Properties of concrete prepared with waste tyre rubber particles of uniform and varying sizes*. Journal of Cleaner Production, 91, 288–296. <https://doi.org/10.1016/j.jclepro.2014.12.022>
- Su, H., Yang, J., Ling, T.-C., Ghataora, G. S., Dirar, S. (2015b). *Properties of concrete prepared with waste tyre rubber particles of uniform and varying sizes*. Journal of Cleaner Production, 91, 288–296. <https://doi.org/10.1016/j.jclepro.2014.12.022>
- Thomas, B. S., Gupta, R. C., Panicker, V. J. (2016). *Recycling of waste tire rubber as aggregate in concrete: Durability-related performance*. Journal of Cleaner Production, 112, 504–513. <https://doi.org/10.1016/j.jclepro.2015.08.046>
- What a Waste 2.0: A Global Snapshot of Solid Waste Management to 2050. (2019, January 7). *Green Growth Knowledge Platform*. <https://www.greengrowthknowledge.org/research/what-waste-20-global-snapshot-solid-waste-management-2050>
- Xue, J., Shinozuka, M. (2013). *Rubberized concrete: A green structural material with enhanced energy-dissipation capability*. Construction and Building Materials, 42, 196–204. <https://doi.org/10.1016/j.conbuildmat.2013.01.005>

- Yang, Z., Ji, R., Liu, L., Wang, X., Zhang, Z. (2018). *Recycling of municipal solid waste incineration by-product for cement composites preparation*. Construction and Building Materials, 162, 794–801. <https://doi.org/10.1016/j.conbuildmat.2017.12.081>
- Youssf, O., ElGawady, M. A., Mills, J. E., Ma, X. (2014). *An experimental investigation of crumb rubber concrete confined by fibre reinforced polymer tubes*. Construction and Building Materials, 53, 522–532. <https://doi.org/10.1016/j.conbuildmat.2013.12.007>